TRANSPORTATION RESEARCH RECORD 1070

Pavement Response, Evaluation, and Data Collection

TRB
TRANSPORTATION RESEARCH BOARD
NATIONAL RESEARCH COUNCIL
WASHINGTON, D.C. 1986

Transportation Research Record 1070
Price $18.20
Editor: Catherine Nizharadze
Compositor: Joan G. Zubal
Layout: Theresa L. Johnson

mode
1 highway transportation

subject areas
12 planning
24 pavement design and performance
40 maintenance

Transportation Research Board publications are available by ordering directly from TRB. They may also be obtained on a regular basis through organizational or individual affiliation with TRB; affiliates or library subscribers are eligible for substantial discounts. For further information, write to the Transportation Research Board, National Research Council, 2101 Constitution Avenue, N.W., Washington, D.C. 20418.

Printed in the United States of America

Library of Congress Cataloging-in-Publication Data
National Research Council. Transportation Research Board.

Pavement response, evaluation, and data collection.

(Transportation research record, ISSN 0361-1981 ; 1070)
1. Pavements–Performance–Congresses. 2. Pavements–Live loads–Congresses. I. National Research Council (U.S.). Transportation Research Board. II. Series.
TE7.H5 no. 1070 380.5 s 86-23522
[TE251.5] [625.8]
ISBN 0-309-04064-7

Sponsorship of Transportation Research Record 1070

GROUP 2–DESIGN AND CONSTRUCTION OF TRANSPORTATION FACILITIES
David S. Gedney, Harland Bartholomew & Associates, chairman

Pavement Management Section
R. G. Hicks, Oregon State University, chairman

Committee on Pavement Management Systems
George B. Way, Arizona Department of Transportation, chairman
Doyt Y. Bolling, George N. Clark, Billy G. Connor, Santiago Corro Caballero, Michael I. Darter, Asif Faiz, Fred N. Finn, Wouter Gulden, Ralph C. G. Haas, W. Ronald Hudson, William J. Kenis, Ramesh Kher, Joseph P. Kubala, Ram B. Kulkarni, Lawrence E. Larsen, David R. Luhr, Robert L. Lytton, David K. Miles, Leon M. Noel, Robert G. Packard, Christian Peyronne, Rolands L. Rizenbergs, Gerald J. Rohrbach, S. C. Shah, Per Ullidtz, Harold L. Von Quintus

Committee on Strength and Deformation Characteristics of Pavement Sections
J. Brent Rauhut, Brent Rauhut Engineering, Inc., chairman
Joseph H. Amend III, Gilbert Y. Baladi, Richard D. Barksdale, Stephen F. Brown, Albert J. Bush III, George R. Cochran, Billy G. Connor, Amir N. Hanna, R. G. Hicks, Ignat V. Kalcheff, William J. Kenis, Thomas W. Kennedy, Erland Lukanen, Robert L. Lytton, Michael S. Mamlouk, Edwin C. Novak, Jr., Lufti Raad, Quentin L. Robnett, Byron E. Ruth, Gary Wayne Sharpe, James F. Shook, Roger E. Smith, R. N. Stubstad, Marshall R. Thompson, Ulian I. Tufektchiev, Thomas D. White

Committee on Monitoring, Evaluation and Data Storage
William A. Phang, Ministry of Transportation and Communications, chairman
Don H. Kobl, Consultant, secretary
Glenn G. Balmer, A. T. Bergan, Billy G. Connor, Brian E. Cox, Michael I. Darter, Karl H. Dunn, Wouter Gulden, Douglas I. Hanson, William H. Highter, W. Ronald Hudson, Andris A. Jumikis, Scott A. Kutz, W. N. Lofroos, Keith E. Longenecker, K. H. McGhee, Robert L. Novak, Freddy L. Roberts, Ivan F. Scazziga, S. C. Shah, Mohamed Y. Shahin, Herbert F. Southgate, Elson B. Spangler, Shiraz D. Tayabji, Reuben S. Thomas, Loren M. Womack

Soil Mechanics Section
Raymond A. Forsythe, California Department of Transportation, chairman

Committee on Subsurface Drainage
Gary L. Hoffman, Pennsylvania Department of Transportation, chairman
Gordon R. Benson, Robert G. Carroll, Jr., Barry J. Dempsey, Wilbur M. Haas, Kent A. Healy, S. Bennett John, Gary L. Klinedinst, Donald C. Long, Robert H. Manz, Vernon J. Marks, C. Robert McQuary, Lyle K. Moulton, Edwin C. Novak, Jr., Willard G. Puffer, Hallas H. Ridgeway, L. David Suits, William D. Trolinger, Hugh L. Tyner, Walter C. Waidelich, David C. Wyant, Thomas F. Zimmie

George W. Ring III and Neil F. Hawks, Transportation Research Board staff

Sponsorship is indicated by a footnote at the end of each paper. The organizational units, officers, and members are as of December 31, 1985.

TRR 1070

Contents

Measurement and Analysis of Truck Tire Pressures on Texas Highways

DAN R. MIDDLETON, FREDDY L. ROBERTS, and T. CHIRA-CHAVALA

ABSTRACT

Field data indicate that truck tire pressures on Texas highways are increasing. Implications of this increase are important in terms of increasing damage to roadway pavements, particularly flexible pavements. The methodology used in field data collection is described, along with data analysis by variables such as vehicle classification, axle load, commodity being hauled, and tire construction.

Preliminary evidence from the field indicates that truck tire pressures on Texas highways have increased in the past few years. The effect of such an increase on pavements would be an accelerated rate of pavement deterioration. On asphaltic concrete pavements, increases in truck tire inflation pressures would result in more rapid appearance of alligator cracking and rutting, and probably an increase in the rate of occurrence of reflection cracking in overlays. One result of increased deterioration will be an accelerated schedule on planned programs of major maintenance and rehabilitation.

Before this study, a need existed to determine the distribution of tire pressures on Texas highways and to identify the magnitude of the effects of increased tire pressures on individual asphaltic concrete pavements and flexible pavement networks. None of the previous studies evaluating the effects of truck traffic and changing legal load limits has included tire pressures as an explicit variable, although inflation pressures were assumed to increase somewhat with increasing legal load limit.

The objectives of this part of the study were twofold:

1. To determine by actual measurement the distribution of tire pressures and areas of tire footprint on Texas pavements, and
2. To determine by computation the effect of these tire pressures on the life and cost of typical flexible pavements.

The measurement of the tire footprint in the field data collection was not accomplished. Several methods were considered and some were actually tested in the field; however, none proved to be feasible for field measurement. Using the measurement systems investigated would have significantly reduced the amount of tire pressure data collected because of the time intensity of the measurement process. It should be noted that in a companion study entitled Experimental Investigation of Truck Tire Inflation Pressure on Pavement--Tire Contact Area and Pressure Distribution, contact areas of tires under various loads were measured in a laboratory setting (1). The study was conducted by the Center for Transportation Research (CTR) at the University of Texas in Austin, and the findings are being used to supplement the results of this study.

D.R. Middleton and T. Chira-Chavala, Texas Transportation Institute, Texas A&M University, College Station, Tex. 77843-3135. F.L. Roberts, Civil Engineering Department, Auburn University, Ala. 36849.

DATA TO BE COLLECTED

First, a standard form was developed for recording survey information. Table 1 gives a list of the desired survey data by the categories of tire, vehicle, site, and other. Because of various constraints, the other data were not collected. Information on vehicle length, width, and headlight height was originally selected in an attempt to camouflage the tire pressure data collection. However, these superfluous measurements were not taken because time was not available. Again, information on the tire contact area was not gathered because of the lack of a practical and accurate means of making the measurement as well as the time constraint.

TABLE 1 Desired Survey Information

Category	Desired Information
Tire	Manufacturer
	Construction (radial, bias)
	Size
	Inflation pressure 1 and 2
	Tread depth
Vehicle	Test number
	AASHTO classification
	Commodity
	License number
	Weight
Site	Air temperature
	Pavement temperature
	Date of survey
	Location
	Weather
Other	Length of vehicle
	Width of vehicle
	Headlight height
	Tire contact area

Site information such as date, location, and weather was recorded once a day, and air and pavement temperatures were recorded approximately hourly. Other information was recorded with each available truck. For each vehicle, a test number and the AASHTO class were recorded, and, if time and personnel were available, the vehicle license number and weight were recorded.

As a minimum, the following tire information was gathered on each vehicle: inflation pressure, manufacturer, construction (radial, bias), size, and tread depth. A second pressure (Pressure 2) was also taken on a few trucks in an attempt to determine change in tire inflation pressure after cool down.

In many cases, the tread depth varied across the

width of the tire. The reading was taken fairly consistently at a distance of 2 in. from the outside edge of the tire.

The weight in pounds of each axle group was recorded by project personnel as the vehicle was weighed by the Texas Department of Public Safety (DPS). Because weights and tire information were in most cases recorded separately by two different people, a system was needed to combine the two sets of data for each truck. This was done by using the truck license plate numbers.

METHODOLOGY USED FOR SITE SELECTION

Coordination with the License and Weight Division of the DPS was necessary for all data collection. The DPS was already involved in an ongoing enforcement program in which trucks were stopped at various locations throughout the state to check weights, vehicle registration, and so forth. Therefore, the logical means of collecting tire pressure information was in conjunction with the DPS operations.

Three primary factors were considered in making site selection:

- Availability of DPS personnel and equipment,
- Roadside safety considerations at the site, and
- Commodities being hauled through the area.

The normal procedure used by project staff to schedule field data collection with the DPS was as follows. First, a geographic area in the state was identified where certain commodity movements were known to occur. Seasonal fluctuations in commodity movement were also important, with the best survey conditions occurring during the peak season. Next, a DPS captain in Austin designated the proper person to contact in the vicinity of the site selected. This contact person had authority in the desired area to make the necessary commitments for DPS personnel to meet project staff at a selected site.

The limitation on DPS equipment often meant scheduling difficulties. Only a limited number of semiportable platform scales were available to the many DPS offices. The typical weighing system used a van towing a trailer to haul the scales. These were rotated to the various DPS offices in a given region on a scheduled basis. Therefore, DPS assistance for data collection depended not only on the availability of their personnel but also on the location of the semiportable scales.

The second important factor in choosing data collection sites was traffic safety around the site. Only a relatively few sites existed where several trucks could be stopped at one time without forming a queue that extended into the through-traffic lanes. Even some weigh strips were of insufficient length to accommodate stopped vehicles.

The commodities of particular interest were those chosen in another project entitled Identification of Special-Use Truck Traffic. They were aggregated into three industries: timber, agriculture, and surface mining. Specific commodities for each are as follows:

1. Timber:
   - Raw timber
   - Wood products
2. Agriculture:
   - Grain
   - Beef cattle
   - Produce
   - Cotton
3. Surface mining:
   - Sand and gravel
   - Limestone

Figure 1 is a state map showing the locations of data collection. These sites were selected partly because of the commodities that flowed through them. Other reasons for their selection were availability of DPS enforcement personnel and proximity to project staff headquarters.

Of these sites, the primary timber products were found in a 40-county area in east Texas. Agricultural produce was found near the Rio Grande Valley and beef cattle were found in the panhandle area of the state. The primary surface mining products, such as crushed stone and sand and gravel, were hauled on a multitude of roads throughout the state; the sites selected for the survey were in the Dallas-Fort Worth area. Few, if any, ideal sites existed for collecting truck tire and weight data. Even where weigh strips were

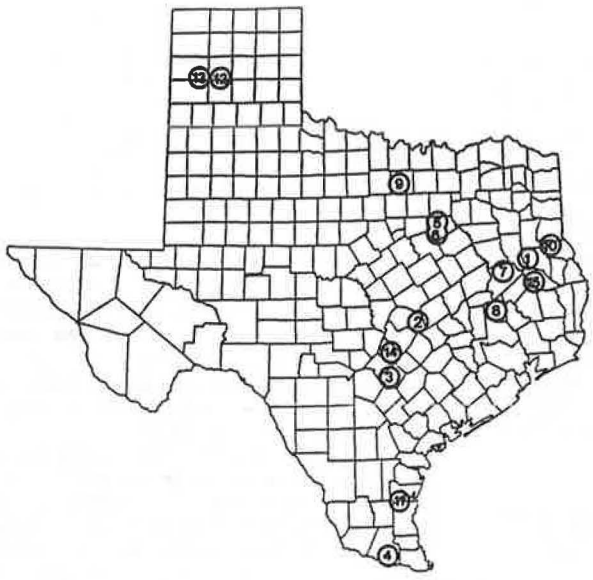

FIGURE 1 Locations of tire pressure data collection.

available for stopping trucks, there were almost always parallel roads available for bypassing the enforcement activities. However, the survey results are not necessarily biased because of this potential for avoidance.

PROCEDURE AT THE SITE

At each data collection site, at least two project persons were required to collect tire pressure information and two DPS officers were required to check and/or weigh trucks. All trucks, whether loaded or empty, were required to stop at these sites. Empty vehicles were often waved on by DPS officers, but at other times a vehicle registration and/or operator's license check was performed.

Project personnel activities were as follows:

- Surveyor No. 1 physically measured tire inflation pressures and tread depths.
- Surveyor No. 2, working alongside Surveyor No. 1, recorded the following information: tire inflation pressure, tread depth, tire manufacturer, tire construction (radial, bias), AASHTO vehicle classification, commodity, truck license number, and information about the site.
- Surveyor No. 3 recorded axle weights and truck license number; this person was not always used.

Tire pressure study information could not be collected as fast as DPS officers could weigh trucks. Therefore, at busy locations, tire pressures could not be measured simultaneously with the weighing because of the excessive queue of trucks that resulted. The more desirable simultaneous operation was modified in those cases to check as many trucks as possible either before being weighed or after, if a violation was detected by DPS. Checking only trucks with violations could introduce bias to the results if there is a correlation between weight and tire pressure (see the section on Analysis of Tire Pressure Data that follows).

The typical data collection procedure involved measuring and recording data on the outside tire along one side of the truck only, beginning at either the front or the rear. The inside tire of the dual was measured only if some problem occurred on the outside tire. Securing information such as brand name on the inside tire was considerably more difficult than doing so for the outside tire.

In most cases, truck drivers were cooperative in allowing their tire pressures to be checked. Because data collection always involved the DPS officers, their presence may have been a factor in the level of cooperation experienced. Several drivers did express concern about the valve stems leaking air after the pressure had been checked. This concern was valid because some valve stems did stick partially open after the pressure was measured. However, the problem could usually be corrected relatively quickly.

TABLE 2 Number of Trucks in Sample

AASHTO Classification	No. of Vehicles	Percent
3-S2	1,033	69.5
2-S2	52	3.5
SU-2	90	6.1
SU-1	86	5.8
Double (3-2)	11	0.7
Double (2-S1-2)	6	0.4
2S1	13	0.9
Missing or unknown	195	13.1
Total	1,486	100.0

ANALYSIS OF TIRE PRESSURE DATA

The objectives of analyses of tire measurement were to identify significant factors affecting tire pressure and to develop tire pressure distributions. The data were divided into sets basically by AASHTO truck class. Analysis of tire pressure measurements was carried out separately for each of four AASHTO classifications: 3-S2, 2-S2, SU-2, and SU-1.

Preliminary Analysis

The sample included measurements on a total of 1,486 trucks. As indicated by the data in Table 2, 70 percent were 3-S2, 6 percent SU-2, 6 percent SU-1, 4 percent 2-S2, 2 percent other truck types, and 13 percent unknown truck types.

Table 3 gives the distribution of truck types at each of the 12 survey locations. At the majority of these locations, virtually all trucks passing the survey station were stopped for tire measurements. These locations were Nacogdoches, Weslaco, Dallas, Wells, Teneha, and Lufkin. At Huntsville, only those trucks stopped by the DPS officers for violations were surveyed for tire pressures.

Figures 2 and 3 show cumulative distribution plots of tire pressures for trucks by tire construction (radial, bias), and with the front axle separated

TABLE 3 Survey Locations and Percent Truck Type at Each Location

Location	Highway Classification	Percent Truck Type					Total No. of Trucks
		3-S2	2-S2	SU-2	SU-1	Other	
Nacogdoches, U.S. 259 and S.H. 204	U.S. 259, two-lane, rural	86.0	3.0	7.0	4.0	—[a]	29
Taylor, U.S. 79	Two-lane, rural	81.0	2.0	7.0	7.0	3.0	85
Seguin, I-10	Interstate, rural	72.0	8.0	8.0	10.0	2.0	245
Weslaco, U.S. 83	Four-lane divided, rural	61.0	5.0	11.0	17.0	7.0	127
Dallas F.M. 1389	Two-lane, rural	78.0	—[a]	16.0	3.0	3.0	64
Wells, U.S. 69	Two-lane, rural	96.0	4.0	—[a]	—[a]	—[a]	22
Huntsville, I-45	Interstate, rural	78.0	6.0	7.0	6.0	3.0	167
Teneha, U.S. 59	Two-lane, rural	90.0	—[a]	2.0	8.0	—[a]	39
U.S. 77 Riviera	Four-lane divided, rural	86.0	2.0	5.0	3.0	4.0	205
Amarillo, U.S. 287	Four-lane divided, rural	86.0	2.0	1.0	3.0	8.0	80
Vega, U.S. 385	Two-lane, rural	94.0	—[a]	3.0	—[a]	3.0	34
Lufkin, S.H. 103	Four-lane divided	91.0	2.0	3.0	4.0	—[a]	128

[a]None observed during survey.

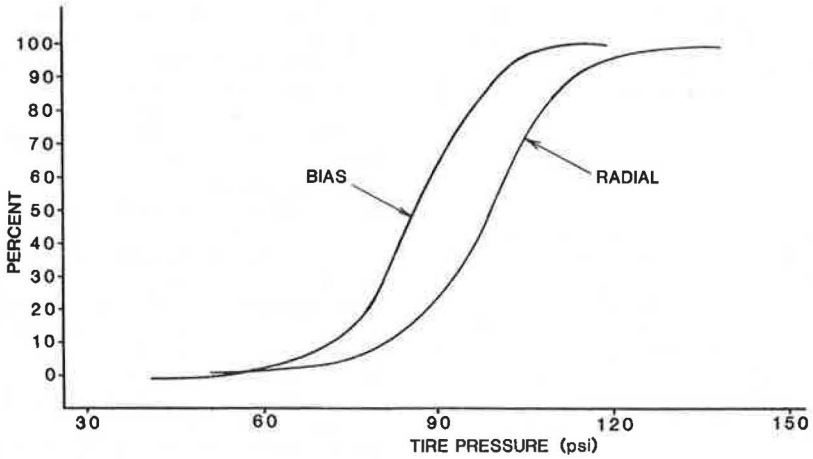

FIGURE 2 Cumulative distribution of tire pressures for front axles of 3-S2 trucks.

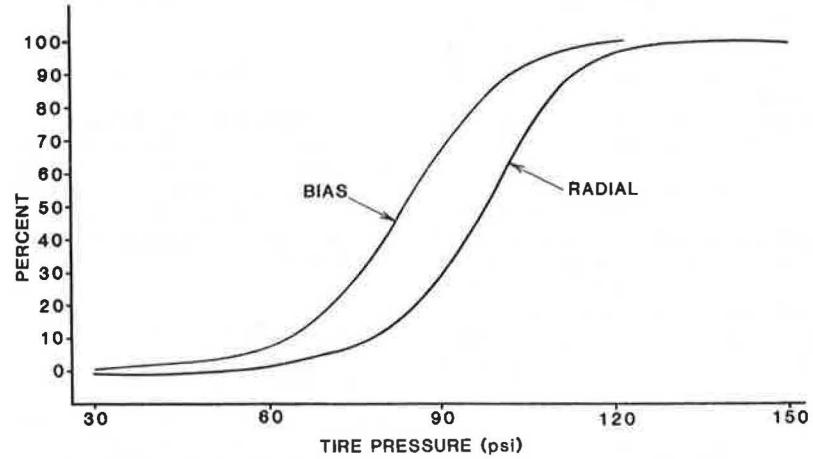

FIGURE 3 Cumulative distribution of tire pressures for non-front axles of 3-S2 trucks.

from all other axles. Figure 4 shows the cumulative distributions of front axle tire pressures among the four AASHTO classes by tire construction. In this figure, the difference in inflation pressure between bias and radial tires is clearly indicated. For a particular AASHTO vehicle, radial tires had higher inflation pressures than did the bias tires. The differences between AASHTO class, although smaller, can also be observed from this figure. For bias tires, 3-S2 vehicles showed higher pressures than did SU-2, 2-S2, and SU-1 vehicles, in that order. For radial tires, the highest tire pressures were measured for 3-S2 trucks, followed by SU-2, 2-S2, and SU-1 trucks.

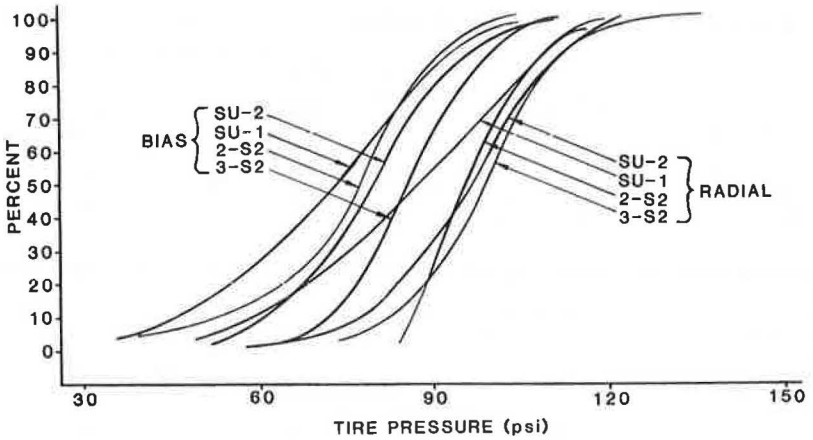

FIGURE 4 Cumulative distribution of tire pressures by tire construction and AASHTO class.

TABLE 4 Tire Pressures by Major Manufacturers for 3-S2 Trucks

Manufacturer	Tire Pressure		
	Mean	Standard Deviation	No. of Axles
Michelin			
Radial	99.0	13.2	730
Bias	94.9	11.1	11
Goodyear			
Radial	98.1	13.9	656
Bias	85.5	16.0	222
Bridgestone			
Radial	99.2	14.9	322
Bias	87.7	14.5	53
Firestone			
Radial	99.8	16.0	116
Bias	83.7	15.1	106
Dunlop			
Radial	98.6	16.5	110
Bias	87.7	17.8	33
General			
Radial	95.4	16.1	80
Bias	84.4	15.8	58
Goodrich (B.F.G.)			
Radial	97.7	13.2	70
Bias	83.8	14.6	96
Cooper			
Radial	94.6	11.7	17
Bias	77.9	14.1	48
Next top 10			
Radial	95.3	15.0	283
Bias	86.6	14.3	171
All other			
Radial	94.9	14.3	264
Bias	85.2	15.8	265

Table 4 gives a summary of tire inflation pressure data by major tire manufacturers for 3-S2 trucks. After adjusting for tire construction, little variation is apparent in the average inflation pressure among manufacturers. Table 5 gives tire inflation pressure data for the 3-S2 trucks by commodities hauled. From that table it can be observed that the inflation pressure was highest for trucks hauling produce and grain on radial tires with an average pressure of 105 psi. For bias tires, the differences in average inflation pressure among different commodities were relatively small.

Figure 5 is a histogram of the axle weight data collected for 3-S2 trucks. The distributions of axle weights for front axles and for tandem axles are shown separately.

Statistical Analysis

The statistical analysis of tire pressures involved an in-depth investigation of the variability in tire pressures and the factors affecting this variability. Based on the results of the preliminary analysis, the following independent variables were examined:

- Tire construction (radial, bias);
- AASHTO truck class;
- Axle location (front, rear, other);
- Tire size (diameter);
- Tread depth (<8/32 in., ≥8/32 in.);
- Commodity carried;
- Axle weight; and
- Survey location.

Tread depth was included as a dichotomous variable to reflect whether the tread depth was inadequate or of reasonable depth.

The collection of axle weight and commodity data was not as complete as the data collected on other variables. The data in Table 6 indicate that a high percentage of axle weight data (about 80 percent) was missing. For commodity, the proportion of cases with missing information was about 55 percent, as indicated in Table 7.

The high percentage of data on axle weight and commodity missing, plus the large subset of 3-S2 trucks, led to the following three analyses:

1. Analysis of the effects of tire and truck factors,
2. Analysis of the effect of axle weights for 3-S2 trucks only, and
3. Analysis of the effect of commodity for 3-S2 trucks only.

TABLE 5 Tire-Pressure Distribution by 10 Major Commodities for 3-S2 Trucks Only

Commodity	Radial			Bias		
	No.	Mean	Standard Deviation	No.	Mean	Standard Deviation
Produce	95	106.2	12.1	10	79.1	20.7
Grain	39	105.6	13.7	11	90.2	14.0
Cattle	36	101.6	19.8	10	87.3	9.1
Lumber	39	100.6	12.6	27	81.8	19.1
Steel	113	98.8	17.5	55	87.9	13.1
Rock, sand or gravel, and limestone	257	97.8	12.4	117	84.0	12.2
Logs	62	96.2	13.4	13	87.7	5.8
Cement	62	95.1	15.6	22	87.6	16.4
Empty	138	95.2	12.2	40	83.8	12.8
Gasoline	121	95.1	13.2	26	85.1	12.1

Effects of Tire Construction, AASHTO Class, Axle Location, Tire Size, and Tread Depth

An analysis of variance (ANOVA) was first conducted to determine the effect of the following five variables on tire pressures:

Variable	Level
Tire construction	Radial or bias
AASHTO class	3-S2, 2-S2, SU-2, SU-1
Axle location	Front or all other
Tire diameter	≤22.5 or >22.5
Tread depth	<8/32 in. or ≥8/32 in.

Table 8 gives the five-variable ANOVA results for all of the significant factors. Tire construction, AASHTO class, and tread depth were found to be significant in explaining the variability in tire pressures. Of these three variables, tire construction was by far the most significant in explaining the differences in tire pressures, followed by AASHTO class. The influence of tread depth was the smallest. Tire diameter and axle location were not significant, nor were any of the two-factor interactions among the five variables.

Table 9 gives a summary of tire pressures by tire construction, AASHTO class, and tread depth. Of the three significant variables, tire construction was the most important. After adjusting for the other two variables, radial tires on the average showed pressures that were up to 20 psi higher than did those of bias tires. The next most significant variable was AASHTO class, in which 3-S2 trucks showed higher average tire pressures than did 2-S2, SU-2, and SU-1 trucks. The largest difference in average tire pressures (10 to 15 psi) was detected between 3-S2 trucks and SU-1 trucks. The effect of tread depth was relatively small, particularly for 3-S2 and 2-S2 trucks. Of these trucks, those with tires in reasonable condition (tread depth ≥8/32 in.)

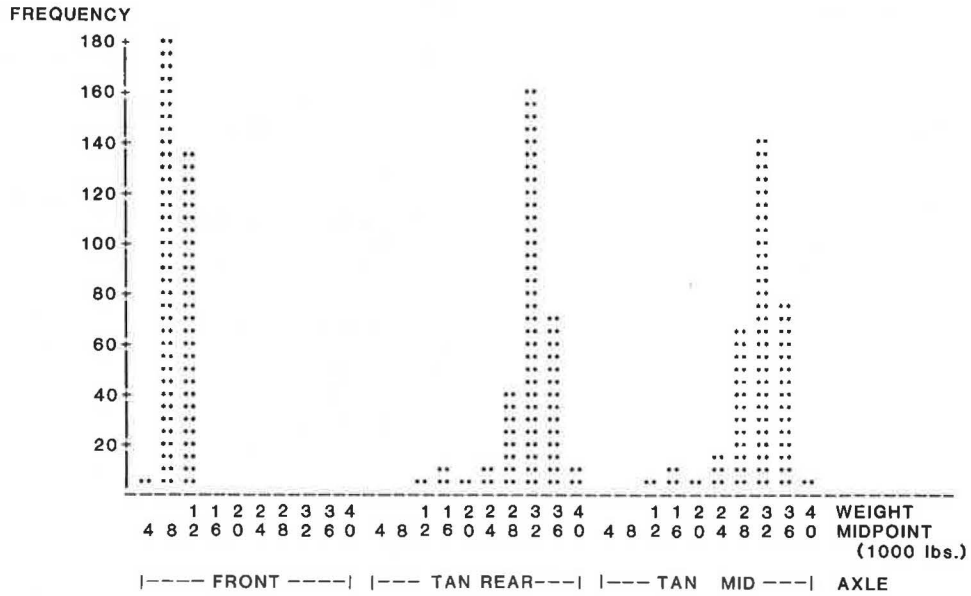

FIGURE 5 Histogram of axle weights for 3-S2 trucks.

TABLE 6 Percentage of Data on Axle Weight Missing

AASHTO Class	No. Complete	No. Missing	Percent Missing
3-S2	871	3,028	77.7
2-S2	29	145	83.3
SU-2	47	173	78.6
SU-1	22	129	85.4

TABLE 7 Percentage of Data on Commodity Missing

AASHTO Class	No. Complete	No. Missing	Percent Missing
3-S2	487	546	52.9
2-S2	26	26	50.0
SU-2	40	50	55.6
SU-1	39	47	54.7

TABLE 8 Five-Variable ANOVA Results (unbalanced design)

Variable	F-Value[a]	p-Value	Remark
Tire construction	144.92	0.0000	Significant
AASHTO class	14.92	0.0001	Significant
Tread depth	8.54	0.0035	Significant

[a]Based on Type III SS (see SAS).

indicated an average inflation pressure that was 4 psi higher than that of worn tires. For SU-1 and SU-2 trucks, this difference was about 6 to 7 psi. Table 9 also indicates that only one tire pressure was observed for SU-1 trucks with a radial tire and tread depth of <8/32 in. To reduce the importance of this single observation on the overall result, another ANOVA analysis was conducted without this observation to retest the effect of tire construction, AASHTO class, and tread depth. The result of this analysis is given in Table 10, which indicates that the significance of all three variables remained unaltered.

TABLE 9 Summary of Tire Pressures by Tire Construction, AASHTO Class, and Tread Depth

AASHTO Class	Tread Depth	Tire Pressure		
		No.	Mean	Standard Deviation
3-S2	<8/32 in.			
	Radial	422	95.1	14.9
	Bias	222	81.2	15.2
	≥8/32 in.			
	Radial	1,997	98.5	13.6
	Bias	709	86.1	14.4
2-S2	<8/32 in.			
	Radial	10	90.9	22.0
	Bias	28	78.0	18.5
	≥8/32 in.			
	Radial	51	95.3	13.0
	Bias	61	74.6	17.5
SU-2	<8/32 in.			
	Radial	19	91.6	14.9
	Bias	23	77.4	17.9
	≥8/32 in.			
	Radial	56	97.9	12.5
	Bias	94	83.6	14.2
SU-1	<8/32 in.			
	Radial	1	101.0	–
	Bias	34	65.7	20.0
	≥8/32 in.			
	Radial	35	88.3	18.8
	Bias	75	73.4	15.3

TABLE 10 ANOVA Result on Tire Construction, AASHTO Class, and Tread Depth[a]

Variable	F-Value	p-Value	Remark
Tire construction	91.57	0.0001	Significant
AASHTO class	18.97	0.0001	Significant
Tread depth	7.87	0.0051	Significant

[a]Excluding one observation (see text).

Effect of Axle Weight for 3-S2 Trucks

Because of the small samples of SU-1, SU-2, and 2-S2 trucks with complete axle-weight information, only

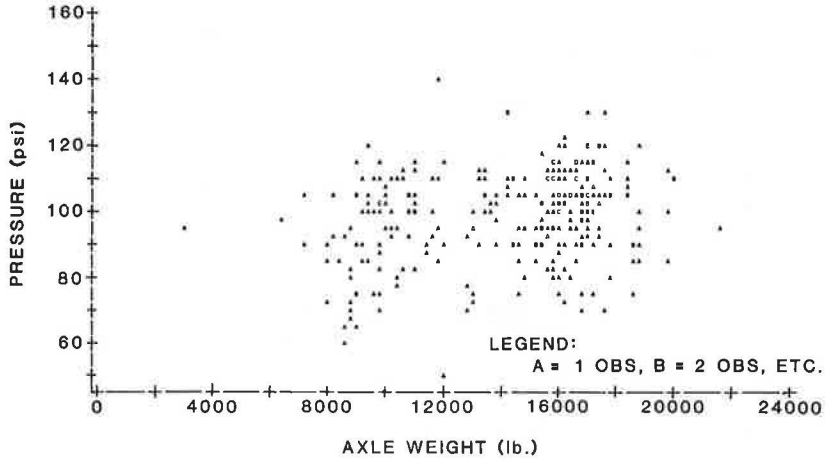

FIGURE 6 Tire pressure versus axle weights for radial tires with >8/32-in. tread depth (3-S2 trucks).

the 3-S2 truck subset was analyzed. A regression analysis was conducted to assess the influence of axle weight on tire pressures. Axle weight was found to be statistically significant in explaining the variability in tire pressures. The following four relationships were obtained from the analysis for all combinations of tire construction and tread depth:

Radial, <8/32 in.: pressure = 83.03
+ 0.0007 (axle weight) (1)

Radial, ≥8/32 in.: pressure = 88.70
+ 0.0007 (axle weight) (2)

Bias, <8/32 in.: pressure = 70.34
+ 0.0007 (axle weight) (3)

Bias, ≥8/32 in.: pressure = 76.01
+ 0.0007 (axle weight) (4)

where pressure is the measured inflation pressure in psi and the axle weight is in pounds.

These equations suggest that to change the inflation pressure 1 psi, axle weight must increase by about 1,400 lb. This magnitude of pressure-weight elasticity may be considered by many to be practically nonsignificant. Figure 6 shows a typical scatterplot of tire pressures versus axle weights. The scatterplots for radial and bias tire constructions appear to be almost the same after taking into account the differences in mean tire pressure. Therefore, only one plot for radials is included.

Effect of Commodity for 3-S2 Trucks

An ANOVA was conducted to test the effect of commodity and tire construction for 3-S2 trucks only. The result is given in Table 11, which indicates that the averages of tire pressure were affected by the principal effects of tire construction and commodity types; the interaction effect between tire construction and commodity was not statistically significant at an alpha level of 0.02. The tire pressure distributions by major commodity types for 3-S2 trucks are given in Table 5. For the ANOVA, commodity types were rearranged into 10 categories: produce; feed; cattle; logs; stone, sand, and gravel; food and beverages; solid bulk; liquid and gas bulk; heavy cargo; and all others.

TABLE 11 Result of ANOVA on Commodity and Tire Construction for 3-S3 Trucks

Source	Type III Sum Squared[a]	Degree of Freedom	p-Value
Tire construction	9,241.95	1	0.0001
Commodity	7,616.03	9	0.0001
Tire construction x commodity	3,885.52	9	0.0229[b]

[a]See SAS (1982 Edition).
[b]Not significant at an alpha level of 0.02.

RELEVANCE OF TIRE PRESSURE IN PAVEMENT CONSIDERATIONS

One of the primary reasons for conducting this field study was to determine the level of the truck tire pressures on Texas highways and to relate those tire pressures to distress produced by axle loads. To accomplish that objective, it was necessary to determine if significant differences existed in tire pressures for tires of different construction, axle load, truck type, and commodity. The most important of these factors are discussed in the following sections.

Tire Construction

Because tire construction significantly affects the pressure transmitted to the roadway surface, it was imperative that an assessment be made of the variation in tire pressure by tire construction. The average tire pressure by vehicle type and tire construction is given in Table 9 and shown in Figure 4. The ANOVA and multiple regression analysis performed indicated that tire pressures for radial tires were considerably higher than those for bias tires. After accounting for truck type and tread depth, radial tires showed a pressure that was on the average 12 to 21 psi higher than that of bias tires.

From a practical standpoint, an evaluation of the effect of the mean tire pressure differences between radial and bias construction must come from analyses similar to those reported by Roberts and Rosson (2). Figure 7 shows the effect of increased tire pressure on the strain in a pavement structure that consists of an 8-in. granular base, the modulus of which is characterized by three different stress-sensitive formulations, over an asphalt concrete surface that has a modulus of 400 ksi and thicknesses of 1, 1.5,

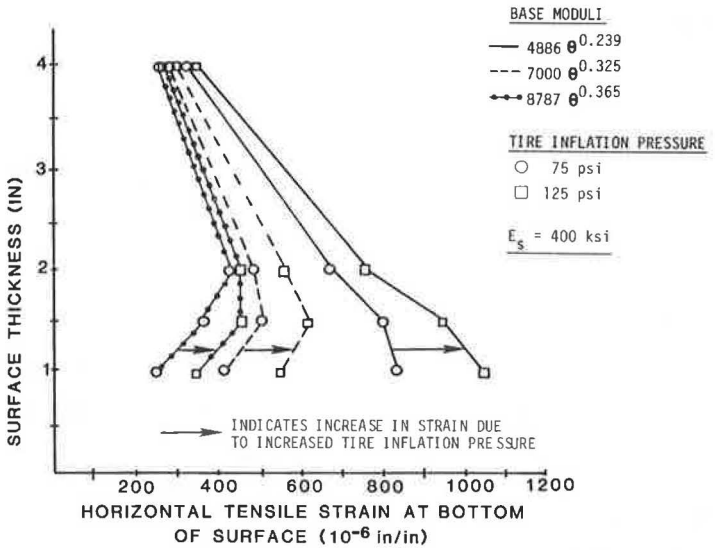

FIGURE 7 Effects of increased tire pressure on tensile strain for a surface modulus of 400 ksi.

2, and 4 in. The effect of increased inflation pressure is shown in Figure 7 by the arrows. The increases in strain are highest as the surface thickness decreases. It must be remembered that although the percent increase in strain may not be high for the 2-in. surface, strain in a fatigue equation is inverted and raised to an exponent of about 5. Therefore, even fairly small increases in strain can produce significant reductions in fatigue life.

Axle Load

The data on tire pressure variation versus axle load almost certainly have some bias because of the nature of the data collection efforts. Although all trucks were stopped after data collection efforts began, at some sites only those vehicles detained for weight or other violations were included in the tire pressure survey. However, it is instructive to review those data for trends. Analysis of the survey data indicated that axle weight was statistically significant in explaining the difference in tire pressure for at least 3-S2 vehicles. It is difficult to dispute that tire pressure is affected by axle load and ambient temperature. However, because tire carcass design affects heat buildup, and therefore tire pressure, it is difficult in an uncontrolled field experiment to confirm all the relationships that should occur.

Figure 6 is a scatterplot between axle load and tire pressure for the 3-S2 class. These figures attest to the wide variation in tire pressure and also to a large, although expected, difference between load on the steering axle and the other axles of the vehicle.

Commodity

Table 5 gives a summary of the variation in tire pressures by commodity for the 3-S2 vehicle. It is interesting to note that only four commodities showed mean tire pressures higher than 100 psi: farm produce, grain, cattle, and lumber. For most commodities, mean tire pressures were approximately 95 psi. Because of the small sample size for other vehicle types, tire pressure distributions by commodity would not be reliable.

SUMMARY

Tire pressure data collected on Texas highways indicate that the mean tire pressures are considerably higher than the values historically used in the design of pavement structures and higher than those of the AASHO Road Test from which load equivalence factors were developed. ANOVA on the collected data indicates that observed tire pressures are significantly affected by tire construction, truck type, tread depth, commodity, and axle weight. However, relatively small sample sizes for trucks other than the 3-S2 in this sample do not allow definitive statements to be made for the other vehicle types.

ACKNOWLEDGMENT

This phase of the project was sponsored by the Texas State Department of Highways and Public Transportation and the FHWA, U.S. Department of Transportation.

REFERENCES

1. K.M. Marshek, W.R. Hudson, R.B. Connell, H.H. Chen, and C.L. Saraf. Experimental Investigation of Truck Tire Inflation Pressure on Pavement--Tire Contact Area and Pressure Distribution. Research Report 386-1. Center for Transportation Research, University of Texas, Austin, Aug. 1985.
2. F.L. Roberts and B.T. Rosson. Establishing Material Properties for Thin Asphalt Concrete Surfaces on Granular Bases. Research Report FHWA-TX-85-345-1. Texas Transportation Institute, Texas A&M University, College Station, Jan. 1985.

Publication of this paper sponsored by Committee on Pavement Management Systems.

Experimental Determination of Pressure Distribution of Truck Tire-Pavement Contact

KURT M. MARSHEK, HSIEN H. CHEN, RICHARD B. CONNELL, and W. RONALD HUDSON

ABSTRACT

The results are presented of an experimental determination of pressure distributions beneath statically loaded truck tires using a pressure-sensitive film. A load frame fitted with a hydraulic ram was used to statically load a bald and treated 10-20 bias ply truck tire. The use of pressure-sensitive film allowed the net contact area--as well as the entire pressure distribution--to be captured, and the data to be stored by using an automated print reading system. The results indicate that the treaded tire produced the highest pressures in the tire shoulder region for the cases studied, except for the overinflated case. High inflation pressures caused the peak pressures to move from the tire shoulder toward the tire centerline. The results also indicate that heavy axle loads produced regions of high pressure in the tire shoulder region. Experiments conducted on bald tires show similar trends; however, the overall pressure distribution is more continuous because of the lack of treads.

One of the major costs incurred by highway departments in the United States is maintaining public roads in a serviceable condition. A variety of factors are known to contribute to pavement damage, including climate, traffic density, and the loads from automobile and truck tires. Historically, the subject of contact pressure distribution between a tire and pavement has received little attention for several reasons, including the following: (a) simplifying assumptions made in past road design work have made knowledge of the actual pressure distribution unnecessary, and (b) measurements of the contact pressure at all locations (points) in the tire footprint are difficult to make. The actual contact pressure distribution between the tire and the pavement will undoubtedly play a larger role in highway pavement design.

The common assumption is made that the contact pressure is uniform and equal in magnitude to the tire inflation pressure, and that it acts on an area that is circular in shape (1). The theoretical relationships used by highway engineers in design work are simplified considerably by this assumption. However, previous investigations have demonstrated that the actual pressure distribution deviates considerably from the uniform pressure model (2,3).

To determine the shape and size of the contact pressure area, Flugrad and Miller modeled the tire as a modified standing torus in their finite element analysis and predicted an elliptical contact pressure area (4). Another study, by Mack et al., also modeled the tire as a standing torus, and predicted an elliptical contact area as did Flugrad and Miller (5).

O'Neil determined experimentally the net contact pressure area of a statically loaded tire by coating the tire with oil, loading the tire on paper, and allowing graphite particles to stick to the oily parts of the paper (3). Tracing of the image obtained then gave the desired net contact area.

For statically loaded tires, O'Neil used a nylon pin and proving ring assembly to determine the normal and tangential pressure distributions exerted by the tire (3). A study by Marshek et al. in progress at the University of Texas at Austin uses a digitizing camera and data acquisition system to determine the contact pressure distribution and the net contact area from pressure-sensitive film prints of statically loaded truck tires. The camera digitizes the print and then, using this data base (a) displays the pressure distribution, and (b) calculates the net contact area by summing the picture elements on the television monitor (pixels) on the digitized image, the color intensity of which defines them as a contact area. Clark demonstrated that the pressure distribution for a statically loaded tire is a good approximation for the pressure distribution of a freely rolling tire (6).

Lippmann and Oblizajek used specially designed microtransducers mounted in a ground steel bed to record three components (normal, radial, and tangential) of the pressure distribution under freely rolling tires (7). Shimada et al. conducted a study using piezoelectric sensors mounted in a rotating drum to measure various contact pressure forces at high speeds (2).

The objective of this study is to determine the contact pressures that exist beneath statically loaded truck tires using pressure-sensitive film. The data obtained will indicate what effect the tread pattern, tire inflation pressure, and axle load have on the resulting tire-pavement contact pressure distribution.

EXPERIMENTAL APPARATUS

The experimental apparatus used in this study consisted of the following components: a load frame for statically loading tires, pressure-sensitive film for capturing the pressure distribution, an optical device (densitometer) for converting color intensity

K.M. Marshek, H.H. Chen, and R.B. Connell, Mechanical Engineering Department, University of Texas at Austin, Austin, Tex. 78712. W.R. Hudson, Center for Transportation Research, University of Texas at Austin, Austin, Tex. 78712.

to pressure, a bidirectional (X-Y) table for precise movement of the print beneath the densitometer, and an HP 3054A data acquisition system.

Tires

The first tire studied was a smooth 10-20 bias ply truck tire used for skid testing. The data from this tire will represent one extreme in the range of tread patterns found in use (as with a tire worn bald) and will thus allow broader conclusions to be drawn about tread patterns and the resulting pressure distributions. The second truck tire studied was a used 10-20 bias ply tire with 3/8 in. of tread depth remaining. This tire is representative of the type of tire and tire condition commonly found on highways today.

Load Frame

The truck tires studied were statically loaded with the load frame shown in Figure 1. This frame was designed so that a hydraulic ram mounted above the tire assembly could deliver a load to the tire through a shaft running through the tire hub. This design allowed the tire to be loaded to better simulate actual use, in contrast to loading the tire, for example, by placing weights on the top of the tire.

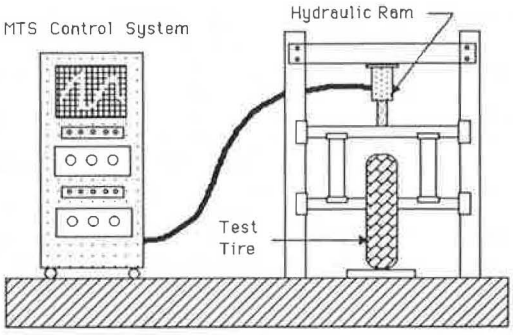

FIGURE 1 Tire load frame.

Pressure-Sensitive Film

A pressure-sensitive film was used, which is capable of capturing the static pressure distribution between contacting bodies. This film consists of an A-sheet and a C-sheet, as shown in Figure 2, the A-sheet containing capsules of developer and the C-sheet providing a developing layer on which the developer acts. The capsules are made in a variety of sizes so that they break when exposed to a certain pressure level. Statistical distribution of the different capsule sizes allows a range of pressures to be captured.

When the two sheets are in their proper orientation and subjected to a pressure, a number of the capsules break and release the developer onto the developing layer; the developer from the A-sheet produces a red spot on the C-sheet, with the intensity of color obtained being proportional to the applied pressure.

Densitometer

The prints developed are read with an optical device called a densitometer (shown in Figure 3). The densitometer consists of the reading head and a chassis that contains a voltmeter and calibration controls.

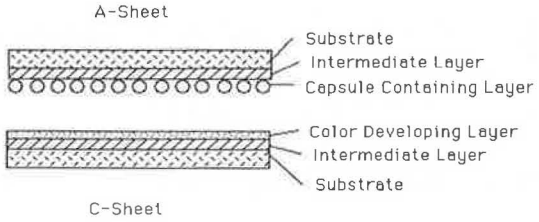

FIGURE 2 Pressure-sensitive film.

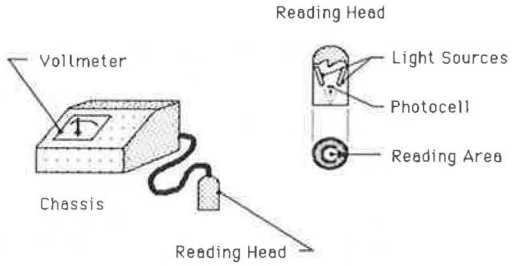

FIGURE 3 Densitometer and schematic diagram of densitometer reading head.

The reading head consists of two symmetrically placed light sources and a photocell. The light sources project beams of light, which pass through a circular opening (0.118 in. in diameter) in the base of the head, striking the print directly below the head, and then reflecting back to the photocell an amount of light proportional to the intensity of color on the print. The photocell outputs a voltage that is proportional to the pressure that was applied to the film; the response of the photocell is that of a first-order system with a time constant of 0.8 sec. The output of the densitometer photocell was connected to a precision voltmeter located in a data acquisition system.

The print developed can be read with the densitometer to determine the pressure at any point or region desired. One important advantage gained by using the densitometer is that a grid reading resolution can be specified, that is, the user can divide the resulting contact area into a grid size with step sizes as small or large as required. This characteristic is important because large pressure gradients occurring in extremely small distances are commonplace, particularly when dealing with bodies such as treaded tires the contact surfaces of which contain numerous discontinuities.

X-Y Table

The small measuring area (0.044 in.^{2}) of the densitometer compared with the large contact area of the truck tire footprint made it necessary to devise a means for automating the print reading process. This was accomplished in part through the use of a bidirectional (X-Y) table that featured high-speed, precision stepper motors driven by an on-board digital control unit. An RS232 interface in the control unit permitted direct control of the X-Y table and data taking by the HP 3054A data acquisition system described in the next section. Errors resulting from miscommunication between the densitometer and the X-Y table controller were avoided because of the exclusive control of the HP3054A over the data-taking process; the print reading time also was kept to a minimum.

Data Acquisition System

An HP 3054A data acquisition system was used extensively throughout all phases of this study. It consisted of the following components: an HP 9816S computer, a dual disc drive, a data acquisition unit, a dot matrix printer, and a multiple pen plotter.

Because of the small measuring area of the densitometer, approximately 6,000 points were measured for each truck tire print in order to map the entire pressure distribution in the contact area. Figure 4 shows the schematic diagram of the print reading system.

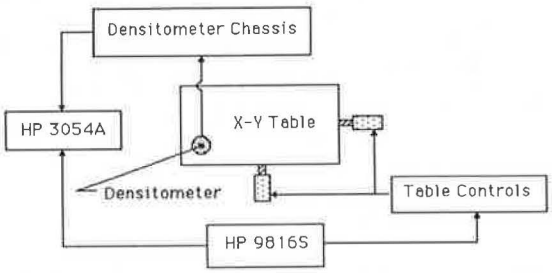

FIGURE 4 Print reading system.

EXPERIMENTAL PROCEDURE

The load application was divided into three parts. The first part was a load ramp in which the load on the tire was increased linearly from zero to full load over a 2-min time period. Part two of the loading consisted of maintaining the full tire load on the paper for 2 min. After this, the tire load was quickly released, the A-sheet was separated from the C-sheet, and the C-sheet was set aside to finish developing. All prints obtained during a testing session were read within 1 hr after the session ended because it was believed that the color intensity on the film might fade with time.

To obtain a pressure print, the A-sheet and C-sheet were taped firmly in their proper orientation to the flat steel plate to prevent erroneous pressure values from being recorded due to the presence of shear forces between the sheets. Also, a piece of shimstock (with a thickness of 0.001 in.) was placed between the tire and the top piece of pressure paper so that expansion of the tire on application of the load was restrained by the shimstock; therefore, only the normal tire load was transmitted to the paper (see Figure 5).

To keep the calibration and experimental procedures as similar as possible, a scheme was devised whereby a known load could be applied to a rubber cube with 1-in. sides (and a Young's modulus roughly equal to the moduli of the truck tires tested) by

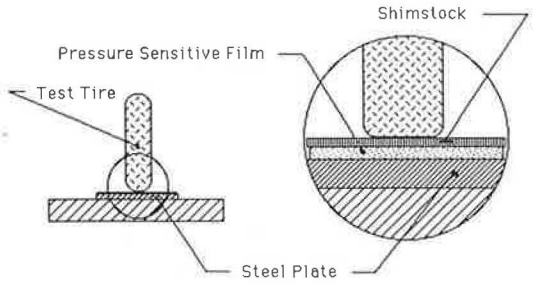

FIGURE 5 Shimstock and pressure-sensitive film configuration.

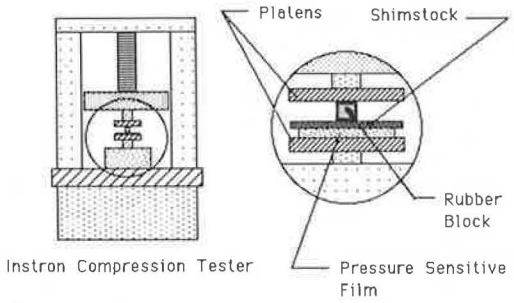

FIGURE 6 Calibration test equipment.

using an Instron compression tester, as shown in Figure 6. Examples of calibration prints obtained with the rubber block and a complete description of the calibration procedure are given by Connell (8).

The data points used to construct the calibration curve were obtained by using the same loading procedure as was used for the tire. The same steel plate and pressure-sensitive film configuration was used, the only difference being that the face of the rubber block touching the shimstock was lubricated to achieve a more uniform pressure distribution. The uniform distribution of known pressure intensity was desired for the calibration prints because the average voltage measured by the densitometer in each of these prints was used as a data point on the calibration curve.

Data points were obtained for each pressure level by averaging voltages in the calibration prints. A second-order polynomial was fitted through the data points to obtain the calibration curve used to convert the voltage arrays to pressures. Because of the sensitivity of the film to its environment, careful attention was paid to ensure that the atmospheric conditions (temperature and relative humidity) were sufficiently close for both calibration and experimental test sessions.

Experiments were conducted with truck tires to demonstrate the effect of tread pattern, tire inflation pressure, and axle load on the resulting contact pressure distribution. Because the pressure-sensitive film is expensive, and because it required about 6 hr to read a developed print, a minimum number of tests were conducted that would still satisfy the goals of this study.

Experiments were conducted by using three different tire inflation pressures (75, 90, and 110 psi) to demonstrate the effect the inflation pressure had on the distribution of pressure in the tire footprint. Two different axle loads were used with this study; the first was a 4,500-lbf load and the second was a 5,400-lbf load (a 20 percent overload).

EXPERIMENTAL RESULTS

The data read by the densitometer from the six pressure prints were stored on disc in the form of arrays of voltages. From the voltage data base, various parameters could be determined, including the net contact area of the tire footprint and the pressure distribution throughout. In addition, the data base could be reduced or converted into equivalent forms (such as equivalent but smaller arrays of pressures and forces); this made it possible to use the data (a) as a means of drawing pressure distributions, (b) to substantiate conclusions about the distribution, and (c) as input to computer programs analyzing pavement performance.

The first form of output used consists of numerical prints that show the pressure that acts on each

grid area in the contact patch; Figure 7 shows a sample numerical pressure print for treaded tire at 90 psi inflation pressure and an axle load of 4,500 lbf. The numerical prints were made by printing the arrays of pressures values in matrix form. General trends in the pressure distribution are difficult to determine from the numerical prints because of the overwhelming amount of data presented for each test conducted. The prints do, however, give a location and the individual pressures that exist in the contact patch.

Operations were performed on the data to reduce the data from an array of 6,000 points (either pressure or force) per print to a number of points appropriate to the application. In general, the operations on the data were performed to accomplish one of two goals: the first goal was to reduce the data to a form suitable for plotting, and the second was to convert the data to an equivalent form compatible with the input requirements of pavement analysis programs.

A three-dimensional plot was chosen over a two-dimensional plot despite the usual assumption that the pressure distribution varies little along the length (in the direction of travel) of the tire. The three-dimensional plots were rotated so that the view chosen best illustrates the pressure profiles along both axes of the footprint (see Figure 8).

The grid dimensions used to make the three-dimensional plots were made nonuniform to preserve regions of high pressure that were isolated because of the presence of the tire shoulder or a tread gap. A moving average scheme was then used to reduce the data to obtain a single pressure or force acting on each unit area. The plots shown in Figure 8 optimize the viewing variables so that the two axes and the presence of high pressures at the tire shoulder and along tread gaps can clearly be observed.

A computer graphics program was used to convert each data base of numerical pressure values into discrete points of color on a graphics terminal; controls in the graphics program associated a particular pressure level with a specific color (e.g., yellow points might indicate pressures between 120 and 140 psi). After the entire data base for each print had been read into the graphics program, plots on the color graphics terminal were photographed with a 35-mm camera. Prints made from the slides give a striking summary of the experimental results, showing both the localized pressures and the general trends in pressure found in the contact patch beneath statically loaded truck tires. Prints of the 35-mm slides are given by Connell (8).

DISCUSSION OF RESULTS

The tread type, that is, the particular pattern of treads, plays a dominant role in the determination of the shape of the pressure distribution. The bald tire represents one end of the tread spectrum, the treaded tire the other. The plots shown in Figure 8 illustrate that a bald tire produces a uniform pressure distribution with significant gradients only at the tire center and shoulder.

FIGURE 7 Sample numerical pressure print.

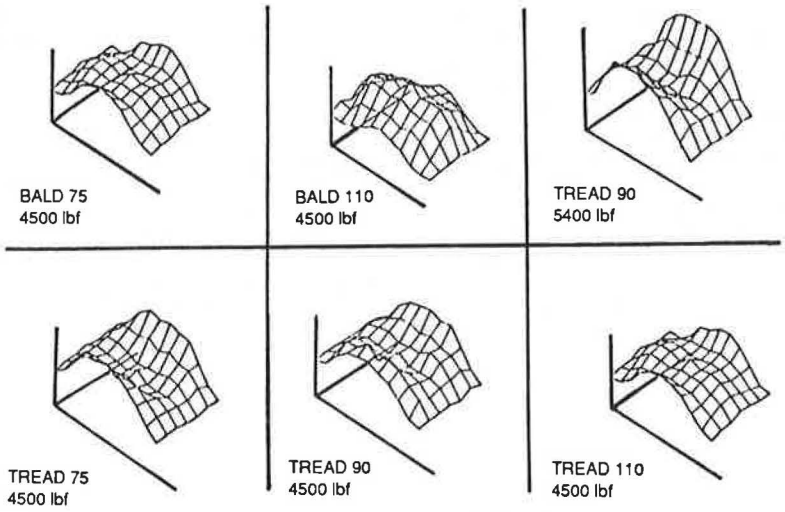

FIGURE 8 Three-dimensional plots of pressure distributions.

With a treaded tire, the pressure distributions have large discontinuities at the tread gaps, within which the pressure is zero. The gaps separate regions of significantly different nonzero pressure levels. This can clearly be observed on the copies of the pressure prints, particularly for the overloaded case (treaded tire at 90 psi and 5,400 lbf), where the circumferential tread gap separates high pressures on the shoulder from medium pressures directly on the other side. This region between the shoulder of the tire and the circumferential gap usually carries the highest pressures.

For a given load, inflation pressure determines the regions of high pressure. Increasing the inflation pressure reduces the crown curvature, thus shifting the high-pressure regions at the tire shoulder to the center of the contact patch.

One other effect of inflation pressure was observed with the treaded tire that supports the use (by highway engineers) of the inflation pressure as the magnitude of the uniform pressure delivered by a tire. The region in the center of the tire, bounded by a circumferential gap on either side, consistently maintained pressures close to the inflation pressure (plus or minus 15 psi) for all of the tests conducted. The high pressures occurred near a tread gap or in the shoulder region where the stress concentration drove the pressures above the range stated.

The axle load is the final parameter the effect of which on the contact pressure distribution was studied. A comparison of the numerical and three-dimensional plots obtained for the treaded tire at rated inflation pressure but for two different axle loads immediately makes clear the following: the pressures in the center region of the tire remain relatively unchanged whereas pressures in the shoulder region increase dramatically.

SUMMARY

The results of this study can be summarized as follows:

1. The tread pattern on a tire was found to have a significant effect on the size of the contact area and the shape of the pressure profiles. Smaller contact areas for treaded tires were observed because the presence of the tread gaps reduced the number of contact points in the tire footprint. The tread gaps were also demonstrated to separate adjacent regions of vastly different pressure levels. High pressures were consistently found at tread-gap interfaces and at the tire shoulder. As the tread wears, three results can be expected: an increase in the net contact area, a reduction of the peak pressures, and a more continuous distribution.

2. The tire inflation pressure, in general, determined the location of regions of high pressure in the contact patch. Low inflation pressures resulted in large contact regions and high pressures near the tire shoulder region. High inflation pressures produced a significant reduction in contact area and a shifting of high pressures toward the center region of the contact patch.

3. The axle load also affected the contact area and pressure distribution. The 4,500-lbf axle load saturates the center region of the tire footprint with contact pressures approximately equal to the tire inflation pressure. The 5,400-lbf axle load caused deformations in the tire sidewalls and an increase in the load carried by the tire shoulder region.

ACKNOWLEDGMENTS

The authors are pleased to acknowledge the combined efforts and support of the Center for Transportation Research and the Mechanical Engineering Department at the University of Texas at Austin and the Texas State Department of Highways and Public Transportation, in cooperation with the FHWA, U.S. Department of Transportation.

REFERENCES

1. K.B. Woods (ed.). Highway Engineering Handbook. McGraw-Hill, New York, 1960.
2. T. Shimada, T.S. Furuya, and K. Ikehara. A Study of Contact Forces of a Radial Tire at High Speed. Bridgestone Tire Company, Inc., Akron, Ohio, 1984.
3. E.W. O'Neil, Jr. Measurement of Pneumatic Tire Contact Pressure for Static Loading. M.S. thesis. North Carolina State University, Raleigh, 1969.
4. D.R. Flugrad and B.A. Miller. Experimental and Finite Element Study of a Standing Torus Under Normal and Tangential Loads. Iowa State University, Ames, 1981.

5. M.J. Mack, Jr., D.E. Hill, and J.R. Baumgarten. Analytical and Experimental Study of a Standing Torus with Normal Loads. Tire Modeling, NASA Conference Publication 2264. National Aeronautics and Space Administration, Washington, D.C., 1982.
6. S.K. Clark. Mechanics of Pneumatic Tires. Report NBS-Mono-122. Michigan University, Ann Arbor, Nov. 1971,853 pp.
7. S.A. Lippmann and K.L. Oblizajek. The Distribution of Stress Between the Tread and Road for Freely Rolling Tires. Transaction 740072. Society of Automotive Engineers, Warrendale, Pa., 1974.
8. R.B. Connell. Experimental Determination of Truck Tire Contact Pressures and Their Effect on Flexible and Rigid Pavement Performance. M.S. thesis. University of Texas at Austin, Austin, 1985.

Publication of this paper sponsored by Committee on Strength and Deformation Characteristics of Pavement Sections.

Effect of Truck Tire Inflation Pressure and Axle Load on Flexible and Rigid Pavement Performance

KURT M. MARSHEK, HSIEN H. CHEN, RICHARD B. CONNELL, and CHHOTE L. SARAF

ABSTRACT

Results are presented of an investigation into the effect of truck tire inflation pressure and axle load on flexible and rigid pavement performance as determined by using computer analysis programs. The flexible and rigid pavement analyses were conducted with both an experimental nonuniform contact pressure distribution and a uniform circular contact pressure distribution as input to the computer programs. The results indicated for the flexible pavement analysis that high inflation pressures and heavy axle loads cause higher tensile strains at the bottom of the surface course, but that only heavy axle loads and not increased inflation pressures are responsible for higher compressive strains at the top of the subgrade course. The rigid pavement analysis indicated an insignificant difference between results obtained by using an experimental and a uniform contact pressure distribution model.

A variety of factors are known to contribute to pavement damage, including climate, traffic density, and the loads from automobile and truck tires. Historically, the subject of the effect of truck tire inflation pressure has received little attention for several reasons, including the following: (a) simplifying assumptions made in past road design procedures have made knowledge of the actual pressure distribution unnecessary, and (b) it is difficult to make measurements of the contact pressure over the entire contact area. The influence of tire inflation pressure as well as the contact pressure distribution between the tire and the pavement will both undoubtedly play a larger role in highway design after their role in causing pavement damage is better understood.

The contact pressure distributions for truck tires loaded at various axle loads and tire inflation pressures were obtained experimentally by using a pressure-sensitive film technique (1). These experimental data were used to determine the effects that the magnitude and shape of the truck tire contact pressure distribution have on the stresses, strains, and deformations developed in the pavement. Computer programs, typical of those used by highway engineers in pavement analysis and design work, are used to determine the strains and stresses of interest for both flexible and rigid pavements. The strains and stresses for an experimental contact pressure distribution will be compared with those obtained by using a uniform pressure model.

The objective of this paper was to determine the effect of tire inflation pressure, tire axle load, and tire pressure distribution model on the strains

K.M. Marshek, H.H. Chen, and R.B. Connell, Mechanical Engineering Department, University of Texas at Austin, Austin, Tex. 78712. C.L. Saraf, Center for Transportation Research, University of Texas at Austin, Austin, Tex. 78712.

and stresses in flexible and rigid pavements. A significant portion of this paper will concentrate on flexible pavements because of their anticipated sensitivity to the pressure distribution. Tensile stresses in rigid pavements will also be investigated. The pavement descriptions and computer models used in the analysis of pavement stress (strain) will be described.

FLEXIBLE PAVEMENT MODEL

Figure 1 shows the flexible pavement model with surface, base, and subgrade courses. The surface courses in this study had thicknesses (H_S) between 1 and 4 in. and a Young's modulus (E) of 400 ksi (note that the modulus would depend on the season of the year). The base and subgrade had thicknesses of 8 and 169 in., respectively, and Young's moduli of 20 and 6 ksi, respectively. The course thicknesses and Young's moduli chosen correspond for the most part with those of a road with low traffic volume.

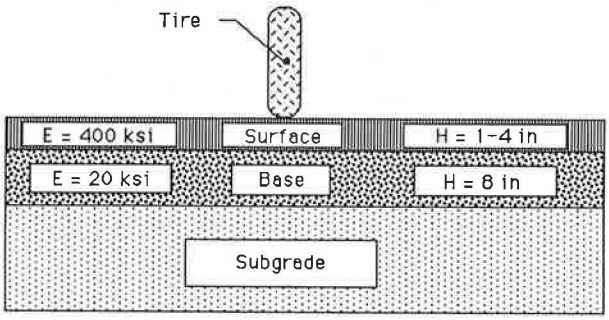

FIGURE 1 Flexible pavement model.

Pressure Distribution Model for BISAR

BISAR uses a common form of data input, that of a circle with a uniform pressure acting on the circular area (see Figure 2) or concentric circles with different pressures acting on each annular area (see Figure 3).

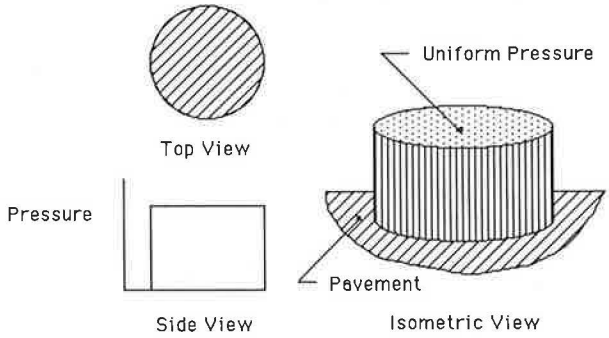

FIGURE 2 Uniform pressure distribution.

The traditional approach has been to assume that the contact area is circular in shape (2). This assumption simplifies the equations used in the analysis. In addition, three assumptions were made about pressure: that it is uniform, that it acts on the circular area, and that it is equal in magnitude to the tire inflation pressure. The simplified theoretical analysis was believed to be of sufficient accuracy for design work. However, premature failure

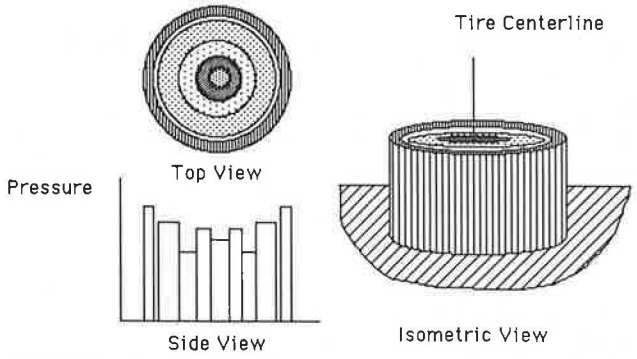

FIGURE 3 Concentric cylinder pressure distribution.

of pavements could be caused by an underestimation of the strains and stresses due to truck tire loading. A more realistic model of the pressure distribution is shown in Figure 3. A half-section view of this pressure distribution, which is used as input to program BISAR, is shown in Figure 4. The computer input data are specified by a pressure distribution and the radial distances associated with each pressure level.

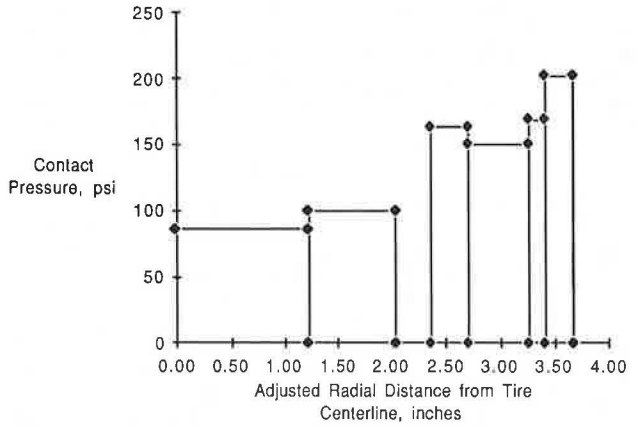

FIGURE 4 Sample input to computer program BISAR.

To match a given tire load, the radial distances are uniformly adjusted so that the sum of the forces (pressure intensity multiplied by the annular area on which it acts) equals the applied load. The form of data input, that of concentric circles, permits the use of pressure distributions containing localized annular regions of high pressure and the resulting large pressure gradients (such as those that occur at a tread gap and a tire shoulder). The pressure distribution input to BISAR for the six cases studied in this paper is given by Marshek et al. (3).

Regions of high contact pressure along the tire contact width were visually identified from numerical prints of the experimental pressure distributions; lines were then drawn along the length of the print to identify these regions. The region of high contact pressure between the tire shoulder and circumferential gap was of special interest for this case because of the magnitude of the pressures that exist in the region. Therefore, this region was divided into four smaller areas to preserve the extremely high pressures (which occurred on a local level throughout this region) that would be lost if an averaging scheme were used over a larger area. Relatively low pressures from the gap to the tire centerline make this region less significant in the

analysis; therefore, larger areas were used in this region. The distance between the tire centerline and the section line is an approximate radial distance.

A representative pressure distribution is obtained by drawing two lines across the tire print, which creates 14 enclosed regions containing different pressure values in each region. Averaging the pressures in each region determines the pressure that acts on the corresponding annular area of the input pressure profile.

The radial distances defining the areas on which the pressures act were adjusted so that the total tire load equaled that used in obtaining the experimental data. This step was necessary because the experimental and input pressure distributions have different forms. For example, the high pressures that act only at the tire shoulder in the experimental distribution completely encircle the print on the computer input model. The radial distances are adjusted in a manner that keeps the relative size of each region proportional to the corresponding region on the actual tire footprint.

Computer Model BISAR

The flexible pavement modeled with the program BISAR (4) consists of three courses (surface, base, and subgrade) with full friction between adjoining layers. The thickness of the course, Young's modulus, and Poisson's ratio for each course are assumed uniform throughout the pavement and are specified as input to BISAR. The frictional condition (no friction or no slip) that exists between adjacent courses is also user-specified (4).

The output variables of BISAR are the stresses, strains, and deflections developed in each course in response to the applied load. Strain is the most useful variable when dealing with flexible pavements because theoretical relationships used in pavement design generally involve the strains developed in each course. The tensile strain at the bottom of the surface course and the compressive strain at the top of the subgrade were studied because they are known to contribute to pavement damage.

Damage to flexible pavements is caused by a number of different mechanisms, with the resulting damage usually being indicative of the mechanism involved. Because the computer models used calculate only responses to load (such as displacements, stresses, and strains), only types of damage that may be related to those responses may be studied. This excluded types of damage such as frost heave, bleeding, pumping, and so on--leaving two major mechanisms to be addressed: fatigue cracking damage and rutting.

When a surface course with a relatively high stiffness is subjected to high pressures or heavy loads, it is able to carry and transmit the load without developing large compressive strains. However, the high stiffness causes large tensile and shear strains to be developed at the bottom of the surface course. The tensile and shear strains cause lateral movement of the material in the surface course away from the region below the tire contact zone and are responsible for longitudinal cracking.

Compressive strains are more of interest when a surface course with low surface stiffness is used. In this case, high compressive strains are found in all the pavement layers in response to a heavy tire load. These strains, particularly those in the subgrade, are responsible for most of the rutting observed. Past studies have indicated that 70 to 95 percent of the compressive strain is found in the subgrade layer; therefore, the vertical compressive strain at the top of the subgrade is of most interest (5). This strain will be the second output variable (the tensile strain at the bottom of the surface course being the first) of interest from the computer program BISAR.

RIGID PAVEMENT MODEL

A rigid pavement is modeled as a two-layer system resting on a Winkler foundation in the computer program JSLAB (6). Material properties and slab dimensions are shown in Figure 5. The slab size is 15 ft long and 12 ft wide. The frictional condition existing between adjacent layers is assumed fully bonded. The maximum horizontal (edge) stress at the bottom of the slab is the desired output variable.

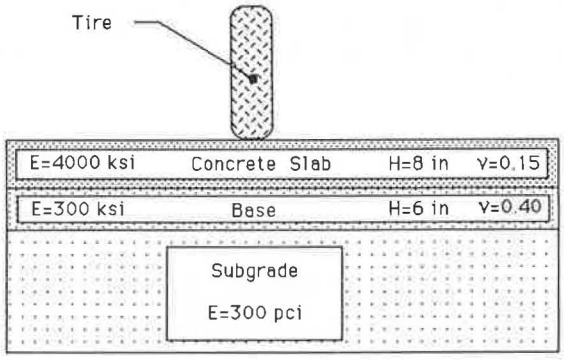

FIGURE 5 Rigid pavement diagram and parameter values used in JSLAB.

RIGID PAVEMENT ANALYSIS PROGRAM (JSLAB)

The computer program JSLAB was used in this study to show what effect different input pressure distribution models had on the tensile stress at the bottom of the slab where the tensile stress is at a maximum. This is the critical stress for a rigid pavement, provided that the material is relatively homogeneous and contains no stress concentrations.

Pressure Distribution Model for JSLAB

The form of input used by JSLAB is an array of pressures acting at specific locations in the tire footprint (see Figures 6 and 7). In addition, the program allows the user to apply the tire load anywhere on the slab. This permits a worst-case analysis to be performed, as when the tire load is applied at the corner of the slab.

76	86	99	112
104	112	124	156
117	114	112	143
126	134	119	151
133	118	125	147
91	99	113	141
79	89	88	96

94	85	99
113	97	103
105	88	119
109	103	105
115	91	108
105	90	107
104	87	100

105	98	87	79
140	114	127	116
129	122	142	125
143	130	140	152
129	115	151	132
133	111	107	103
96	85	97	81

FIGURE 6 Pressure array used in computer program JSLAB.

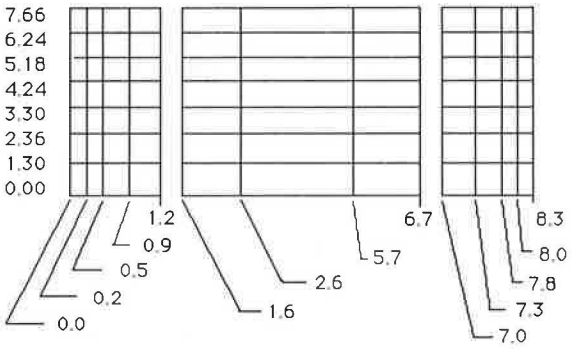

FIGURE 7 Grid spacing used in JSLAB (dimensions in inches).

PRESENTATION AND DISCUSSION OF RESULTS

The computer programs BISAR and JSLAB used in the flexible and rigid pavement analyses, respectively, determined the strains and stresses that occur throughout a pavement structure in response to truck tire loading. Comparisons demonstrate the effects that the tangential braking, tread type, inflation pressure, and axle load have on the stresses and strains developed in the pavement.

Effect of Braking Force on the Tensile Strain at the Bottom of the Surface

Figure 8 shows the tensile strain at the bottom of the surface course for the case of the treaded tire at an inflation pressure of 90 psi and an axle load of 4,500 lbf. The plot shows the pure normal loading

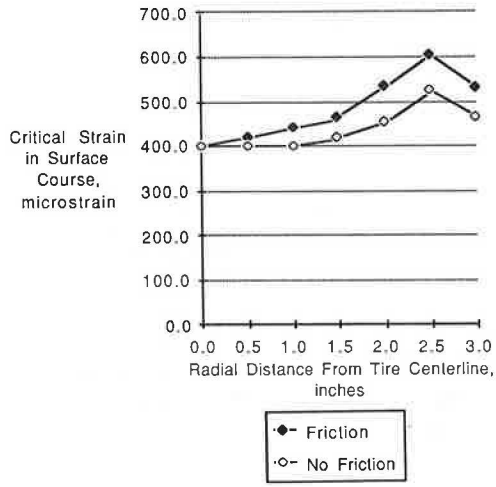

FIGURE 8 Effect of braking force on critical tensile strain at the bottom of a 1-in. thick surface pavement.

case as well as the case in which a tangential load (e.g., developed during braking), equal to 30 percent of the normal load, is superimposed onto the normal load. The strain for both cases is the same under the center of the tire. However, the tangential loading produces higher strains elsewhere, with a maximum difference of about 13 percent being observed at a radial distance of 2.5 in.

Effect of Tread Type (Bald or Treaded Tire) on Tensile Strain at the Bottom of the Surface

Figure 9 shows the effect of the tread type (bald or treaded tire) on critical tensile strains at the bottom of a 1-in. surface pavement at two different inflation pressures (i.e., 75 psi and 110 psi). (Note that tread 7545 indicates the treaded tire at 75 psi inflation pressure and an axle load of 4,500 lbf.) Using a 1-in. surface thickness permitted trends in strain to be more easily observed. A more realistic surface course would be 2 to 4 in. thick when normal-to-heavy wheel loads were anticipated (7). The overinflated treaded tire (inflation pressure of 110 psi) generally produces higher tensile strains than the bald tire, except for the underinflated case (inflation pressure of 75 psi) for the same axle load. When underinflated, the bald tire maintains a higher average pressure under the center of the tire (less shoulder effect), causing the strains to be higher at radial distances of approximately 1.5 in. and less. The treaded tire produces the tensile strain of greatest magnitude because of the regions of high pressure near the tire shoulder.

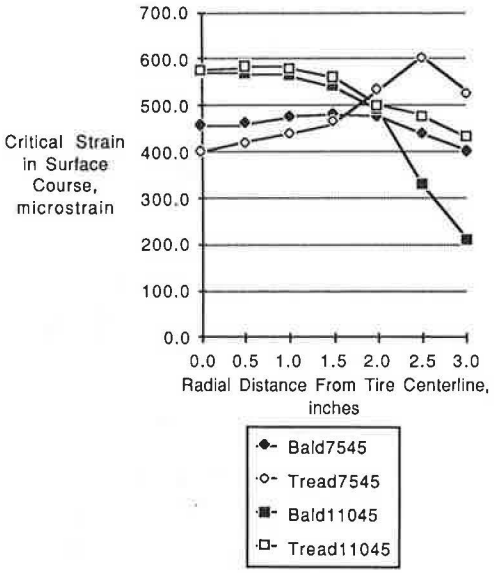

FIGURE 9 Effect of tread type on critical tensile strain at the bottom of a 1-in. thick surface pavement.

The critical tensile strain produced by three different pressure input models (i.e., bald, treaded, and uniform) is plotted against surface course thickness in Figures 10 and 11. For the underinflated case (Figure 10), the treaded tire distribution produces significantly higher strains for thin surface thicknesses than does the bald tire distribution or uniform pressure model. As the surface thickness is increased, agreement between the three models improves; the models predict similar results with surface thicknesses greater than about 2.5 in. The uniform pressure model consistently underestimates the strains for the underinflated case.

Figure 11 shows that for the overinflated case, the uniform pressure model always overestimates the strain produced. As was discussed previously, the treaded tire produces larger strains than the bald tire for all surface thicknesses. In addition, the most significant difference between the strains pro-

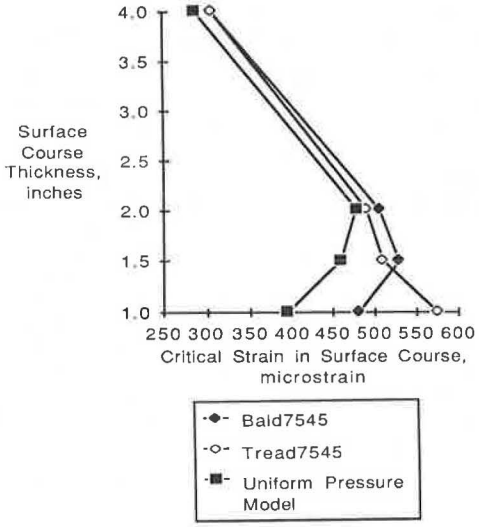

FIGURE 10 Effect of pressure distribution model (75 psi) on critical tensile strain at the bottom of the surface.

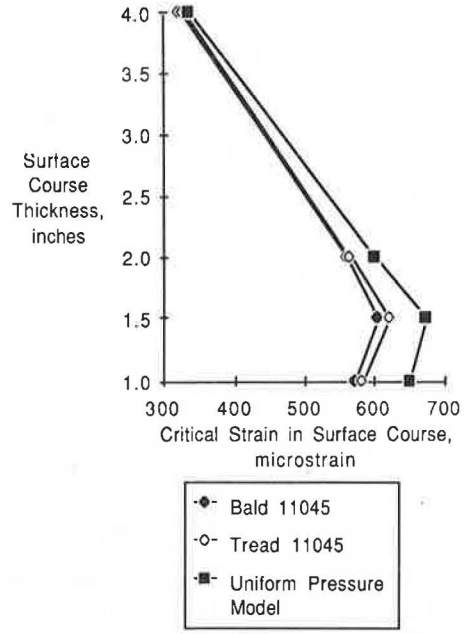

FIGURE 11 Effect of pressure distribution model (110 psi) on critical tensile strain at the bottom of the surface.

duced for the three pressure distribution models occurs for thin surface layers.

Effect of Tire Inflation Pressure and Axle Load on Tensile Strain at the Bottom of the Surface

Figure 12 shows plots of the tensile strain at the bottom of the surface course for the treaded tire at three inflation pressures with a surface course thickness of 1 in. This plot demonstrates how inflation pressure determines the shape of the strain contour as well as the location of the maximum strain. For an underinflated tire, the high shoulder pressures produce the largest strains at a radial distance of about 2.5 in. Increasing the inflation

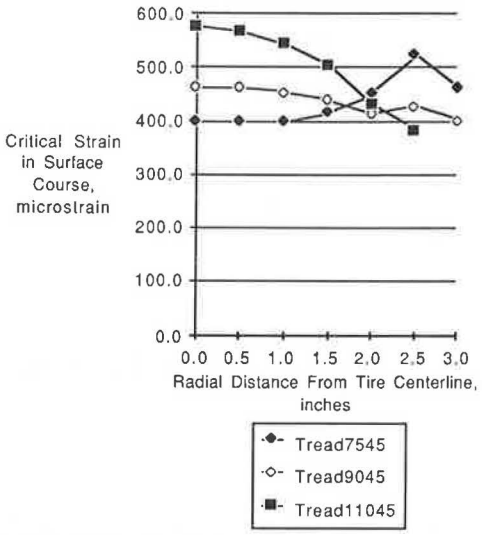

FIGURE 12 Effect of inflation pressure on tensile strain at the bottom of a 1-in. thick surface pavement.

pressure moves the highest strains toward the region beneath the center of the tire in response to the increased contact pressure on the corresponding area of the surface course.

Figure 13 shows the effect of inflation pressure on the critical tensile strains for surface course

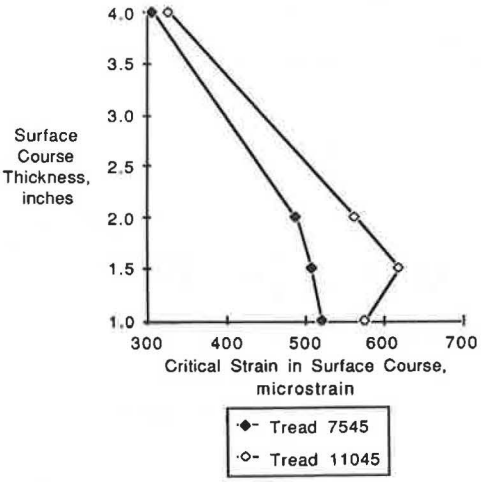

FIGURE 13 Effect of inflation pressure on critical tensile strains at the bottom of the surface.

thicknesses from 1 to 4 in. The overinflated tire consistently produces higher strains than the underinflated tire. For a typical surface course thickness (2 to 4 in.), although the difference between the strains for the underinflated and overinflated cases is small, the pavement life reduction due to high inflation pressure may be significant. In general, the pavement distress is an exponential function of strains in the pavement. To evaluate the additional pavement damage produced by the increase in tire inflation pressure, a strain ratio of two different inflation pressures needs to be calculated and related to the known fatigue and permanent deformation laws.

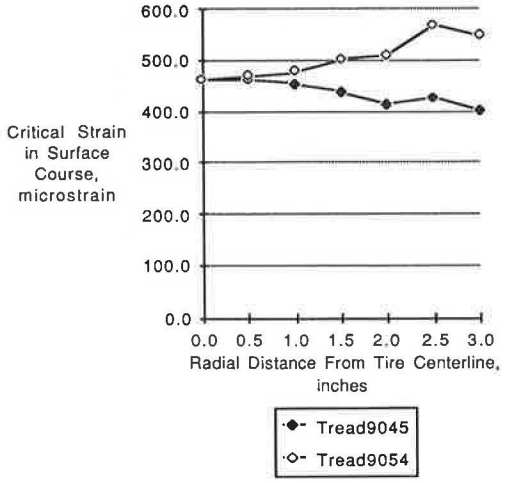

FIGURE 14 Effect of axle load on tensile strain at the bottom of a 1-in. thick surface pavement.

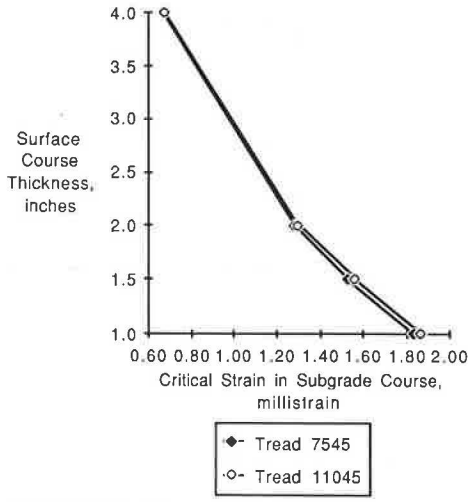

FIGURE 16 Effect of inflation pressure on critical compressive strains at the top of the subgrade.

Effect of Tire Inflation Pressure and Axle Load on Compressive Strain at the Top of the Subgrade

Figure 14 shows the critical tensile strain developed at the bottom of the surface course by applying 4,500-lbf and 5,400-lbf loads to the treaded tire (at inflation pressure rated at 90 psi). The maximum critical strain for the overloaded case occurs roughly 2.5 in. from the tire centerline because the overloaded tire produced a high contact pressure region between the circumferential tread gap and the tire shoulder. Figure 15 shows the maximum critical strain obtained for two axle loads and the usual range of surface course thicknesses. For a 20 percent increase in axle load, the overloaded tire consistently produces the highest strains with a difference of about 20 percent being observed for a typical surface course thickness.

In addition to the tensile strain in the surface course, the vertical compressive strain at the top of the subgrade is also of interest because this strain is known to play a major role in pavement rutting damage. Figure 16 shows that an increase in inflation pressure produces a small increase in the compressive strain developed at the top of the subgrade for the usual range of surface course thicknesses.

From Figure 17 it can be observed that the axle load has a significant effect on the compressive strains developed at the top of the subgrade. The figure indicates that a 20 percent increase in axle load produces approximately a 20 percent increase in the critical subgrade compressive strain for a typical surface course thickness.

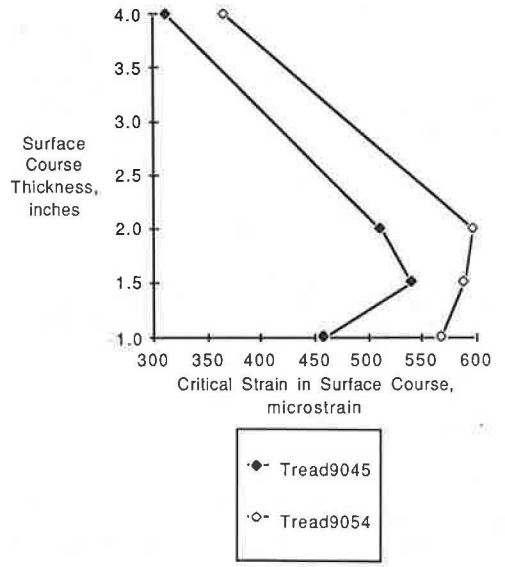

FIGURE 15 Effect of axle load on critical tensile strains at the bottom of the surface.

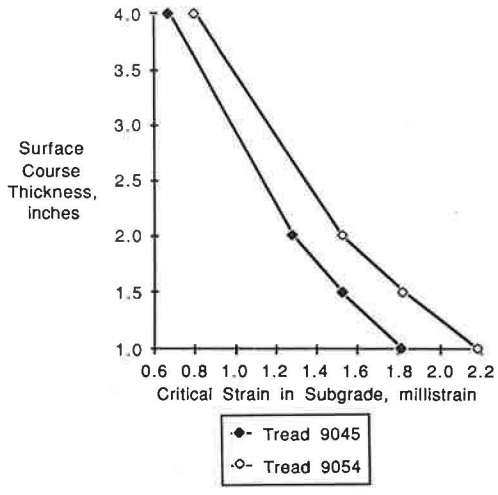

FIGURE 17 Effect of axle load on critical compressive strains at the top of the subgrade.

Rigid Pavements

Figure 18 shows the edge stress at the bottom of the slab versus the distance along the wheel path for the case of the treaded tire at 4,500-lbf load and the uniform pressure model, both at an inflation pressure of 110 psi. The tensile stress for both cases is almost identical. Although not demonstrated in this paper, only the axle load (among the variables considered) affects the magnitudes of the

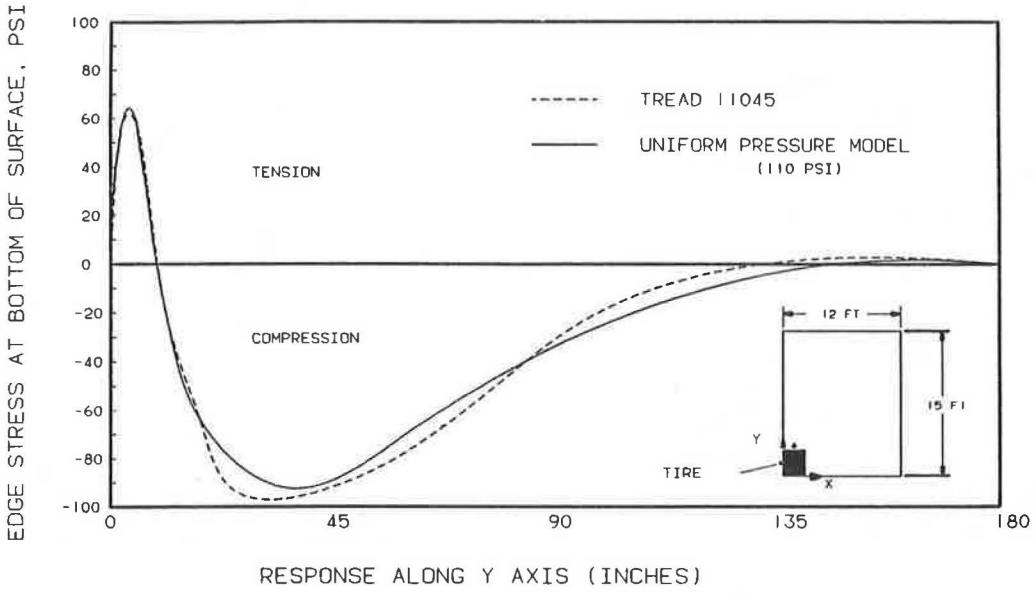

FIGURE 18 Effect of inflation pressure on critical tensile stresses in concrete slab.

stresses developed in a rigid pavement in response to tire loads.

CONCLUSIONS

Based on the limited number of tire contact pressure distributions and pavements discussed in this paper, the following conclusions can be drawn.

For flexible pavements:

- Superimposing a tangential load (braking force) onto the normal load has little effect on the strains produced under the center of the tire. However, for radial distances larger than about 1.0 in., the effect of braking force becomes more significant; the maximum difference in the surface tensile strains occurs at a radial distance of about 2.5 in. Therefore, the effect of braking force should be considered because it affects most stronqly the strains of interest (the maximum tensile strains in the thin and flexible pavement).
- Tread type (bald or treaded tire) has a smaller effect on the critical tensile strains developed at the bottom of the thicker surface course. A treaded tire produced slightly higher strains than did the bald tire, which indicates that as a tire wears a small decrease will occur in the maximum tensile strain produced.
- Tire inflation pressure has a significant effect on the critical tensile strains at the bottom of the surface course. Inflation pressure determines not only the magnitude of the tensile strains produced but also the location of the maximum tensile strain relative to the tire centerline. An underinflated tire produced a maximum strain under the tire shoulder, whereas an overinflated tire produced a maximum strain near the tire centerline. Although little difference exists between the magnitudes of the tensile strains produced for the two cases, particularly when a realistic surface course thickness of 4 in. is used, the pavement life reduction due to high inflation pressure may be significant because the strain ratio not the difference is a significant factor in determining the pavement damage life.
- Inflation pressure will have an insignificant effect on the compressive strains developed at the top of the subgrade. For surface course thicknesses between 2 and 4 in., the effect of inflation pressure is negligible. Therefore, inflation pressure is an insignificant factor with respect to subgrade rutting.
- Axle load was the most significant factor causing high strains in flexible pavements. Regions of high pressure (between the tire shoulder and circumferential gap) produce significant increases in the tensile strain at the bottom of the surface course, with the maximum strains occurring below these high-pressure regions. The increase in tensile strain is a function of the surface course thickness; the effect is most dramatic in pavements with thin surface courses. The axle load increases the tensile and horizontal shear strains in the surface course, making axle load the primary factor (among those studied) in causing fatigue cracking.
- The effect of the axle load on the critical strains in the subgrade is relatively uniform for all surface course thicknesses. Increasing the axle load increases the maximum compressive strain by a proportional amount, regardless of surface course thickness. Therefore, axle load plays a significant role in subgrade rutting damage.

For rigid pavements:

- Close agreement between the tensile stresses obtained when using the experimental and uniform pressure models indicates that pressure distribution has little effect on rigid pavement damage. The uniform pressure model gives almost identical results (when compared with the experimental model) for predicting tensile stresses.

ACKNOWLEDGMENTS

The authors are pleased to acknowledge the combined efforts and support of the Center for Transportation Research and the Mechanical Engineering Department at the University of Texas at Austin and the Texas State Department of Highways and Public Transportation, in cooperation with the FHWA, U.S. Department of Transportation.

REFERENCES

1. K.M. Marshek, W.R. Hudson, R.B. Connell, H.H. Chen, and C.L. Saraf. Experimental Investigation of Truck Tire Inflation Pressure on Pavement--Tire Contact Area and Pressure Distribution. Report 386-1. Center for Transportation Research, University of Texas at Austin, Austin, 1985.
2. S.K. Clark. Mechanics of Pneumatic Tires. Report NBS-Mono-122. Michigan University, Ann Arbor, Nov. 1971, 853 pp.
3. K.M. Marshek, W.R. Hudson, H.H. Chen, C.L. Saraf, and R.B. Connell. Effect of Truck Tire Inflation Pressure and Axle Load on Pavement Performance. Report 386-2F. Center for Transportation Research, University of Texas at Austin, Austin, 1985.
4. BISAR, Computer Program User's Manual. Koninklijke/Shell-Laboratorium, Amsterdam, The Netherlands, 1972.
5. E.J. Yoder and M.W. Witczak. Principles of Pavement Design. John Wiley and Sons, Inc., New York, 1975.
6. S.D. Tayabji and B.E. Colley. Analysis of Jointed Concrete Pavements. Portland Cement Association, Skokie, Ill., 1981.
7. K.B. Woods (ed.). Highway Engineering Handbook. McGraw-Hill, New York, 1960.

Publication of this paper sponsored by Committee on Strength and Deformation Characteristics of Pavement Sections.

Rigid Bottom Considerations for Nondestructive Evaluation of Pavements

WAHEED UDDIN, A. H. MEYER, and W. RONALD HUDSON

ABSTRACT

Mechanistic analysis of dynamic deflection basins for evaluating in situ moduli of pavement-subgrade systems has become an important part of nondestructive pavement evaluation techniques. Discussed is the influence of a rock layer on the evaluation of in situ moduli by using the multilayered linear elastic theory. The value of Young's modulus of elasticity of the subgrade overlying a rock layer can be significantly overestimated if a semi-infinite subgrade is assumed in applying the linear elastic layer theory to analyze deflection basins. An algorithm has been developed to correct this type of error for two cases: (a) when the subgrade thickness is known and (b) when depth to the rock layer is unknown. For the Dynaflect and falling weight deflectometer systems, a rigid bottom can be considered for the second case by assigning a subgrade thickness as a function of the wave length of compression wave in the subgrade. The computer programs FPEDD1 (for flexible pavements) and RPEDD1 (for rigid pavements) incorporate procedures for evaluating in situ moduli with regard to rigid bottom considerations in pavement-subgrade systems.

Nondestructive testing (NDT) is an indispensable part of pavement condition monitoring procedures. Recent surveys (1,2) indicate that dynamic deflection measuring devices are used by a majority of agencies for nondestructive pavement evaluation. Among these, the Dynaflect is the single most popular and widely accepted NDT device, followed by the Road Rater and falling weight deflectometer (FWD). Several agencies are currently evaluating FWDs because of improvements in their operating characteristics and their ability to apply variable and heavy dynamic loads. These devices use seismic sensors to measure surface deflections when the pavement surface is excited by dynamic loads.

The deflection basins formed by the dynamic deflection measurements from an array of seismic sen-

W. Uddin, Austin Research Engineers, Inc., 2600 Dellana Lane, Austin, Tex. 78746. A.H. Meyer and W.R. Hudson, University of Texas at Austin, Austin, Tex. 78712.

sors are used in conjunction with the thickness information and the multilayered linear elastic theory for calculating in situ Young's moduli of the pavement layers. This is accomplished through an iterative procedure of matching the measured deflections with theoretical deflections calculated by using an assumed set of Young's moduli. Uddin et al. presented a review of these iterative procedures (3). Several other papers are related to this topic (4-7). The proposed AASHTO Guide (8) also recommends the use of in situ moduli, calculated from NDT deflection data, for overlay design of pavement structures.

Discussed in this paper are the sources of errors in the moduli calculated from the iterative application of the multilayered linear elastic theory, particularly with regard to rigid bottom considerations.

DEFLECTION BASIN MATCHING APPROACH

Only the Dynaflect and FWD are discussed in this paper. The Dynaflect is a steady-state vibratory device that is instrumented to measure peak-to-peak dynamic deflections on the pavement surface. The Dynaflect applies a harmonic load of a 1,000-lb peak-to-peak amplitude through two steel wheels that are 20 in. apart. Peak-to-peak surface deflections are measured by five geophones secured on a lower-raise bar and spaced at 12 in. such that the first geophone is located midway between the loading wheels. The radial distances of the geophones from each loading wheel are 10.00, 15.62, 26.00, 37.36, and 49.03 in. Geophones are calibrated in the field at a driving frequency of 8 Hz before making deflection measurements.

An FWD applies an impulse load by dropping a known mass from a predetermined height. The Dynatest Model 8000 FWD system, used in this study, can generate a low load of approximately 2,000 lb, as well as a very high peak force of more than 20,000 lb, by using different configurations of mass and height. The load is transmitted to the pavement surface through a loading plate 11.8 in. in diameter. A load cell is used to measure peak dynamic force. Use of a minimum of six and a maximum of seven geophones is assumed in this study. The first sensor is located in a hole at the center of the loading plate for measuring maximum peak deflection. The remaining sensors can be positioned along the lower-raise bar. The geophones are assumed to be 12 in. apart in this study, with radial distances 0.0, 12.0, 24.0, 36.0, 48.0, 60.0, and 72.0 in. from the center of the loading plate. Only peak deflections are recorded by the FWD.

Both the Dynaflect and FWD systems are mounted on lightweight trailers. The static weight of a Dynaflect trailer is approximately 1,800 lb and an FWD trailer weighs approximately 2,000 lb. Restated, deflections measured by these two devices are dynamic displacements of the pavement-subgrade system when the pavement surface is excited by the dynamic forces they generate.

Analyzing Dynamic Deflection Basins

In a layered linear elastic model of a pavement, each layer can be characterized by its Young's modulus of elasticity, E, and Poisson's ratio, μ. Reasonable values of Poisson's ratio can be assumed for typical pavement materials; these generally fall in a narrow range. In the iterative application of the layered theory for calculating in situ moduli of pavement layers, surface deflections are calculated by using known values of layer thicknesses and loading and an assumed set of moduli for a semi-infinite subgrade. Assumptions made in developing the FPEDD1 and RPEDD1 programs are as follows:

1. The principle of superposition is valid for calculating response due to more than one load. The peak-to-peak dynamic force of the Dynaflect is modeled as two pseudostatic loads of 500 lb, each uniformly distributed on circular areas (each 3 in.^{2}).
2. The peak dynamic force of the FWD is assumed to be equal to a pseudostatic load uniformly distributed on a circular area represented by the FWD loading plate.
3. Gravity stresses are neglected.
4. The effects of static trailer weights on the response of the pavement-subgrade system are also ignored. Considering the light static weights of these trailers and the measurement of only dynamic deflections, this is not an unreasonable assumption.
5. Subgrade is characterized by an average modulus value.
6. In considering a rigid bottom, the rock layer underlying the subgrade is assumed to extend infinitely in vertical and horizontal directions.
7. Deflection basins are measured on locations away from pavement edges and discontinuities such as cracks and joints.

In this iterative procedure, the theoretical deflection basin is compared with the measured basin. The discrepancies in the theoretical and measured deflections are related to the required correction in the values of moduli assumed in the first iteration. The moduli are then corrected for the second iteration. When the discrepancies fall within allowable tolerances, the corrected values of moduli are treated as the estimated in situ moduli. Two types of tolerances are primarily provided in the FPEDD1 and RPEDD1 computer programs; these are described in detail elsewhere (3,9).

The tolerances for activating changes in the moduli of various layers are summarized in Table 1. From numerous layered theory computations, it was found that no significant difference existed in theoretical deflection if a correction in the modulus of a given layer did not exceed its tolerance level (9).

TABLE 1 Tolerances for Activating Changes in Moduli (for use in basin-fitting subroutines)

Pavement Type	Program	Tolerances in Moduli (%)		
		TOLR31	TOLR32	TOLR33
Rigid	RPEDD1 (subroutine BASINR)	4.0	3.0	0.05
Flexible	FPEDD1 (subroutine BASINF)	4.0	2.0	0.10

Note: TOLR31 is used for E_1 (Young's modulus of surface layer); TOLR32 is used for intermediate layers; and TOLR33 is used for subgrade modulus.

The second type of tolerance is the maximum permissible discrepancy in measured and calculated deflections. The programs do not attempt any iteration if the maximum discrepancy, based on the first set of moduli, does not exceed 1.5 percent. Further iterations are stopped if the discrepancies increase in a given iteration. A second cycle of iterations is performed if the maximum discrepancy exceeds 10 percent. These tolerances make the basin-fitting procedures efficient.

The evaluation of in situ moduli by using the

deflection basin matching approach poses three major problems:

1. The possibility of nonuniqueness of the estimated in situ Young's moduli (in a multilayered pavement, several combinations of moduli can yield similar deflection basins);
2. Errors in the calculated in situ moduli due to nonlinear behavior of granular layers and subgrade; and
3. Errors due to the assumption of a semi-infinite subgrade when a rock layer exists at a shallow depth of subgrade.

The nonuniqueness of predicted moduli can lead to substantial errors, particularly in the moduli of pavement layers above the subgrade. The methodology incorporated in the FPEDD1 and RPEDD1 computer programs (3,9) ensures unique results. The methodology relies on generating seed moduli primarily as functions of measured deflections, radial distances of sensors from the load(s), and thicknesses of pavement layers. In addition, the seed moduli of upper layers of a pavement are also functions of the subgrade seed modulus. Applications of this methodology have been presented elsewhere (10,11). An example for verifying the methodology is shown in Figure 1; it shows a hypothetical concrete pavement with preassigned values of moduli (called true moduli), the seed moduli generated by the RPEDD1 program, and the final predicted moduli derived by matching deflection basins. The pavement consists of a 10-in. portland cement concrete (PCC) layer, 6-in. stabilized base, and semi-infinite subgrade.

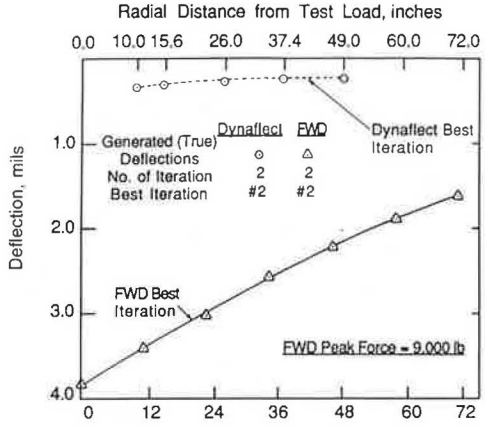

	True Moduli* (psi)	Input Moduli (psi)	Predicted Young's Moduli (psi): Dynaflect Basin	Predicted Young's Moduli (psi): FWD Basin
PC Concrete	4,000,000	0	3,862,000	4,000,000
Stabilized Base	150,000	0	249,300	150,000
Subgrade	25,000	0	23,300	23,920

* Predesignated moduli

FIGURE 1 Prediction of Young's moduli for a hypothetical rigid pavement.

The empirical equations for predicting seed moduli were developed for Dynaflect and FWD from the theoretical deflection data generated by numerous layered theory computations. In the case of FWD, the methodology uses normalized deflections (1,000 x deflection at a given sensor/peak FWD force) to predict seed moduli. The prediction of seed moduli also eliminates user dependency for the assumption of the initial set of moduli in the iterative scheme for matching deflection basins.

Because of the nonlinear behavior of granular layers and cohesive subgrades, it is generally suspected that the moduli of these materials predicted from a light load device (e.g., the Dynaflect) may be significantly different from the moduli associated with heavy wheel loads such as the 18-kip single-axle load. Uddin et al. (3,10,11) applied the equivalent linear analysis for correcting the Dynaflect moduli of these materials. This is based on strain-sensitive models for granular and cohesive soils used in the field of earthquake engineering. A detailed treatment of applying correction to in situ moduli for nonlinear behavior is presented by Uddin (9). This step is omitted in the case of FWD deflection basins. It is recommended that a peak FWD force of 9,000 lb or more be used if the FWD data are collected for the purpose of in situ material characterization.

CONSIDERATION OF RIGID BOTTOM

The semi-infinite thickness of subgrade is an inherent assumption in the use of the elastic layered theory for calculating a deflection basin. The presence or assumption of a rock layer at some finite depth necessitates consideration of a rigid layer instead of a semi-infinite subgrade because it can significantly affect the deflection basin, as shown in Figure 2. Ignorance of this condition may

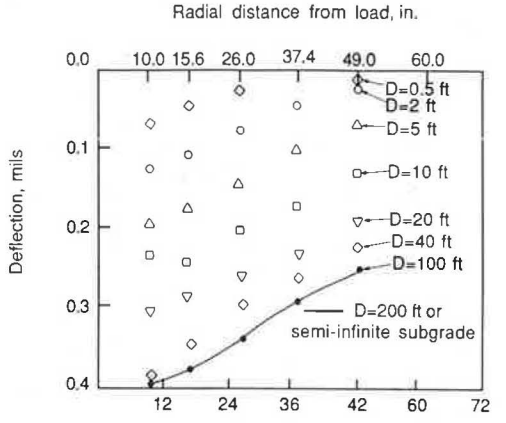

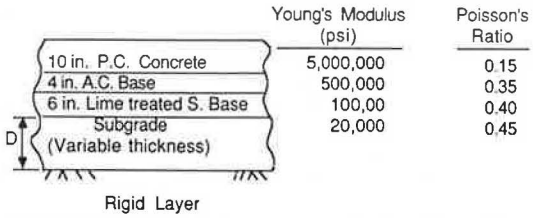

FIGURE 2 Effect of the presence of a rigid layer at varying depths on theoretical Dynaflect deflection basins.

result in significant errors in moduli derived from deflection basins, as demonstrated by McCullough and Taute (12). If the thickness of the subgrade overlying a rock layer is known from design-construction records and other evidence then its value should be entered in the input of the basin-matching programs.

Case of Unknown Thickness of Subgrade

This condition is undoubtedly more common in NDT data. The error involved in overpredicting deflection because of the assumption of a semi-infinite subgrade is obvious. Some researchers, such as Wiseman et al. (6), have considered using an arbitrary depth of subgrade to the rigid layer. Researchers at the U.S. Army Corps of Engineer Waterways Experiment Station (4) assume a rigid bottom at 20 ft for the evaluation of in situ moduli from their deflection basin matching programs. A subgrade thickness of 20 ft has been arbitrarily selected for the dynamic analysis of the Road Rater deflection basins (7). However, significant effects are reported for certain ranges of subgrade thicknesses by the researchers at the University of Texas at Austin based on their dynamic analyses of dynamic deflection tests (13). The assumption of an arbitrary thickness of subgrade may therefore significantly affect the moduli calculated from the static analyses of deflection basins.

The inherent weakness of the current state of the art is the use of static analyses (i.e., iterative application of multilayered linear elastic theory) to calculate in situ moduli from measured dynamic deflection basins. However, in the field of nondestructive pavement evaluation, the current state of knowledge for proper dynamic analyses of dynamic deflection basins is in the research and development stage. The layered theory is still the best tool available in the absence of any reliable and valid method of dynamic analysis.

EVALUATION OF MODULI FOR A KNOWN ROCK LAYER

If a rock layer is suspected at a pavement site, every effort should be made to extract information about the thickness of the subgrade. In this case, the pavement structure can be properly modeled for the iterative application of the elastic layered theory. However, the problem of nonuniqueness may still remain a source of significant error in the predicted moduli for the conventional basin matching approach in which iterations start from user-specified values of moduli.

The FPEDD1 and RPEDD1 programs ensure the uniqueness of predicted moduli by correcting the seed modulus of subgrade for the finite thickness of subgrade. For this purpose, a parametric study was made by using different rigid and flexible pavements to investigate the influence of variations in the depth of subgrade of Sensor 5 deflection. Based on layered theory computations, the ratio (RAT5) of Dynaflect Sensor 5 deflection for several subgrade thicknesses (D, in.) to the Sensor 5 deflection for a semi-infinite subgrade was determined for various pavement structures. The ratio (RAT5) approached zero if a rocklayer was assumed at 1 ft or a shallower depth below the pavement. A power function was used to develop a regression equation based on the values of RAT5 and D. The programs compute RAT5 if the thickness of the subgrade layer is entered by the user. The equivalent Sensor 5 deflection W_5' for a semi-infinite subgrade case is then calculated by using the following relationship:

$$W_5' = W_5/RAT5 \quad (1)$$

where W_5 is the measured Sensor 5 deflection.

The regression equations developed from numerous theoretical basins are then used to predict subgrade moduli. These equations are based only on Sensor 5 deflections. The R-squared values associated with these equations are above 0.95. In the case of the FWD, the Sensor 5 deflection is normalized by the program to 1,000 lb for substituting its value in Equation 1 and in the predictive equations. The subgrade seed modulus (corrected for the influence of subgrade thickness on measured deflections) is used to calculate seed moduli of upper layers of the pavement. The evaluation of in situ moduli is then performed by converging to measured deflections by using basin fitting routines.

Application

Several theoretical deflection basins generated for various hypothetical pavement-subgrade systems were analyzed to verify the predictions of moduli; this is a rational method of checking the accuracy of predictions before subjecting the methodology to field applications. Figure 3 shows this point; a deflection basin--predicted assuming 50 ft of subgrade--has been analyzed for a hypothetical pavement with preassigned moduli by using the RPEDD1 program. In this figure, HERRP represents maximum discrepancy in the theoretical and the best-fit deflections.

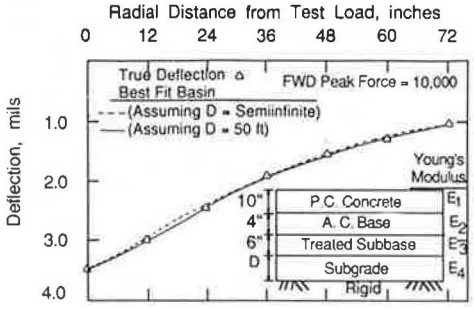

Young's Moduli	Assigned Moduli	Input Moduli	Predicted (Iteration #2)	Percent Difference	HERRP (Percent)
E_1 (psi)	4,000,000	0	3,085,000	-22.9	
E_2 (psi)	400,000	0	273,100	-31.7	
E_3 (psi)	100,000	0	129,000	+29.0	2.98
E_4 (psi)	30,000	0	34,610	+15.4	

(a) D = Semi-infinite subgrade (no. of Iterations 2)

Young's Moduli	Assigned Moduli	Input Moduli	Predicted (Iteration #2)	Percent Difference	HERRP (Percent)
E_1 (psi)	4,000,000	0	3,921,000	-2.0	
E_2 (psi)	400,000	0	430,000	+7.5	
E_3 (psi)	100,000	0	129,000	+29.0	3.72
E_4 (psi)	30,000	0	28,850	-3.8	

(b) D = 50 ft subgrade (no. of iterations 2)

FIGURE 3 A theoretical FWD deflection basin generated for a hypothetical pavement to study rigid bottom consideration.

Figure 4 shows an example of predicted in situ moduli from an FWD deflection basin analyzed by the FPEDD1 program. At this flexible pavement site, approximately 5 ft of subgrade soil exists over the bedrock, according to the available records. The false assumption of a semi-infinite subgrade would have resulted in a significant overprediction (more than 100 percent) of the subgrade modulus. An example of the moduli estimated from the Dynaflect and FWD deflection basins is another flexible pavement site where a 15-ft subgrade layer exists over the bedrock. The results are summarized in Tables 2 and 3. For this case, the FPEDD1 program predicted a subgrade modulus of 16,700 psi from the analysis of the Dynaflect deflection basin. The program corrected this value to 10,300 psi for the nonlinear behavior

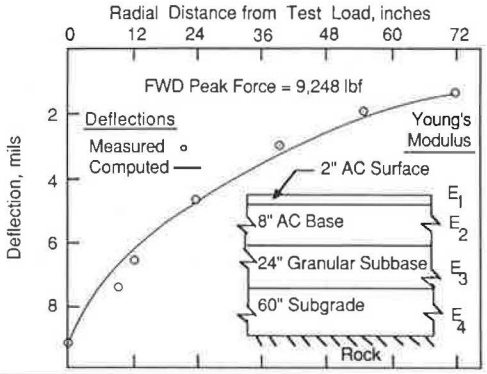

Location	Poisson's Ratio	Young's Moduli (psi) Layer	Input	Predicted
St. 200 US 75	0.35	E_1	0	591,00
Southbound,	0.35	E_2	0	590,00
Oklahoma	0.40	E_3	0	32,000
(June, 1984)	0.45	E_4	0	10,300

FIGURE 4 Prediction of in situ moduli from an FWD deflection basin analyzed by the FPEDD1 program.

TABLE 2 Dynaflect and FWD Deflection Basins: Measured and Predicted Deflections

Dynaflect Sensor No.	Deflections (mils) Measured	Predicted	FWD[a] Sensor No.	Deflections (mils) Measured	Predicted
1	0.93	0.97	1	19.2	19.5
2	0.70	0.80	2	13.9	14.1
3	0.46	0.53	3	10.9	12.1
4	0.29	0.34	4	6.7	5.8
5	0.21	0.21	5	3.3	3.1
			6	1.8	1.7
			7	1.0	1.0

Note: Measured on the flexible pavement of southbound U.S. 69 in Oklahoma (Station 220).
[a]Peak force = 8,776 lbf.

TABLE 3 Prediction of In Situ Moduli from the Dynaflect and FWD Deflection Basins

Pavement Layers	Poisson's Ratio	Young's Modulus Dynaflect	FWD (psi)
2.75-in. AC wearing course[a]	0.35	151,000	114,000
8-in. AC base course	0.35	245,000	163,000
180-in. subgrade overlying rock bottom	0.45	10,300[b]	10,700

[a]AC = asphalt concrete.
[b]Corrected for nonlinear behavior.

of the subgrade soil. Obviously, differences exist in the two sets of moduli from the Dynaflect and FWD basins for surface and base layers; these differences could be attributed to the loading mode effect and device dependency as related to measured deflections. Figure 5 shows another example of a flexible pavement site where prior knowledge of the presence of a rock layer of a shallow depth was available.

The examples just discussed indicate the usefulness of the methodology incorporated in the FPEDD1 and RPEDD1 computer programs. This study did not include any laboratory tests. Some researchers may

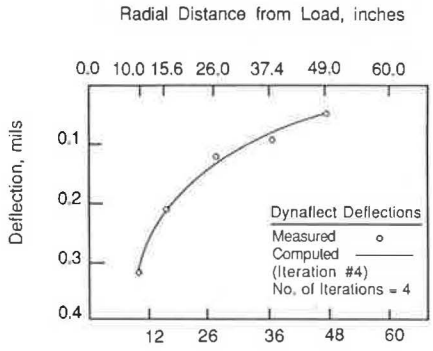

Pavement		Young's Moduli (psi)		
Loop 360 SB (Site #3) St. 404 + 52 (May 83)	Poisson's Ratio	Input	Predicted	Corrected for Nonlinearity
1.5 in. AC Surfacing	0.35	0	407,000	--
12.0 in. Flexible Base	0.40	0	100,000	55,300
20 ft. Subgrade Rockfill	0.45	0	70,000	50,030
Overlying Bedrock				

FIGURE 5 Prediction of in situ moduli for a flexible pavement with known depth of subgrade to rock by using the flexible pavement evaluation program FPEDD1.

consider comparisons with the moduli determined from laboratory tests to be more convincing. The following three points should be considered while making any inferences from a comparison of in situ moduli with laboratory moduli, particularly in the case of subgrade moduli:

1. Generally, a large scatter in resilient modulus relationships is obtained in the laboratory because of the influence of degree of saturation, water content, density, sampling disturbances, and variability associated with operators. In the case of subgrade soil, a possibility exists of even greater variability related to the depth from which the sample is extracted. On the other hand, the in situ subgrade modulus estimated from a given deflection basin is an average value over the entire depth of the subgrade.
2. The in situ stress and environmental conditions cannot be truly duplicated in laboratory.
3. The resilient modulus, based on laboratory tests, is calculated as a function of a stress parameter in the case of unbound materials and subgrade soils. It is interesting to note that the values of appropriate stress parameters are based on layered theory computations.

A RATIONAL APPROACH FOR CONSIDERING THE RIGID BOTTOM

In this section, a rational approach for assigning a finite thickness to the subgrade is presented. This approach eliminates the need for arbitrary selection of a depth to the rigid bottom. All dynamic deflection devices generate disturbance in the pavement-subgrade system. It is unlikely that the zone of influence of the dynamic test loads extends to infinite depth. In such cases, the FPEDD1 and RPEDD1 programs predict a finite thickness of subgrade. This predictive procedure is based on concepts taken from theory of stress wave propagation in elastic media. Basically, the predicted thickness of subgrade

is a function of frequency of loading (f) and compression wave velocity (V_p).

By looking at wave motion induced by the Dynaflect, long wavelengths result from low excitation frequency (8 Hz). For typical subgrade soils, half wavelengths will be more than 35 ft. It has been observed from the dynamic analysis of simulated Dynaflect tests that if the subgrade thickness is more than 35 ft, almost no significant difference exists between dynamic deflections and the static deflections computed by the elastic layered theory (13).

A simplified approach for calculating the predominant frequency excited by the FWD is the representation of the FWD load signal by an idealized load-time history: if the duration of the FWD load signal is 25 msec, the period can be approximated to 50 msec by assuming a harmonic wave form. Therefore, frequency, being the inverse of period, can be taken as 20 Hz. This is supported by extensive field measurements using a Fourier Spectrum Analyzer made during a previous study at the University of Texas (14). It was found from the time history and power spectra for the FWD that the predominant frequency excited by the FWD was approximately 20 to 21 Hz.

The step-by-step procedure for assigning a finite thickness to the subgrade is described in the following list.

1. An initial estimate of the Young's modulus of the subgrade, ENAT, is made by using the predictive relationships based on the Sensor 5 deflection. A value of Poisson's ratio (μ) for the subgrade is assigned.
2. The dynamic parameter (M) of the subgrade is calculated by using the following relationship:

$$M = \lambda + 2G \quad (2)$$

where

λ and G are Lame's constants,
$G = ENAT/2(1 + \mu)$, and
$G = \mu \cdot ENAT/(1 + \mu)(1 - 2\mu)$.

Equation 2 can be rewritten as follows:

$$M = [ENAT(1 - \mu)]/[(1 + \mu) \times (1 - 2\mu)] \quad (3)$$

3. Mass density, ρ, of the subgrade soil is calculated from the unit weight of the soil. (The unit weight of the soil is assigned based on the soil type.)
4. The wavelength of the P-wave, L_p, is then calculated by using the following relationship:

$$L_p = (M/\rho)^{0.5}/f \quad (4)$$

where f is the frequency of the driving force (8 Hz for the Dynaflect and for the FWD; the predominant frequency can be taken as 20 Hz, as discussed previously).
5. The thickness of the subgrade is assumed to be one-half of L_p.

In the FPEDD1 and RPEDD1 programs, the procedure just described for assigning a finite thickness to the subgrade is activated through an option in the input data. An example of using this option is shown in Figure 6.

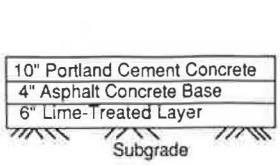

	Poisson's Ratio	Young's Modulus of Elasticity
10" Portland Cement Concrete	0.15	E_1
4" Asphalt Concrete Base	0.30	E_2
6" Lime-Treated Layer	0.40	E_3
Subgrade	0.45	E_4

Columbus Bypass, Sh-71 (Southbound, Station, 1186 + 50), Texas

FWD Peak Force = 8960 lbf. (FWD test in the ℄ of Travel Lane)

(a) PREDICTED MODULI (psi)

Layer	Semi-Infinite Subgrade	Rigid Bottom option*
E_1	5,320,000	4,870,000
E_2	486,000	371,000
E_3	169,000	50,000
E_4	36,100	25,200

(b) FWD DEFLECTIONS (mils)

Sensor No.	Measured	Semi-infinite Subgrade	Rigid Bottom*
1	2.4	2.5	2.9
2	2.3	2.2	2.2
3	2.0	1.9	2.0
4	1.6	1.6	1.6
5	1.4	1.4	1.3
6	1.2	1.2	1.0
7	1.0	1.0	0.8

*Predicted Subgrade thickness = 15.1 Feet

FIGURE 6 Analysis of an FWD deflection basin by the PREDD1 program using the rigid bottom option.

SUMMARY AND CONCLUSIONS

Various sources of errors associated with the in situ moduli of pavement layers based on the application of elastic layered theory and basin fitting approach have been discussed in this paper, particularly with respect to the rigid bottom considerations. It is shown that the use of seed moduli generated by self-iterative procedures is desirable to ensure uniqueness of the predicted in situ moduli and eliminate user-dependency aspects of these procedures. This methodology has been successfully used in the FPEDD1 and RPEDD1 computer programs. These programs also incorporate equivalent linear analyses for correcting the Dynaflect moduli with regard to the nonlinear behavior of granular layer and cohesive subgrade. The principal findings are as follows.

1. Ignorance of rigid bottom considerations may lead to substantial errors in the predicted moduli of a pavement-subgrade system. The subgrade modulus may be significantly overpredicted if a semi-infinite subgrade is falsely assumed, when actually bedrock exists at a shallow depth.
2. A procedure has been described for taking into account the influence of a rock layer if the subgrade thickness is known. This procedure relies on correcting the seed modulus of subgrade for the known depth to the rock layer.
3. A rational approach has been outlined to assign a finite thickness to the subgrade if no rock exists at shallow depths. This depth is taken as a function of the frequency of loadings and the velocity of compression wave in the subgrade. This option eliminates the need to assign an arbitrary thickness to the subgrade if the consideration of rigid bottom is required in the deflection basin analysis.

Various procedures discussed in this paper have been applied to the Dynaflect and FWD. However, the concepts can be equally applied to other dynamic load NDT devices, for example, the Road Rater.

ACKNOWLEDGMENTS

The research study was conducted as part of the Cooperative Highway Research Program sponsored by the

Texas State Department of Highways and Public Transportation and the FHWA, U.S. Department of Transportation, at which time the first author was a graduate student at the University of Texas at Austin. Appreciation is extended to K.H. Stokoe II, Professor of Civil Engineering at the University of Texas at Austin, for his interest during the course of this research. Thanks are also due to John Nixon of ARE, Inc., for providing some field deflection basin data for the evaluation of in situ moduli.

Discussion

Anastasios M. Ioannides*

Since the publication of Westergaard's pioneer works in the 1920s, the behavior of slabs-on-grade has been investigated on the basis of plate theory. On the other hand, Uddin, Meyer, and Hudson, as well as a few other investigators (15-17), have proposed using layered elastic analysis for both flexible and rigid pavements. Such a unified procedure is philosophically and practically attractive, and would allow the characterization of the pavement as a multilayered system. This is more realistic than the current use of the subgrade modulus, k, in a two-layer (or at most three-layer) system assumed when plate theory is employed.

However, using the layered elastic theory inevitably restricts the scope of all analyses to the case of interior loading. Current layered elastic theory computer codes cannot provide any information on pavement response under edge and corner loads or on the efficiency of load transfer systems at the pavement joints. This latter aspect of behavior is evidently considered an overriding consideration by the Federal Aviation Administration, U.S. Department of Transportation. A 1978 Advisory Circular entitled Airport Pavement Design and Evaluation changed the design criterion for portland cement concrete (PCC) airport pavements from the maximum stress under an interior load to that of the maximum stress when the load is placed near an edge (18). This approach to design is more realistic because it can be shown that the maximum stress in PCC pavements occurs under edge loading. Furthermore, it is almost impossible to place an aircraft on most pavement slabs in a manner that produces anything approaching a true interior loading condition (19). It has also been shown that nearly all distress in jointed concrete pavements is related to joints (20).

The possibility of analyzing the top layer of a pavement system as a plate, while retaining Burmister's multilayer theory for the remainder, has been investigated by Pickett and Ai (21). However, these authors point out that such a substitution "without modification would result in appreciable error in cases of practical importance, since it does not take into account the effects of shear in the pavement on deflection and does not properly take into account horizontal shear at the interface between subgrade and pavement." On the other hand, Parker et al. contend that "the representation of the top layer as a thin elastic plate or as an elastic layer is really not that different when the top layer is a PCC slab" (16).

To investigate this issue further, a comparison is presented here of the layered elastic and plate theories for the case of interior loading on a semi-infinite pavement system. This system consists of a top layer or PCC slab resting on a Boussinesq half-space, characterized by E_s and μ_s. From the point of view of the layered elastic theory, this half-space is the special case of a multilayered system consisting only of one layer. The problem with plate theory is the standard one: a plate on an elastic solid foundation. The analyses were performed using computer programs ELP15 (22) and WESTER (23), respectively. The equations presented by Losberg are used in WESTER for the responses according to plate theory (24).

The parameters selected for the various system components ranged between wide limits in order to ensure that most practical conditions are included in the factorial of runs conducted. The plots of nondimensional maximum response in Figures 7-9 indicate that the governing consideration when comparing the layered elastic and plate theories is the

*University of Illinois at Urbana-Champaign, Urbana, Ill. 61801.

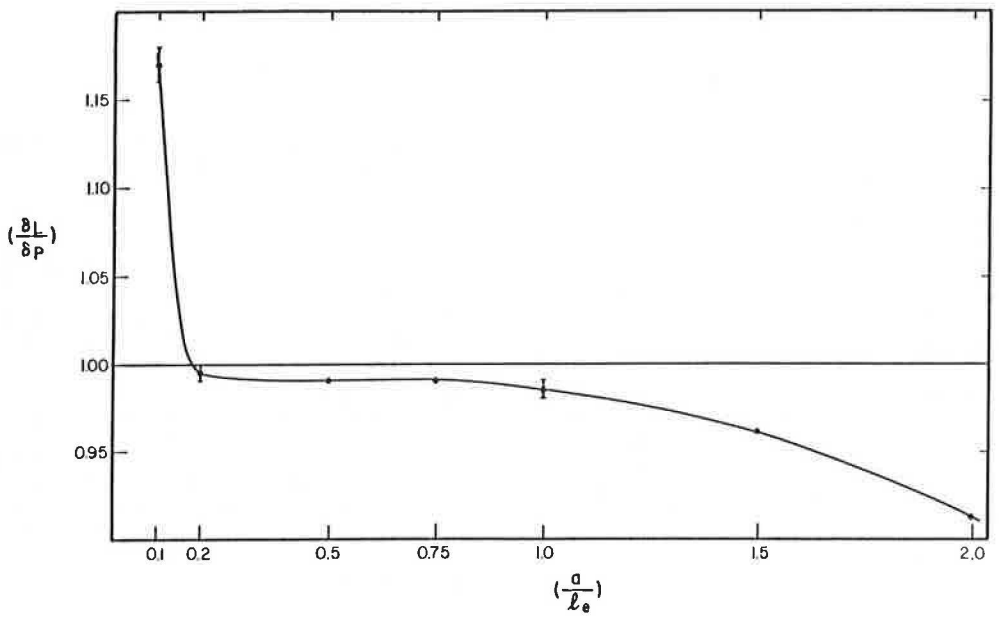

FIGURE 7 Comparison of layered elastic and plate theories: maximum deflection.

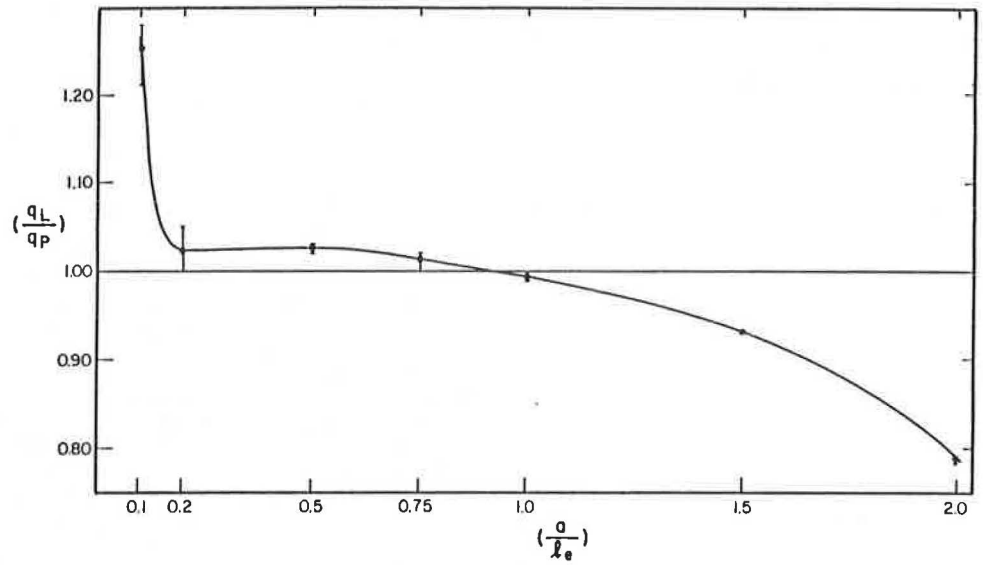

FIGURE 8 Comparison of layered elastic and plate theories: maximum subgrade stress.

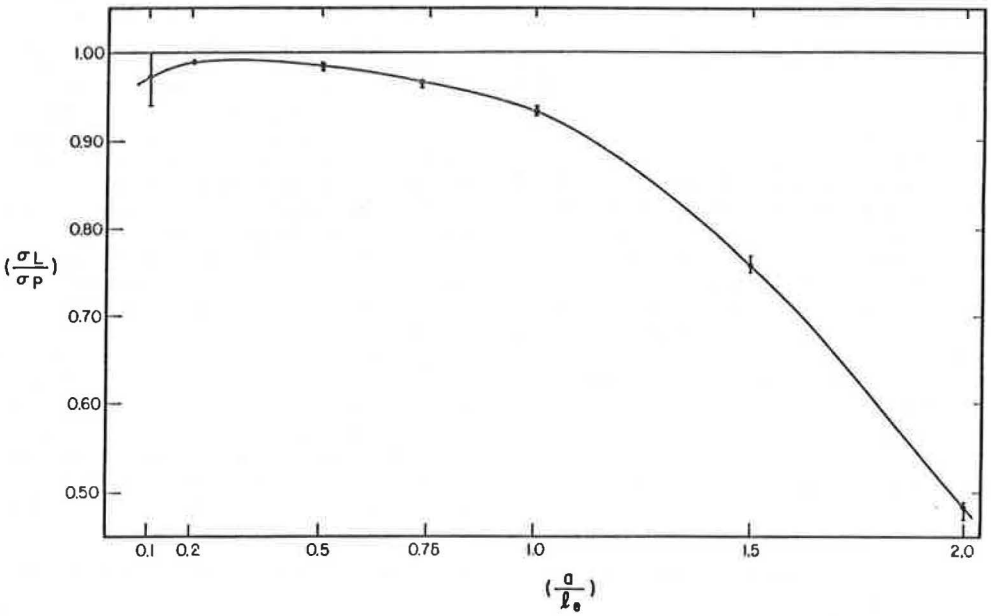

FIGURE 9 Comparison of layered elastic and plate theories: maximum bending stress.

value of the ratio (a/ℓ_e) of the radius of the applied load to the radius of relative stiffness of the pavement system.

Good agreement between the two theories is obtained when (a/ℓ_e) is between 0.2 and 1.0; considerable discrepancies occur outside this range. Values of (a/ℓ_e) greater than 1.0 are principally of academic interest only, but in practice several cases may arise in which (a/ℓ_e) takes values below 0.2. In such cases, widely divergent results may be expected from the two theories.

Note that the comparison presented here refers only to the interior loading condition. Similar comparisons for edge and corner loading are not feasible because of the inherent limitations of the layered elastic theory. Furthermore, the comparison is with the plate theory used in conjunction with an elastic solid foundation. It is generally admitted that the dense liquid and elastic solid models can only be correlated in a limited number of special cases. As a result, a comparison between the layered elastic theory and the plate theory used in conjunction with a dense liquid foundation would have limited significance and would not be of a general nature. Such a comparison was attempted by Barker (17).

The fairly good agreement between the two theories within the prescribed range of $(a\ell_e)$ values has only been established for the case of the semi-infinite half-space. A similar comparison for the multilayered foundation case is feasible, at least theoretically, by using WESLAYER (25) or RISC (26) finite element programs for the plate theory investigation. Unfortunately, the application of the finite element method in conjunction with a multilayered subgrade has not yet been developed to the point where it is generally practical to use because such programs make substantial demands on computer resources.

REFERENCES

1. R.E. Smith and R.L. Lytton. Synthesis Study of Nondestructive Testing Devices for Use in Overlay Thickness Design of Flexible Pavements. Report FHWA/RD-83/097. ERES Consultants, Inc., Champaign, Ill., April 1984.
2. J.P. Zaniewski and W.R. Hudson. Procedures for the Analysis of Pavement Condition Data. Draft Interim Report. ARE, Inc., Austin. Tex., July 1984.
3. W. Uddin, A.H. Meyer, W.R. Hudson, and K.H. Stokoe II. Project Level Structural Evaluation of Pavements Based on Dynamic Deflections. In Transportation Research Record 1007, TRB, National Research Council, Washington, D.C., 1985, pp. 37-45.
4. A.J. Bush III and D.R. Alexander. Pavement Evaluation Using Deflection Basin Measurements and Layered Theory. In Transportation Research Record 1022, TRB, National Research Council, Washington, D.C., 1985, pp. 16-29.
5. S. Husain and K.P. George. In Situ Pavement Moduli from Dynaflect Deflection. In Transportation Research Record 1043, TRB, National Research Council, Washington, D.C., 1985, pp. 102-112.
6. G. Wiseman, J. Greenstein, and J. Uzan. Application of Simplified Layered Systems to NDT Pavement Evaluation. In Transportation Research Record 1022, TRB, National Research Council, Washington, D.C., 1985, pp. 29-36.
7. M.S. Mamlouk. Use of Dynamic Analysis in Predicting Field Multilayer Pavement Moduli. In Transportation Research Record 1043, TRB, National Research Council, Washington, D.C., 1985, pp. 113-121.
8. Proposed AASHTO Guide for Design of Pavement Structures. Draft. AASHTO, March 1985.
9. W. Uddin. A Structural Evaluation Methodology for Pavements Based on Dynamic Deflections. Ph.D. dissertation. University of Texas at Austin, Austin, Dec. 1984.
10. W. Uddin, A.H. Meyer, and W.R. Hudson. A Flexible Pavement Structural Evaluation System Based on Dynamic Deflections. Presented at the 1985 Annual Meeting of Association of Asphalt Paving Technologists, San Antonio, Tex., Feb. 1985.
11. W. Uddin, A.H. Meyer, W.R. Hudson, and K.H. Stokoe II. A Rigid Pavement Structural Evaluation System Based on Dynamic Deflections. Presented at the 3rd International Conference on Concrete Pavement Design and Rehabilitation, Purdue University, Lafayette, Ind., April 1985.
12. B.F. McCullough and A. Taute. Use of Deflection Measurements for Determining Pavement Material Properties. In Transportation Research Record 852, TRB, National Research Council, Washington, D.C., 1982, pp. 8-14.
13. J.M. Roesset and K-Y. Shao. Dynamic Interpretation of Dynaflect and Falling Weight Deflectometer Tests. In Transportation Research Record 1022, TRB, National Research Council, Washington, D.C., 1985, pp. 7-16.
14. J.S. Heisey, K.H. Stokoe II, W.R. Hudson, and A.H. Meyer. Determination of In Situ Shear Wave Velocities from Spectral Analysis of Surface Waves. Research Report 256-2. Center for Transportation Research, University of Texas at Austin, Austin, Nov. 1982.
15. W.R. Barker and W.N. Brabston. Development of a Structural Design Procedure for Flexible Airport Pavements. Technical Report S-75-17 (also, Report FAA-RD-74-199). U.S. Army Engineer Waterways Experiment Station, Vicksburg, Miss., Sept. 1975.
16. F. Parker, W.R. Barker, R.C. Gunkel, and E.C. Odom. Development of a Structural Design Procedure for Rigid Airport Pavements. Report FAA-RD-77-81. U.S. Department of Transportation, 1977.
17. W.R. Barker. Introduction to a Rigid Pavement Design Procedure. Proc., Second International Conference on Concrete Pavement Design, Purdue University, Lafayette, Ind., April 1981.
18. Airport Pavement Design and Evaluation. Advisory Circular 150/5320-60. Federal Aviation Administration, U.S. Department of Transportation, Dec. 1978.
19. E.J. Barenberg and D.M Arntzen. Design of Airport Pavements as Affected by Load Transfer and Support Conditions. Proc., Second International Conference on Concrete Pavement Design, Purdue University, Lafayette, Ind., April 1981.
20. D.M. Arntzen, E.J. Barenberg, and R. Krauce. Airfield Pavement Demonstration Validation Study. ASCE, Transportation Engineering Journal, Vol. 106, No. TE6, Nov. 1980.
21. G. Pickett and D.K.Y. Ai. Stresses in Subgrade Under Rigid Pavement. Proc., 33rd Annual Meeting, Highway Research Board, Washington, D.C. Jan. 1954.
22. J. Michelow. Analysis of Stresses and Displacements in an N-Layered Elastic System Under a Load Uniformly Distributed on a Circular Area. California Research Corporation, Richmond, 1963.
23. A.M. Ioannides. Analysis of Slabs-On-Grade for a Variety of Loading and Support Conditions. Ph.D. thesis. University of Illinois at Urbana-Champaign, Urbana, 1984.
24. A. Losberg. Structurally Reinforced Concrete Pavements. Doktorsavhandlingar Vid Chalmers Tekniska Hogskola, Gothenburg, Sweden, 1960.
25. Y.T. Chou. Structural Analysis Computer Programs for Rigid Multicomponent Pavement Structures with Discontinuities--WESLIQID and WESLAYER; Report 1: Program Development and Numerical Presentations; Report 2: Manual for the WESLIQID Finite Element Program; Report 3: Manual for the WESLAYER Finite Element Program. Technical Report GL-81-6. U.S. Army Engineer Waterways Experiment Station, Vicksburg, Miss., May 1981.
26. K. Majidzadeh, G.J. Ilves, and H. Sklyut. Mechanistic Design of Rigid Pavements--Volume 1: Development of the Design Procedure. Final Report, DTH11-9568 (draft). Nov. 1983.

Publication of this paper sponsored by Committee on Strength and Deformation Characteristics of Pavement Sections.

Characterizing Premature Deformation in Asphalt Concrete Placed over Portland Cement Concrete Pavements

SAMUEL H. CARPENTER and THOMAS J. FREEMAN

ABSTRACT

An analytical study of the problem of premature deformation in asphalt concrete overlays of concrete pavements is presented; topics that have not been investigated previously are suggested for consideration. Premature deformation is considered to be the development of failure level rutting after only 1 or 2 years of service. The study indicates that there are stress and strain fields in an overlay that have not been considered in previous analysis procedures, which could indicate why premature rutting developing on Interstate pavements could be different when the original surface is concrete than when it is asphalt. The strain energy of distortion, or octahedral shear stress, was chosen from a study of failure theories as best representing the stress state relating to the onset of inelastic deformation under one load cycle rather than only the vertical stress as is usually used. Analysis indicates that different stress conditions can develop in the overlay when it is placed on a concrete surface compared with when it is placed on an asphalt surface. Interface bonding between the overlay and the original surface alters this stress state, which is very much closer to a failure condition than previously believed. The computer analysis indicates that current testing does not model the material behavior at a stress level or with boundary conditions comparable to those existing in the field. Material nonlinearity under field conditions, and the proximity of the existing stresses to a failure state for that material, may indicate why current procedures have not been able to accurately characterize a material's potential for rapid permanent deformation failure within the first 1 or 2 years.

In recent years, the performance of asphalt concrete (AC) overlays on heavily trafficked Interstate concrete pavements has not been as good as was expected. Reasons suggested for this include changes in the asphalt cements, changes in equipment for compaction and placement, changes in mixing equipment or procedures, and changes in traffic. Whatever the reason, an increase has been noted in the premature deformation of these AC overlays. Premature deformation here refers to the failure of an overlay within 1 or 2 years after it has been placed, and not the gradual steady-state appearance of rutting under long-term traffic.

The problem produced by changes in asphalt cement or equipment and procedures is beyond the scope of this paper. The problems of altered traffic conditions and mix design considerations can be investigated in the laboratory or with computer simulation. Presented in this paper is the initial phase of a study designed to describe developments in a mixture placed over a concrete pavement that could be used to account for any noted increase in the occurrence of premature deformation.

CHARACTERIZATION OF PREMATURE DEFORMATION

To accurately characterize the development of any distress, the stress or strain conditions causing the distress to occur must be accurately determined. The stress or strain must also relate directly to the development of the distress. As an extreme example, the radial strain in the asphalt layer should not be used to predict the rutting potential in the subgrade even though a relationship may be developed. The response parameters indicate what is happening in the material being investigated.

Current testing for permanent deformation typically uses the triaxial unconfined compressive test either with repetitive or creep loading. The one response parameter selected to model the pavement in the laboratory is typically vertical stress. For example, VESYS uses a 20 psi vertical stress, and creep testing usually starts with a similar value. These stresses relate directly to deformation resistance in a material, but the question is whether they relate to the failure mechanism that actually develops in the pavement when premature deformation is occurring. Using compressive stress may not accurately indicate the failure taking place because it may have only a proportional and/or nonlinear relationship with the mechanism occurring in the overlay, not a direct unique relationship.

At low stress levels, the compressive stress is proportional to the deformation and presents the proper relationship for gradual accumulation of rutting over a prolonged time. This test has not provided an accurate relationship with any mode of deformation that develops rapidly, which may be why some computer models have a difficult time modeling the rapid failure of a pavement. This inadequacy is not due to an inadequacy in the theoretical modeling

S.H. Carpenter, University of Illinois at Urbana-Champaign, Urbana, Ill. 61801. T.J. Freeman, ERES Consultants, Inc., Champaign, Ill. 61820.

process, but rather through the use of a parameter that does not completely model the existing stress or strain state in the overlay to describe the behavior of the pavement.

The development of premature deformation being studied in this paper is better related to failure under a one-time load than it is to the gradual accumulation of strain under repeated loadings because of the rapidity with which it occurs. Although failure theory is not exactly applicable to this situation, rapid failure clearly indicates that the stress-strain condition in the asphalt layer could be closer to a failure value than previously believed, depending on pavement type, conditions, and material quality. Thus, the principles of failure mechanics may be more applicable to bituminous mixes placed as an overlay than previously believed. Although failure mechanics is more appropriate in studying incipient failure, the rapid shear failure being investigated here is more similar to incipient failure than to the accumulation of rutting in a normal pavement.

FAILURE THEORY

Failure theories involve the application of mechanics to predict the stress-strain condition in a sample at failure. If the stress-strain condition of an in-place material exceeds the failure stress-strain value predicted from the theory, the material will fail under that one loading.

In examining failure related to ductile behavior, the theories of octahedral shear stress or maximum strain energy of distortion stand out as most applicable to the situation in which failure is predominantly ductile and not brittle fracture (1).

Researchers have demonstrated the applicability of the octahedral shear stress failure theory in ductile metals (1). For most paving materials, the Mohr-Coulomb failure criteria are more commonly accepted. Although the two theories are completely different, enough similarities exist to suggest that the octahedral shear stress parameter warrants further study as an indicator of potential for failure in a pavement material. A schematic comparison of the octahedral shear stress failure and the Mohr-Coulomb failure conditions is shown in Figure 1.

The equation developed from theory for the octahedral shear stress is

$$\tau_{oct} = (1/3)[(\sigma_1 - \sigma_2)^2 + (\sigma_2 - \sigma_3)^2 + (\sigma_3 - \sigma_1)^2]^{1/2} \quad (1)$$

where σ is the principal stresses in the material and τ_{oct} is the octahedral shear stress.

The companion equation for the strain energy of distortion is

$$E.D. = [(1 + u)/6E][(\sigma_1 - \sigma_2)^2 + (\sigma_2 - \sigma_3)^2 + (\sigma_3 - \sigma_1)^2] \quad (2)$$

where

E = elastic modulus,
u = Poisson's ratio, and
E.D. = strain energy of distortion.

These equations indicate that the octahedral shear stress failure theory provides a complete description of the total stress state in the material; a single parameter such as the vertical compressive principal stress commonly used in current laboratory repeated loading studies cannot. The equations also indicate a similarity in the theoretical failure condition for ductile metals and materials that are assumed to follow the Mohr-Coulomb failure. According to the octahedral shear stress failure theory, inelastic deformation will occur when the octahedral shear stress (strain energy of distortion) exceeds a value of 0.47 times the uniaxial tensile strength (strain energy of distortion) at failure under a uniaxial tension test. A study of the Mohr-Coulomb failure theory shows that at failure the octahedral shear stress is exactly equal to 0.47 times the deviator stress on the sample at failure.

A direct tension test involves decreasing the major principal stress on the sample until failure occurs under this tensile stress. The other principal stresses are generally zero. A tensile test can be simulated in a triaxial test under a given set of confining conditions if the vertical stress on the cylindrical sample is allowed to decrease until failure occurs, rather than allowing the vertical stress to increase to failure. In this test the sample fails in extension under the given stress condi-

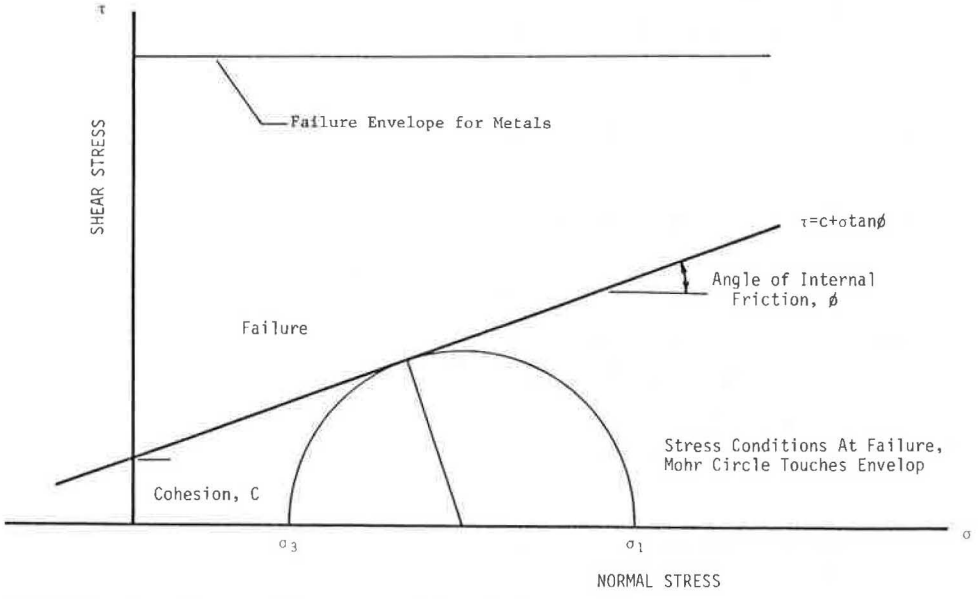

FIGURE 1 Mohr-Coulomb failure representation of stress conditions.

tions, and the deviator stress is equal to a quasi-tensile strength of the sample under the given stress conditions. Thus, a similarity of failure conditions exists between the two theories even though they are not the same. More important, the octahedral shear stress or strain energy of distortion theory provides a single numerical parameter that describes the total stress state in the material that accurately relates to the onset of inelastic deformation, or yield, in the material. It is not stated in this theory that permanent deformation cannot occur until the stress level exceeds failure.

The hypothesis for the remainder of this paper is that the octahedral shear stress provides a unique numerical indicator that allows the engineer to examine how close to failure an AC mixture may be after it is placed. Further, it allows the mixture quality to be examined and included in the analysis through a description of the failure envelope. If the Mohr failure envelope can be defined for a bituminous mixture and the stress condition in that material when placed on a pavement can be accurately predicted, then a comparison can be made between the stress in the material produced by a wheel loading and the stress that will cause failure under one load. Although it is not expected that failure under one wheel load is likely to occur, the proximity of the stress state in the pavement to the stress state defined by the failure envelope can provide an indication of how close to failure the material in the pavement may be and the potential for premature deformation to develop. If the stresses in the existing overlay sections placed on portland cement concrete (PCC) pavements today show excessively high octahedral shear stresses compared with similar installations in flexible pavements, a rationale exists for expecting more rapid deformation in the overlay sections on concrete pavements.

COMPARISON OF OVERLAYS

The initial phase of this investigation was set up to determine if a significant difference could be found between the octahedral shear stresses in an overlay of a rigid pavement and those in an overlay of a flexible pavement. The two standard sections selected for the comparison are shown in Figure 2. These sections were selected as representative of a typical high-volume pavement that might receive an overlay and were not designed to be equivalent. The computer program BISAR was used to calculate the stress state in overlays placed on each pavement section.

Standard pavement design and analysis techniques use a standard 18,000-lb equivalent single axle load (ESAL), which produces a contact pressure of 70 psi. These were used for the bulk of the calculations and comparisons performed in this study. The applicability of these parameters will be discussed in a subsequent section of this paper. The first item noted in examining stress conditions in the overlays is that the maximum octahedral shear stress or strain energy of distortion does not always occur under the centerline of the wheel load nor does it always occur at the bottom of the AC layer. These are the traditional locations for maximum values of stresses or strains used in pavement analysis, and a traditional investigation such as that done by Roberts and Kennedy would not note the difference observed here (2). Contours of the strain energy of distortion are shown in Figures 3 and 4 for several thicknesses of overlay over both flexible and rigid pavements.

No significant difference between the maximum octahedral shear stress values for the two pavement types was noted. However, the distributions of the stress under the wheel load were significantly different between the two pavement types. This difference indicates that the stress condition that exists in an overlay placed on a flexible pavement is different from that existing in an overlay placed on a rigid pavement. Similar findings were noted for the radial strain in the overlay, as shown in Figures 5 and 6. A significant radial tensile strain exists in the overlay on the rigid pavement, but it does not necessarily occur at the locations traditionally used in pavement design. Again, this indicates the need to avoid a traditional analysis when investigating new concepts or when examining a specific distress type. These findings indicate that a new approach may be required for analyzing a mixture for placement as an overlay because significantly different shear and radial tensile stresses and strains are developing in the mixture. The presence and

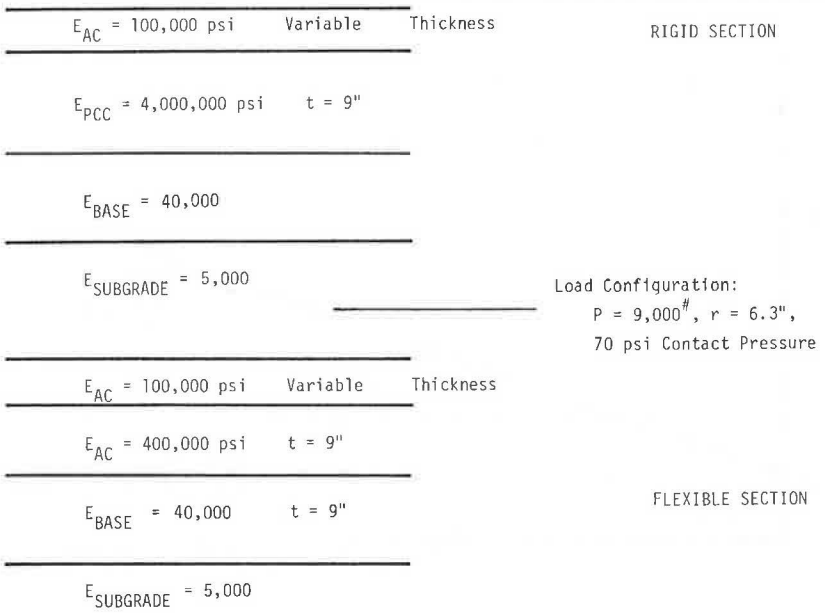

FIGURE 2 Pavement cross sections used in overlay analysis.

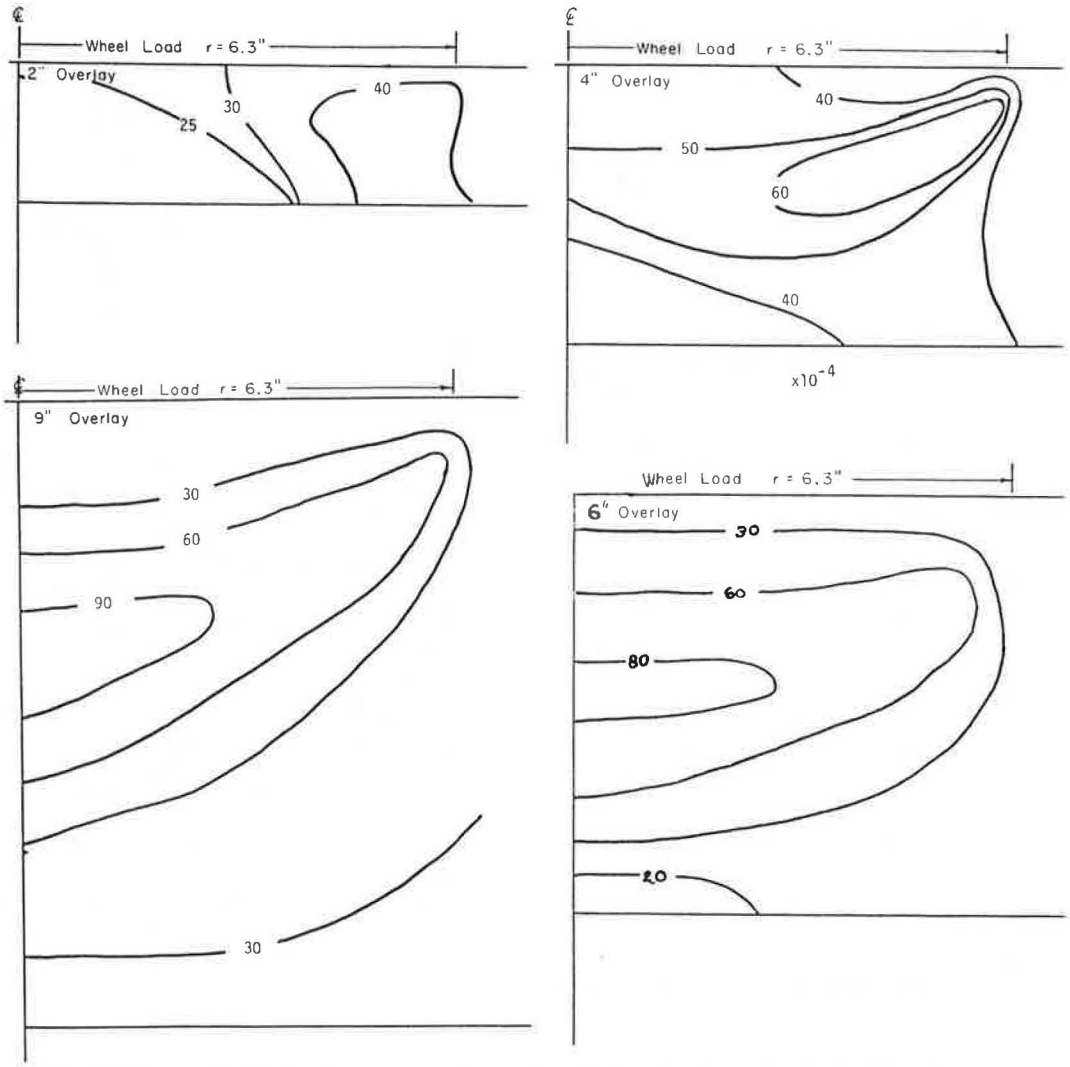

FIGURE 3 Distribution of strain energy of distortion (x 10^{-4}) for AC/PCC pavements for a perfect bond condition.

magnitude of these stresses may also indicate the need for different mix design considerations.

The octahedral shear stress varies considerably with the thickness of the overlay, as shown previously. As the overlay becomes thicker, the maximum value increases and moves under the centerline of the wheel load at the middepth portion of the overlay. Thus, if the bottom of the overlay was examined, only low stress levels would be reported even though a problem of shearing in the middle of the mixture could be developing.

Figure 7 shows a failure envelope developed by using an estimated angle of internal friction and a measured tensile strength, and as such can be considered as representing a potential material quality level. The stress condition produced by a standard wheel is shown and the stress level usually used in laboratory repeated load triaxial testing is also shown. At this temperature and loading rate, an unconfined sample would fail with an applied octahedral shear stress of 85 psi. The octahedral shear stress induced by the loadings is shown with each Mohr's circle. These values have been used to calculate the ratio of actual stress to failure stress, R. These ratios clearly indicate that the standard wheel load is three times closer to failure than the stress usually used to characterize permanent deformation in the laboratory.

Because the failure envelope may change with different boundary conditions such as temperature and rate of load (3), these ratios are only relative indicators and their magnitude can change. The point is that failure in the field under traffic will be significantly different from that predicted in the laboratory. This point was evident in the 1974 study by Morris et al., which examined permanent deformation under stress conditions varying from compression to tension (4). The unifying factor they did not develop was the octahedral shear stress, which unifies all the stress conditions.

To evaluate the impact that differences in stress state have on performance requires data indicating how the behavior of a mixture changes as the stress state approaches failure. It must be demonstrated whether current laboratory testing produces the same performance that develops in the field, or whether laboratory testing should be changed to better account for the conditions developing in the field. Material behavior assumed to be linear at low stress levels may be decidedly nonlinear as the stress level increases. The magnitude of the in situ stresses relative to the failure envelope becomes crucial

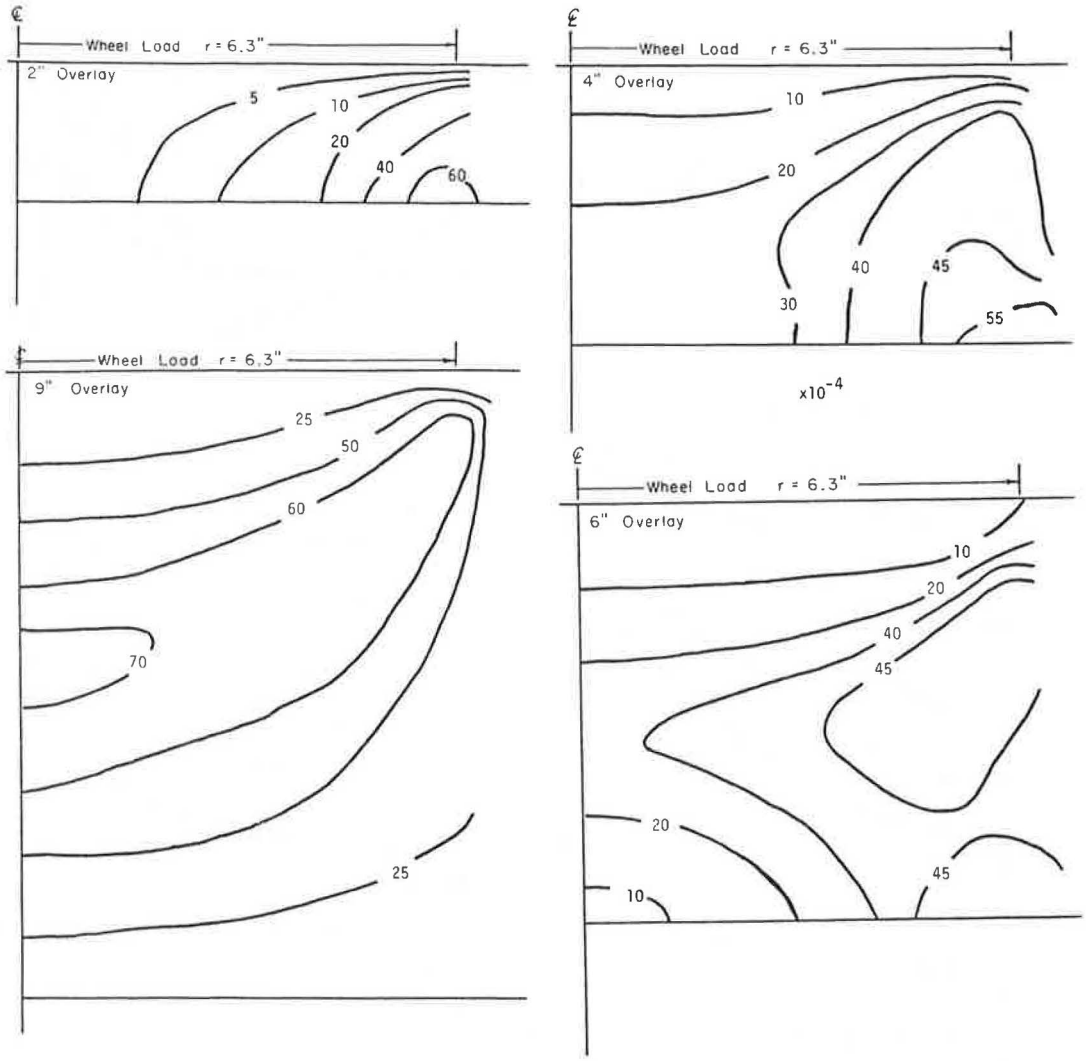

FIGURE 4 Distribution of strain energy of distortion (x 10^{-4}) for AC/AC pavements for a perfect bond.

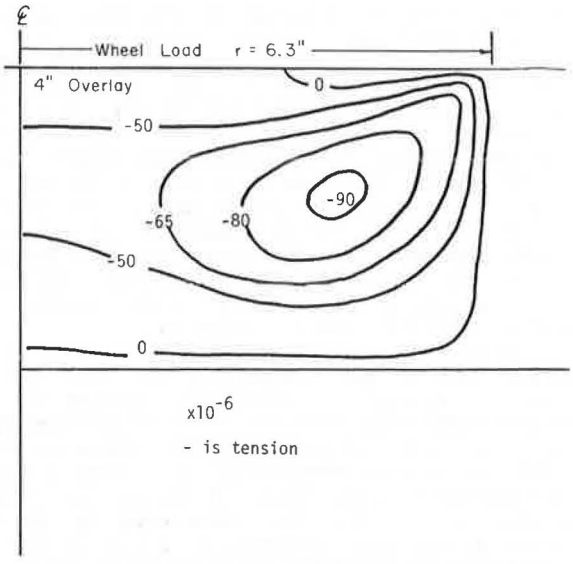

FIGURE 5 Distribution of radial strain under standard wheel load for 4-in. AC/PCC pavement.

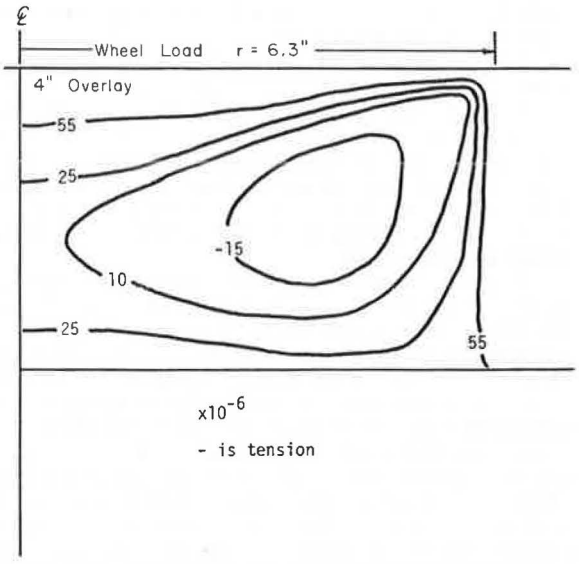

FIGURE 6 Distribution of radial strain under standard wheel load for 4-in. AC/AC pavement.

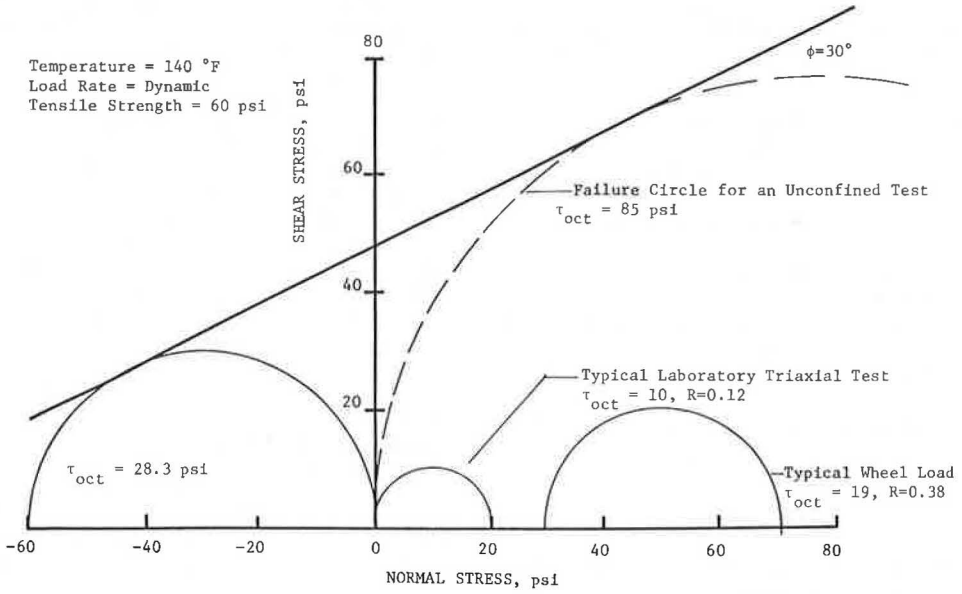

FIGURE 7 Mohr circles for the stress state in an overlay and for a typical unconfined repeated loading test in the laboratory.

when the material behavior has the potential to become nonlinear under different conditions. It then becomes important to be able to accurately define the conditions in the pavement that can change.

PAVEMENT DIFFERENCES

As discussed in the previous section, the comparisons between the stresses produced in different pavement configurations did not indicate a significant difference in the maximum stresses developing in the two pavement types that would account for a noted preference for premature deformation to develop in an overlay of a rigid pavement rather than a flexible installation. The next consideration is to determine the potential differences that could develop between the overlay on a flexible pavement and that on a rigid pavement, and to determine the effect, if any, that these differences would have on the octahedral shear stress state in the mixture.

Some differences that could produce different effects on the two pavement structures include the following:

1. Two different materials being placed in direct contact in the rigid pavement while two similar materials are placed for the flexible pavement.
2. Differences in performance related to discontinuities in the original surface being different in the two pavements (i.e., fatigue cracking or thermal cracks in the flexible pavement in contrast with joints or D-cracking in the rigid pavement).
3. Differences in the moisture conditions in the rigid pavement compared with those in the flexible pavement.
4. Construction differences necessitated because of pavement differences.

These differences, although not structural, can alter performance when they affect the interface of the two materials--the old pavement and the new overlay. In a flexible pavement, the new AC can soften the old pavement during placement and produce a relatively good bond. However, in a rigid pavement, there can be no softening or rehealing and the potential for a good bond is lower in this pavement from the beginning.

The ability of moisture to separate two materials is heightened when the materials are very different. The increased presence of moisture in a badly cracked concrete pavement after overlay indicates that more water may be available to collect at the interface in a rigid pavement than in a flexible pavement (5). In the Illinois Cooperative Highway Research Program entitled Predicting the Progression of D-Cracking, laboratory evidence is being obtained that indicates that (a) the thermal characteristics of the two different materials in the rigid installation interact to promote disbonding under the action of freeze-thaw cycling, and (b) moisture accentuates this disbonding. The bonding between the old surface and the new overlay appears to be the most significant single factor that could produce a structural difference between the overlay mixture in a flexible installation and that in a rigid installation. Although the problem has not been thoroughly investigated, the potential for disbonding would appear to be higher for the rigid installation than it is for the flexible installation.

ANALYTICAL COMPARISONS OF BOND LOSS

The consideration of bond loss at the interface of the two layers was studied with the BISAR computer program. This elastic layer program provides the capabilities of allowing the interface between two layers to move and of providing different strains in the upper and lower layer, simulating a loss of bond to varying degrees. The program utilizes a compliance factor to allow the upper and lower layers to move an amount proportional to the selected compliance and the applied loading at the interface.

This compliance can be presented as being proportional to the inverse of the stiffness with which the two layers are being restrained from moving relative to each other (shear modulus). A bond of 0 indicates an infinitely high stiffness, which does not allow any movement between the two layers; this level of bond is the typical assumption used in all elastic layer programs. A compliance with an extremely high value would indicate a very low stiffness, which would allow a large amount of relative movement between the two layers. A study by Uzan et

al. on flexible pavements defined some limiting values typical of pavement materials (6). The values used in that study are presented in the following table.

Compliance	Bond Condition
0	Perfect bonding
2	25% loss of bond
20	75% loss of bond
10,000	95% loss of bond

The same pavement configurations used in calculating the octahedral shear stress and strain energy of distortion shown previously were analyzed with the BISAR program applying the different bond factors at the interface. As expected, the octahedral shear stress increased dramatically as the bonding decreased, and the position of the maximum octahedral shear stress also changed considerably.

Position of Maximum Octahedral Shear Stress

Figure 8 shows the distribution of the strain energy of distortion as the bond decreases for the 4-in. overlay being studied. The location of the maximum shifts to the bottom of the layer as the bonding decreases; this occurs as the direct result of the loss of restraint on the bottom of the layer. As the resistance to slip is lowered, the movement at the bottom of the layer increases because it will not be as confined as it is on the top, where the wheel is in contact with the pavement. This outward movement reduces the confining stress on the mixture at the interface, which increases the stress state.

Similar trends were noted for the flexible and rigid installations. The changes in the strain energy of distortion with bonding are shown in Figures 9 and 10 for the two pavement types. The increase in the strain energy of distortion indicates that when bond is lost the stress situation will be far more critical than when the bond is good. These calculations allow the stresses developed in a pavement with different boundary conditions to be quantified for study in the laboratory, which was not previously possible.

One significant difference can be noted between the flexible and rigid installations. When bonding is lost, the inherent flexibility of the flexible pavement produces a significantly higher octahedral shear stress than that found in the rigid installation, where the rigidity of the old surface does not allow any extra stress to be produced by a bending action of the pavement. Potentially, the flexible pavement could develop the most critical stress condition.

It is generally believed that the bonding in an asphalt overlay of a flexible surface will provide the best bond and that the potential for long-term performance of this bond will be good. For this reason, the flexible pavement situation is not expected to indicate a severe loss of bonding unless exten-

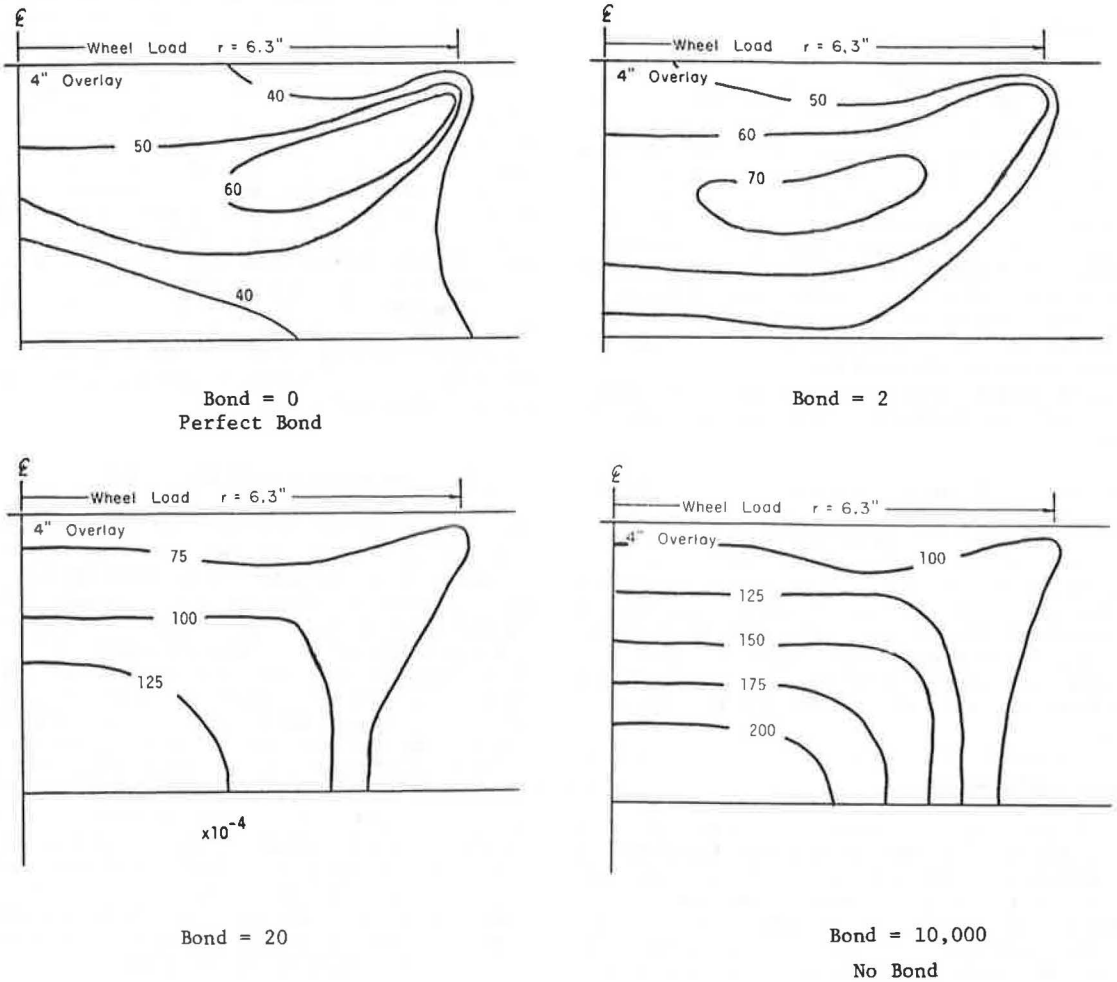

FIGURE 8 Change in the strain energy of distortion with a change in interface bond.

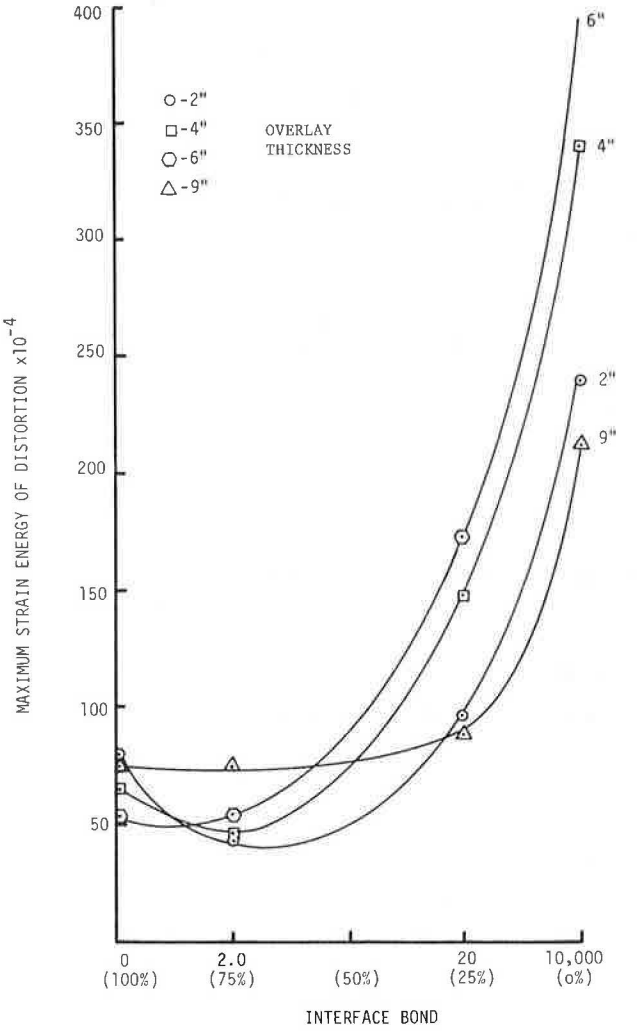

FIGURE 9 Variation of maximum strain energy of distortion for various thicknesses of AC/AC as a function of bonding.

sive material problems are present. On the other hand, the rigid pavement has absolutely nothing going for it to reduce the potential for loss of interface bond. It is likely that the bond will deteriorate quickly if moisture is introduced into the system, and a winter's thermal activity would accelerate the debonding even faster. Thus, a rigid pavement has the highest potential for loss of bond over the long term; this is in addition to a high potential for immediate loss of bond if the construction sequences are not controlled, the pavement surfaces are not cleared, and tack coats are not used properly. The results of loss of bond have been most noticeable in mixtures placed over orthotropic plate bridge decks when the epoxy bond has not cured properly.

The poor condition of the interface expected in an overlay of a rigid pavement will produce octahedral shear stresses with magnitudes in the range of 35 to 40 psi. The maximum octahedral shear stress expected in a flexible pavement overlay should remain in the range of 15 to 20 psi. Therefore, the rigid pavement has the highest potential to produce the most severe stress condition in the overlay.

Implications for Performance

The increased stress state produced by loss of bonding develops through a decrease in the horizontal principal stress (confining pressure) resulting from the slip at the interface. For a complete loss of bonding, the horizontal principle stress can theoretically become negative, producing a tensile stress. The smaller the secondary principle stress, the larger the octahedral shear stress. This stress condition has been recognized by previous researchers such as McLeod (7), but could never be calculated to determine its quantitative effect on the state of stress in the bituminous mixture.

The stress condition corresponding to no bond is plotted as a Mohr's circle in Figure 11 to demonstrate the total effect on performance potential. As interface bonding is lost, the Mohr's circle moves closer to the failure envelope, which represents failure, and hence the material's quality level. Again, this failure envelope has been constructed by using a measured tensile strength and an estimated angle of internal friction, and should be considered as being only an indicator of a true failure envelope. The closer the Mohr's circle representing the stress state existing in the pavement moves to the failure envelope, the higher the potential for premature deformation to occur. The size and location of the Mohr's circle in this figure, relative to failure, clearly indicates that an unconfined repeated load test could model pavement behavior for this material only if the vertical stress was approximately 70 psi, not 20 psi as usually used.

Testing at these higher stress levels should be done if premature deformation failure is suspected; this testing may be prudent whenever an overlay is placed on a heavily trafficked concrete Interstate pavement. Because repeated loading tests conducted at the lower stress levels have not demonstrated consistent relationships with temperature, it may be suspected that the testing stress levels are too far

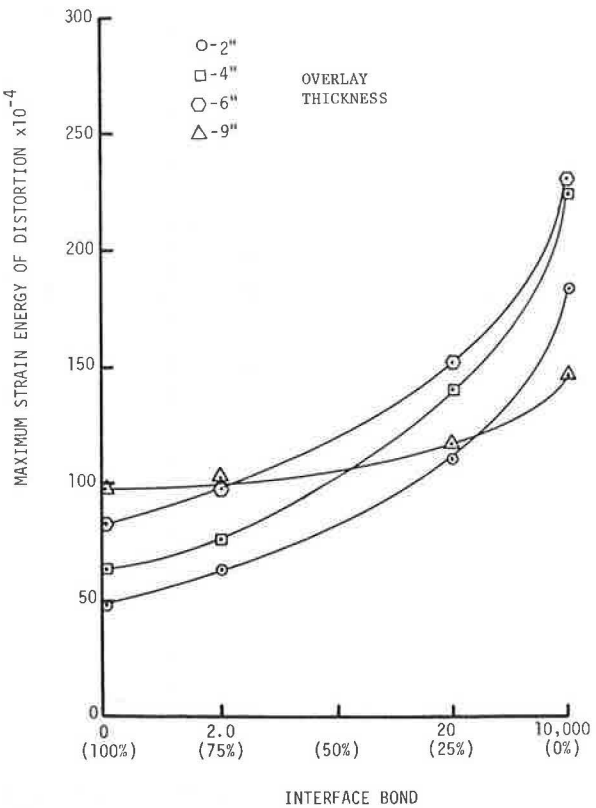

FIGURE 10 Variation of maximum strain energy of distortion for various thicknesses of AC/PCC as a function of bonding.

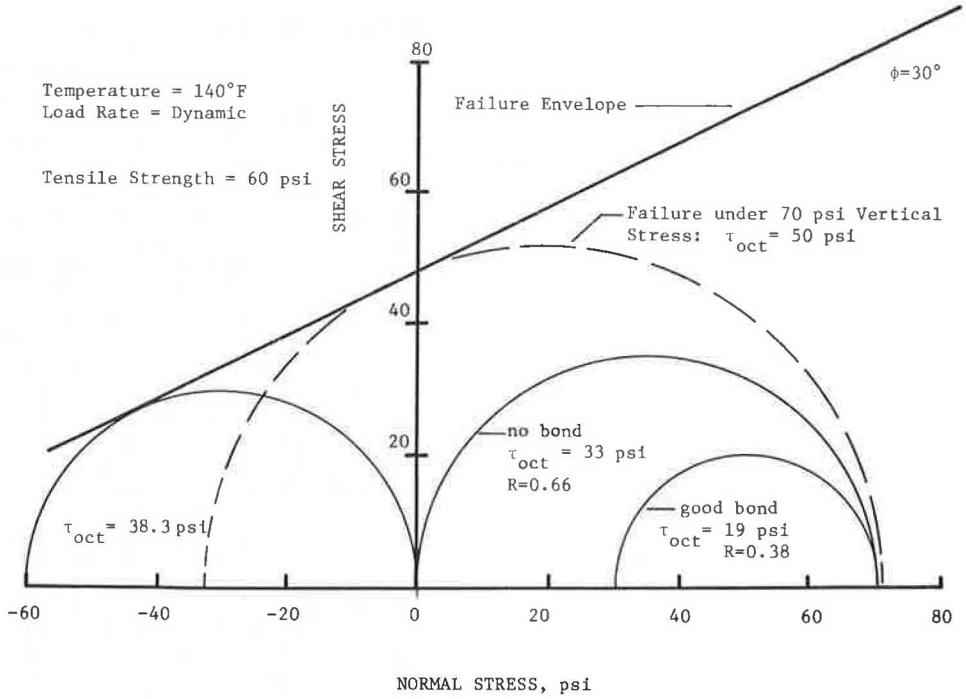

FIGURE 11 Mohr circle representation for stress state in an overlay as the interface bond is lost.

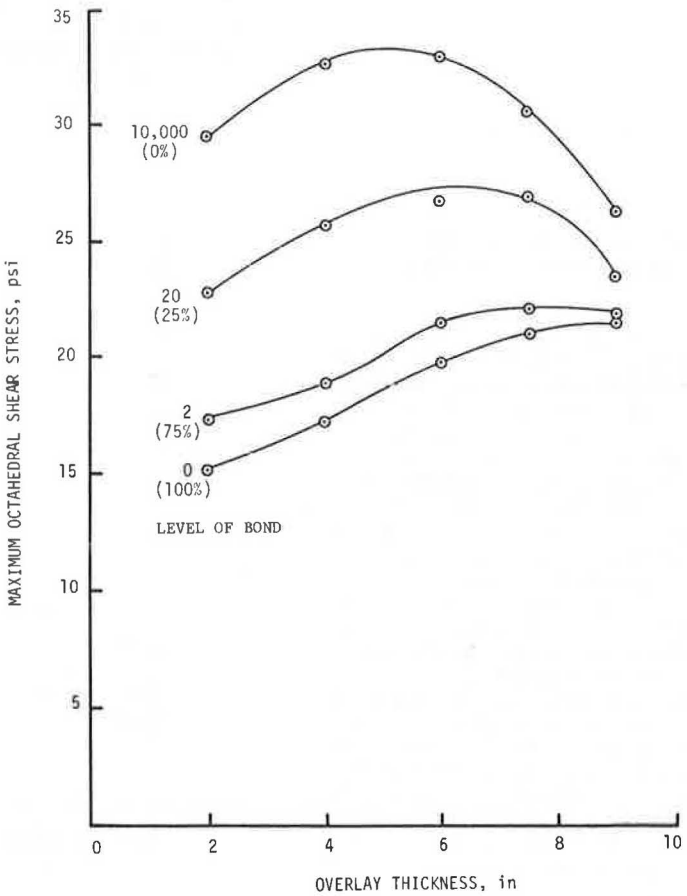

FIGURE 12 Variation of the maximum octahedral shear stress for the rigid pavement sections for various bonds.

below the actual pavement stress to fully activate the material properties that control premature deformation. Precise determination of the stress state in the overlay and the failure criteria under conditions existing in the pavement (temperature and load rate) will be necessary to accurately characterize how close to failure a mixture actually is through laboratory testing.

DESIGN CONSIDERATIONS

Thickness

Unlike the vertical compressive stress, which is practically independent of the overlay thickness, the octahedral shear stress or strain energy of distortion does change with thickness because it depicts a complete stress state. Figure 12 shows the variation in maximum octahedral shear stress as a function of the overlay thickness and degree of interfacial bonding for the rigid pavement. This figure clearly indicates that there is an interaction between thickness, interfacial bonding, and the stress state. In general, thinner overlays develop less octahedral shear stress, which translates to a lower potential for permanent deformation to develop. This helps explain why extremely thin overlays typically do not show rutting as the main failure distress. It is interesting to note that the better the bond, the less important the thickness of the overlay becomes in resisting permanent deformation.

When bond is lost, the critical thickness is in the 5- to 6-in. range. This thickness will have a higher potential for permanent deformation than an overlay only 2 in. thick. Not only is there more material to undergo deformation but the stresses that activate this permanent deformation are going to be higher. A mixture that performed satisfactorily at 2 or 3 in. may not perform well at 6 in. because of the increased stress state. At this point in the study it is not known whether this difference in stress state is significant, but the potential for poorer performance exists.

Material Property Determination

A Mohr's failure envelope must be determined for the bituminous mixture before comparisons of performance can be made using the techniques proposed in this paper. When a Mohr's failure envelope is determined for a particular material, the stress conditions required in the pavement for failure to occur for any vertical principal (compressive) stress from the wheel load and a given tensile strength material property can be calculated from the geometry of the failure envelope. This equation is as follows:

$$\sigma_1 = \sigma_3[(1 + \sin \phi)/(1 - \sin \phi)] + [\sigma_t(1 + \sin \phi) \div \cos \phi] [(1 + \sin \phi)/(1 - \sin \phi)]^{1/2} \quad (3)$$

where

σ_t = tensile strength,
ϕ = the angle of internal friction, and
σ_1, σ_3 = the principal stresses.

Because the potential for failure is proportional to the relative magnitude of the stress state in the pavement to the failure envelope, it is vital to accurately define the Mohr failure envelope in the laboratory under the exact conditions existing in the field that produce stress in the overlay material. These conditions include temperature and rate of loading. Pavement temperatures of interest when premature deformation occurs are generally in the range of 120 to 140°F for the upper 2 in. The loading rate is that which is produced by a moving truck wheel. Triaxial testing to develop a failure envelope should be done at these levels if any comparison is to be made between the existing stress state, the failure envelope, and the short-term performance of the pavement (3). This requirement is a drawback because it is difficult to test at these extremes. Although this is a limitation, it does not make the approach any less correct or applicable to the problem.

With the appropriate computer analysis, the octahedral shear stress in the pavement structure under a given wheel load can be computed. The ratio of the actual stress in the pavement to the failure stress predicted by theory indicates the potential for premature deformation to develop. The closer this value is to unity, the more likely it is that rutting will develop at an accelerated rate. However, in all likelihood failure as exhibited through premature deformation will initiate at a ratio considerably less than unity. Because existing triaxial data have not been developed for the actual conditions in the pavement, few material property indicators are available for construction of a failure envelope representative of the pavement at this time. Future testing as part of this project will develop failure envelopes for typical mixtures and gradations at the extreme values to demonstrate the influence on rutting.

This approach can provide a unifying concept for designing a mixture to resist premature deformation, an item not adequately addressed in current laboratory research testing because of equipment limitations and the lack of accurate modeling of the actual conditions in the pavement. The octahedral shear stress or strain energy of distortion provides a single number to indicate the total stress state in the mixture that is necessary if any procedure is to assess the quality of a mixture for design considerations. This approach also has the long-term potential to allow design of different mixes for different traffic situations. Where lower percentages of truck traffic are predicted, a mixture with a lower failure envelope could be selected over another mixture that may be more expensive because of use of special imported materials required. Current mix design testing cannot begin to provide this type of information. However, this approach will require extensive testing and evaluation before its applicability can be established. Even then the approach may not be implementable in a DOT type of laboratory.

Traffic

The analysis presented here was done for the loading conditions typically used for design or analysis of a pavement, namely a single wheel with a 9,000-lb load, and a resulting contact pressure of 70 psi. Dual wheels may slightly increase the octahedral shear stress under the centerline of each wheel because of the overlapping stress field, but the single-wheel configuration represents a good indication of the loading spectrum for permanent deformation. However, the actual loading conditions on an Interstate pavement are not close to typical nor are they conservative.

Legislation has legalized increased loadings not considered when the pavement was designed or the materials were selected. Mix design procedures were

TABLE 1 Tire Pressure Readings

Reading No.	Air Pressure	Reading No.	Air Pressure
1	94	19	94
2	110	20	100
3	101	21	102
4	94	22	130
5	100	23	100
6	100	24	88
7	104	25	108
8	82	26	80
9	75	27	108
10	80	28	104
11	100	29	86
12	96	30	90
13	86	31	91
14	110	32	72
15	90	33	103
16	105	34	100
17	95	35	100
18	94	36	92

Note: All readings were taken on May 3, 1984, from the last axle on the trailer; they were conducted on FAI-57 in Marion, Illinois.

established long before newer load limits were enacted, and evidence increasingly indicates that the percentage of overloading is rising. This is supported by numerous reports of increases in tire pressures on trucks in service and reports of new weigh-in-motion installations, which indicate the magnitude of overloading. Results of a survey conducted on FAI-57 at Marion, Illinois, are given in Table 1. These measurements indicate that actual loading conditions are considerably more severe than those usually assumed for design and analysis. The average tire pressure was 96 psi on this Interstate, with measurements up to 130 psi. If a 120-psi vertical stress is used for the vehicle loading in the analysis presented in this paper, the bituminous materials are likely approaching a failure state under every loading. This is demonstrated in Figure 13 for comparison with the 70-psi tire pressure used in this study.

A large number of loadings of this magnitude would significantly accelerate the appearance of rutting in a short time period, particularly during the hot summer months. These loadings would be particularly damaging if the interface bonding was nonexistent or had deteriorated for some reason. Under these conditions, failure would appear in a short time, as has been observed recently on several Interstate pavements.

SUMMARY AND CONCLUSIONS

The problem of premature deformation, rutting that develops in a short time, in some bituminous overlays of concrete pavements may be the result of material, pavement, and/or load interactions that are considerably different from the more commonly accepted interactions that have been investigated previously. Current technology has not accurately predicted this phenomenon of premature deformation. Consideration of failure theory in examining this type of failure indicates that viable approaches exist that provide parameters suitable for indicating a total stress state in the material related directly to the type of failure observed. Specifically, the octahedral shear stress or strain energy of distortion developing in the overlay more closely relates to permanent deformation than other stress parameters used in the laboratory to characterize bituminous mixtures. The information presented in this paper can be interpreted to support the following conclusions:

1. Actual stress-strain levels in a pavement overlay mixture are significantly higher than levels used in the laboratory to characterize permanent deformation, and current vehicle loadings are increasing these differences to the point at which a marginally acceptable mixture may fail under a very few loads.
2. The octahedral shear stress in an asphalt

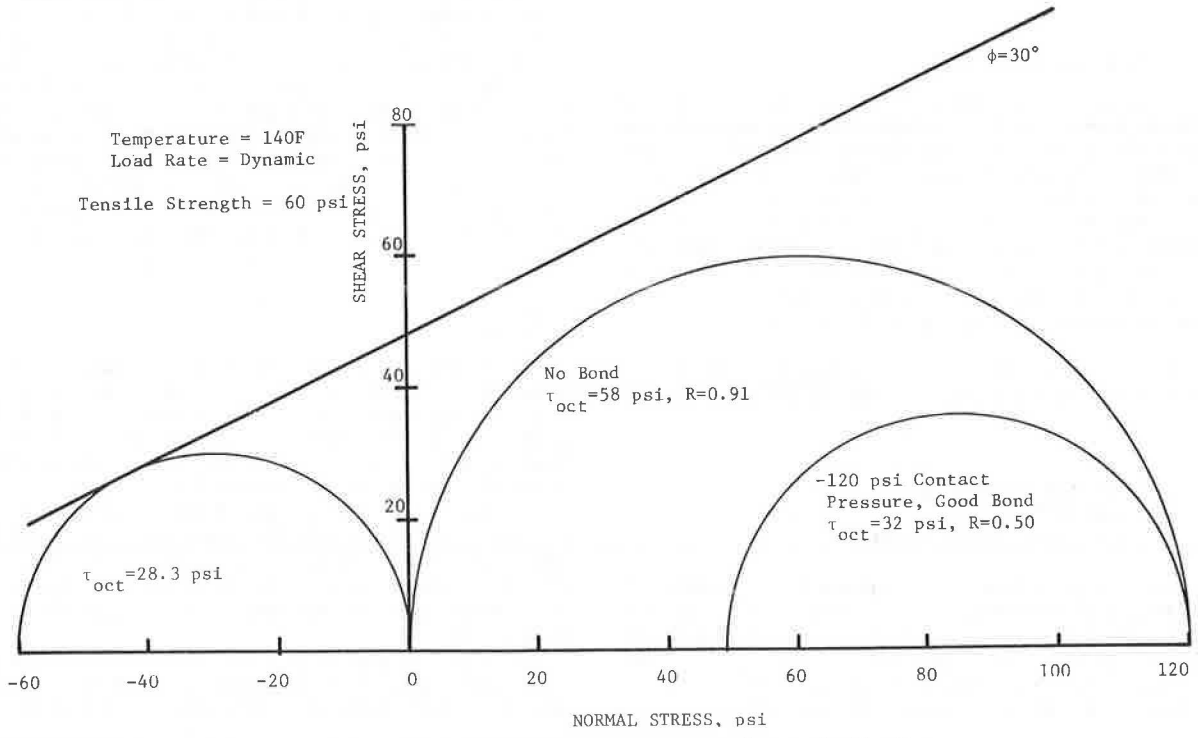

FIGURE 13 Mohr circle representation of the stress state in an overlay under heavy wheel loading.

mixture provides a unique parameter capable of describing the stress state in the mixture. When the Mohr-Coulomb failure envelope is defined, the octahedral shear stress in the pavement can indicate how close to failure the mixture may be when loaded. Adjustments to mix quality can be made to improve the relationship between loading and failure stresses.

3. By using octahedral shear stress to indicate the total stress state in the mix, it can be demonstrated how varying pavement conditions can alter the potential for premature deformation. These pavement conditions include original pavement type, temperature, rate of load, and--most critically--the condition of the bond at the interface between the overlay and the original surface.

4. Laboratory testing of mixes must be changed to allow testing to be performed at the boundary conditions found in the actual pavement, primarily temperature, rate of load, and stress level, as indicated by the octahedral shear stress.

5. Interface bonding needs to be investigated, particularly for high-volume rigid pavement installations where the potential for loss of bonding is greatest and the need for good bonding is also greatest.

6. Further in-depth studies into the actual loading conditions of today's trucks need to be conducted to accurately define the loading parameters that should be used to characterize mixture performance.

7. Laboratory testing using triaxial compression and tensile strength determinations and repeated loadings must be conducted to validate the possible applicability of the octahedral shear stress as a mixture design parameter for laboratory use. The results must be substantiated by field performance data.

ACKNOWLEDGMENTS

This paper was prepared as a part of the study entitled Structural Characterization of Bituminous Mixes Used as Overlays on Heavily Trafficked Concrete Pavements, by the Department of Civil Engineering in the Engineering Experiment Station, University of Illinois at Urbana-Champaign. This study is funded by the FHWA, U.S. Department of Transportation, as a part of the DOT's Program of University Research. The authors would like to extend their appreciation to all those who provided data to this study.

REFERENCES

1. F.B. Seely and J.O. Smith. Advanced Mechanics of Materials. John Wiley & Sons, Inc., New York, 1966.
2. F.L. Roberts and T.W. Kennedy. Asphalt Concrete Overlay Design Considerations. Report FHWZ/TX-84/13+318-1F. Center for Transportation Research, University of Texas at Austin, Austin, Feb. 1984.
3. S.H. Carpenter and T.J. Freeman. An Analytical Study of Bituminous Mixtures Used as Overlays on Concrete Pavements. Interim Report. FHWA, U.S. Department of Transportation, Jan. 1984.
4. J. Morris, R.C.G. Haas, P. Reilly, and T.T. Hignell. Permanent Deformation in Asphalt Pavements Can Be Predicted. Proc., Association of Asphalt Paving Technologists, Vol. 43, 1974, pp. 41-76.
5. D. Janssen. The Influence of Asphalt Concrete Overlays on the Durability of Portland Cement Concrete Pavements. Ph.D. dissertation. Civil Engineering Department, University of Illinois, Urbana, Aug. 1985.
6. J. Uzan, M. Livneh, and Y. Eshed. Investigation of Adhesion Properties Between Asphaltic-Concrete Layers. Proc., Association of Asphalt Paving Technologists, Vol. 47, 1978, pp. 495-521.
7. N.W. McLeod. A Rational Approach to the Design of Bituminous Paving Mixtures. Proc., Association of Asphalt Paving Technologists, Vol. 21, 1952, pp. 82-224.

Publication of this paper sponsored by Committee on Strength and Deformation Characteristics of Pavement Sections.

Typical Curves for Evaluation of Pavement Stiffness from Dynaflect Measurements

BOUTROS E. SEBAALY and MICHAEL S. MAMLOUK

ABSTRACT

Currently, no direct solution exists that provides the pavement in situ layer moduli from deflection measurements. Current methods evaluate the pavement layer moduli from deflection measurements by using either empirical approaches or static layered elastic computer programs with iterative solutions. In this study, mechanistically based typical curves and tables are developed to evaluate the moduli of the four highway pavement layers--surface, base, subbase, and subgrade--from the Dynaflect measurements based on both static and dynamic analyses. The curves and tables are developed by using the Chevron computer program for the static analysis and the DYNAMIC computer program for the dynamic analysis. The results are applicable to a large number of typical combinations of layer thicknesses and material moduli. If the layer thicknesses are known and the Dynaflect measurements are determined, the four moduli of the pavement layers can be evaluated. The curves and tables developed are simple to use, without the need for previous empirical relationships or computer analysis. The study demonstrates that the static and dynamic predictions of the layer moduli are different in most cases. However, the research technique used in this study needs field verifications or other independent validation procedures to support the obtained results.

The rational rehabilitation of rapidly deteriorating highway pavements requires knowledge of the stiffness of existing pavements. Nondestructive testing (NDT) is being widely used to evaluate the load-carrying capability of pavements. Unlike laboratory testing, NDT is fast and accurate and can provide the in situ layer moduli with a minimum of disturbance and cost.

The nondestructive evaluation of pavements generally follows one of two main techniques: wave propagation or surface deflection measurements. The deflection measurement tests have been extensively used by many highway agencies because of their simplicity and their ability to model real traffic load intensities and durations. Therefore, the layer moduli computed from surface deflection measurements are more nearly representative of field conditions.

One of the most widely used deflection measurement devices is the Dynaflect, which applies a steady-state harmonic load with a peak-to-peak load of 1,000 lb and a frequency of 8 Hz. The force is transmitted to the pavement through two 4-in.-wide steel wheels with a 16-in. outside diameter, spaced 20 in. apart. The peak-to-peak deflections are measured by using five deflection sensors (geophones) located midway between the two steel wheels and at four other locations 1 ft apart, as shown in Figure 1.

Different modes of loading (static, harmonic, transient, etc.) result in different deflection measurements for the same load intensities (1-3), as shown in Figure 2. The pavement response is highly dependent on the mode of loading, load frequency, or both as shown in Figure 3. To date, most methods of analysis treat different modes of loading identically. The dynamic analysis has recently been applied to pavement response to deflection measurement devices in several studies (4-8). These studies indicate that the dynamic response of pavement may be significantly different from the static response because of the inertia of the pavement system. Because the Dynaflect applies loads with an 8-Hz frequency, a resonant condition might occur if the natural vibration frequency of the pavement structure is close to that frequency. In this case, the pavement deflection is magnified and, unless the dynamic analysis is used, the interpretation of results may be misleading.

The first step in the evaluation process is the estimation of the layer moduli, after which a decision is made to determine the required overlay thickness based on previous field correlations. No direct theoretical solution is currently available to evaluate the layer moduli if the surface deflections and the layer thicknesses are known. In the current techniques, iterative solutions are used in which initial estimates of the moduli are assumed and the corresponding surface deflections are computed. The estimated moduli are then adjusted to improve the fit between the computed and the measured deflections.

Although this method provides a reasonable degree of accuracy, it requires use of a computer, which may not be accessible, and the experience to use it, which may not be available. Also, because the layer moduli are sensitive to deflection measurements and any iteration procedure allows a certain amount of tolerance, the resulting solution is not unique. In addition, all the commonly available multilayer computer programs are based on static analyses that do not match the dynamic loads applied by NDT devices.

Typical curves were recently developed to estimate the layer moduli from surface deflections by using the static method of analysis (9). The objective of this study was to provide typical curves and tables to enable the highway engineer to estimate the in situ moduli of pavement layers from surface deflections by using the dynamic analysis. The curves

Center for Advanced Research in Transportation, Arizona State University, Tempe, Ariz. 85287.

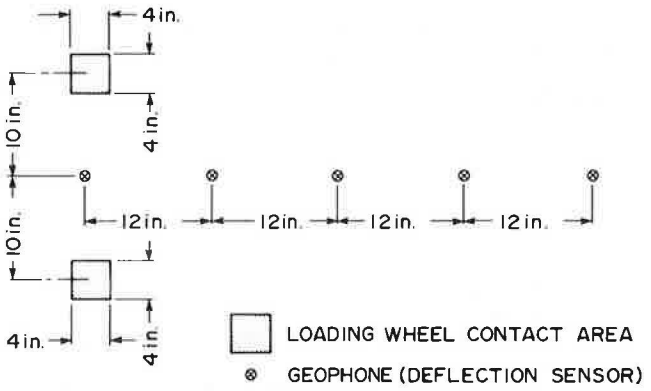

FIGURE 1 Location of Dynaflect loading wheels and geophones.

and tables can be easily used with an acceptable degree of accuracy, without the need for using the computer. Moreover, the static solution can also be obtained by using these curves and tables, and a comparison between the static and the dynamic predictions can be made.

ASSUMPTIONS

In this study, the pavement structure is assumed to consist of four layers: surface, base, subbase, and subgrade. The materials are idealized to be homogeneous, isotropic, and linear elastic or viscoelastic. Thus, the material of each layer is characterized by Young's modulus, Poisson's ratio, mass density, and material damping ratio. Further, the analysis assumes existence of laterally unbounded soil and pavement layers, underlain by a rigid bedrock at a finite depth. Full interface bonding (no slip) conditions are assumed at the layer interfaces.

NONLINEARITY AND STRESS SENSITIVITY

For many years it has been known that the subgrade material is nonlinear. However, if the load is repeated several times, the effect of nonlinearity is reduced. For example, Figure 4 shows a typical stress-strain relationship for a soil specimen subjected to a triaxial state of stress in which the axial stress is varied in a pulsating form while the confining pressure is kept constant. It can be observed that the nonlinearity is apparent when the

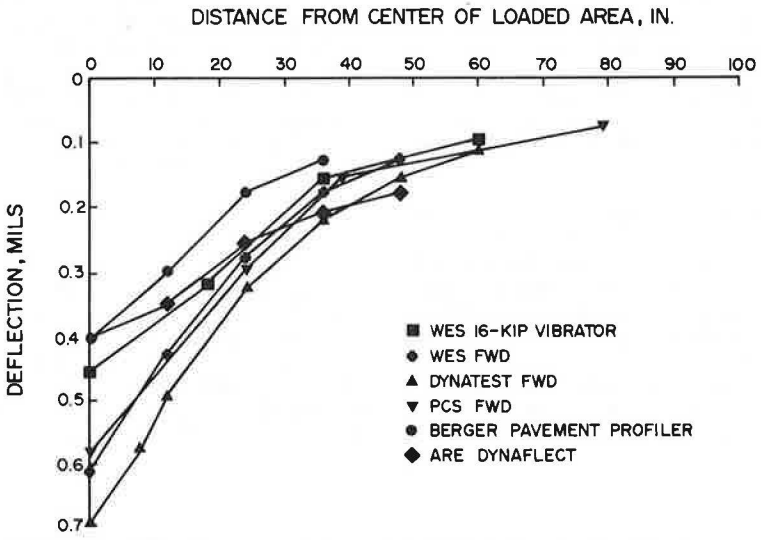

FIGURE 2 Deflection measurements of six NDT devices as a flexible airport pavement normalized to 1,000-lb force level *(2)*.

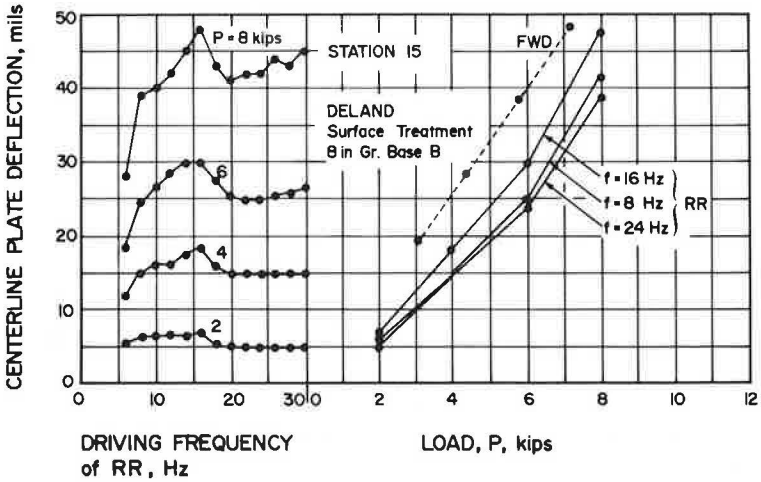

FIGURE 3 Road Rater 2008 and falling weight deflectometer data *(3)*.

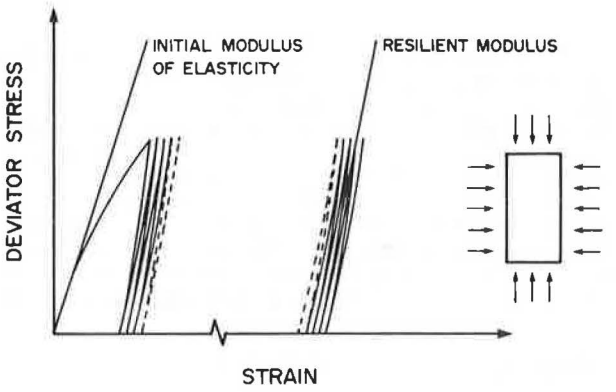

FIGURE 4 Definition of resilient modulus.

load is applied for the first time, after which the material can be assumed to be linear without significant error.

In Figure 4, the initial slope of the curve when the load is applied for the first time can be defined as the initial modulus of elasticity, or initial Young's modulus. The deviator stress divided by the recoverable strain is defined as the resilient modulus, as represented by the slope of the second line in Figure 4. Therefore, the resilient modulus is the modulus of the material after many load repetitions at which the effect of nonlinearity becomes small. This indicates that if a repeated type of load is applied, the resilient modulus can be used instead of Young's modulus in a linear analysis with a reasonable approximation.

On the other hand, the stress-strain relationship is affected by the state of stress of the material. However, when the load is applied several times, the resilient modulus does not change considerably when the state of stress is changed. For example, Figure 5 shows a typical stress-deflection diagram from repetitive plate load testing on a subgrade material according to ASTM test procedure D1195 (10). It is shown in this figure that the stress divided by the recoverable deflection is almost constant regardless of the applied stress level. According to the Boussinesq solution for one-layer systems (11),

$$\Delta = pa/E(F) \quad (1)$$

or

$$E = (p/\Delta)aF$$

where

Δ = deflection,
p = stress,
a = radius of plate,
E = Young's modulus,
F = a factor that is a function of z/a and r/a,
z = depth of the point of interest, and
r = lateral distance between load and the point of interest.

Thus, if p/Δ is almost constant for repeated loads at different stress levels, the modulus of the material remains approximately constant.

It should be noted that laboratory resilient moduli obtained for soil samples subjected to triaxial states of stress (AASHTO T274) vary at different confining pressures. This change of resilient modulus with change in confining pressure appears to contradict the previous field results shown in Figure 5. This contradiction, however, is expected because the confining pressure in the laboratory test is usually kept constant when the axial load is changed, whereas the stresses in the three orthogonal directions are simultaneously changed when the load is applied in the field.

METHOD OF ANALYSIS

The dynamic solution used in this study is based on the Helmholtz equation, which is the governing equation for steady-state elastodynamics (12). Because no exact solution to this equation is available for harmonic loadings applied on a multilayered system, a simplified numerical solution is used (13). It is assumed in this solution that the displacement fields

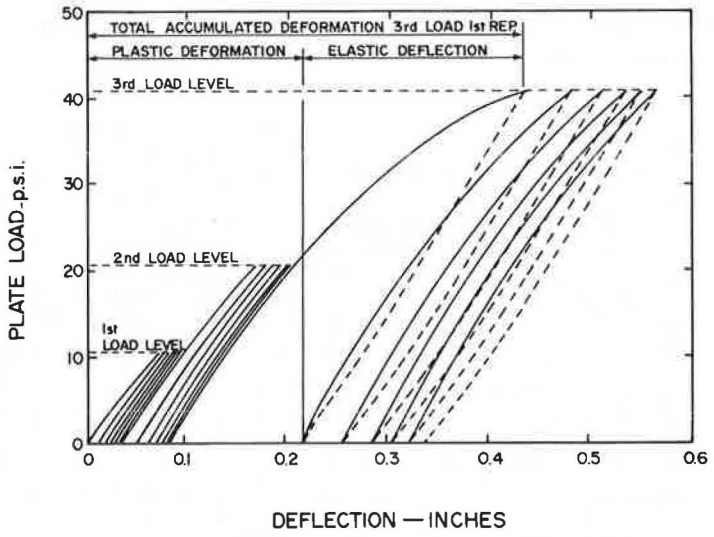

FIGURE 5 Typical load-deflection diagram from repetitive plate load testing *(10)*.

vary linearly (in the direction of layering) between adjacent interfaces. Therefore, it is important that sufficiently thin artificial sublayers be specified in order to preserve accuracy. The dynamic solution is developed in the computer program DYNAMIC (13).

The input data required in the computer program are number of layers (and sublayers), layer thicknesses, depth to bedrock, mass densities, Young's moduli, Poisson's ratios, and material damping ratios representing the viscous effect. The computer program also requires information on diameter of the load plate, location of the load with respect to various layers, frequency of loading, and locations where results are required. The current version of the program is capable of computing the in-phase and out-of-phase deflections in the vertical, radial, and tangential directions at any location throughout the pavement system. Because the solution assumes linear material behavior, the results are obtained due to a load intensity of 1 psi. Further, the DYNAMIC program with zero load frequency was checked versus the Chevron program under identical conditions; it was found that it provided the same results.

Note that the bedrock reflects the waves generated by the dynamic excitations, and consequently the pavement response is influenced by the depth to bedrock. However, in the static analysis the depth to bedrock is not as significant as it is in the dynamic analysis. Also, the density is not required in the static analysis to characterize the materials because the inertial effect is ignored.

To simulate the load applied by the Dynaflect, an 8-Hz harmonic load is assumed to be uniformly distributed on a circular area of 16 $in.^2$ at the pavement surface. The vertical deflections are computed at distances of 10.0, 15.6, 26.0, 37.4, and 49.0 in., representing various geophone locations. Because the loads on the two wheels are simultaneous, the response due to the two wheels can be obtained by superposition. By using this load representation, two minor approximations are made. The first approximation is the assumption that the contact areas are circular instead of rectangular, and the second approximation is the use of uniformly distributed loads instead of rigid wheels. The errors resulting from these two approximations are small, particularly away from the load.

DEVELOPMENT OF TYPICAL CURVES AND TABLES

A number of typical curves and tables are developed in this study to aid the highway engineer in evaluating the in situ pavement moduli from the Dynaflect deflection data. The Chevron computer program was used to evaluate the surface deflections for a wide range of layer thicknesses and moduli combinations due to a load intensity of 1 psi. Typical Poisson's ratios of 0.35, 0.4, 0.4, and 0.45 were used for surface, base, subbase, and subgrade materials, respectively. A total of 15 thicknesses and 10 moduli combinations were used (150 pavement sections x 4 moduli). The surface thicknesses ranged from 2 to 6 in., the base thicknesses from 4 to 8 in., and the subbase thicknesses from 4 to 12 in. The subgrade was assumed to be semi-infinite. A wide range of layer moduli was also used with typical modulus ranges for each layer.

To expand the scope of the study, the deflection values obtained in the previous step (using static analysis) were used to backcalculate the corresponding layer moduli using the dynamic analysis with subgrade thicknesses of 30 and 60 ft. An iterative scheme was used based on the fact that surface deflections remote from the loaded area are primarily governed by the stiffness of the deeper layers (6,14). In this procedure, the modulus values used in the static solution were assumed as initial moduli for the dynamic solution. The DYNAMIC program is used to calculate deflections at various geophone locations. The calculated deflections are compared with measured deflections. If the deflections do not agree, the moduli are changed through an iterative procedure until a set of modulus values is determined that produces deflections from the DYNAMIC program that match the deflections obtained from the Chevron program. A match is considered adequate when the error in deflection at each geophone location does not exceed 3 percent.

In the DYNAMIC program typical mass densities of 145, 140, 140, and 125 lb/ft^3 were used for surface, base, subbase, and subgrade materials, respectively. Also, a typical material damping ratio of 5 percent was used (15). Meanwhile, Poisson's ratios that were used in the static analysis were also used in the DYNAMIC program. It should be emphasized that minor errors in estimating these parameters do not significantly change the results.

Following the preceding procedure, three sets of layer moduli are available (1,800 moduli). The first set of moduli is associated with the static prediction, and the other two sets of moduli are associated with the dynamic analysis with 30- and 60-ft subgrades. All three sets of moduli have the same deflections but are computed either with different procedures or with different subgrade thicknesses.

The goals were to minimize the number of relationships and maximize the range of applications while maintaining simplicity of use. Therefore, several considerations had to be kept in mind during the development of the typical curves. Because the materials are assumed to be linear, doubling the layer modulus values results in reducing the surface deflections by a factor of 1/2, and so forth. Therefore, normalized curves are developed by dividing the five computed deflections by the computed deflection at Geophone Number 1. This results in five deflection ratios (δ/δ_1) with a unit value at the first geophone. In this case the deflection curves represent certain deflection shapes rather than actual deflection measurements. The normalized curves are shown in Figures 6-13 for various layer thickness combinations. For each thickness combination, 10 normalized curves are shown (A to J) representing 10 moduli ratios.

Three sets of tables have also been prepared to be used with the curves. Table 1 gives the static constants and Tables 2 and 3 present the dynamic factors for 30- and 60-ft subgrades for all thickness and curve combinations. The static constant is defined as the layer modulus based on static analysis times deflection of Geophone Number 1 during the original development of the curves times 31.25 times 2. The factor 31.25 is the peak-to-peak load intensity applied by the Dynaflect on each loading wheel, whereas the factor 2 is used to account for the two wheels. On the other hand, the dynamic factor is defined as the modulus obtained by using dynamic analysis divided by the modulus obtained using the static analysis.

USE OF TYPICAL CURVES AND TABLES

To use the typical curves, the user is expected to know the layer thicknesses from pavement records and the peak-to-peak deflection readings of the five

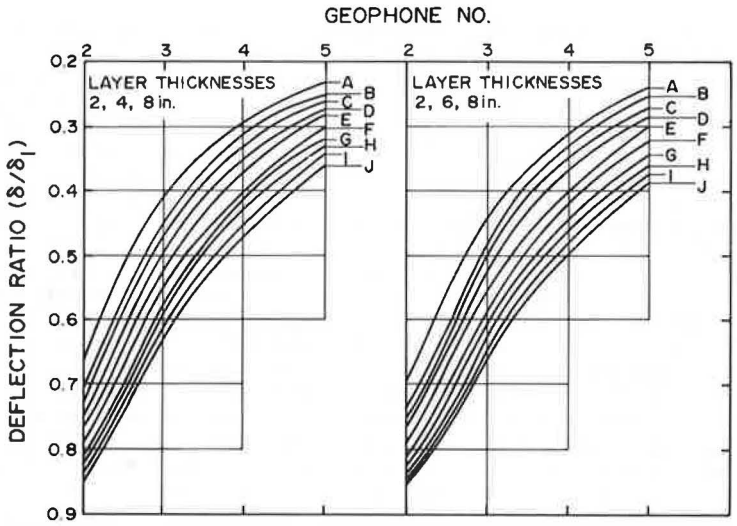

FIGURE 6 Typical normalized deflection curves for layer thicknesses 2, 4, and 8 in. and 2, 6, and 8 in.

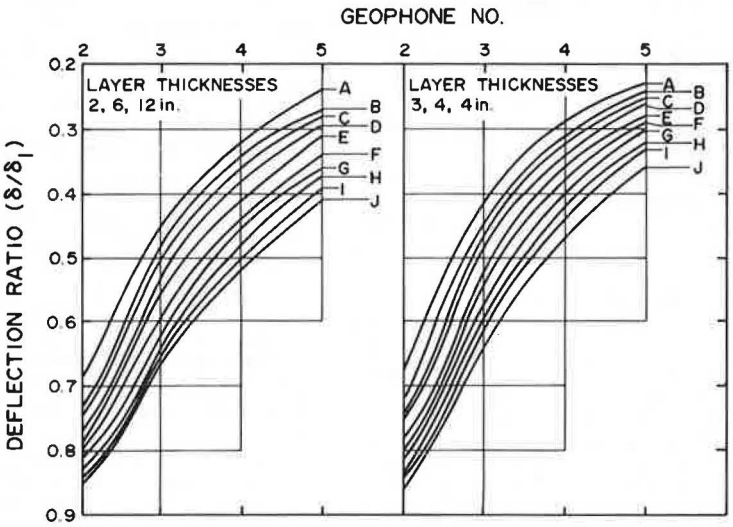

FIGURE 7 Typical normalized deflection curves for layer thicknesses 2, 6, and 12 in. and 3, 4, and 4 in.

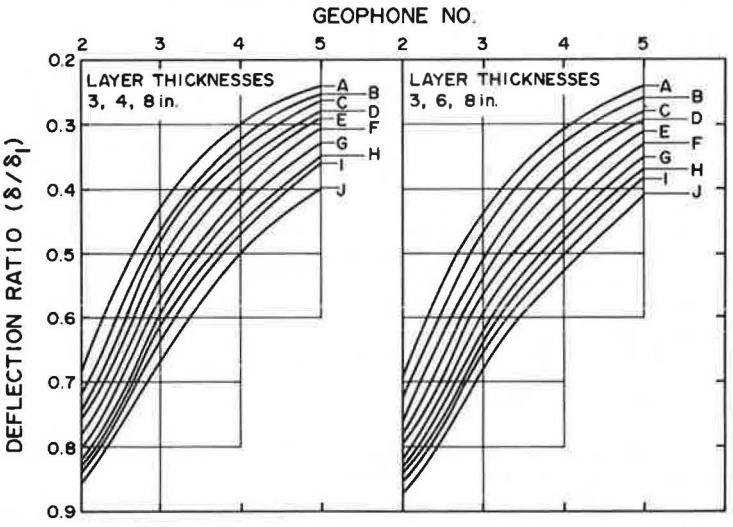

FIGURE 8 Typical normalized deflection curves for layer thicknesses 3, 4, and 8 in. and 3, 6, and 8 in.

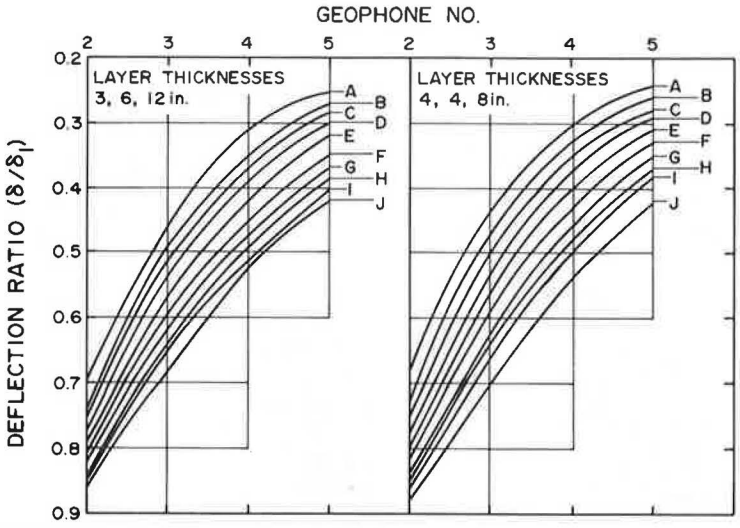

FIGURE 9 Typical normalized deflection curves for layer thicknesses 3, 6, and 12 in. and 4, 4, and 8 in.

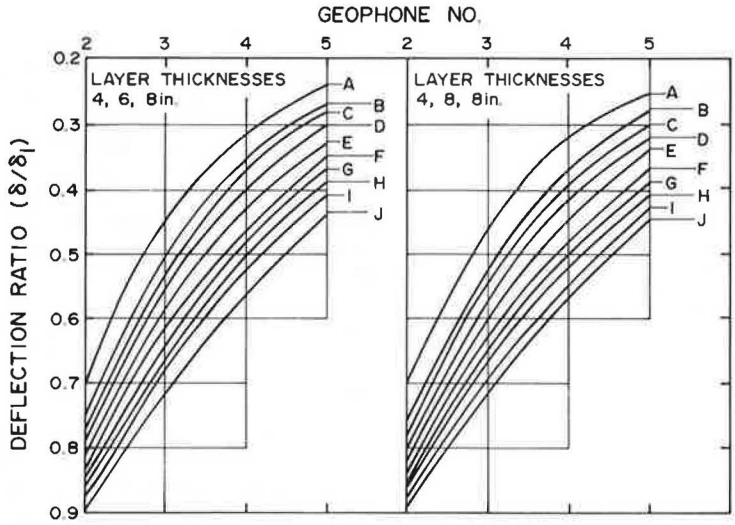

FIGURE 10 Typical normalized deflection curves for layer thicknesses 4, 6, and 8 in. and 4, 8, and 8 in.

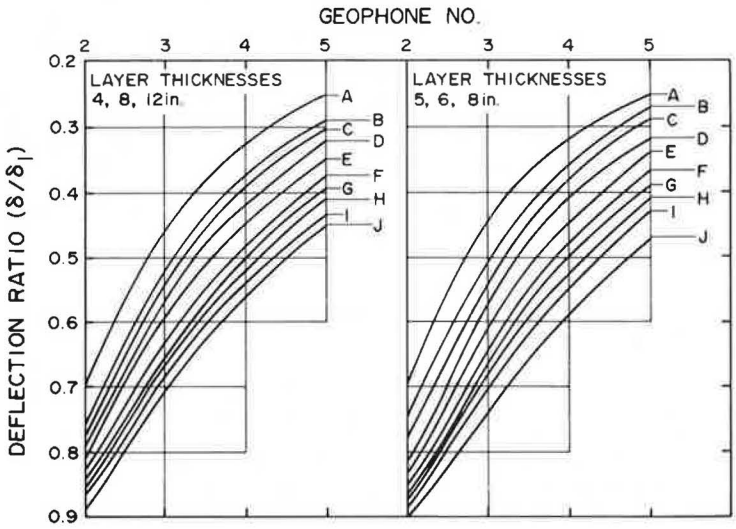

FIGURE 11 Typical normalized deflection curves for layer thicknesses 4, 8, and 12 in. and 5, 6, and 8 in.

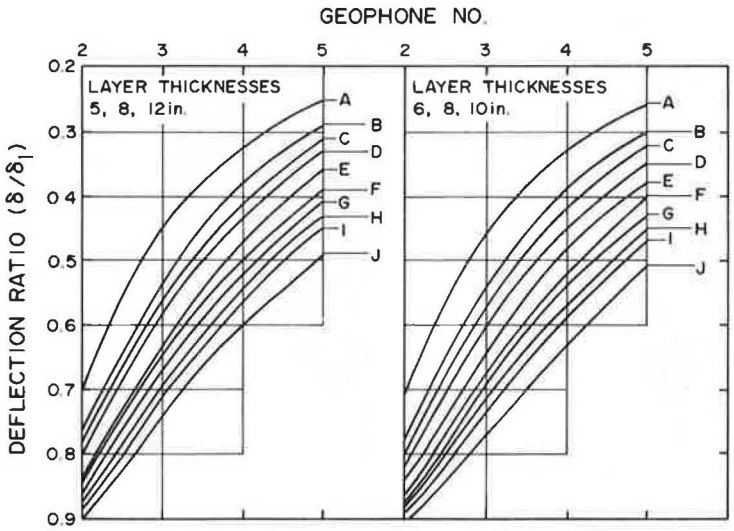

FIGURE 12 Typical normalized deflection curves for layer thicknesses 5, 8, and 12 in. and 6, 8, and 10 in.

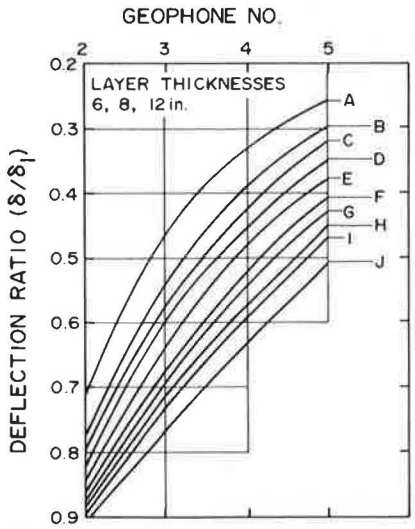

FIGURE 13 Typical normalized deflection curves for layer thicknesses 6, 8, and 12 in.

geophones of the Dynaflect. The deflection ratios are determined, which are the deflection values divided by the deflection at Geophone Number 1. The graph corresponding to the appropriate thickness combination is entered with the deflection ratios and the geophone numbers. The values are plotted and the closest typical curve (A-J) is then determined.

To obtain the layer moduli based on the static solution, the following equation is used:

$$E_{i(static)} = [(\text{static constant})_i]/\delta_1 \quad (2)$$

where

$E_{i(static)}$ = modulus of layer i based on static analysis (psi);
i = 1, 2, 3, and 4, representing the surface, base, subbase, and subgrade, respectively;
$(\text{static constant})_i$ = value given in Table 1 for Layer i (lb/in.); and
δ_1 = measured peak-to-peak deflection at Geophone Number 1 (in.).

It should be noted that interpolation is allowed in using these curves, but should be used with caution because the curves are not always parallel.

If the layer moduli are sought based on dynamic analysis, the user first has to estimate the approximate depth to bedrock from construction or geological records. The dynamic factors of various layers are then obtained from either Table 2 or Table 3, or interpolated between both tables, and used in the following equation:

$$E_{i(dynamic)} = \{[(\text{static constant})_i]/\delta_1\} (\text{dynamic factor})_i \quad (3)$$

where

$E_{i(dynamic)}$ = modulus of Layer i based on dynamic analysis (psi), and
$(\text{dynamic factor})_i$ = value given in Table 2 or Table 3, or interpolated between both tables for Layer i.

The typical modulus for asphalt concrete is approximately between 100,000 and 700,000 psi, depending on the temperature, and the granular base and subbase moduli should range between 20,000 and 100,000 psi. Typical values of subgrade moduli vary from 3,000-5,000 psi for cohesive clay soils to 20,000-30,000 psi for fine-grained sandy soils. These typical ranges of moduli were used in the development of the curves and tables in this study. Thus, it is not expected that moduli outside of these ranges be obtained based on dynamic analysis if the curves and tables are used.

TYPICAL EXAMPLE

A Dynaflect test was performed on a four-layer flexible pavement with surface, base, and subgrade thicknesses of 4, 4, and 8 in., respectively. Geological records indicate that the bedrock is deep. The Dynaflect peak-to-peak surface deflections are 0.002806, 0.002250, 0.001571, 0.001125, and 0.000860 in. at Geophones 1, 2, 3, 4, and 5, respectively. Using the typical curves and tables developed in this study, it is required that the modulus values of various pavement layers be estimated as well as that of the subgrade based on static and dynamic analyses.

TABLE 1 Static Constants

Thicknesses (in.)	Layer	Curve A	B	C	D	E	F	G	H	I	J
2, 4, 8	1	21.9	12.7	19.4	108	3,285	4,356	3,903	7,207	7,779	1,934
	2	11	10.6	46.3	27.3	109	149	221	111	211	835
	3	40	34	47.3	58.5	55.9	58.9	60.7	75.9	68.4	59.5
	4	22.6	22.1	21.9	21.4	19.9	18.7	17.9	17.1	16.6	16
2, 6, 8	1	21.9	39	20.6	6,427	2,871	3,767	674	4,761	2,507	4,319
	2	22.4	42.1	91.4	64.3	43.1	117	201	178	448	699
	3	41.3	50.5	50.9	73.9	69.6	50.9	64.8	36.3	27.7	16.4
	4	23	21.7	20.9	19.6	18.4	17.4	16.8	16.2	15.9	15.6
2, 6, 12	1	20.8	15.5	499	1,738	2,550	320	3,900	4,344	7,790	2,840
	2	28.6	64.2	298	72.3	119	129	108	118	128	693
	3	36.6	48.2	71.3	40.5	47.9	53.7	40.8	43.3	37.6	27.8
	4	22.6	21.3	20.5	18.7	18	16.8	16.2	15.4	14.9	14.3
3, 4, 4	1	24	13.3	62.8	2,318	3,518	4,780	5,881	424	5,711	9,289
	2	19.1	11.1	31.4	29	52.8	39.8	44.1	47.2	50.2	54.9
	3	86.3	31.5	168	193	81.7	109	92.9	219	172	104
	4	24.6	22.3	22.7	21.7	20.7	19.6	18.9	17.9	17.4	16.3
3, 4, 8	1	453	818	1,144	2,045	3,058	2,828	2,032	1,150	1,945	13,688
	2	34.2	46.2	47.1	34.1	45.9	99.8	200	446	476	593
	3	81.7	29.1	56.4	70.8	61.8	58.3	56.2	54.9	53.1	18.3
	4	23.3	20.6	21.5	20.2	19.2	18	17.2	16.5	15.9	17
3, 6, 8	1	432	765	1,029	1,819	1,965	1,370	4,239	1,615	1,913	3,546
	2	43.6	61.5	73	72.8	105	154	88.9	561	556	257
	3	43.6	38.3	42	45.5	41.8	41.6	63.4	18.7	21.4	26.1
	4	22.7	21.9	20.3	19.1	18	17	16.4	16	15.3	14.6
3, 6, 12	1	377	696	792	179	587	1,150	307	4,421	7,200	5,959
	2	32.9	69.0	40.8	98	109	103	98.5	104	113	172
	3	59.8	35.8	43.3	42.9	39.8	40.7	33.5	31.9	26.4	28.8
	4	19.5	20.6	19.5	18.6	17.4	16.4	15.8	15.1	14.6	13.8
4, 4, 8	1	446	784	52.9	1,358	1,766	1,618	1,039	292	444	3,045
	2	17.6	19.6	26.5	23.8	42.1	48.7	273	584	577	491
	3	89.8	80.4	73.9	81	64.1	35.8	47.6	90	73	22.6
	4	23.3	21.7	21	19.4	18.2	17.2	16.4	15.7	15.2	14.3
4, 6, 8	1	426	715	92.5	1,012	1,011	1,010	1,688	3,524	3,178	9,805
	2	29.5	44.2	53.8	65.5	104	153	154	29.5	224	151
	3	57.3	48.5	53.9	44.7	39.5	35.4	26.3	122	13.3	13.1
	4	22.7	20.6	19.8	18.5	17.4	16.3	15.7	14	14.7	13.5
4, 8, 8	1	326	652	43.3	209	618	1,218	1,720	2,025	4,238	1,729
	2	37.8	60.7	43.7	99	112	116	132	156	24.2	282
	3	45.2	34.8	59.4	52.3	28.7	20.6	15.2	12.2	159	11.4
	4	22.2	19.7	18.9	16.7	16.5	15.8	15.4	14.8	12.2	13.3
4, 8, 12	1	174	30.7	104	321	1,915	1,179	2,109	190	733	387
	2	41.8	64.5	77.9	82.9	80.2	100	104	380	379	84.8
	3	35.8	37.6	35.1	32.6	37.9	26.4	20.9	37.1	16.9	30.7
	4	22	19.4	18.4	17.3	15.5	15.4	14.8	14	13.6	12.5
5, 6, 8	1	320	186	913	735	736	612	1,278	4,519	1,376	1,124
	2	28.1	18.3	22.8	65.7	108	174	169	452	304	525
	3	50.4	147	126	39.9	34	31	20.6	11.3	13.7	11.3
	4	22.4	21.3	17.8	17.8	16.6	15.5	15	11.6	14	13
5, 8, 12	1	374	33.3	759	238	995	336	658	689	1,294	356
	2	58.7	66.3	68.7	85.6	130	127	134	174	176	356
	3	22.4	35.7	27	31.6	15.3	29.4	23.1	21.6	15.6	28.2
	4	22.7	19	18.4	16.7	16.7	14.8	14.2	13.6	13.1	11.8
6, 8, 10	1	111	132	79.6	1,232	192	191	1,258	584	253	333
	2	36.1	63.8	88.9	44.7	205	16.7	18.9	214	326	416
	3	38.3	30.8	32.8	23.2	23	26.6	126	12.7	23.8	24.7
	4	21.6	18.7	17.5	15.9	15.7	14.5	12	13.3	12.4	11.4
6, 8, 12	1	125	47.8	91.9	173	281	215	354	268	240	3,610
	2	35.5	67.9	81.8	94.9	116	162	174	241	266	19.7
	3	39.7	32.4	31.1	30.2	26.3	26.3	21.9	24.7	29.1	35.5
	4	21.3	18.6	17.4	16	14.9	14.3	13.7	12.8	12.2	11.1

The first step is to determine the deflection ratios δ/δ_1 as 0.8, 0.56, 0.4, and 0.31 at Geophones 2, 3, 4, and 5, respectively. By plotting these deflection ratios on the figure corresponding to layer thicknesses of 4, 4, and 8 in. (Figure 9), it can be observed that the data fit Curve E. The static constants are obtained from Table 1 as 1,766, 42.1, 64.1, and 18.2 for the surface, base, subbase, and subgrade, respectively. By using Equation 2, the moduli of various materials are calculated as follows:

$E_{1(static)}$ = 1,766/0.002806 = 629,400 psi.

$E_{2(static)}$ = 42.1/0.002806 = 15,000 psi.

$E_{3(static)}$ = 64.1/0.002806 = 22,800 psi.

$E_{4(static)}$ = 18.2/0.002806 = 6,500 psi.

To obtain the layer moduli based on the dynamic analysis, the dynamic factors are determined. These factors are obtained from Table 3 as 0.402, 2.7, 0.666, and 0.797 for the surface, base, subbase, and subgrade, respectively. By using Equation 3, the moduli are as follows:

$E_{1(dynamic)}$ = 629,400 x 0.402 = 253,000 psi.

$E_{2(dynamic)}$ = 15,000 x 2.7 = 40,500 psi.

$E_{3(dynamic)}$ = 22,800 x 0.666 - 15,200 psi.

$E_{4(dynamic)}$ = 6,500 x 0.797 = 5,200 psi.

SIGNIFICANCE OF THE DYNAMIC ANALYSIS

The inertia of the pavement system is reflected in the dynamic factors given in Tables 2 and 3. Ob-

TABLE 2 Dynamic Factors for 30-ft Subgrade

Thicknesses (in.)	Layer	Curve A	B	C	D	E	F	G	H	I	J
2, 4, 8	1	4	13.3	1.32	5	0.25	0.25	0.338	0.25	0.286	2.07
	2	4	8	3.72	3.97	1.21	0.976	0.715	1.51	0.844	0.24
	3	0.823	1.12	0.723	0.771	0.881	0.987	1.09	0.949	1.14	1.35
	4	0.969	0.98	0.901	0.842	0.824	0.775	0.737	0.701	0.669	0.627
2, 6, 8	1	4	4	1.3	0.075	0.25	0.25	1.63	0.322	0.75	0.75
	2	1.96	1.85	0.972	1.5	2.67	1.07	0.656	0.802	0.335	0.232
	3	0.796	0.694	0.699	0.544	0.619	0.987	0.848	1.69	2.38	3.94
	4	0.952	0.897	0.85	0.819	0.781	0.722	0.653	0.629	0.592	0.52
2, 6, 12	1	4	9.36	0.5	0.25	0.25	2.55	0.25	0.296	2	0.977
	2	1.46	1.13	0.28	1.2	0.859	0.844	1.09	1.02	0.974	2
	3	0.851	0.753	0.466	0.895	0.798	0.81	1.2	1.19	1.45	2
	4	0.919	0.85	0.813	0.773	0.709	0.646	0.604	0.556	0.523	0.484
3, 4, 4	1	4	13.3	5	0.25	0.25	0.25	0.25	0.477	0.44	0.473
	2	2.51	8	3.33	4	2.67	4	4	4	4	4
	3	0.416	1.27	0.25	0.25	0.646	0.584	0.792	0.37	0.512	0.844
	4	0.975	0.993	0.924	0.891	0.85	0.812	0.779	0.753	0.722	0.672
3, 4, 8	1	0.2	0.2	0.25	0.25	0.25	0.355	0.594	1.42	1.03	0.267
	2	1.33	1.77	2.03	3	2.67	1.34	0.725	0.342	0.337	0.308
	3	0.695	0.706	0.7	0.602	0.743	0.92	1.07	1.19	1.32	4
	4	0.958	0.917	0.888	0.842	0.796	0.745	0.702	0.661	0.629	0.538
3, 6, 8	1	0.2	0.2	0.25	0.25	0.34	0.636	0.25	0.868	0.894	0.843
	2	0.991	1.24	1.17	1.25	1.02	0.753	1.43	0.233	0.246	0.582
	3	0.744	0.899	0.817	0.832	0.96	1.12	0.835	2.99	2.8	2.29
	4	0.951	0.875	0.846	0.794	0.742	0.685	0.648	0.585	0.558	0.513
3, 6, 12	1	0.2	0.2	0.3	2.3	1.02	0.662	2.91	0.269	0.2	0.423
	2	1.14	1.01	1.94	0.84	0.877	0.984	1.09	1.07	1.02	0.731
	3	0.473	0.875	0.732	0.8	0.902	0.998	1.33	1.5	1.91	1.75
	4	0.966	0.845	0.812	0.739	0.688	0.618	0.567	0.524	0.494	0.455
4, 4, 8	1	0.2	0.2	5	0.351	0.397	0.564	1.05	5	4	0.993
	2	2.54	4	3.33	4	2.67	0.25	0.48	0.233	0.246	0.308
	3	0.373	0.439	0.477	0.49	0.657	1.36	1.14	0.649	0.851	2.68
	4	0.957	0.904	0.841	0.818	0.77	0.71	0.665	0.62	0.586	0.528
4, 6, 8	1	0.2	0.2	2.59	0.42	0.61	0.79	0.561	0.359	0.482	0.267
	2	1.44	1.62	1.49	1.3	0.952	0.696	0.738	4	0.548	0.868
	3	0.557	0.664	0.593	0.792	0.81	1.2	1.8	0.414	4.04	4
	4	0.936	0.869	0.806	0.767	0.711	0.653	0.604	0.6	0.522	0.484
4, 8, 8	1	0.249	0.2	5	1.82	0.885	0.578	0.483	0.547	0.296	1.32
	2	1.07	1.07	1.65	0.77	0.784	0.808	0.754	0.663	4	0.405
	3	0.673	0.84	0.486	0.804	1.14	1.82	2.73	3.63	0.267	4
	4	0.914	0.828	0.763	0.723	0.661	0.594	0.541	0.5	0.496	0.43
4, 8, 12	1	0.444	4	1.97	1.1	0.25	0.534	0.348	5	1.59	5
	2	0.927	0.95	0.878	0.847	0.956	0.837	0.846	0.233	0.246	1.14
	3	0.81	0.733	0.779	0.897	0.758	1.27	1.76	1.02	2.41	1.26
	4	0.88	0.791	0.742	0.675	0.62	0.544	0.495	0.452	0.43	0.387
5, 6, 8	1	0.26	0.787	0.25	0.535	0.766	1.18	0.668	0.25	1	2.01
	2	1.48	4	3.33	1.2	0.833	0.553	0.605	0.233	0.358	0.215
	3	0.618	0.225	0.243	0.821	0.993	1.25	2.07	4	3.48	4
	4	0.928	0.861	0.855	0.738	0.679	0.622	0.568	0.65	0.487	0.436
5, 8, 12	1	0.2	3.52	0.25	1.38	0.452	1.72	1.02	1.28	0.819	5
	2	0.638	0.884	0.922	0.767	0.554	0.607	0.6	0.475	0.482	0.25
	3	1.26	0.74	0.938	0.866	1.76	1.05	1.46	1.64	2.38	1.26
	4	0.826	0.772	0.687	0.657	0.539	0.521	0.475	0.435	0.404	0.376
6, 8, 10	1	0.68	0.866	2.36	0.25	2.24	2.9	0.5	1.45	4	5
	2	1.04	0.899	0.703	1.38	0.335	0.444	4	0.37	0.249	0.2
	3	0.735	0.836	0.763	1.11	2.24	1.12	0.25	2.67	1.49	1.35
	4	0.87	0.764	0.716	0.644	0.548	0.511	0.524	0.423	0.408	0.367
6, 8, 12	1	0.59	2.34	1.99	1.76	1.52	2.47	1.74	3	4	0.437
	2	1.04	0.822	0.744	0.643	0.586	0.438	0.425	0.311	0.29	4
	3	0.7	0.775	0.783	0.843	0.969	1.08	1.41	1.3	1.15	0.889
	4	0.868	0.753	0.699	0.637	0.57	0.496	0.451	0.42	0.393	0.356

viously, when the dynamic factor is close to 1 the inertial effect can be neglected, otherwise it is significant. It can be easily observed from the tables that the dynamic factors vary widely between 0.2 and 13.3 for all pavement sections, which indicates that the static analysis either underestimates or overestimates the layer moduli. In fact, the moduli of some layers are underestimated and the moduli for other layers are overestimated in the same pavement section with no consistent trend because of the use of static analysis. For example, by using static analysis, a modulus for an upper layer that is lower than that for a lower layer may be obtained. This discrepancy between static results and actual material properties is mainly due to the inconsistency between the type of load in the field and the method of analysis. Also, the inconsistency in the dynamic factor values indicates that Tables 2 and 3 cannot easily be reduced to simpler or smaller tables because the dynamic response of pavement is a complex function of material properties, layer thicknesses, loading mode, loading frequency, or some combination of these.

The results also indicate that the effect of changing the depth to bedrock on the layer moduli is not as large as the effect of changing the method of analysis (static versus dynamic). This is explained, in many cases, by the similarity of factors in Tables 2 and 3.

LIMITATIONS

Although the curves and tables developed in this paper provide a simple and convenient method for evaluating the layer stiffnesses of existing pave-

TABLE 3 Dynamic Factors for 60-ft Subgrade

Thicknesses (in.)	Layer	Curve A	B	C	D	E	F	G	H	I	J
2, 4, 8	1	4.37	13.6	1.38	5.09	0.255	0.255	0.341	0.254	0.29	2.09
	2	4.34	8.11	3.83	4.02	1.23	0.992	0.721	1.53	0.854	0.243
	3	0.852	1.13	0.745	0.781	0.888	1	1.11	0.963	1.16	1.38
	4	0.996	1	0.946	0.872	0.86	0.823	0.774	0.736	0.69	0.66
2, 6, 8	1	4.12	4.06	1.33	0.076	0.255	0.253	1.69	0.327	0.763	0.775
	2	2.02	1.88	1	1.53	2.71	1.08	0.686	0.82	0.342	0.244
	3	0.828	0.706	0.728	0.552	0.629	1.01	0.895	1.73	2.4	4.17
	4	1	0.926	0.894	0.858	0.819	0.749	0.716	0.658	0.631	0.592
2, 6, 12	1	4.12	9.38	0.496	0.253	0.252	2.58	0.251	0.298	0.204	0.98
	2	1.5	1.14	0.273	1.22	0.871	0.843	1.1	1.03	0.983	0.201
	3	0.885	0.69	0.46	0.912	0.816	0.833	1.21	1.21	1.47	2.04
	4	0.965	0.9	0.863	0.813	0.742	0.69	0.639	0.59	0.563	0.515
3, 4, 4	1	4.04	13.7	5.15	0.254	0.254	0.253	0.253	0.481	0.445	0.474
	2	2.49	8.13	3.43	4.05	2.7	4.06	4.05	4.05	4.05	4.06
	3	0.413	1.3	0.258	0.252	0.656	0.595	0.802	0.375	0.521	0.859
	4	1.02	1.03	0.97	0.927	0.877	0.835	0.804	0.779	0.744	0.69
3, 4, 8	1	0.206	0.201	0.253	0.249	0.254	0.359	0.598	1.42	1.04	0.267
	2	1.38	1.77	2.05	2.99	2.71	1.36	0.737	0.341	0.342	0.308
	3	0.716	0.705	0.684	0.598	0.753	0.945	1.1	1.19	1.35	4.06
	4	1.01	0.971	0.922	0.878	0.835	0.771	0.74	0.668	0.653	0.57
3, 6, 8	1	0.164	0.199	0.253	0.253	0.346	0.643	0.257	0.88	0.897	0.844
	2	0.821	1.25	1.19	1.26	1.03	0.76	1.49	0.239	0.25	0.594
	3	0.83	0.909	0.819	0.845	0.975	1.15	0.888	3.06	2.86	2.35
	4	1	0.885	0.893	0.826	0.773	0.718	0.702	0.619	0.596	0.534
3, 6, 12	1	0.204	0.203	0.298	2.31	1.01	0.671	2.92	0.272	0.199	0.423
	2	1.15	0.992	1.91	0.854	0.871	1.01	1.11	1.08	1.01	0.733
	3	0.466	0.825	0.716	0.815	0.895	1.01	1.37	1.53	1.9	1.78
	4	1.01	0.913	0.866	0.777	0.714	0.657	0.604	0.551	0.494	0.471
4, 4, 8	1	0.206	0.201	5.14	0.356	0.402	0.568	1.06	5.02	4.01	1.01
	2	2.62	4.02	3.48	4.05	2.7	0.255	0.485	0.234	0.25	0.308
	3	0.384	0.441	0.499	0.498	0.666	1.38	1.58	0.654	0.86	2.73
	4	1.01	0.934	0.884	0.853	0.797	0.751	0.689	0.652	0.623	0.556
4, 6, 8	1	0.239	0.203	2.65	0.424	0.616	0.795	0.566	0.367	0.49	0.264
	2	1.55	1.64	1.57	1.3	0.968	0.705	0.751	4.02	0.557	0.864
	3	0.517	0.67	0.612	0.811	0.961	1.23	1.83	0.421	4.13	4.08
	4	0.991	0.915	0.85	0.812	0.748	0.695	0.65	0.642	0.542	0.525
4, 8, 8	1	0.257	0.202	5.15	1.85	0.894	0.582	0.484	0.551	0.295	1.34
	2	1.1	1.1	1.7	0.78	0.797	0.822	0.768	0.678	4.19	0.408
	3	0.684	0.857	0.504	0.824	1.17	1.87	2.79	3.72	0.287	3.97
	4	0.986	0.885	0.81	0.753	0.693	0.628	0.577	0.532	0.547	0.47
4, 8, 12	1	0.447	4.12	1.98	1.08	0.254	0.538	0.35	5.11	1.61	5.07
	2	0.935	0.979	0.888	0.837	0.988	0.846	0.864	0.242	0.251	1.15
	3	0.818	0.755	0.791	0.896	0.81	1.29	1.77	1.11	2.41	1.38
	4	0.939	0.831	0.791	0.735	0.683	0.585	0.539	0.524	0.469	0.451
5, 6, 8	1	0.265	0.791	0.254	0.538	0.763	1.19	0.664	0.247	0.98	1.95
	2	1.5	4.06	3.4	1.21	0.831	0.562	0.618	0.235	0.363	0.198
	3	1.62	0.226	0.248	0.833	0.992	1.27	2.14	4.11	3.59	3.55
	4	0.985	0.906	0.898	0.778	0.682	0.674	0.61	0.701	0.505	0.486
5, 8, 12	1	0.202	3.55	0.251	1.37	0.452	1.74	1.02	1.3	0.811	5
	2	0.642	0.894	0.56	0.778	0.563	0.607	0.607	0.477	0.491	0.249
	3	1.26	0.758	0.953	0.889	1.79	1.1	1.47	1.67	2.38	1.3
	4	0.86	0.809	0.742	0.709	0.567	0.568	0.519	0.426	0.441	0.386
6, 8, 10	1	0.687	0.871	2.36	0.258	2.31	2.94	1.55	1.45	3.99	0.49
	2	1.05	0.909	0.714	1.42	0.345	0.448	4.12	0.364	0.253	0.199
	3	0.744	0.845	0.793	1.14	2.33	1.14	0.26	0.272	1.52	1.38
	4	0.918	0.83	0.771	0.676	0.575	0.541	0.55	0.481	0.438	0.394
6, 8, 12	1	0.592	2.29	1.96	1.75	1.51	2.43	1.77	2.99	3.84	0.434
	2	1.05	0.807	0.732	0.644	1.69	0.43	0.423	0.31	0.279	3.8
	3	0.711	0.754	0.77	0.865	0.996	1.06	1.41	1.32	1.14	0.911
	4	0.919	0.794	0.736	0.689	0.613	0.495	0.495	0.446	0.391	0.403

ments, they have some limitations. In a small number of cases, field deflections may cross one or more of the typical curves. In such cases interpretation of results may not provide accurate estimates. Another source of error might develop because of the use of a backcalculation procedure in developing the tables. Because backcalculations in many cases do not result in unique solutions, the estimated moduli may not be accurate. However, this error is not expected to significantly alter the prediction of the load-carrying capacity of the pavement system or the required overlay thickness. Field verifications or other independent validation procedures are still needed to support the results obtained in this study.

Also, the typical curves and tables are intended to be used with the Dynaflect data only because the Dynaflect has some unique characteristics that are different from those of other nondestructive devices, such as load magnitude, frequency of loading, location of loading wheels, and location of geophones. Moreover, the layer thicknesses used in this study may not completely cover all thicknesses encountered in the field. However, the limitations associated with the use of the curves and tables are believed to be insignificant when their usefulness and simplicity are taken into consideration.

It should be noted that the Dynaflect has some limitations, such as the small load magnitude, which might not accurately detect the material properties at deep layers, and the fixed loading frequency, which might result in a resonant pavement response.

SUMMARY

Because there is no direct solution for providing the pavement layer stiffnesses from deflection mea-

surements, typical curves and tables are developed in this study to aid the highway engineer in this respect. These curves and tables provide the layer moduli of typical highway pavements from the peak-to-peak deflection readings of the Dynaflect. The development of the curves and tables is based on the principles of mechanics using both static and dynamic analyses. Pavement sections are used with four typical layers: surface, base, subbase, and subgrade. Materials are assumed to be homogeneous and isotropic, with linear elastic behavior in the static solution and linear viscoelastic behavior in the dynamic solution. Typical Poisson's ratios, material damping ratios, and mass densities are assumed. If the layer thicknesses and the approximate depth to bedrock are known, the layer moduli can be predicted with a reasonable degree of accuracy. The curves are simple to use without the need for previous empirical relations or computer analysis.

The inertial effect of the pavement structure in most cases proved to be influential in evaluating the layer moduli. The dependence on the static solution in the interpretation of the dynamic Dynaflect deflections can either underestimate or overestimate the moduli, which may have significant effects on the predicted load-carrying capacity, the required overlay thickness, or both.

ACKNOWLEDGMENT

The authors wish to thank the Center for Advanced Research in Transportation and the Department of Civil Engineering at Arizona State University for making their facilities available to them.

REFERENCES

1. D.R. Alexander. Correlation of Nondestructive Pavement Evaluation Test Results with Conventional Quality Control and In-Situ Strength Tests Obtained on an MX Road Test Section. U.S. Army Engineer Waterways Experiment Station, Vicksburg, Miss., Feb. 1985.
2. J.W. Hall. Comparative Study of Nondestructive Pavement Testing--MacDill Air Force Base. U.S. Army Engineer Waterways Experiment Station, Vicksburg, Miss., 1984.
3. M.S. Hoffman and M.R. Thompson. Comparative Study of Selected Nondestructive Testing Devices. In Transportation Research Record 852, TRB, National Research Council, Washington, D.C., 1982, pp. 32-41.
4. M.S. Mamlouk and T.G. Davies. Elasto-Dynamic Analysis of Pavement Deflections. Transportation Engineering Journal, ASCE, Vol. 110, No. 6, Nov. 1984, pp. 536-550.
5. T.G. Davies and M.S. Mamlouk. Theoretical Response of Multilayer Pavement Systems to Dynamic Nondestructive Testing. In Transportation Research Record 1022, TRB, National Research Council, Washington, D.C., 1985, pp. 1-7.
6. M.S. Mamlouk. Use of Dynamic Analysis in Predicting Field Multilayer Pavement Moduli. In Transportation Research Record 1043, TRB, National Research Council, Washington, D.C., 1985, pp. 113-121.
7. J.M. Roesset and K-Y. Shao. Dynamic Interpretation of Dynaflect and Falling Weight Deflectometer Tests. In Transportation Research Record 1022, TRB, National Research Council, Washington, D.C., 1985, pp. 7-16.
8. B.E. Sebaaly, T.G. Davies, and M.S. Mamlouk. Dynamics of the Falling Weight Deflectometer. Journal of Transportation Engineering, ASCE, Vol. 111, No. 6, Nov. 1985.
9. M.S. Mamlouk. Evaluation of In-Situ Pavement Moduli from Deflection Measurements. Journal of Testing and Evaluation, ASTM, Vol. 13, No. 1, Jan. 1985, pp. 60-68.
10. D.A. Kasianchuk and G.H. Argue. A Comparison of Plate Load Testing with the Wave Propagation Technique. Proc., 3rd International Conference on the Structural Design of Asphalt Pavements, Vol. 1, London, 1972, pp. 444-454.
11. E.J. Yoder and M.W. Witezak. Principle of Pavement Design. McGraw-Hill, New York, 1975.
12. A.C. Eringen and E.S. Suhubi. Elastodynamics, Vol. 2, Linear Theory. Academic Press, New York, 1975.
13. E. Kausel and R. Peek. Dynamic Loads in the Interior of a Layered Stratum: An Explicit Solution. Bull. of the Seismological Society of America, Vol. 72, No. 5, Oct. 1982, pp. 1459-1481.
14. W.P. Kilareski and B.A. Anani. Evaluation of In-Situ Moduli and Pavement Life from Deflection Basins. Proc., 5th International Conference on the Structural Design of Asphalt Pavements, Delft University of Technology, Delft, The Netherlands, Vol. 1, 1982, pp. 349-366.
15. F.E. Richart, Jr., J.R. Hall, Jr., and R.D. Woods. Vibrations of Soils and Foundations. Prentice-Hall, Englewood Cliffs, N.J., 1970.

Publication of this paper sponsored by Committee on Strength and Deformation Characteristics of Pavement Sections.

Nondestructive Pavement Testing by Wave Propagation: Advanced Methods of Analysis and Parameter Management

ROBERT A. DOUGLAS and GEORGE L. ELLER

ABSTRACT

Wave propagation methods for the nondestructive testing of pavements use an impulsive input of force at a point on the surface of a pavement structure in order to generate surface waves. Surface waves are dispersive in layered systems such as pavements. Two accelerometers acquire the shape of the surface wave as it passes. The two wave shapes experience signal analysis to determine the details of the dispersion that has taken place. The results are used to plot the several elements of the dispersion field: the graph of wave speed versus wavelength for the pavement structure. The dispersion field is the principal product of the wave propagation test. Success in determining layer properties depends on the accuracy with which the several dispersion curves may be computed that combine to form the dispersion field for the structure. The results of analysis are found to be strongly dependent on test parameters, pavement geometry, and the signal analysis methods chosen. Current test methods and methods of analysis sometimes lead to ambiguity, phase problems with reflections, and near-field distortions. The purposes of this work were to examine, find the causes for, and seek to remedy inconsistencies displayed at intervals by the analysis. Several recommendations have resulted; one is that current broadband methods be replaced by the medium-band method; another is that a Bessel transform developed by the authors replace the Fourier transform for analysis of signals at long wavelengths. Other methods overcome the errors in phase caused by reflections.

Nondestructive pavement testing by wave propagation (NDPT/WP) has been under development in the United States for some years and several hardware systems exist. Although some awareness of the method exists, few engineers are familiar with its details. Its progress can be traced in technical reports of the U.S. Air Force and in the reports of other federal and state agencies that have contributed to the work (1-5); however, little has appeared in the literature until several recent papers by Nazarian and Stokoe (6,7). Their experimental methods have many useful features.

The NDPT/WP method is attractive in respects that have made it of particular interest to the U.S. Air Force. Although based on low levels of strain, which may cause relating the properties to performance under moving wheel loads to appear somewhat arbitrary, the method deals with fundamental parameters, the elastic constants. This means that the equipment and method may be used with structures for which there is no available history. The results, described by Douglas and Eller (8), are current in situ parameters.

Another advantage of the NDPT/WP method is that the results are from tests of a simple character, not calling for experienced operators. The data are then subjected to sophisticated signal analysis methods. NDPT/WP follows the pattern of simple test-sophisticated analysis. Also, the equipment is not expensive, and it can be transported easily by light aircraft, small vans, or even backpack.

As a result of one or more of those advantages, interest in the wave propagation method is increasing as engineers come into contact with it. Administrators at various levels of responsibility have begun to inquire how and when they might utilize the method.

However, it has taken some years to bring this method to its current state, and improvement of the method continues as expert systems built into the analysis are modified to treat new situations. This is because this application of wave propagation theory is more sophisticated than radar and the medium is not air; rather, the layered structure of a pavement is an inverted geologic structure that combines the often intractable stuff of soil mechanics with the mechanics and mathematics of both linear and nonlinear manmade materials.

This research has caused the authors to examine in detail the elements of the method of analysis. It may be useful for those not familiar with the method to follow the development of the analysis up to this time in order to see where anomalies have appeared and how the improvements mentioned will function.

INITIAL SIMPLICTY

The early form of this method is described by Jones in his work at the Road Research Laboratory in England during the 1950s and 1960s; three of his publications are particularly informative (9-11).

All of the NDPT/WP methods are based on the dispersion of surface waves in a layered medium. Surface waves remain attached to the free surface and move parallel to the surface as they expand outward from a source. They decay rapidly with depth below the

Civil Engineering Department, North Carolina State University, Raleigh, N.C. 27695-7908.

surface. Waves with short wavelengths may be detected only in the uppermost layer, and increasingly longer wavelengths penetrate to deeper and deeper levels. The general scheme is that by using surface waves of different wavelengths, the wave speed associated with each layer could be determined; the wave speeds could then be used to find the elastic constants of each individual layer. The process is described in detail by Jones (11), Finn et al. (12), and Nielsen and Baird (1).

The analysis is built about the fundamental relationship among the wavelength (WL), wave speed (WS), and period (T), as

$$WL = WS \times T \quad (1)$$

Instead of the period T, the time associated with the passage of a single wavelength, the relationship may be written in terms of the frequency F (the reciprocal of T) as

$$WL = WS \times (1/F) \quad (2)$$

The first employment of an NDPT/WP system took advantage of Equation 2 in a direct manner. A vibrator generated a single frequency at a time so that F, and its inverse T, would be known quantities. In a test, an accelerometer would be moved by increments to successive locations away from the source until a series of minimum readings was obtained. These represented the nulls at the nodal points of the standing wave pattern set up by the vibrator. Thus, the wavelengths were measured, null to null to null.

The first wavelengths were associated with surface layer behavior. The next sets of wavelengths, each shorter than the one before, indicated lower speeds and were associated with the next layers down. After the structure had been explored adequately at one frequency, another frequency was selected and the process repeated. An improvement was to use an accelerometer array to trigger the array to capture the signals, then to use a Fourier transform to sort out the components of the wave, each of the same frequency and varying from the others only in wavelength (1,2).

The method was thoroughly tested and found to be successful but time consuming. The vibrator and power supply needed were large, expensive, and difficult to transport.

CURRENT METHOD

A major change took place in the mid-1970s (2): the vibrator was replaced by a broadband system based on single impulsive loading. A falling weight was used. It created many frequencies at one time, and a single thump (no other term for the impact process has stuck) would contain the entire range of frequencies needed.

In the current method, several accelerometers are arranged radially away from the source, to be triggered either by the thump or by arrival of the wave at the gauges if pretrigger capabilities exist in the recording diagnostics. Any two gauges form a gauge pair and the concept of a gaugelength (GL) between two gauges is now required.

Figure 1 shows accelerometer records from a lightly damped broadband input. The change in shape between the two records is the trademark of dispersive propagation. A linear change of size is not the same at all because it can occur as the consequence of distance of travel or through altering the gain setting of the diagnostics and does not imply dispersion. The broadband response of each accelerometer of an array is stored; a dispersion analysis can then be conducted for any two gauges.

A Fourier transform of each of the sets of data is performed, usually by FFT (fast Fourier transform) software. Two new sets of information are obtained, describing magnitude versus frequency and phase angle versus frequency for each gauge. It is phase versus frequency that is used for the dispersion analysis.

AMBIGUITIES OF ANALYSIS

The meaning of phase angle lies in the answer to this question: at a particular gauge, at the time of recording, and for a particular frequency, what was the position in time of that frequency as recording started? Was it at the beginning of the cycle? The phase angle would be zero (or was that phase angle 360 degrees?). Was it halfway along the first lobe of a sine curve? The phase angle would be 90 degrees.

Computation of wavelength is based on phase difference (PD), the difference between the phases computed for two frequencies. The wavelength (WL) comes from the relationship

$$WL = GL/(PD/360) \quad (3)$$

and wavespeed, from Equation 2 becomes

$$WS = WL \times F \quad (4)$$

or, in terms of Equation 3,

$$WS = (GL \times F/(PD/360) \quad (5)$$

In Equation 3, the term (PD/360) establishes the fraction of a wavelength corresponding to the gaugelength. If the two phases differed by 30 degrees, the gaugelength would be 30/360 of a wavelength. But was the phase difference 30 degrees, or 30 degrees plus 360 degrees, or 30 degrees plus 720 degrees?

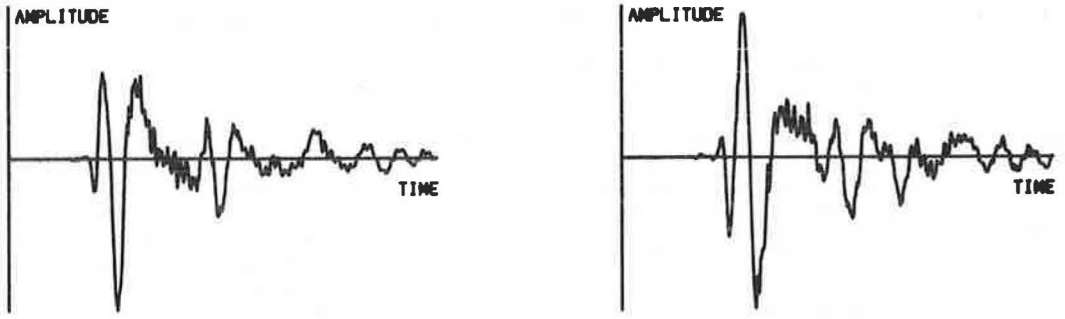

FIGURE 1 Lightly damped signals.

The individual values of phase do not disclose the phase difference uniquely. Attempts have been made to create an expert system to examine the data by using programmed rules to determine the correct value of each of the wavelengths in the broadband response, but they have been only partially successful.

Currently, this program for dispersion analysis computes the phase difference for several (selectable) of the different possible values of the phase difference, as well as the possibilities of lead and lag at each value; it also plots those possibilities. Figure 2 shows two signals captured at a gauge pair from an input with medium damping. Figure 3 shows the results obtained from an analysis of those two signals by using the authors' typical plotter output from which it is visually possible to identify the several dispersion curves that make up the dispersion field. The abscissa and ordinate are wavelength and wave speed, respectively. The lines that extend radially from the origin are lines of constant frequency. Figure 4 shows elements of the dispersion field identified by examination of Figure 3.

Figure 5 shows a choice that must be made continually. The start is at the lowest, rightmost point, moving left and up until, at the approximate coordinates (10,2500), a choice must be made: go left and up, or right and up, or left and down? In this case, go left and up. Soon it would be necessary to make another choice, then others. Figure 6 shows the high-frequency portion of a dispersion field from a different test, in which a number of choices exist.

A troublesome rule is that only one point may be chosen on a given frequency line. The signal comes to each accelerometer from different parts of the pavement structure, each segment arriving at a different time. The accelerometer reports the sum of the magnitudes of the signals it receives. The analysis and computation of phase by FFT averages the results for a given frequency. The result is some kind of average, which is sometimes erroneous.

The decisions involved in determining the family of curves in the dispersion field are based on knowledge of what is possible and what is probable, and on experience. Figure 7 shows the general geometry to be expected of the dispersion field from a structure with two layers over a half space. Jones (10,11), Vidale (13), and Watkins, Lysmer, and Monismith (14) describe the relationship of the dispersion field for simple layered structures. Figure 8 shows a line of constant frequency superimposed on the elements of the dispersion field. It shows that at each frequency, an individual accelerometer registers inputs from different elements of the dispersion field, yet the analysis can provide only a single composite value.

PROBLEM OF REFLECTIONS

Where cracks exist in a layer, or if the pavement is jointed, reflections occur and distort the dispersion field. On airfield pavements, often the entire test setup is on a single slab. Reflections from side joints and ends return quickly and after the phase values. Figures 9 and 10 show two sets of first and second gauge results from tests on a large slab, each set for the same thump and gauge pair arrangement,

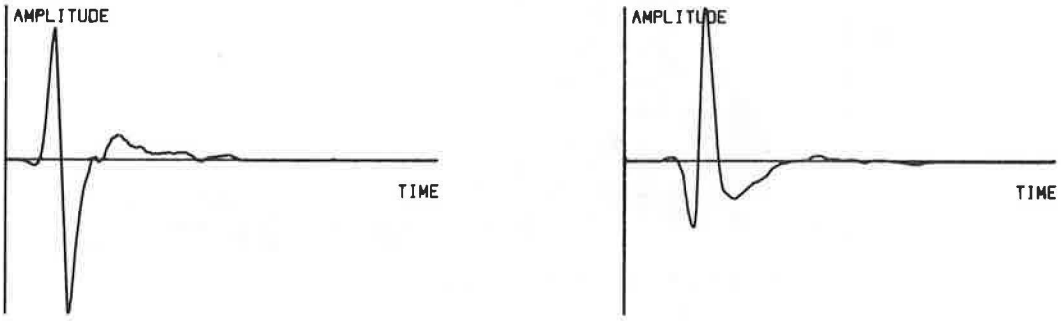

FIGURE 2 Medium damped signals.

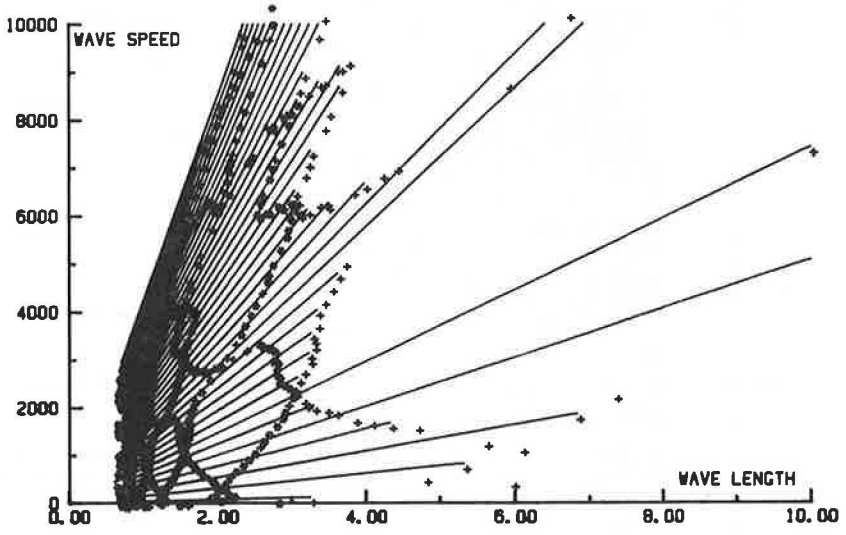

FIGURE 3 Dispersion field before identification.

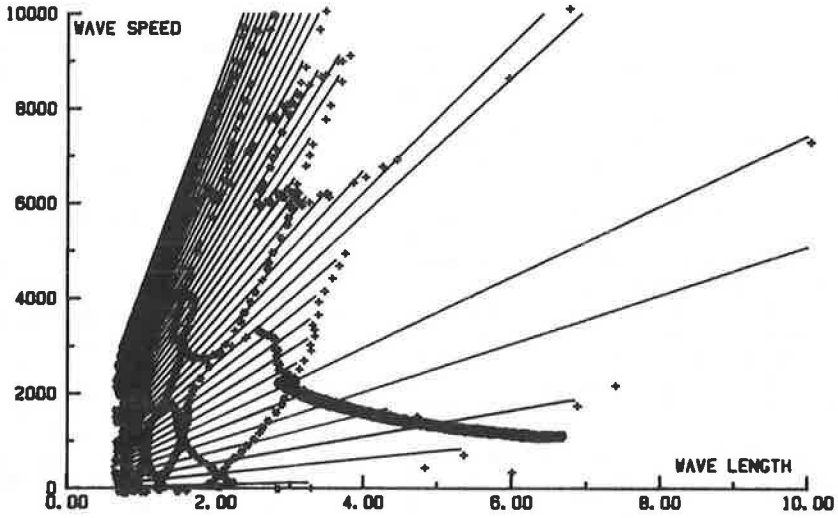

FIGURE 4 Dispersion field after identification.

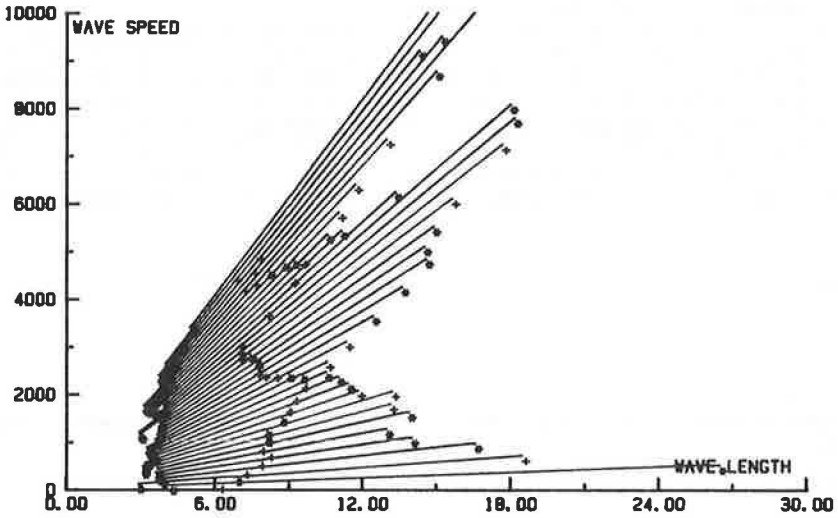

FIGURE 5 Alternate paths in a dispersion field.

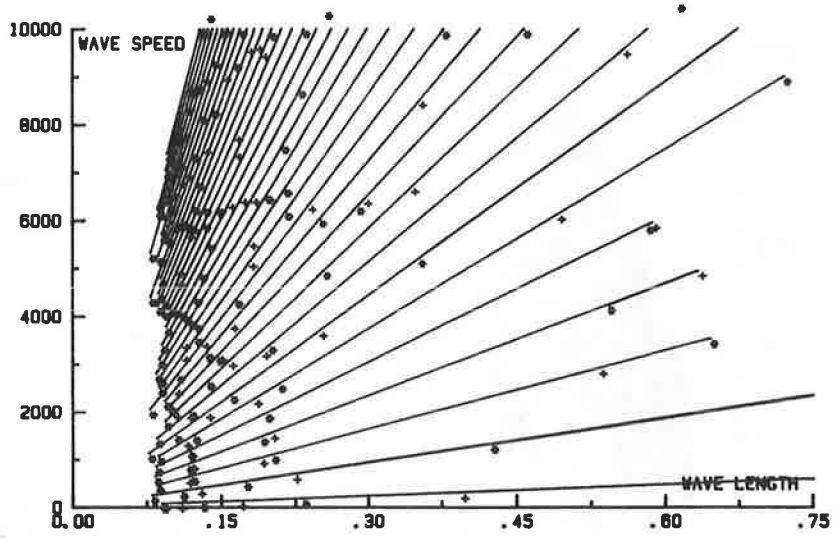

FIGURE 6 Multiple solutions.

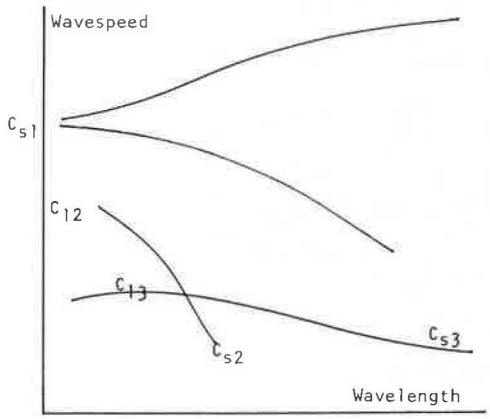

FIGURE 7 Elements in a dispersion field.

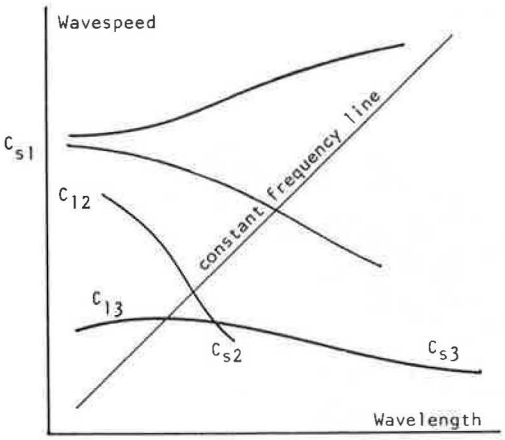

FIGURE 8 Constant frequency line.

but at different orientations with respect to the boundaries of the slab. The pavement structure was the same in each case, as were the gauge length and the thump.

Figure 9 shows records with the thump and gauges so far from the boundaries of the large portland cement concrete slab (60 ft on a side) that reflections did not return during the test period. Figure 10 shows the signals when the line formed by thump and gauges is moved close and parallel to a lateral boundary. The signals are visibly different than those in Figure 9.

Figures 11 and 12 show two dispersion fields that were computed from the two pairs of signals of Figures 9 and 10. The differences are obvious, yet the results are from the same pavement structure and should be the same. Figure 13 shows three dispersion fields from a similar test superimposed (low-frequency portions only), and demonstrates vividly the magnitudes of the errors that can result from reflections. The problem of reflections is an acute one because interpretation of the dispersion field in order to determine accurate values for the material constants depends on a dispersion field without distortion. Changes in procedure and analysis to minimize these effects are described later.

NEAR-FIELD PROBLEM

In the analysis itself, a problem is buried that can distort the dispersion field significantly in the region of longer wavelengths that is associated with deeper layers. The user of the Fourier transform unwittingly adopts a number of assumptions that may not be appropriate to the particular signal processing problem that is involved. Above all, the Fourier transform of data should be used only for problems whose solutions are suitably described by sinusoids.

The situation here involves the responses of the buried layers for which the wavelengths are longer

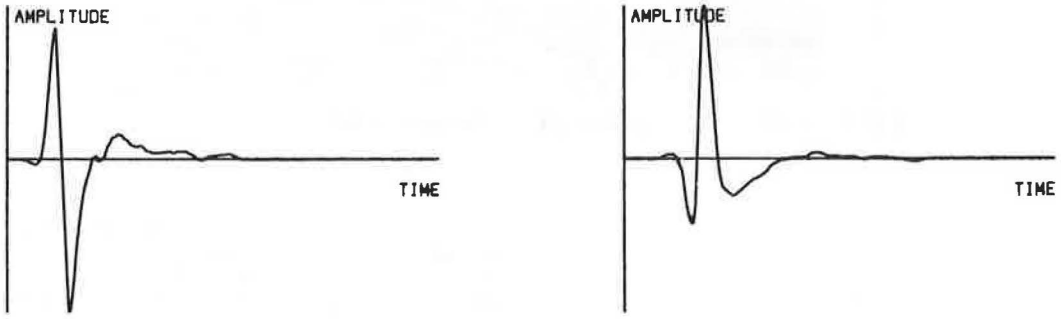

FIGURE 9 Signals from first and second gauges: no reflections.

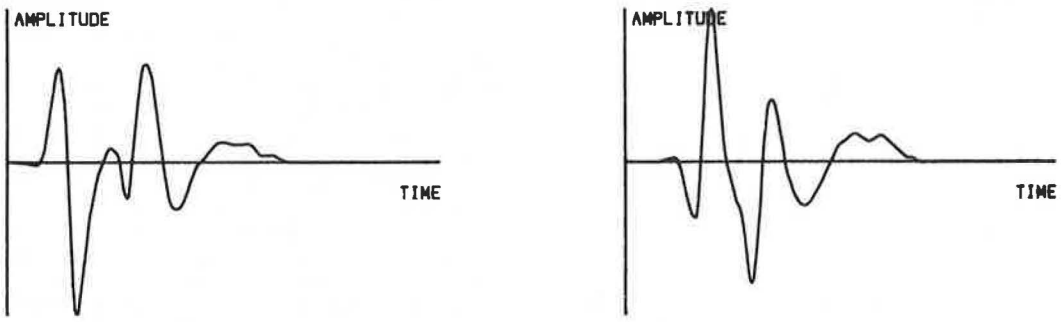

FIGURE 10 Signals from first and second gauges: reflection from side.

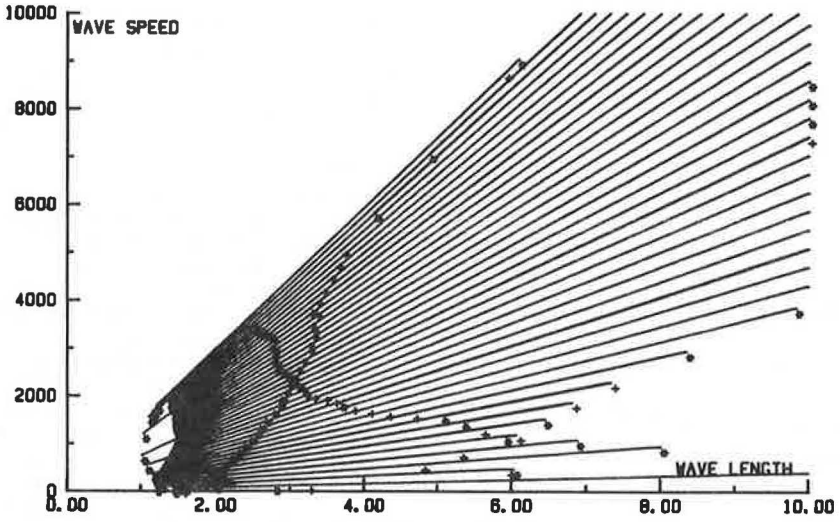

FIGURE 11 Reflections in dispersion field: no reflection.

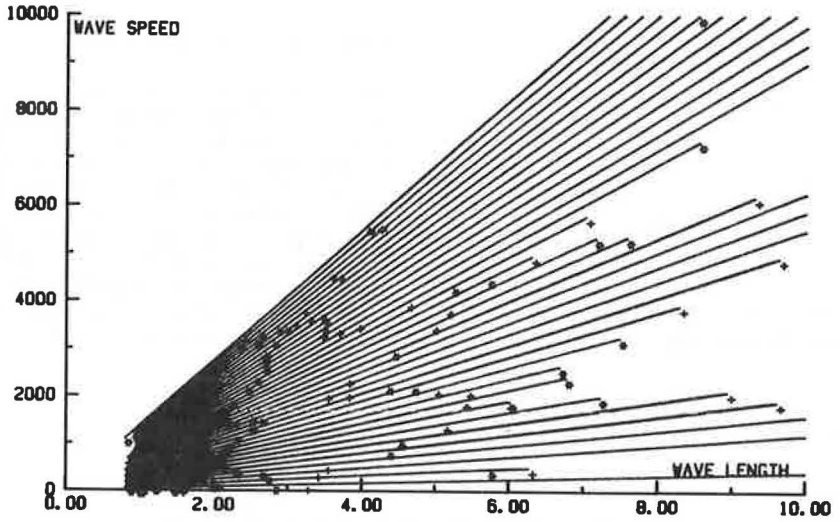

FIGURE 12 Reflections in dispersion field: reflection from side.

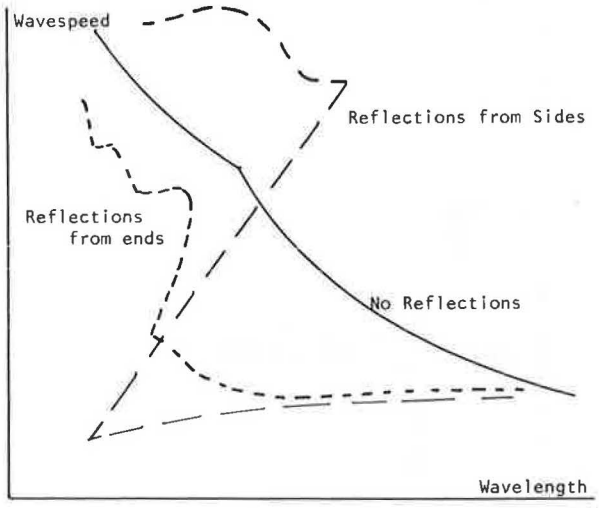

FIGURE 13 Effect of reflection conditions.

and the wave speeds lower than for the surface layer. The duration of the captured signal is involved. It tends to be shortened rather than lengthened to minimize reflections and avoid plate vibration modes.

The traveling waves that are created by a thump on the surface are described by Bessel functions [see Schroedinger (15), Weinstock (16), and Tasi (17)]. Figure 14 shows the irregular nature of the Bessel functions J_o and Y_o for early values of the arguments. Figure 15 shows how the disturbance from the source travels outward in the form of several Bessel functions, looking similar to a snake with its head raised, and with the largest values in the first few cycles. The first few zeros of the function are irregular, but then the functions become sinusoidal. When many zeros are involved, the Bessel functions approximate sinusoids and could serve as the sine and cosine terms of a Fourier transform.

If the signal must be truncated, then for short records, long wavelengths, and low wave speeds, possibly only one or two zeros of a Bessel function of any one argument may appear on the time signal. To

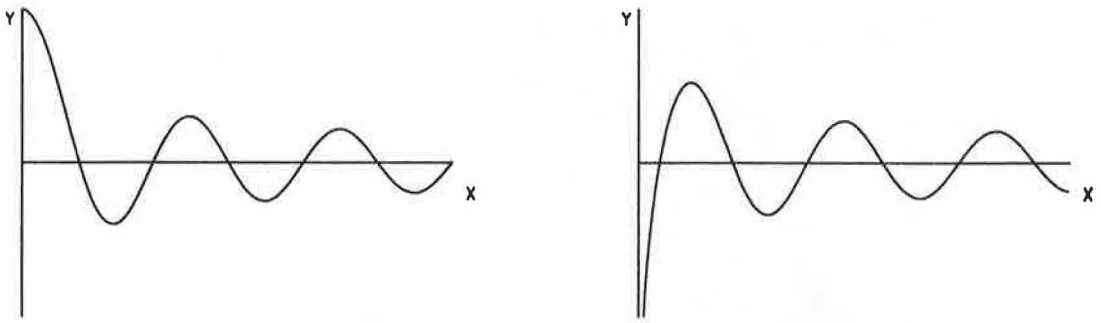

FIGURE 14 Bessel functions.

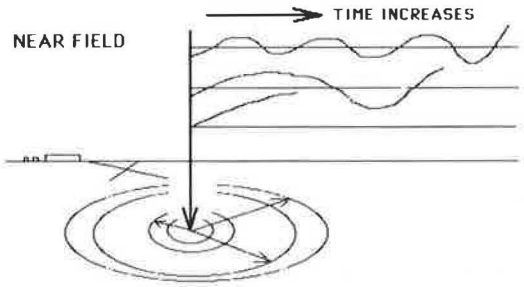

FIGURE 15 Emerging Bessel functions.

interpret that irregular signal by a Fourier transform would result in whimsical answers.

The obvious recourse is to utilize a transform based on Bessel functions of suitable arguments, and, instead of phase and phase difference, to return to the more intuitively acceptable concept: at what time did the function pass the first gauge, and at what later time did it pass the second gauge? The time interval and gaugelength will immediately give wave speed.

To demonstrate this behavior by the Fourier transform, Figure 16 shows the spurious dispersion field that results when the Fourier transform and its appropriate dispersion computations are applied to synthetic time signals for first and second gauges. The two artificial signals are created from Bessel functions of only three different arguments, each assigned a particular wavespeed. The true solution is only three single points in the dispersion field. The solution via the Fourier transform indicates a complete dispersion field, not dissimilar from those of customary tests. Figure 17 shows the same dispersion field, replotted to enlarge the high-frequency, short-wavelength portion, which does not exist.

Modified Transform Method for Fourier Portion of Analysis

The protocols of the FFT assume that the signal being transformed repeats in time; that is, wraparound is an inherent assumption of the correlation being made, with all frequency elements assumed to have been in the signal from the beginning. In NDPT/WP tests, the contributions from different channels enter the combined signal at different times; thus the information associated with each different frequency changes during the signal in response to each new input.

Repeating an earlier statement, the Fourier transform recognizes only two pieces of information for each frequency: a magnitude and a phase angle, each as an average involving the entire signal. The Fourier transform may be altered so that sine and cosine parts are evaluated in parallel, and so that phase is determined as a running sum during the computations rather than at the end. By this means it would be possible to determine the time of entry of information from new sources. If time of entry of information can be determined, the time difference between the entries of information at first and sec-

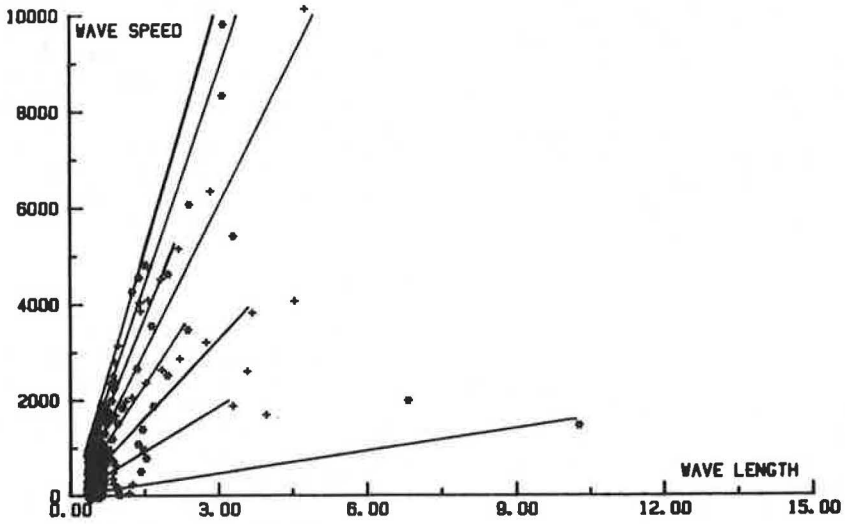

FIGURE 16 Fourier interpretation of three Bessel points.

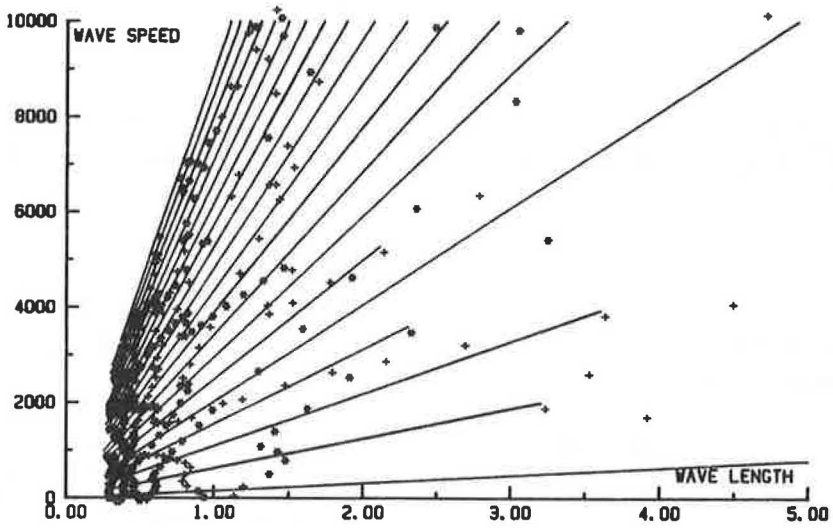

FIGURE 17 High-frequency part of Fourier interpretation.

ond gauges would be a quantity computed directly rather than being deduced on a basis of multiple phase differences with leads or lags. The computation of wave speed would be reduced to the simplicity of Equation 2, and velocity would be found by dividing gaugelength by transit time.

A Bessel Transform for Deeper Buried Layers

The authors' current work on a special-purpose Bessel transform to evaluate long wavelength portions of experimental data has been encouraging. Because of the layered nature of a pavement system, the authors use a few selected arguments rather than the regularly spaced frequencies of the Fourier transform. Cross correlations between J_0 arguments and the first and second signals produce good results for the elapsed times, but it was necessary to discard the concept of wraparound. Instead, parity of comparisons is accomplished by using a truncated Bessel argument for both first and second gauge comparisons and limiting the range of cross correlation so that the function never moves past the end of the data.

The shortcoming of this Bessel transform is principally that of excessive computation time. The first exploration into such a transform was by use of a spreadsheet. The results were successful in showing the entry points of several signal components at each of the arguments used; however, the run time was several hours on a microcomputer because of continual reference to disc. The second version was programmed. The speed, although increased, could still be further improved. However, this shortcoming is not considered to be significant; it can be overcome in part by more effective programming, and completely with greater memory. Microcomputers will be completely adequate for this work now that the memory available to them is at the megabyte level.

Field Techniques

The entire method is being improved as the influence of individual parameters is determined. The relationship of the thump distance to the gauge length (Figure 18) is an example of this. Larger bases for accelerometers minimize errors from the lack of homogeneity of material immediately beneath as well as errors from any localized bond failures.

The authors have found a change in technique that

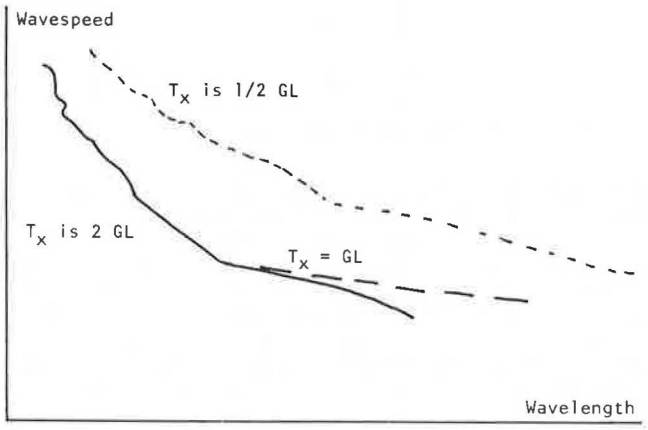

FIGURE 18 Effect of gauge length on thump distance.

substantially diminishes the consequences of reflections. The accelerometers are essentially unidirectional, with transverse sensitivity only 5 percent of the axial sensitivity. By mounting an accelerometer horizontally rather than vertically, and with the axis parallel to the lateral boundary, the reflections from that boundary become negligible. Figures 19 and 20 show the results from a test in which gauge pairs were placed side by side, one set with axes vertical in the customary position and the other set with the axes horizontal and parallel to the side boundary. Signals were recorded for both pairs simultaneously, from the same thump. Figure 19 shows the dispersion field with customary vertical gauge axes; Figure 20 shows the Rayleigh wave speed and also the longitudinal wave speed for the layer.

FUTURE RESEARCH

Several problems of a different type have yet to receive sufficient attention. Accuracy of results must be determined and documented. A method based on wave propagation is expected to produce results that are measures of fundamental quantities, in contrast with comparative studies; yet it has been learned that many parameters of test and analysis become involved in the results, and how to overcome their effects is being learned. To establish the accuracy of the method and the success of the corrective measures

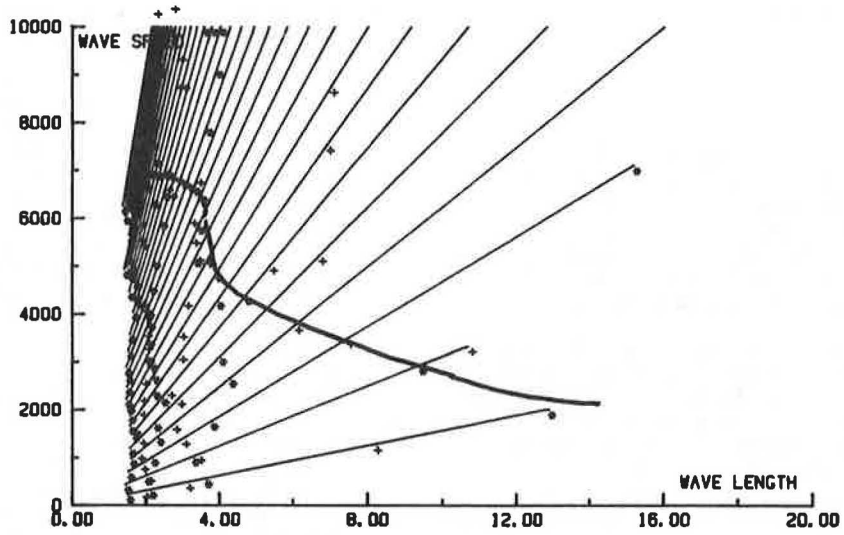

FIGURE 19 Effect of gauge axis orientation: axes vertical.

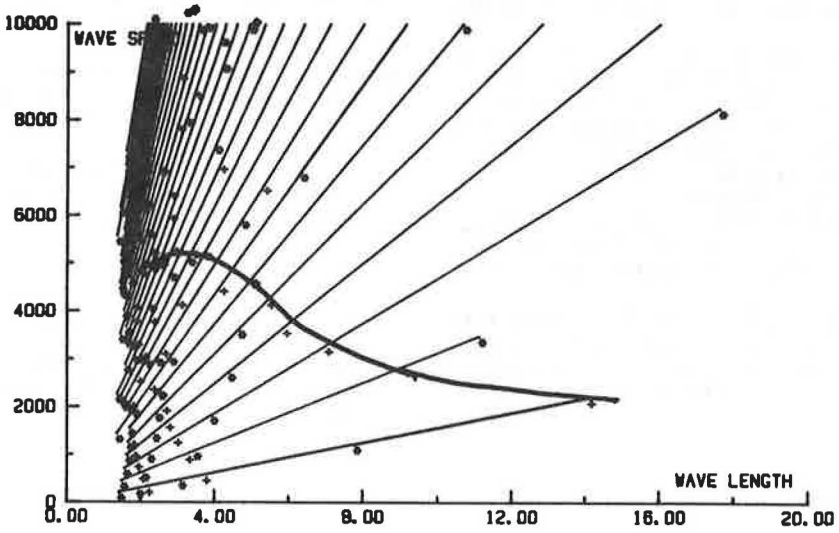

FIGURE 20 Effect of gauge axis orientation: axes horizontal.

that are being instituted, a separate method is needed. Cross-hole measurements are an obvious choice, but the tests needs to be modified substantially to deal with the thin layers of a pavement structure.

Linearity is another problem. To what extent are the results dependent on linear behavior by the individual layers of a pavement structure? Do the results vary if the energy and momentum levels associated with the thump are changed? Within what ranges of gauge location and energy and momentum level are results constant?

A continuing problem will be determining the nature of response from pavement structures that are less than ideal. The structures reasonably well understood at the current time involve few layers, and they display monotonic variation or properties with depth. What happens when there are flexible overlays to jointed rigid pavements? What happens when there are many layers present? What is the sensitivity of the method? What is the least value of the variation in properties that would permit two different layers to be identified?

CONCLUSIONS

As the problems described in this paper are overcome, nondestructive pavement testing by wave propagation nears the end of its development phase; however, answers must be found to the questions posed in the preceding section before it is fully ready to be adopted into practice. Fortunately the several systems currently in the field are providing shakedown results, and experience gained from them has helped to identify the problems the authors have discussed. Those same systems in the field will be useful testbeds for debugging these latest modifications to the analysis.

ACKNOWLEDGMENTS

The work described in this paper has been supported by the U.S. Air Force Engineering and Services Center, Tyndall Air Force Base, Florida. Project Officers associated with the work are John A. Centrone,

Paul Y. Thompson, James Murfee, and Robert R. Costigan.

REFERENCES

1. J.P. Nielsen and G.T. Baird. Pavement Evaluation System. Final Report. University of New Mexico, Albuquerque, Aug. 1976.
2. J.P. Nielsen and G.T. Baird. Evaluation of an Impulse Testing Technique for Nondestructive Testing of Pavements and Recommended Follow-On Research. University of New Mexico, Albuquerque, July 1977.
3. M.C. Wang. An Evaluation of the Air Force Pavement Nondestructive Testing Method. Final Report. U.S. Air Force Summer Faculty Research Program, Tyndall Air Force Base, Florida, 1981.
4. R.A. Douglas. Evaluation of the Nondestructive Testing of Airfield Pavements: Wave Propagation Aspects. Final Report. U.S. Air Force Summer Faculty Research Program, Tyndall Air Force Base, Florida, 1982.
5. H.R. Marien and G.T. Baird. U.S. Air Force Nondestructive Airfield Pavement Evaluation Method. Presented at meeting of TRB Task Force on Nondestructive Evaluation of Airfield Pavements, June 1981.
6. S. Nazarian, K.H. Stokoe II, and W.R. Hudson. Use of Spectral Analysis of Surface Waves Method for Determination of Moduli and Thicknesses of Pavement Systems. In Transportation Research Record 930, TRB, National Research Council, Washington, D.C., 1983, pp. 38-45.
7. S. Nazarian and K.H. Stokoe II. Nondestructive Testing of Pavements Using Surface Waves. In Transportation Research Record 993, TRB, National Research Council, Washington, D.C., 1984, pp. 67-79.
8. R.A. Douglas and G.L. Eller. Soil Properties at Depth from Surface Measurements. Proc., Symposium on Interaction of Non-Nuclear Munitions with Structures, Panama City Beach, Fla., April 1985.
9. R. Jones. A Vibration Method for Measuring the Thickness of Concrete Road Slabs In Situ. Concrete Research, Vol. 7, No. 97, July 1955.
10. R. Jones. In Situ Measurement of the Dynamic Properties of Soil by Vibration Methods. Geotechnique, Vol. 6, No. 1, 1958.
11. R. Jones. Surface Wave Technique for Measuring the Elastic Properties and Thickness of Roads: Theoretical Development. British Journal of Applied Physics, Vol. 13, No. 21, 1962.
12. F.N. Finn, B.F. McCullough, K. Nair, and R.G. Hicks. Plan for Development of a Nondestructive Method for Determination of Load-Carrying Capacity of Airfield Pavements. Final Report 1062-2(F). U.S. Naval Civil Engineering Laboratory, Port Hueneme, Calif.; Materials Research and Development Co., Oakland, Calif., Nov. 1966.
13. R.F. Vidale. The Dispersion of Stress Waves in Layered Media Overlying a Half-Space of Lesser Acoustic Rigidity. Ph.D. dissertation. University of Michigan, Ann Arbor, 1964.
14. D.J. Watkins, J. Lysmer, and C.L. Monismith. Nondestructive Pavement Evaluation by the Wave Propagation Method. Report TE-74-2. University of California at Berkeley; California Department of Transportation, Sacramento, July 1974.
15. E. Schroedinger. Zur Dynamik Elastisch Gekoppelter Punktsysteme. Annalen der Physik, 4, 44, 916, 1914.
16. R. Weinstock. Propagation of a Longitudinal Disturbance on a One-Dimensional Lattice. American Journal of Physics, Vol. 38, No. 1289, 1970.
17. J. Tasi. Far-Field Analysis of Nonlinear Shock Waves in a Lattice. Journal of Applied Physics, Vol. 44, No. 4569, 1973.

Publication of this paper sponsored by Committee on Strength and Deformation Characteristics of Pavement Sections.

Dynamic Analysis of Falling Weight Deflectometer Data

BOUTROS E. SEBAALY, MICHAEL S. MAMLOUK, and TREVOR G. DAVIES

ABSTRACT

The response of pavement systems to falling weight deflectometer (FWD) blows is evaluated by using a multidegree of freedom elastodynamic analysis. This analysis is based on a Fourier synthesis of a solution for periodic loading of elastic or viscoelastic horizontally layered strata. The method is verified for selected flexible pavement sections for which high-quality field and laboratory data are available in the literature. FWD deflection measurements at various geophone locations are compared by using dynamic as well as static analyses. The results indicate that inertial effects are important in the prediction of the pavement response. Conventional static analyses yield significantly different results and therefore yield erroneous (unconservative) predictions of pavement moduli backcalculated from deflection data. Elastodynamic analyses, based on fundamental material parameters (Young's modulus, mass density), appear to provide a useful vehicle for correlating pavement response between different loading modes (impulse, vibratory, etc.). Because resonance is a less important factor in the displacement response characteristics of pavements subjected to transient loading, deflection data obtained from transient loading devices are, in general, easier to interpret.

Rehabilitation of rapidly deteriorating pavements is receiving increasing attention from highway engineers. Because building new roads in the United States is a rare event at the current time, the main concern is directed toward upgrading the existing ones. Therefore, the need for rational and fast methods of assuring the integrity of pavement structures becomes more evident.

Nondestructive testing has proven to be an effective method for evaluating the load carrying capacity of pavements. Unlike seismic techniques, deflection measurements have gained widespread popularity among highway agencies. Deflection devices apply various types of loading: static (Benkelman beam), harmonic (Road Rater and Dynaflect), and impulsive [(falling weight deflectometer (FWD)]. Field studies have indicated that deflections of the FWD correlate closely with pavement deflections induced by moving wheel loads (1,2). However, interpretation of FWD deflection data remains somewhat problematic. A point of discrepancy arises because FWD measurements are interpreted as static deflections in many studies, thus ignoring the fact that the load of the FWD is dynamic.

Most previous analyses of the data obtained from dynamic loading devices have been based either on empirical approaches or elastostatic and viscoelastostatic models. Empirical approaches are not transferable, and in the static analyses the inertia of pavements is ignored. Unless the inertial effect of pavements is incorporated in the analysis, misleading results may be obtained.

One approach to dynamics is to represent the pavement system by a combination of masses, springs, and dashpots, that is, the single degree-of-freedom analysis (3-5). Although these single degree-of-freedom models can take into consideration inertial effects, one of their major shortcomings is the assumption that loads, deflections, stresses, and strains are applied in one direction, that is, the vertical direction. In reality, when a vertical load is applied, stresses and strains are developed in all directions throughout the pavement structure. Thus, by using a single degree-of-freedom representation, the deflections at points away from the load (at various geophone locations) cannot be predicted.

A three-dimensional elastodynamic solution was recently applied to nondestructive testing of pavements by Mamlouk and Davies (6-8) and by Roesset and Shao (9). It was demonstrated that the pavement surface profile differs in several respects from the stationary deflection basins assumed in static analyses. The pavement surface takes a wave form propagation outwards from the point of excitation in a manner similar to that produced by exciting a surface of water. These waves are highly affected by the mode of loading, loading frequency, or both. Static analyses of dynamic deflections may result in significant errors, particularly if a resonant condition is encountered or if the radiation damping is large. Also, it was reported that the material damping (the viscous effect) is insignificant compared with the radiation damping in the pavement structure (the dynamic effect). Field observations indicate that different dynamic devices result in different deflection readings--a behavior that cannot be explained by a static analysis (1,10,11).

The purpose of this study is to provide a rational interpretation of the FWD performance based on elastodynamic analysis. The dynamic response of selected flexible pavements is verified by using field data. In this study, static and dynamic analyses of pavement response are compared and the errors resulting from ignoring the inertia of pavements are evaluated.

B.E. Sebaaly and M.S. Mamlouk, Center for Advanced Research in Transportation, Arizona State University, Tempe, Ariz. 85287. T.G. Davies, Department of Civil Engineering, University of Glasgow, Glasgow, Scotland.

FWD OPERATING CHARACTERISTICS

The FWD delivers a transient force impulse to the pavement surface. The device uses a weight that is lifted to a given height on a guided system and then

dropped. The falling weight strikes a plate that transmits the force to the pavement. By varying the mass of the falling weight, the drop height, or both, the impulse force can be varied. The FWD has a relatively small preload compared with the actual loading. The preload during the period the weights are dropping is usually in the range of 3 to 14 percent of the maximum load. The mass usually weighs about 200 lb and is dropped from a height varying from 0.13 to 1.3 ft. The weight drops onto a set of springs or a rubber buffer system to provide a load pulse in approximately a half-sine wave form. In most cases, the load is transmitted to the pavement through a 12-in.-diameter loading plate. The pulse duration is usually 30 to 40 msec.

The springs or the rubber buffers are usually loaded within their elastic range so that the force applied to the pavement can be found by equating the initial potential energy of the system to the stored strain energy of the springs when the mass is at rest. Therefore,

$$F = (2Mghk)^{1/2} \quad (1)$$

where

F = applied force (lb),
M = falling mass (lbm),
g = acceleration of gravity (ft/sec^2),
h = drop height (ft), and
k = spring constant (lb/ft).

The deflections are measured at the pavement surface at the center of the load and at several radial distances from the plate center. Velocity transducers (geophones) are usually used to measure deflections.

FWD DYNAMICS AND TRAFFIC SIMULATION

To investigate the dynamics of the FWD, two separate problems have to be addressed: the dynamics of the FWD and the dynamic response of the pavement system to the pulse loading. For the FWD, a simple discrete mass-spring model suffices to represent the device, as shown in Figure 1. The total displacement of the

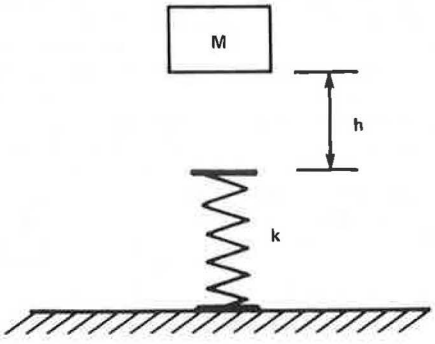

FIGURE 1 Discrete mass-spring model of FWD.

FWD system after time t can be given by the following equation:

$$z = s[(1 - \cos \omega t) + (2h/s)^{1/2} \sin \omega t] \quad (2)$$

where

s = compression of the spring under the static loading (ft),
ω = natural frequency of the oscillation of the system (Hz), and
h = drop height (ft).

The compression-time relation described by Equation 2 is shown in Figure 2. The first term in Equation 2 represents the response of the spring if the free fall of the mass is zero. In this case, the compression of the spring reaches twice the static value, that is, 2s. The second term is dominant for large drop heights. For example, because FWD spring stiffness is approximately 6 kips/in. and the mass is approximately 200 lbm, the static compression of the spring is only 40 mils. Thus, even for drop heights as low as 1.5 in., the maximum spring compression is predicted to within 10 percent by the second term in Equation 2 alone (in this case, 0.35 in. instead of the correct 0.39 in.). Because for larger drop heights the error is even smaller, the compression-time relation for all practical purposes becomes

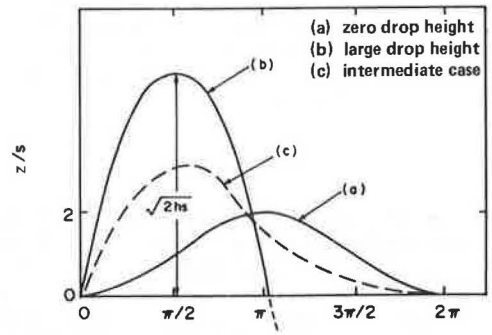

FIGURE 2 Three compression time relations.

$$z = (2h/s)^{1/2} \sin \omega t \quad (3)$$

Also, after the loading and unloading cycle is complete, the mass loses contact with the spring for a time period after which contact takes place again. A previous study indicated that, even for the most conservatively low drop heights, this elapsed time is approximately 180 msec, and therefore the initial impulse imparted by the FWD is effectively independent of the subsequent rebound (12).

As far as traffic simulation is concerned, previous studies concluded that a fixed-in-place nondestructive testing device of current design cannot simulate exactly the loading effect of a moving wheel (1,2). This conclusion is suggested by the disagreement between the considerably higher accelerations induced by the FWD (more than 4 g) and the low acceleration induced by moving wheels (approximately 0.1 g). Also, differences between the pulse duration of the FWD (25 to 60 msec) and that of moving trucks (about 200 msec) have been observed. Nevertheless, field results on deflections compare favorably. Moreover, better simulation can be achieved by simultaneously decreasing the drop height and increasing the mass of the drop weight. In this case, the full compression-time relation (Equation 2) may have to be adopted.

DYNAMIC ANALYSIS

In this analysis, the pavement system is idealized as layered viscoelastic continuum overlying the bedrock at a finite depth, as shown in Figure 3. Each material is characterized by Young's modulus, Pois-

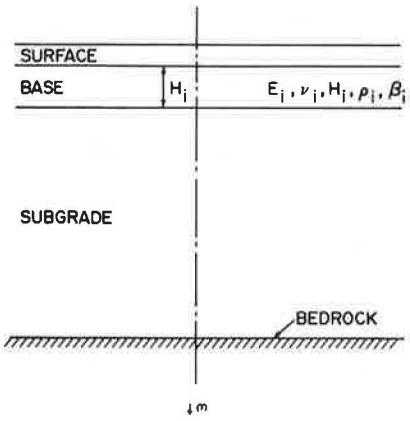

FIGURE 3 Flexible pavement characterization as a multilayer viscoelastic system.

son's ratio, material damping, and mass density. The assumptions of material linearity and isotropy as well as the no-slip conditions at the layer interfaces are invoked. The thicknesses of various layers as well as the depth to bedrock are assumed to be known.

The dynamic solution was obtained by using the multilayer computer program DYNAMIC. The solution is based on the Helmholtz equation of elastodynamics for harmonic loading (13). Because no direct solution to the elastodynamic equation is available for multilayered systems, a numerical solution must be used (7,14). This solution provides the in-phase and out-of-phase displacements at any location throughout the pavement structure. Unlike the single degree-of-freedom representations, the three-dimensional nature of the pavement system is considered in this solution. Further, the static solution can be easily derived from the dynamic solution simply by using a frequency of zero. This is valid because the Helmholtz equation of elastodynamics reduces to Navier's equation of elastostatics when the frequency is reduced to zero.

Because the FWD applies a transient load on the pavement surface, Fourier transformations can be used to represent the transient mode by a series of harmonic loadings with various frequencies and amplitudes. The FWD loading impulse is assumed to be periodic with a period T that is essentially divided into two time periods: (a) loading pulse width, T_p, and (b) rest period, T_R, as shown in Figure 4. The pulse width, T_p, is a function of the loading device as well as of the pavement system properties, varying from 25 to 60 msec for most FWD devices. Because a repeated loading function is used in the analysis, the second period, T_R, is chosen in such a way that the pavement fully recovers from deformation during this time so that the response to each impulse is isolated from earlier ones. After the evaluation of Fourier coefficients of the load impulse expansion, the phase lag, frequency, and amplitude of each harmonic load are obtained. Thus, the solution for the displacement response is sought in the so-called frequency domain (14). The responses of each of the harmonic loadings are summed in the time domain, which results in the full response of the impulse loading generated by Fourier expansion. The number of terms used in the Fourier expansion is a function of the pulse parameters and the degree of approximation sought.

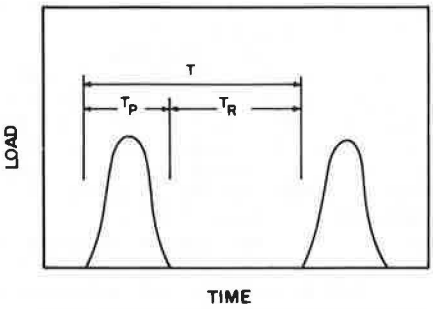

FIGURE 4 Assumed periodicity of FWD impulses.

APPLICATIONS AND RESULTS

To verify the validity of the model described in this paper, a theoretical analysis was performed on selected typical in-service flexible pavement sections. The theoretical results are compared with data reported from FWD measurements and laboratory testing on pavement sections Bement, Deland, Monticello, and Sherrard performed by Hoffman and Thompson (1). Each section consists of a surface layer and a base course above the subgrade, as shown in Figure 3. The material types and layer thicknesses of various pavement sections are given in Table 1. No information was available concerning the thickness of the subgrade above the bedrock. A 50- to 60-ft subgrade thickness was assumed based on field observations indicating that the bedrock is deep.

TABLE 1 Material Types and Layer Thicknesses of Pavement Sections

Section	Layer	Type	Thickness (in.)
Bement	Surface	Asphalt concrete	4
	Base	Soil cement	6
	Subgrade	A-7-6 (24)	720[a]
Deland	Surface	Surface treatment	0.5
	Base	Granular	8
	Subgrade	A-7-6 (21)	720[a]
Monticello	Surface	Asphalt concrete	3.5
	Base	Plant-mixed CAM	8
	Subgrade	A-6 (8)	720[a]
Sherrard	Surface	Asphalt concrete	4
	Base	Crushed stone	14
	Subgrade	A-4 (6)	720[a]

[a]Assumed values.

Table 2 gives the material properties of the pavement sections selected for analysis. The modulus values were reported by Hoffman and Thompson (1) as a result of an extensive laboratory program on the four pavement sections (Bement, Deland, Monticello, and Sherrard). The resilient properties of the subgrade soils were produced by subjecting the samples to repetitive loadings of varying magnitudes, according to the method proposed by Thompson and Robnett (15). For asphalt concrete layers and stabilized materials, the specimens were subjected to repeated diametral loads, and the diametral resilient modulus was computed. The modulus values used in this study were within ± 1 standard deviation from the laboratory mean values, and typical Poisson's ratios were assumed.

The experimental results indicated a difference in temperature between field and laboratory conditions, which was also taken into account. A typical

TABLE 2 Pavement Material Properties

Section	Layer	Moduli[a] (ksi)	Poisson's Ratio[b]	Density[b] (lb/ft^3)
Bement	Surface	170	0.35	145
	Base	1700	0.4	140
	Subgrade	7.5	0.45	115
Deland	Surface	30	0.35	145
	Base	9	0.4	140
	Subgrade	9	0.45	115
Monticello	Surface	450	0.35	145
	Base	650	0.4	140
	Subgrade	8	0.45	115
Sherrard	Surface	500	0.35	145
	Base	35	0.4	140
	Subgrade	10	0.45	115

[a] From laboratory testing.
[b] Assumed values.

material damping ratio of 5 percent was used throughout the analysis (16). The FWD used to obtain the deflection measurements (1) had a 12-in.-diameter baseplate and produced an impulse load of 8 kips with a loading duration ranging from 30 to 40 msec. The deflections were measured with velocity transducers (geophones) located at 0, 1, 2, and 3 ft from the center of the loading plate. In the analysis, the loading impulse induced by the FWD was generated by a series of harmonic loads using the Fourier expansion, as discussed earlier. The half-sine impulse representation was found to be adequately modeled by using only the first 10 terms of the Fourier series.

By using a pulse duration of 40 msec and a rest period of 180 msec, it was found that the shape of the half-sine wave load impulse was accurately reproduced. Figure 5 shows the theoretical impulse synthesized from the Fourier expansion. The actual and theoretical impulses had the same duration and their amplitudes did not differ by more than 2 percent. The 10 frequencies used in the analysis and their relative amplitudes are given in Table 3 and shown in Figure 6. By examining Figure 6, it can be observed that the FWD pulse cannot be simply represented by a single load frequency because it is a complex combination of a number of harmonic loadings with different frequencies and magnitudes. It should be noted that the highest frequency is 45.5 Hz, which is sufficiently low to avoid the numerical difficulties associated with the high-frequency response of the discrete layer formulation (14).

The analysis indicated the existence of a short time lag between the application of the load impulse and the response of the pavement at all four geophone

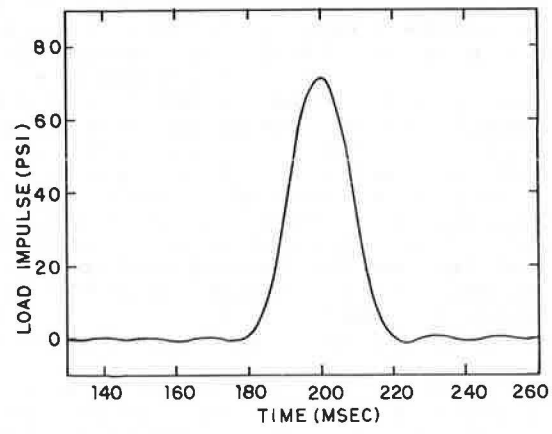

FIGURE 5 Theoretical representation of FWD impulse.

TABLE 3 Frequency Content of FWD Load Impulse Obtained by Fourier Series Expansion

Frequency (Hz)	Relative Amplitude	Cumulative Amplitude (percent)
0	51	9
4.5	100	26.8
9.1	94	43.5
13.6	84	58.4
18.2	72	71.2
22.7	58	81.5
27.3	44	89.3
31.8	25	93.8
36.4	20	97.3
40.9	11	99.3
45.5	4	100.0

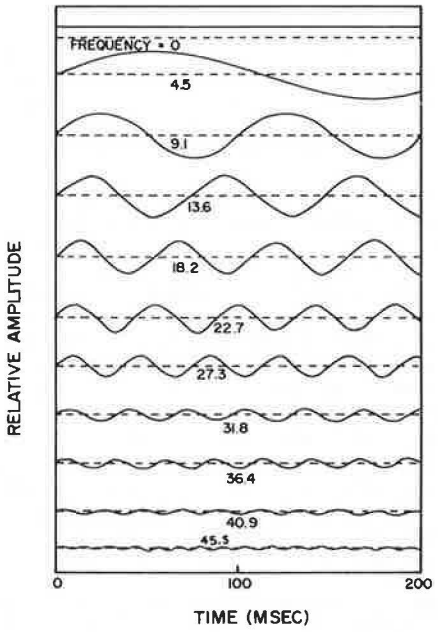

FIGURE 6 Equivalent theoretical harmonic components of FWD impulse.

locations. Figure 7 shows the phase lag for the center of the baseplate at the Bement section, which is almost typical for the other three locations. The phase lag is small, only 4 to 6 msec at the peak deflection, and no discernible flattening occurs with respect to the initiating impulse. This phase lag is mainly a consequence of inertia and not of material damping. Also, the results indicate that small phase lags (not more than 1.5 msec) exist between peak deflections at successive geophones. This analysis proves also that little difference in the peak acceleration occurs between the falling mass itself and the pavement. This conclusion varies somewhat from the experimental results (1). This variation may be due to the existence of the cushioning material between the FWD and the pavement that was used to distribute the road more evenly.

In addition to the dynamic formulation discussed earlier, a static analysis was performed for comparison. The static solution was obtained by using the same DYNAMIC computer program at zero frequency. Samples of the DYNAMIC program results with zero frequency were verified by using the Chevron computer

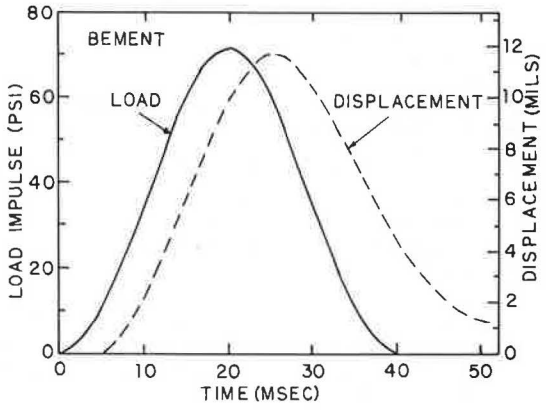

FIGURE 7 FWD load impulse and pavement displacement response at center of baseplate.

program under similar conditions with a rigid base. The two programs provided identical results.

Comparisons between the experimental data of the FWD and the results of the numerical model used here are shown in Figures 8-11. Each figure shows field deflections as well as deflections obtained by using the static (zero-frequency) analysis and the dynamic model at various geophone locations. The results indicate that in all four pavement sections the dynamic analysis values were within ±15 percent of the field deflections and as low as 3 percent in some cases. The dynamic curves crossed the field results in all figures, indicating that in most cases the highest error occurs below the center of the baseplate. It is probable that part of the discrepancy at some locations is a consequence of the approximate estimation of the subgrade thickness. Meanwhile, the static analysis always yielded average deflection values approximately 25 to 30 percent higher than those obtained from the elastodynamic analysis. In most cases, these static deflections were 20 to 40 percent different from the field deflections.

SUMMARY

Published field data on pavement response to the FWD were analyzed by using an elastodynamic technique. Because of the inertia of the pavement system, the displacement impulse slightly lags the loading impulse, although its shape closely reflects the half-sine loading curve. Such analysis shows close agreement with the field data, with a maximum error of ±15 percent. On the other hand, the static analysis of the pavement response to the FWD always resulted in average surface deflections 20 to 40 percent larger than field measurements. This indicates that the static analysis of the FWD overestimates (by backcalculating from deflection data) the stiffnesses of the pavement layers. It is expected that larger differences between static and dynamic results would

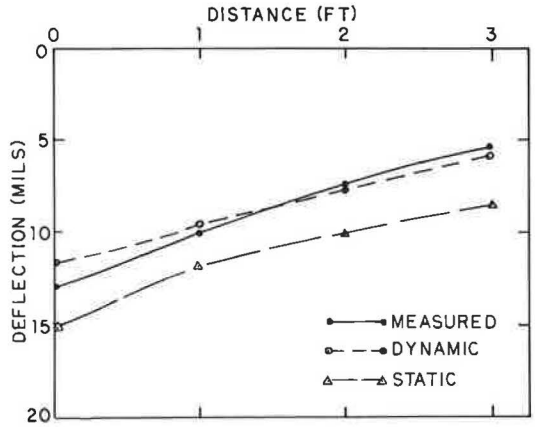

FIGURE 8 Measured, static, and dynamic deflections at various geophone locations for Bement section.

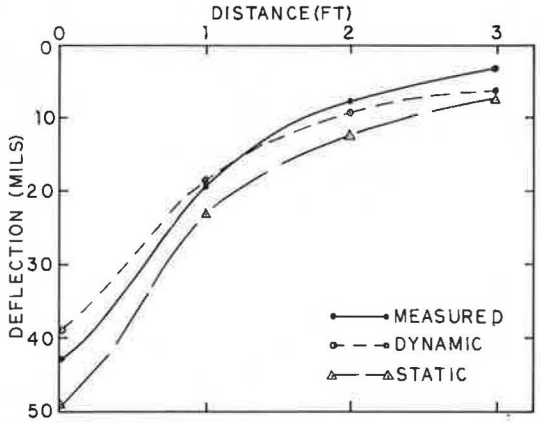

FIGURE 9 Measured, static, and dynamic deflections at various geophone locations for Deland section.

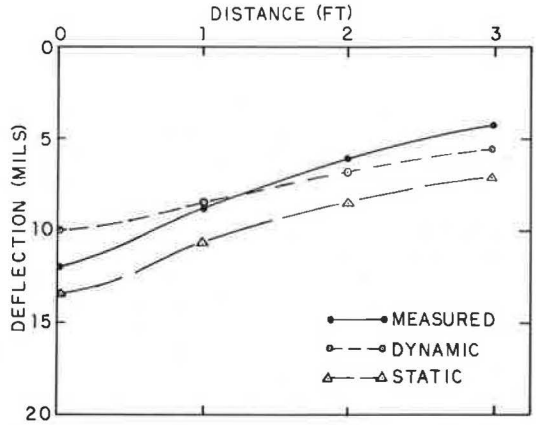

FIGURE 10 Measured, static, and dynamic deflections at various geophone locations for Monticello section.

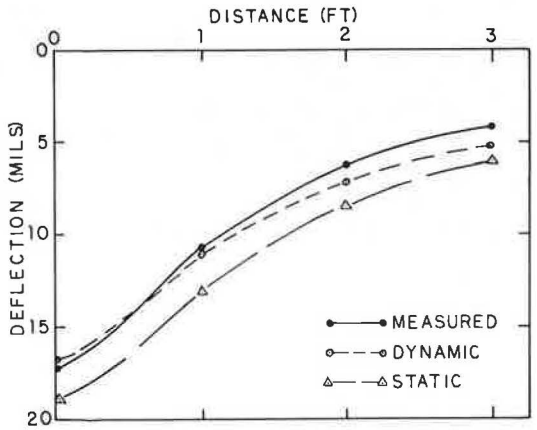

FIGURE 11 Measured, static, and dynamic deflections at various geophone locations for Sherrard section.

have been obtained if the subgrade was smaller than that used in this study.

The FWD appears to be suitable for the nondestructive testing of pavements because it simulates the shape and temporal nature of moving wheel loading reasonably closely. In addition, the hazards of resonance associated with periodic loading devices such as the Dynaflect and the Road Rater are less acute with the transient loading of the FWD.

ACKNOWLEDGMENTS

The authors wish to thank E. Kausel of the Massachusetts Institute of Technology for providing the computer program for harmonic loading and M.R. Thompson of the University of Illinois for providing the field data that were used in this study. The Department of Civil Engineering and the Center for Advanced Research in Transportation at Arizona State University are acknowledged for making their facilities available to the authors.

REFERENCES

1. M.S. Hoffman and M.R. Thompson. Nondestructive Testing of Flexible Pavements--Field Testing Program Summary. Transportation Engineering Series 31, Illinois Cooperative Highway and Transportation Research Program, Series 188, University of Illinois at Urbana-Champaign, Urbana, June 1981.
2. M.S. Hoffman and M.R. Thompson. Comparative Study of Selected Nondestructive Testing Devices. In Transportation Research Record 852, TRB, National Research Council, Washington, D.C., 1982, pp. 32-41.
3. R.A. Weiss. Pavement Evaluation and Overlay Design: A Method that Combines Layered-Elastic Theory and Vibration Nondestructive Testing. In Transportation Research Record 700, TRB, National Research Council, Washington, D.C., 1979, pp. 20-34.
4. R.A. Weiss. Subgrade Elastic Moduli Determined from Vibratory Testing of Pavements. U.S. Army Engineer Waterways Experiment Station, Vicksburg, Miss., Oct. 1977.
5. M.S. Hoffman. Loading Mode Effects on Pavement Deflections. Journal of Transportation Engineering, ASCE, Vol. 109, No. 5, Sept. 1983, pp. 651-668.
6. M.S. Mamlouk and T.G. Davies. Elastodynamic Analysis of Pavement Deflections, Transportation Engineering Journal, ASCE, Vol. 110, No. 6, Nov. 1984, pp. 536-550.
7. T.G. Davies and M.S. Mamlouk. Theoretical Response of Multilayer Pavement Systems to Dynamic Nondestructive Testing. In Transportation Research Record 1022, TRB, National Research Council, Washington, D.C., 1985, pp. 1-7.
8. M.S. Mamlouk. Use of Dynamic Analysis in Predicting Field Multilayer Pavement Moduli. In Transportation Research Record 1043, TRB, National Research Council, Washington, D.C., 1985, pp. 113-121.
9. J.M. Roesset and K-Y. Shao. Dynamic Interpretation of Dynaflect and Falling Weight Deflectometer Tests. In Transportation Research Record 1022, TRB, National Research Council, Washington, D.C., 1985, pp. 7-16.
10. D.R. Alexander. Correlation of Nondestructive Pavement Evaluation Test Results with Conventional Quality Control and In-Situ Strength Tests Obtained on an MX Road Test Section. U.S. Army Engineer Waterways Experiment Station, Vicksburg, Miss., Feb. 1985.
11. J.W. Hall. Comparative Study of Nondestructive Pavement Testing--MacDill Airforce Base, U.S. Army Engineer Waterways Experiment Station, Vicksburg, Miss., 1984.
12. B.E. Sebaaly, T.G. Davies, and M.S. Mamlouk. Dynamics of the Falling Weight Deflectometer. Journal of Transportation Engineering, ASCE, Vol. 111, No. 6, Nov. 1985.
13. A.C. Eringen and E.S. Subhubi. Elastodynamics, Vol. 2, Linear Theory. Academic Press, New York, 1975.
14. E. Kausel and R. Peek. Dynamic Loads in the Interior of a Layered Stratum: An Explicit Solution. Bull. of the Seismological Society of America, Vol. 72, No. 5, Oct. 1982, pp. 1459-1481.
15. M.R. Thompson and Q.L. Robnett. Resilient Properties of Subgrade Soils. Final Report. Report UILU-ENG-76-20009. Transportation Engineering Series No. 14, June 1976.
16. F.E. Richart, Jr., J.R. Hall, Jr., and R.D. Woods. Vibrations of Soils and Foundations. Prentice-Hall, Englewood Cliffs, New Jersey, 1970.

Publication of this paper sponsored by Committee on Strength and Deformation Characteristics of Pavement Sections.

Use of Falling Weight Deflectometer Data in Predicting Fatigue Cracking

RAM B. KULKARNI, EZIO ALVITI, and BILLY CONNOR

ABSTRACT

A statistical model was developed for the Alaska Department of Transportation and Public Facilities to predict the occurrence of cracking on paved Alaskan highways. The department has been conducting visual surveys of pavement condition since 1978 on the statewide network of highways. In addition, a falling weight deflectometer has been used since 1982 to provide an indication of the pavement's structural strength. The pavement condition history and deflections were used in a stepwise multiple regression analysis to predict the percentage of pavement area cracked (including the cracked area that was patched) as a function of variables such as pavement age, traffic volume, and deflections. Initially an attempt was made to develop a regression equation to predict the percent cracking for each mile-long road segment. However, this analysis could not produce a regression equation that was statistically significant (the highest correlation coefficient was less than 0.5). An alternative approach was then tried. Rather than predict cracking for each individual mile, it was considered adequate to predict average cracking for each construction project (which might consist of several miles built at the same time). Miles within each construction project that had similar deflections (and hence similar structural strength) were grouped, and average values of cracking and other variables were calculated for each group. Regression analysis of the grouped data produced statistically significant relationships (with correlation coefficients in the range of 0.7 to 0.9). The study demonstrates the development of a performance prediction model with limited inventory and deflection data.

Pavement deflection data have been used in the past by the Alaska Department of Transportation and Public Facilities (DOTPF) to monitor the performance of their highways. These data were used in an earlier study to develop a model for predicting fatigue cracks in the pavements (1). Deflection measurements at the center of the load were used for this purpose.

Two years ago, the Alaska DOTPF acquired a falling weight deflectometer (FWD) to measure pavement deflections. This equipment, in addition to measuring the deflection at the center of the load, records deflections at six other points away from the center of the load. The users of the FWD have reported that the measurements obtained with the help of this equipment can be used to define the shape of the deflection basin (2). Further, it was reported that the deflection basin was a better indicator of the damage potential to highway surfaces than the single measurement of surface deflection under the load center (2).

Based on this experience, it was expected that the fatigue damage prediction model could be improved significantly if FWD data were used in place of deflections at the center of the load. Therefore, the primary objective of this study was to develop a model for fatigue crack prediction using the FWD data. A mechanistic approach has been generally used to model a pavement structure as a multilayer elastic system and FWD data are used to estimate mechanistic layered properties necessary for structural analysis.

However, in this study the authors used an empirical approach because the primary purpose was not to explain theoretical causes for the occurrence of fatigue cracking but to statistically correlate fatigue cracking with field observations. One limitation of this approach is that predictions cannot be made beyond the range of available data with a high degree of reliability. On the other hand, major advantages of the empirical approach are that it is well calibrated with past observations of pavement performance and it can be developed with limited inventory and deflection data. Because the data used in the development of a statistical model covered an adequate range of age, traffic, and pavement conditions in Alaska, the model is expected to provide reliable predictions of fatigue cracking on Alaskan highways.

DATA COLLECTION

The data used in this study were contained in two different files. The pavement inventory data files contained the following items:

- Route number;
- Coordinated data system (CDS) mile;
- Mays roughness;
- Bumps (>1 in., >2 in., >3 in.);
- Percent alligatoring (Type I, Type II);
- Patching (%);
- Average rut depth; and
- Rut depth standard deviation.

R.B. Kulkarni and E. Alviti, Woodward-Clyde Consultants, 100 Pringle Avenue, Walnut Creek, Calif. 94596-3564. B. Connor, Alaska Department of Transportation and Public Facilities, Fairbanks, Alaska 99701-6394.

The FWD data files contained the following items:

- Date,
- Temperature (°F),
- Route number,
- CDS mile x 100,
- Load (falling weight), and
- Sensor deflections (sensors 1 to 7, μmm)

All the available inventory data for the years 1981 and 1982 were reviewed for this study. Also, the available FWD data for the years 1982 and 1983 were reviewed for possible use in the analysis.

In addition, data on the surfacing dates on each route were also obtained to determine the age of the pavement on each section of the route.

Finally, data on annual average daily traffic (AADT) and monthly average daily traffic (MADT) for April and May were obtained from the 1981 annual report (3).

DATA ANALYSIS

The data were analyzed in the following manner:

1. Merge pavement inventory files;
2. Estimate age, AADT, and MADT;
3. Select an FWD record for each pavement inventory record;
4. Search for suitable fatigue cracking prediction model;
5. Group data for further analysis; and
6. Search for fatigue cracking model using grouped data.

Merge Pavement Inventory Files

Two pavement inventory files contained 1981 and 1982 data for the state highway system. Because about one-half of the system is surveyed each year, no significant overlap occurred between the two files except for Route 170000. Where overlap did occur, 1982 data were used unless the CDS mile had lower cracking in 1982 and no rehabilitation action was taken in 1981 or 1982. If a -1 appeared as either type of fatigue cracking or patching, the record was omitted. Routes that did not have FWD measurements were also omitted. Finally, portions of routes for which surfacing information was not available were omitted.

The following routes were represented in the merged pavement inventory file:

Route No.	Route Name
130000	Seward/Glennallen Highway
150000	Steese/Elliott/Dalton Highway
170000	Parks Highway
180000	Alaska Highway
190000	Richardson Highway

In the remainder of this paper, these routes will be referenced by the first three digits of the route number. For example, Route 130000 will be referred to as Route 130.

The pavement inventory files recorded the percent alligator (fatigue) cracks by Type I and Type II. Because it may not be practical to predict cracking by Type I and Type II, it was considered appropriate to combine these two types of cracks and treat the total as the observed fatigue cracks.

Although the fatigue cracking data were identified by the year during which they were recorded in the field, a discussion with the Alaska DOTPF staff indicated that some observations might have been recorded during the same period that maintenance work had been done. Thus, it was possible that some of the observations were recorded before maintenance and some of them after maintenance. To reduce this inconsistency, it was decided to combine percentage of patching with the percentage of fatigue cracking to arrive at the total percentage of fatigue cracking in each mile of the route. If this total for any CDS mile exceeded a value of 100.0, it was changed to 100.0.

Estimate Age, AADT, and MADT

The surfacing date was added to each record of the pavement inventory file. An indicator variable, age adjustment (AGE ADJ), was also added to each record to identify which of the two original pavement inventory files it came from. A code of 1 was used for 1981 and a code of 0 was used for 1982. The age of a CDS mile can be calculated by using the formula:

$$\text{AGE} = 82 - \text{LAST FIX} - \text{AGE ADJ} \quad (1)$$

where LAST FIX is the last 2 digits of the year of its most recent surfacing. Because some CDS miles on Routes 180 and 190 were last surfaced in 1982 but were only inventoried in 1981, this formula computed a value of -1 for them. Because the previous surfacing dates were not known, these records had to be excluded from the analysis.

Daily traffic is measured at a selected number of points on each route. The values of AADT and MADT for each CDS mile were computed by using the following procedure:

1. Calculate the value of ADT at both end points of the CDS mile by using linear interpolation.
2. If none of the original points at which ADT data were collected falls within this CDS mile, set ADT to the average of the two values calculated in Step 1.
3. If one or more of the original points at which ADT data were collected falls within this CDS mile, set ADT as follows:
   a. Define N-1 intervals where N includes the two endpoints and the other points falling within this CDS mile;
   b. Compute the average ADT for each of the N-1 intervals;
   c. Multiply the average ADT by the length of the interval as a fraction of a mile for each interval; and
   d. Set ADT for this CDS mile to the sum of all N-1 weighted averages.

In some instances, the number of miles between two points on a route on which ADT is measured is significant. The value of ADT for many of these CDS miles would be a general approximation.

This procedure was first done for annual ADT and then repeated for April and May monthly ADT. April and May were selected because most of the pavement damage due to traffic would be expected to occur during the spring thaw period.

Select an FWD Record for Each Pavement Inventory Record

The FWD data were recorded at every 0.2 CDS mile on each route. For numerous sections of the routes, data were recorded on several occasions during the season. This was done because it was not known when a section of road was in its weakest condition. For most records in the pavement inventory file, more

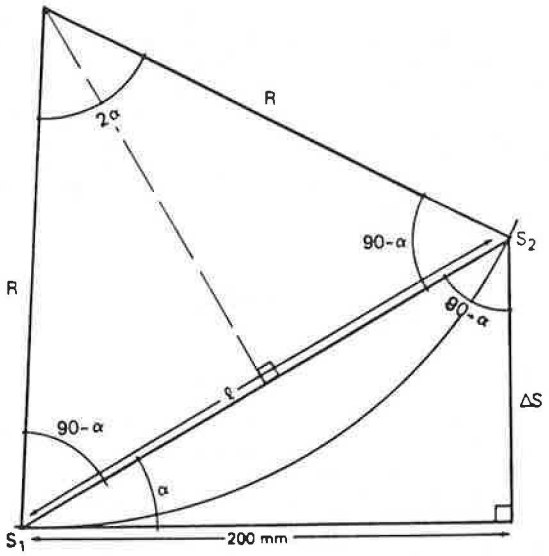

FIGURE 1 Illustration of radius of curvature.

than one FWD record exists. It was decided that a representative record should be selected and that it should represent the CDS mile in its weakest condition. The criterion used to select the FWD record was the radius of curvature. The radius of curvature is the radius of the circle, which is based on the first two sensor readings as described in the following procedure and shown in Figure 1.

1. Let S_1 and S_2 be Sensor No. 1 and Sensor No. 2 readings, respectively.
2. Let $\Delta S = (S_1-S_2)/1{,}000$.
3. Let ℓ be the length of the chord between S_1 and S_2 on the circle. Because the distance between Sensor No. 1 and Sensor No. 2 on the FWD is 200 mm, a right triangle exists the hypotenuse of which is ℓ and the base of which is 200 mm. The Pythagorean theorem allows us to compute ℓ^2 with the following formula:

$$\ell^2 = (\Delta S) + 200^2 \quad (2)$$

4. Also shown in Figure 1 is a right triangle the hypotenuse of which is the radius of the circle, R, and whose base has a length of $\ell/2$.
5. Noting that the three angles of the triangle in Step 3 are the same as those for the triangle in Step 4 and defining the angle α as is shown in Figure 1, the following formulas are derived:

$$\sin \alpha = \Delta S/\ell \quad (3)$$

$$\cos 90 - \alpha = \ell/2/R = \ell/2R \quad (4)$$

$$\cos 90 - \alpha = \sin \alpha \text{ (trigonometric identity)} \quad (5)$$

$$\Delta S/\ell = \ell/2R \quad (6)$$

6. Algebraic manipulation gives

$$R = \ell^2/2\Delta S = [(S_1 - S_2)^2 + 200^2]/[2(S_1 - S_2)] \quad (7)$$

Because smaller values of the radius of curvatures would indicate a pavement with lower structural strength, the FWD record with the smallest radius of curvature was used to represent a CDS mile in its weakest condition. The information on this FWD record was combined with the information on the pavement inventory record to form a single new record.

Search for Suitable Fatigue Cracking Prediction Model

The evaluation of alternative fatigue cracking prediction models was performed by using the multiple linear regression technique and engineering judgment. The first group of regressions was done by using a value of Sensor No. 1 that was adjusted to a standard weight and temperature. The predictor variables that were tried were the seven sensors, radius of curvature, age, AADT, MADT, temperature, and falling weight. A model with an r-squared (R^2) value greater than .20 could not be found. The transformations of these variables that were tried included logarithmic, square root, square, reciprocal, reciprocal square root, and reciprocal square. For temperature and weight, subtracting a constant was tried so that number of degrees above freezing and amount of weight over a specific value could be added to the model. None of these transformations considerably increased R^2 and in most cases actually decreased it. The interaction between age and AADT and MADT was added with no success. Finally, the logarithmic, square root, and reciprocal transformations of fatigue cracking were tried; they also did not yield satisfactory results.

The analysis just described was repeated for Sensor No. 1 with it only adjusted by falling weight; the same results were obtained. The analysis was repeated using the unaltered value of Sensor No. 1. The results were similar to those of the previous two analyses. It should be noted that because the radius of curvature computation depends in part on the value of Sensor No. 1, adjusting its value could, and in many cases did, cause a different FWD record to be selected for a particular pavement inventory record. Because the adjustment for Sensor No. 1 values did not change results significantly, only unadjusted values of Sensor No. 1 were used in subsequent analysis.

Data screening based on fatigue cracking, temperature, falling weight, and route number was tried next. When screening data, records that were in a specified range of one or more variables should be selected. The motivation is that by removing unusual cases, the prediction will be improved. Data screening based on fatigue cracking, falling weight, Sensor No. 1 value, or any combination thereof did not result in a satisfactory model.

At first, selecting records with temperatures in the range of 50 to 80°F appeared to show some promise. But on closer inspection it became apparent that most of the records being excluded were for either Route 170 or Route 180. If only the records corresponding to Routes 130, 150, and 190 are included, then an R^2 of .40 can be achieved. Including only the records of Routes 170 and 180 resulted in an R^2 below .20. A discussion with Billy Connor of the Alaska DOTPF provided valuable insight at this point of the analysis; he said that Routes 170 and 180 were built more recently than the other routes and used different standards. Even the best model that could be found did not explain most of the variation as is reflected in an R^2 below .50. Rather than predicting fatigue cracking for a CDS mile, perhaps predicting the average fatigue cracking for a logical grouping of CDS miles would give better results. This approach is described in the remaining sections of this paper.

Group Data for Further Analysis

A surfacing project on a route covers a consecutive group of CDS miles on that route and is therefore a natural criterion for grouping the data. The data were first ordered by route number and within each

route by CDS mile number. The surfacing projects were then numbered consecutively beginning with Route 130 and continuing through Route 190. A total of 35 surfacing projects were found on the 5 routes. For reasons explained earlier in this paper, age could not be established for two of these projects and they had to be excluded from the analysis.

The data in each project were then divided into 3 groups based on the value of Sensor No. 1. These groups were defined as follows:

Group No.	Range of Sensor No. 1
1	0-600
2	60-1,000
3	1,001+

For some projects, the Sensor No. 1 values fell into only one or two of these ranges and therefore only one or two groups were used in the analysis. A new file with one record for each group in each project was created. These records have the same variables as the CDS mile records plus one more. The value for a variable on the new record is the average of the values for that variable across all the records in the group it represents. The variable added to the record is the case weight, which is the number of CDS miles in the group. Table 1 gives data on the first 4 projects on Route 130. Because of the large number of variables, the table has been divided into two sections. Table 2 gives data on the new file whose records are the group averages. The value in the column labeled CDS is the first CDS mile in the project to which that record corresponds. The column headings used in Tables 1 and 2 are explained in Table 3.

Search for Fatigue Cracking Model Using Grouped Data

Weighted multiple linear regression was used to analyze the averaged data. The variable Case Wgt in Table 2 contains the weights used in the analysis. The variety of models that was tried with this data is similar to those models tried with the original data. None of the transformations appreciably improved the fit of the data, and in most cases resulted in a worse fit. With all five routes present in the analysis, the best fit that could be found had an R^2 of about .30.

The atypical values were smoothed out when the

TABLE 1 Subset of Data Before Grouping

Row	Route	Cds	Date	Project	Temp	Wgt	Radius	S1	S2	S3	S4	S5	S6	S7
1	130	239	820524	1	52	584	101010	695	497	374	247	145	83	48
2	130	240	820524	1	52	572	53619	831	458	275	151	80	43	22
3	130	241	820524	1	52	592	51021	1135	743	531	324	181	110	62
4	130	242	820524	1	52	642	57143	1210	860	617	405	262	141	70
5	130	243	820524	1	52	618	72464	976	700	492	287	167	75	46
6	130	244	820524	1	56	562	82988	582	341	195	108	65	42	27
7	130	245	820524	1	56	651	62696	701	382	412	269	163	88	44
8	130	246	820524	1	56	639	75188	628	362	218	111	60	40	27
9	130	247	820524	1	56	592	98522	612	409	280	164	95	53	29
10	130	248	820524	1	56	588	117647	577	407	305	196	117	71	43
11	130	249	820524	1	56	584	75472	616	351	203	113	70	48	33
12	130	250	820524	1	56	658	81633	680	435	261	136	81	53	32
13	130	251	820428	1	54	755	67114	672	374	194	62	8	5	4
14	130	252	820428	1	54	745	74350	617	348	164	42	17	5	4
15	130	253	820428	1	54	707	62500	775	455	238	91	25	3	7
16	130	254	820428	2	54	740	81633	522	277	134	43	12	6	5
17	130	255	820428	2	54	689	80645	706	458	287	175	76	13	7
18	130	256	820511	3	44	651	71943	811	533	352	210	117	53	21
19	130	257	820511	3	68	603	122699	358	195	122	78	50	29	15
20	130	258	820511	4	68	590	55097	1046	683	435	269	153	66	22
21	130	259	820428	4	67	596	71943	723	445	276	158	61	4	4
22	130	260	820428	4	67	593	56818	722	370	218	127	52	12	3
23	130	261	820428	4	67	626	53764	694	322	145	61	27	11	11

Row	Route	Cds	Project	Crk1	Crk2	Patch	Crk	Last Fix	Age Adj	Age	Adt	Apr	May	Apr+ May
1	130	239	1	14	0	0	14	65	0	17	698	3766	4262	8028
2	130	240	1	4	0	0	4	65	1	16	690	3621	4100	7721
3	130	241	1	0	0	0	0	65	0	17	682	3475	3939	7414
4	130	242	1	100	0	8	100	65	1	16	674	3329	3778	7107
5	130	243	1	32	0	11	43	65	1	16	666	3183	3617	6800
6	130	244	1	52	0	16	68	65	1	16	658	3037	3455	6492
7	130	245	1	100	0	29	100	65	1	16	650	2892	3294	6186
8	130	246	1	100	0	3	100	65	1	16	643	2746	3133	5879
9	130	247	1	44	0	0	44	65	1	16	635	2600	2972	5572
10	130	248	1	36	0	30	66	65	1	16	627	2454	2810	5264
11	130	249	1	68	0	22	90	65	1	16	617	2308	2649	4957
12	130	250	1	47	0	0	47	65	1	16	599	2163	2488	4651
13	130	251	1	85	0	0	85	65	1	16	580	2017	2327	4344
14	130	252	1	33	0	0	33	65	1	16	561	1871	2165	4036
15	130	253	1	48	0	4	52	65	1	16	543	1725	2004	3729
16	130	254	2	22	0	3	25	77	1	4	524	1579	1843	3422
17	130	255	2	0	0	39	39	77	1	4	505	1434	1682	3116
18	130	256	3	7	0	7	14	65	1	16	486	1288	1520	2808
19	130	257	3	6	0	6	12	65	1	16	467	1142	1359	2501
20	130	258	4	0	0	2	2	73	1	8	452	996	1198	2194
21	130	259	4	0	0	45	45	73	1	8	450	850	1037	1887
22	130	260	4	0	0	0	0	73	1	8	450	704	875	1579
23	130	261	4	0	0	24	24	73	1	8	450	559	714	1273

TABLE 2 All Data After Grouping

Row	Route	Cds	Project	Wgt	Crk	Age	Apr+May	Radius	S1	S2	S3	S4	S5	S6	S7
1	130	239	1	2	67.0	16.0	5878.0	100317	579.5	374.0	250.0	152.0	91.0	56.5	35.0
2	130	239	1	11	55.6	16.1	5627.6	74961	709.4	433.7	282.8	152.1	82.5	45.1	26.9
3	130	239	1	2	50.0	16.5	7260.5	54082	1172.5	801.5	574.0	364.5	221.5	125.5	66.0
4	130	254	2	1	25.0	4.0	3422.0	81633	522.0	277.0	134.0	43.0	12.0	6.0	5.0
5	130	254	2	1	39.0	4.0	3116.0	80645	706.0	458.0	287.0	175.0	76.0	13.0	7.0
6	130	256	3	1	12.0	16.0	2501.0	122700	358.0	195.0	122.0	78.0	50.0	29.0	15.0
7	130	256	3	1	14.0	16.0	2808.0	71943	811.0	533.0	352.0	210.0	117.0	53.0	21.0
8	130	258	4	3	23.0	8.0	1579.7	60842	713.0	379.0	213.0	115.3	46.7	9.0	6.0
9	130	258	4	1	2.0	8.0	2194.0	55097	1046.0	683.0	435.0	269.0	153.0	66.0	22.0
10	130	262	5	8	7.1	3.0	861.3	104252	487.5	289.3	181.1	119.9	73.8	39.1	20.4
11	130	262	5	3	10.7	3.0	846.0	72602	749.0	466.3	304.0	214.3	151.3	95.7	52.0
12	130	273	6	21	0.2	1.0	846.0	184802	362.0	248.8	175.3	114.9	69.7	39.9	22.5
13	130	294	7	13	8.8	9.0	846.0	121061	474.3	304.6	200.8	126.1	78.6	50.1	31.8
14	130	294	7	3	17.7	9.0	846.0	100248	711.0	507.0	357.3	229.3	136.7	70.7	43.0
15	150	12	8	5	16.6	14.0	1609.4	50495	843.4	440.6	284.4	166.2	94.6	54.8	33.2
16	150	12	8	3	22.3	14.0	1611.3	34406	1389.3	724.7	480.0	258.3	125.3	70.0	44.3
17	150	20	9	13	0.0	2.0	1522.4	64077	862.5	537.9	364.6	217.2	113.4	34.5	13.6
18	150	20	9	4	0.0	2.0	1503.0	49947	1704.8	1253.3	894.5	558.5	313.3	91.3	36.3
19	170	36	10	3	0.0	10.0	2519.3	119020	511.3	336.3	257.7	172.3	113.7	71.3	49.7
20	170	36	10	1	0.0	10.0	2512.0	96619	637.0	430.0	321.0	205.0	136.0	84.0	56.0
21	170	40	11	8	1.9	7.0	2402.4	109652	498.4	312.3	220.9	131.0	79.5	47.4	31.6
22	170	40	11	4	0.0	7.0	2466.3	86967	702.3	465.3	331.8	190.0	93.5	51.0	21.3
23	170	40	11	1	4.0	7.0	2387.0	67797	1098.0	803.0	690.0	452.0	266.0	128.0	93.0
24	170	53	12	4	1.0	17.0	2324.3	135302	403.8	255.5	176.3	103.5	62.0	33.8	18.8
25	170	57	13	12	7.5	5.0	2218.1	111282	484.6	300.8	207.7	122.8	73.3	40.8	29.8
26	170	57	13	2	0.0	5.0	2244.0	95465	674.5	464.0	321.0	183.0	96.5	39.5	19.5
27	170	71	14	20	0.6	12.0	1976.3	114806	467.1	289.6	198.1	113.4	66.6	39.2	25.4
28	170	71	14	9	0.4	12.0	1954.1	94465	674.4	459.0	332.6	197.9	109.4	53.1	34.2
29	170	71	14	2	2.0	12.0	1908.5	62438	1264.0	936.0	727.0	477.0	252.5	102.5	45.0
30	170	102	15	20	33.9	11.0	1638.2	93935	499.3	284.4	182.3	100.3	61.0	38.7	26.8
31	170	102	15	6	37.8	11.0	1612.8	85351	661.8	426.3	273.5	145.2	70.7	31.3	18.3
32	170	102	15	1	0.0	11.0	1715.0	20388	1377.0	396.0	200.0	73.0	28.0	9.0	15.0
33	170	129	16	13	4.5	10.0	1395.3	82484	517.1	266.3	156.2	80.1	49.8	33.0	23.2
34	170	129	16	16	7.6	10.0	1398.3	58538	697.3	348.8	221.4	128.5	76.0	43.7	26.8
35	170	129	16	1	7.0	10.0	1373.0	60606	1174.0	844.0	624.0	372.0	173.0	46.0	21.0
36	170	176	17	1	1.0	7.0	1700.0	50505	596.0	200.0	119.0	67.0	42.0	30.0	23.0
37	170	176	17	23	53.1	7.0	1599.6	45838	733.7	288.9	176.7	105.0	66.7	46.0	32.3
38	170	176	17	4	100.0	7.0	1496.8	36979	1198.8	627.8	426.0	189.3	82.5	41.8	25.8
39	170	204	18	9	15.2	10.0	1775.8	43216	796.2	329.3	214.2	126.0	69.4	40.9	26.4
40	170	204	18	3	20.3	10.0	1741.7	23097	1942.7	547.3	322.7	131.7	65.0	36.7	22.7
41	170	216	19	23	23.4	10.0	1937.8	41945	762.1	280.7	184.0	116.3	76.9	53.3	38.2
42	170	216	19	3	45.0	11.0	1932.7	24871	1277.3	407.3	259.7	155.3	96.3	62.7	41.0
43	170	242	20	3	10.3	5.0	2241.7	79349	482.7	229.0	155.7	96.0	56.7	34.7	24.0
44	170	242	20	24	20.0	5.0	2177.7	60930	749.4	397.9	288.1	193.6	123.8	81.1	54.5
45	170	242	20	3	21.0	5.0	2183.0	17324	3368.7	2011.7	1548.0	1120.0	805.7	539.3	73.0
46	170	272	21	5	19.2	12.0	2188.8	47464	895.0	472.6	340.2	217.6	126.6	74.2	45.4
47	170	272	21	13	40.1	12.0	2185.2	38605	1350.7	807.0	514.8	225.1	71.9	31.3	22.0
48	170	290	22	11	11.4	7.0	1966.6	47332	891.6	463.7	296.5	166.1	82.5	44.6	27.5
49	170	290	22	14	26.0	7.0	2017.1	38162	1358.2	745.0	462.9	234.0	93.3	49.1	29.6
50	170	315	23	1	2.0	2.0	8103.0	59880	383.0	49.0	159.0	83.0	33.0	11.0	8.0
51	170	315	23	3	.0	2.0	4676.7	53761	741.7	369.0	258.0	158.7	90.0	55.3	36.3
52	170	319	24	1	2.0	7.0	9816.0	53476	724.0	350.0	281.0	200.0	127.0	80.0	55.0
53	180	220	25	15	34.3	-1.0	1757.1	127207	431.5	265.1	189.5	132.5	96.6	59.3	40.4
54	180	220	25	9	35.0	-1.0	1513.8	79065	831.5	569.8	409.8	271.7	178.6	91.8	55.2
55	180	220	25	6	47.5	-1.0	1559.7	60985	1079.7	749.2	535.7	348.0	221.5	90.0	48.5
56	180	250	26	6	11.3	7.0	3879.8	105549	479.7	287.7	202.3	135.3	95.5	55.7	38.0
57	180	257	27	6	5.0	11.0	5188.7	120775	422.3	253.5	174.3	113.5	80.2	50.5	34.8
58	180	257	27	2	32.5	11.0	5726.5	55194	655.5	282.5	203.0	163.5	129.5	86.5	59.5
59	180	265	28	16	0.2	7.0	7808.6	168585	298.2	165.4	109.8	73.6	50.6	33.6	23.7
60	180	281	29	6	10.5	10.0	13317.5	152472	348.2	215.5	150.5	105.8	75.3	48.2	33.7
61	190	74	30	6	3.3	3.0	621.8	131447	497.0	344.3	235.8	138.7	70.8	37.7	22.5
62	190	74	30	2	23.5	3.0	593.0	89113	642.0	403.0	258.0	168.5	84.5	38.0	17.0
63	190	82	31	14	2.4	9.0	780.4	140347	476.0	328.2	221.7	136.2	73.0	38.0	21.4
64	190	82	31	1	0.0	9.0	811.0	117647	652.0	482.0	353.0	228.0	131.0	74.0	41.0
65	190	97	32	5	0.6	3.0	928.2	132891	448.0	296.4	193.2	118.2	71.0	39.0	21.4
66	190	102	33	7	47.1	9.0	1022.2	135314	423.0	270.0	171.7	104.1	62.3	37.3	22.1
67	190	102	33	1	64.0	9.0	1030.0	90090	632.0	410.0	280.0	150.0	50.0	1.0	2.0
68	190	110	34	5	14.4	3.0	1117.8	111581	478.6	285.8	185.2	115.6	73.4	45.2	27.2
69	190	115	35	4	3.5	-1.0	1183.2	165682	364.8	242.8	165.5	103.3	63.8	39.3	23.3

data were averaged. Therefore, no motivation existed to screen out unusual data from the analysis. Dividing the data into two groups of routes, as was done with the original data, could be justified on the basis of inherent differences in the standards to which they were built. As before, one group of routes included Routes 130, 150, and 190, and the other group included Route 170 and 180. Favorable results with respect to both statistical and engineering criteria were achieved for both groups of routes.

Fatigue Cracking Model for Routes 130, 150, and 190

Detailed results of the statistical analysis of this group of routes are given in this section. The fol-

TABLE 3 Definition of Variable Names Used in Tables 1 and 2

Column Heading	Description
Row	Position of record in file
Route	First three digits of route number
CDS	Coordinated data system milepost
Date	Date of FWD data on this record
Project	Number assigned to specific surfacing project
Temp	Temperature (°F)
Wgt	Load (falling weight)
Radius	Radius of curvature
S1-S7	Sensor No. 1 to Sensor No. 7
Crk1	Fatigue cracking, Type I
Crk2	Fatigue cracking, Type II
Patch	Patching
Crk	Sum of Crk1, Crk2, and patch
Last Fix	Surfacing date (1900)
Age Adj	Age adjustment 1:1981 and 0:1982
Age	82 minus Last Fix minus Age Adj
ADT	Annual ADT
Apr	April ADT
May	May ADT
Apr + May	April and May ADT
Case Wgt	Case weight

lowing table gives the regression coefficients, including the constant term with their standard deviations and t-ratios.

Column	Coefficient	S.D. of Coefficient	t-Ratio = Coefficient/S.D.
Constant	-5.329	6.910	-0.77
Age	0.9563	0.4731	2.02
MADT	0.007618	0.0001546	4.93
Radius	-7.029E-06	0.00004609	-0.15

(Note that for three of the variables the data given are averaged values rather than original data: Age, MADT, and Radius.)

The t-ratio can be used to evaluate the reliability of a coefficient. The absolute value of the t-ratio is taken first. If this value is 2.0 or greater, the coefficient is considered reliable. If this value is between 1.0 and 2.0, the coefficient has moderate reliability. If this value is below 1.0, the coefficient should be used with caution, particularly if extrapolations beyond the range of data used in this analysis are required. It can be observed that AGE and MADT have reliable coefficients, whereas the constant term and the coefficient for Radius are not reliable. In equation form, the model can be expressed as follows:

$$Crk = -5.33 + 0.956\ Age + 0.00762\ MADT - 7.03 \times 10^{-6}\ Radius \quad (8)$$

where

Crk = fatigue cracking (%),
Age = time since last surfacing (years),
MADT = April and May ADT, and
Radius = radius of curvature (mm).

The value of R^2 is .796; it is the proportion of the total variation explained by the model. The value of .79 obtained for this model is considered good.

The analysis of variance table is as follows:

Due To	DF	SS	MS = SS/DF	F-Ratio
Regression	3	34,157.4	11,385.8	27.2912
Residual	21	8,761.1	417.2	
Total	24	42,918.6		

The sums of squares (SS), degrees of freedom (DF), mean squares (MS), and F-ratio are given. The SS column divides the total variation into Due to Regression (explained) and Residual (unexplained). The ratio of SS due to regression to total SS is R^2. The residual mean square is an unbiased estimate of the remaining variability in the data. The F-ratio is used to test whether the coefficients are all zero.

The following table gives the minimum, weighted mean, and maximum of each variable in the analysis.

	Crk	Age	MADT	Radius
Minimum	0.0000	1.0000	593.00	34,406
Weighted mean	12.7538	6.5846	1,648.36	109,888
Maximum	67.0000	16.5000	7,260.50	184,802

Using values of Age, MADT, or Radius that are outside these ranges (recall these are average values) should be avoided because extrapolation incurs greater uncertainty of the result.

The original value, predicted value, residual = predicted Crk - original Crk, and the standardized residual are given in Table 4. Standardized residual values are used to more easily locate unusual values or outliers. Values above 2.0 in absolute value are possible candidates for outliers and above 2.5 in absolute value are almost always considered outliers. They may be removed after the first pass but not on the second pass. Here a large standardized residual is left in the data because this is the second pass through the data.

TABLE 4 Predicted Values and Residuals for Roads Built to Older Standards

Row	Route	Project	Cds	Crk	Crk Fit	Residual	Std Res
1	130	1	239	67.0000	54.0481	12.9519	0.96663
2	130	1	239	55.6364	52.4053	3.2311	0.84879
3	130	1	239	50.0000	65.3837	-15.3837	-1.19797
4	130	2	254	25.0000	23.9929	1.0071	0.05035
5	130	2	254	39.0000	21.6686	17.3314	0.86352
6	130	3	256	12.0000	28.1636	-16.1636	-0.81057
7	130	3	256	14.0000	30.8592	-16.8592	-0.84080
8	130	4	258	23.0000	13.9288	9.0712	0.79336
9	130	4	258	2.0000	18.6494	-16.6494	-0.82351
10	130	5	262	7.1250	3.3689	3.7561	0.54984
11	130	5	262	10.6667	3.4752	7.1915	0.63351
12	130	6	273	0.2381	0.7738	-0.5357	-0.22209
13	130	7	294	8.8462	8.8725	-0.0263	-0.00537
14	130	7	294	17.6667	9.0188	8.6479	0.75530
15	150	8	12	16.6000	19.9660	-3.3660	-0.42031
16	150	8	12	22.3333	20.0938	2.2395	0.20772
17	150	9	20	0.0000	7.7317	-7.7317	-1.81808
18	190	9	20	0.0000	7.6834	-7.6834	-0.82613
19	190	30	74	3.3333	1.3535	1.9798	0.24641
20	190	30	74	23.5000	1.4317	22.0683	1.55700
21	190	31	82	2.3571	8.2372	-5.8801	-1.32098
22	190	31	82	0.0000	8.6299	-8.6299	-0.42665
23	190	32	97	0.6000	3.6776	-3.0776	-0.34733
24	190	33	102	64.0000	10.4920	53.5080	2.64358
25	190	34	110	14.4000	5.2719	9.1281	1.03076

In Figure 2, the standardized residuals are plotted against the fitted values to see if they are randomly distributed. A nonrandom pattern could indicate inadequacies of the model or the violation of an important assumption of linear models: homogeneity of variance. The individual sensors are not represented in the model because they did not contribute to the predictive ability of the model.

Fatigue Cracking Model for Routes 170 and 180

The results for Routes 170 and 180 are discussed in this section. The following table gives the regres-

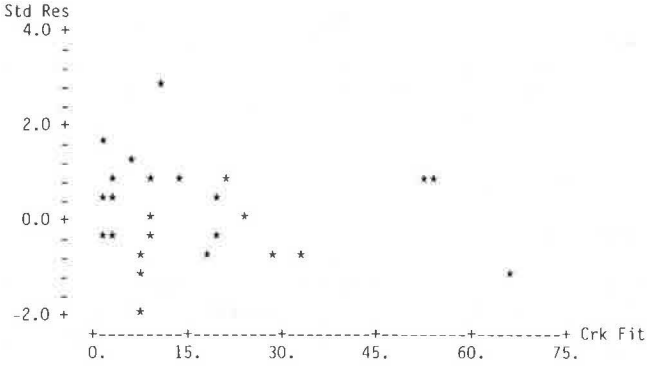

FIGURE 2 Plot of standardized residuals versus fitted values for roads built to older standards.

sion coefficients along with their standard deviations and t-ratios.

Variable	S.D. of Coefficient	Coefficient	t-Ratio = Coefficient/S.D.
Constant	14.094	9.532	1.48
Age	0.1716	0.5613	0.31
Radius	-1.169E-04	0.00006051	-1.93
S1	0.014818	0.007553	1.96
S5	-0.04991	0.02963	-1.68

The t-ratio for Age is low. The remaining coefficients are of moderate quality. In equation form,

$$Crk = 14.1 + 0.172\ Age - 1.17 \times 10^{-4}\ Radius + 0.0148\ S_1 - 0.0499\ S_5 \quad (9)$$

where S_1 is Sensor No. 1 reading in microns and S_5 is Sensor No. 5 reading in microns. Monthly ADT is not in this equation because it is negatively correlated with fatigue cracking. This is most likely due to the amount of interpolation necessary for these routes. The value of R^2 is .50 (rounded from .501), which is a moderately good value.

The hypothesis that all the coefficients are zero is rejected at the .0005 significance level with the value of F-ratio shown in the following analysis of variance table.

Due To	DF	SS	MS = SS/DF	F-Ratio
Regression	4	18,930.4	4,732.59	7.7944
Residual	31	18,822.5	607.18	
Total	35	37,752.8		

The ranges of the predictor variables shown in the following table should be kept in mind when using Equation 9.

	Crk	Age	Radius	S1	S5
Minimum	0.0000	2.0000	17,324	298.19	28.000
Weighted mean	13.0195	8.9297	78,660	755.62	92.371
Maximum	45.0000	17.0000	168,585	3,368.67	805.667

The predicted values and residuals given in Table 5 indicate that two cases are unusual with respect to the rest. However, this is the second pass through the data after having removed outliers from the first pass. The plot of the standardized residuals versus the predicted value of fatigue cracking does not indicate any distinguishable patterns (Figure 3).

TABLE 5 Predicted Values and Residuals for Roads Built to Newer Standards

Row	Route	Project	Cds	Crk	Crk Fit	Residual	Std Res
1	170	10	36	0.0000	3.8032	-3.8032	-0.27169
2	170	10	36	0.0000	7.1689	-7.1689	-0.29235
3	170	11	40	1.8750	5.8966	-4.0216	-0.47755
4	170	11	40	0.0000	10.8703	-10.8703	-0.89296
5	170	11	40	4.0000	10.3652	-6.3652	-0.26172
6	170	12	53	1.0000	4.0862	-3.0862	-0.27659
7	170	13	57	7.5000	5.4662	2.0338	0.31463
8	170	13	57	0.0000	8.9728	-8.9728	-0.52150
9	170	14	71	0.6000	6.3352	-5.7352	-1.19238
10	170	14	71	0.4444	9.6442	-9.1997	-1.17843
11	170	14	71	2.0000	14.9390	-12.9390	-0.76435
12	170	15	102	37.8333	12.2864	25.5470	2.58768
13	170	15	102	0.0000	32.6064	-32.6064	-1.34868
14	170	16	129	4.4615	11.3478	-6.8863	-1.05091
15	170	16	129	7.6250	15.5073	-7.8823	-1.36566
16	170	16	129	7.0000	17.4886	-10.4886	-0.42767
17	170	17	176	1.0000	16.1279	-15.1279	-0.61821
18	170	18	204	15.2222	19.0919	-3.8679	-0.49304
19	170	18	204	20.3333	38.6536	-18.3203	-1.52067
20	170	19	216	23.3913	18.5106	4.8807	1.13050
21	170	19	216	45.0000	27.1948	17.8052	1.28280
22	170	20	242	10.3333	10.0020	0.3313	0.02383
23	170	20	242	20.0417	12.7572	7.2845	1.80210
24	170	20	242	21.0000	22.6325	-1.6325	-0.34562
25	170	21	272	19.2000	17.5496	1.6504	0.15562
26	170	21	272	40.0769	28.0667	12.0102	2.17856
27	170	22	290	11.3636	18.8591	-7.4955	-1.06328
28	170	22	290	26.0000	26.3055	-0.3055	-0.05684
29	170	23	315	2.0000	11.4669	-9.4669	-0.39234
30	170	23	315	0.0000	14.6520	-14.6520	-1.08228
31	170	24	319	2.0000	13.4348	-11.4348	-0.46732
32	180	26	250	11.3333	5.3003	6.0330	0.61585
33	180	27	257	5.0000	4.1229	0.8771	0.09027
34	180	27	257	32.5000	12.7807	19.7193	1.15645
35	180	28	265	0.1875	-2.5166	2.7041	0.61505
36	180	29	281	10.5000	-0.6111	11.1111	1.17380

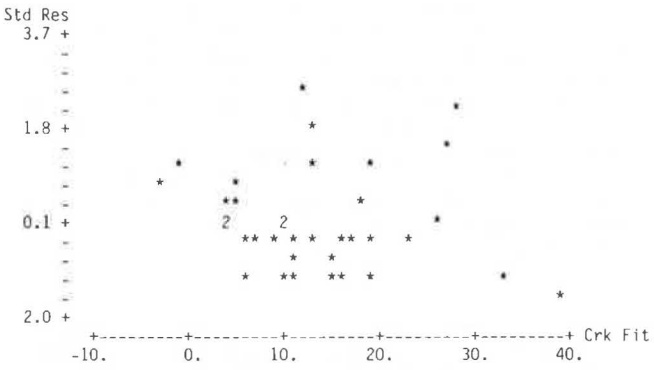

FIGURE 3 Plot of standardized residuals versus predicted value of fatigue cracking for roads built to newer standards.

SUMMARY AND CONCLUSIONS

Deflection measurements at the center of the load (Benkelman beam) were used in the past to develop a fatigue cracking prediction model for highways in Alaska. The Alaska DOTPF has acquired two FWDs to measure deflections for their road deflection inventory. Studies conducted by Alaska DOTPF staff have indicated that the deflection basin measured with the help of FWDs is a better indicator of the damage potential to highway surfaces than the single measurement of deflection under the load. Therefore, the current studies were proposed to develop a fatigue cracking prediction model using FWD data.

The data available on FWD measurements and the fatigue cracking observations were used in developing a suitable fatigue cracking prediction model for Alaskan highways. Preliminary analysis of the data indicated that a careful selection of the data obtained over a period of two to three months (during the thaw season) is needed to relate the deflection basin to fatigue cracking. Therefore, a method of screening and grouping the data has been developed. The data obtained after screening and grouping were used in developing the fatigue cracking prediction models for two groups of routes. The older routes (130, 150, and 190) were in one group and the newer routes (170 and 180) were in the other group. An R^2 of .79 was found for the group of older routes and one of .50 was found for the group of newer routes. Combining all five routes into a single analysis produced an R^2 of .30. If prediction for a route not in this analysis is desired, it will be necessary to classify it as being built to either older standards or newer standards.

To improve the prediction models (increase R^2), it is necessary to modify the existing road inventory procedures so that suitable data for this purpose can be obtained from the survey records. A brief description of some desirable modifications is included in the following section.

RECOMMENDATIONS

Consistency in the fatigue cracking records can be maintained if patching records are subdivided into patching of fatigue cracks and patching of other items. This will allow the appropriate proportion of patching to be included with the observed amount of fatigue cracking.

Any load restrictions imposed during the spring should also be recorded properly so that an estimate of traffic and age can be made for various sections of the route.

The number of points along each route at which traffic data are collected should be increased so that interpolated estimates of ADT are more accurate. To develop reliable prediction models, it would be desirable to establish a reasonable number of control sections along each route. These control sections should be observed more carefully than the regular inventory sections. Any possibility of inconsistency in observations should be avoided (to the extent possible). Chances of error can be minimized if the same personnel and equipment are used for measuring and recording the observations.

REFERENCES

1. R. Kulkarni, C. Saraf, F. Finn, J. Hilliard, and C. Van Til. Life Cycle Costing of Paved Alaskan Highways. Final Report. Department of Transportation and Public Facilities, Fairbanks, June 1982, Vol. I.
2. R.N. Stubstad and B. Connor. Prediction of Damage Potential on Alaskan Highways During Spring Thaw Using the Falling Weight Deflectometer. Final Report. Department of Transportation and Public Facilities, Fairbanks, Aug. 1982.
3. Alaska Highways Annual Traffic and Volume Report. Transportation and Planning Division, Alaska Department of Transportation and Public Facilities, Fairbanks, 1981.

Publication of this paper sponsored by Committee on Strength and Deformation Characteristics of Pavement Sections.

Preliminary Concepts for FWD Testing and Evaluation of Rigid Airfield Pavements

PAUL T. FOXWORTHY and MICHAEL I. DARTER

ABSTRACT

Results are presented of a study on the effects of temperature on repeatability of falling weight deflectometer (FWD) measurements, the behavior of rigid pavement joints, and the backcalculation of E and k in order to form the basis for application of finite element techniques to the classical Westergaard theory of rigid pavement evaluation. Three U.S. Air Force installations were chosen for an in-depth study of pavement response to FWD loads under a variety of environmental and geological conditions. Repeatability of FWD load and deflection measurements at constant temperatures as well as changing temperatures is reported. Effects of temperature on joint load transfer efficiency are analyzed, and predictive models are presented that account for seasonal temperature fluctuations in load-carrying capacity analyses of rigid pavements. A computer program to backcalculate elastic and subgrade reaction moduli from FWD deflection data has been developed, and repeatability of these moduli is established for different climatic conditions. The study has indicated the following: (a) the FWD is remarkably consistent in repeated load and deflection measurements at any slab position for constant temperatures; (b) center slab load and deflection measurements are also consistent under varying temperatures; (c) joint load transfer efficiency is highly temperature dependent but can be accurately modeled for a given joint type; and (d) E and k can be accurately determined from FWD measurements through an iterative computer scheme, and the results are consistent over a wide range of temperatures.

The current destructive test methodologies for obtaining critical airfield evaluation data and conducting the analyses are costly and time-consuming, but, most important, severely affect the operation of the airfield. In many cases the structural evaluation is neglected because airfield management cannot tolerate the schedule interruption that would occur with extensive downtime of the pavements. Fortunately, in recent years great strides have been made in the development of equipment that can rapidly and nondestructively collect data on which an evaluation of load-carrying capacity and future life can be made. Of particular importance in the evaluation of rigid airfield pavements was the development of impulse loading devices, such as the falling weight deflectometer (FWD), which reasonably approximate actual moving aircraft wheel loads (1). Simultaneously, researchers have been developing analytical models that could describe the response of a pavement system to specific loading conditions.

Presented in this paper are the results of several preliminary investigations that are essential in forming a solid foundation for the nondestructive testing and evaluation (NDT & E) of rigid airfield pavements. When coupled with other research done by the authors (see paper elsewhere in this Record), a complete system--including field testing, analyses, and prediction of future performance of each feature--is developed. Elsewhere, Foxworthy provides a comprehensive description of the entire study (2). Implementation of the system will permit rapid completion of field testing with little or no interruption of installation operations, and analysis of field data and presentation of results are possible within hours.

P.T. Foxworthy, Civil Engineering Research Division, U.S. Air Force Weapons Laboratory, Kirtland AFB, N. Mex. 87111. M.I. Darter, University of Illinois, Urbana, Ill. 61801.

TESTING EQUIPMENT AND PAVEMENT CHARACTERIZATION MODEL

An extensive investigation of available nondestructive equipment and engineering models led to the selection of the FWD and the ILLI-SLAB finite element program for this research. Each represents the latest advancements in the state of the art, but more important, they were selected because of the confidence the authors and other research and field engineers have in their ability to simulate actual loading conditions on airfield pavements (1,3).

The testing system is trailer mounted, towed a standard automobile, and weighs between 1,323 and 1,875 lb, depending on the weight of the falling mass used. By varying the drop heights and mass levels, impulse forces ranging between 1,500 and 24,000 lb can be achieved. Deflections are measured using up to seven velocity transducers mounted on a bar, which is lowered automatically with the loading plate. A typical configuration is shown in Figure 1. The entire operation can be controlled by one person from the front seat of the tow vehicle; typically 45 sec is required to complete an entire test sequence.

ILLI-SLAB was developed at the University of Illinois in the late 1970s for structural analysis of jointed, one- or two-layer concrete pavements with load transfer systems at the joints (4). The ILLI-SLAB model is based on the classical theory of a medium-thick plate on a Winkler foundation, and can evaluate the structural response of a concrete pavement system with joints, cracks, or both. Recent efforts by Ioannides et al. to revise and expand ILLI-SLAB have produced a versatile, easy-to-use tool with

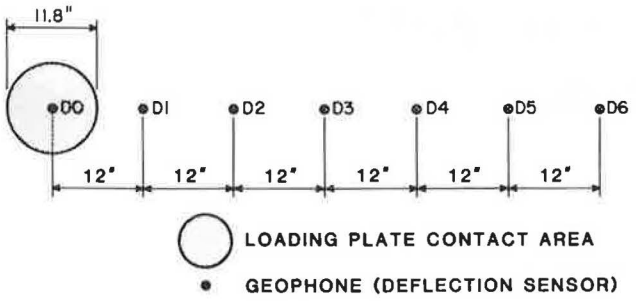

FIGURE 1 Typical location of the loading plate and deflection sensors of the FWD.

improved accuracy (5). Guidelines for proper mesh construction have been provided, and a global coordinate system is currently in place for easy use in analysis. The work by Ioannides has been instrumental in the development of the procedures used throughout this study.

FIELD RESEARCH PROGRAM

The engineer performing NDT & E of an airfield pavement system is faced with what must appear to be an overwhelming task of planning and executing the data collection program. The tremendous number of tests that are possible in a relatively short time period with the FWD permits great flexibility in evaluating many features and distress patterns. However, this flexibility also leads to a certain amount of perplexity in trying to plan the most efficient manner in which to collect and organize such a vast quantity of data. Adding to this confusion are the inevitable variabilities associated with the testing of nonhomogeneous, anisotropic paving materials subjected to wide ranges in climatic conditions. A major objective of this research was to provide specific guidelines to the engineer for conducting the field testing program in light of these inherent variations; to this end, the field research program was designed.

With the introduction of NDT & E in the early 1960s, engineers began to experience significant variation in field test measurements over relatively short time periods. Such variations existed with destructive testing methods, but were largely ignored because of the expense involved in performing repeated testing. To date, little has been formally written on this problem, particularly in regard to rigid airfield pavements, either because equipment manufacturers were reluctant to publicize such information or because testing firms did not have the impetus to explore the problem.

This research effort has attempted to quantify this problem for several aspects of the rigid pavement evaluation process, including the following: (a) the repeatability of FWD deflection and load measurements at the center, edge, and corner of a slab over any given minute, hour, day, month, or season; (b) the effect of pavement, air temperature, or both on FWD deflection and load measurements, backcalculated slab and subgrade moduli, and load transfer efficiencies at joints; (c) the variation in portland cement concrete (PCC) elastic modulus, subgrade modulus, and load transfer efficiency from slab to slab within the same feature; (d) the effect of load magnitude on backcalculated moduli and load transfer efficiency; (e) the influence of type of joint construction on the relationship between load transfer efficiency and temperature; and (f) the consistency of load transfer efficiency along the joint.

FWD Measurement Repeatability

The first major concern addressed during the field research program was the repeatability of the FWD load and deflection measurements. If the validity of these measurements could be established, then confidence could be expressed in the equipment and a firm foundation could be laid for the analysis. To investigate this aspect of the data collection process, a testing program was conducted at Sheppard Air Force Base in Wichita Falls, Texas, to measure loads and deflections for several combinations of load, temperature, and thickness. This installation was selected because of its variety of pavement thicknesses and accessibility to key pavement features.

Testing for repeatability began by devising a test pattern for the FWD consisting of five points on each slab, three load levels, and four complete repetitions. This pattern was repeated for three slabs in each feature and for three features of different thicknesses. The entire test sequence for one slab took approximately 45 min to complete, thus minimizing the effects of air-pavement temperature change on the measurements. Each of the four series of drops at each point on the slab could have been performed consecutively, but by moving the FWD and then returning to approximately the same spot, it was believed that a more realistic measure of repeatability could be achieved.

Table 1 shows the repeatability of the FWD load/deflection ratio at constant temperature for Sheppard Feature T04A, Slab 1, at the corner position. An examination of the data in Table 1, typical of the results at slab joints and corners, reveals that appreciable improvement in the coefficient of variation of the load measurement can be expected as the load level increases. Load measurements typically average about 4 percent variation in the 7,000-lb range whereas deflections average about 5 percent. As loads increase to 15,000 lb, the variation in load measurement drops to about 2 percent whereas that of deflections remains about the same. Finally, 23,000-lb loads display about a 1 percent variation, whereas their corresponding deflections remain at about 5 percent. Results at the center slab positions were nearly identical for load measurements, but load/deflection ratios were even more consistent.

When raw deflection data are examined, good consistency is observed between the first and second drops (made within 30 sec of each other) and the third and fourth drops (also made within 30 sec of each other but nearly 30 min after the first two drops); however, the second pair of drops produced slightly lower deflections and loads, a definite trend that is attributable to increased temperatures in the rubber buffers of the FWD. Differences in the drops can also be partially accounted for by slight inaccuracies in repositioning the FWD and by rounding of the deflection values to the nearest one-tenth mil. However, overall the FWD exhibits remarkable consistency in measuring transient loads and small deflections on such nonuniform materials.

Results of repeatability measurements at constant air-pavement temperatures indicate that excellent consistency exists in FWD measurements for all points on the slab, but particularly at the center slab positions. Thus, the influence of the equipment on the variability of the end product, the backcalculated moduli and load transfer efficiency, is minimal. The contribution of time, temperature, and, to some extent, seasonal changes to the variation in FWD load and deflection measurements at center slab within hourly and daily periods was also examined. Moisture is presumed to play a modest role in the variations observed, but it is difficult to account for it apart from temperature over short time peri-

TABLE 1 Repeatability of FWD Load/Deflection Ratio at Constant Temperature

Load[a] Range	Test No.	Load (lbf)	Sensor Load/Deflection Ratios (lbf/mil) D0	D1	D2	D3	D4	D5	D6
Low	1	7568	2225	4451	4370	5405	6306	6880	8408
	2	7360	2230	4906	4906	5661	6690	6690	8177
	3	6880	2372	4047	4586	5292	6254	6254	7644
	4	7088	2362	4430	4725	5452	5906	7088	7875
Average		7224	2297	4458	4646	5452	6289	6728	8026
Coef. of Var.		.04	.04	.08	.05	.03	.05	.05	.04
Medium	1	15536	1804	4510	4947	5477	6390	6970	8071
	2	15540	1828	4570	5012	5550	6475	7063	8178
	3	14912	1962	4030	4518	4970	5735	6778	7456
	4	14936	1890	4036	4392	4978	5744	6493	7468
Average		15206	1871	4286	4717	5243	6086	6826	7793
Coef. of Var.		.02	.04	.07	.07	.06	.07	.05	.05
High	1	22801	1727	4470	5066	5700	6514	7355	8444
	2	22817	1702	4563	5070	5565	6338	7130	8450
	3	22196	1834	4035	4624	5161	5841	6341	7653
	4	22483	1827	4087	4683	5228	5764	6612	7752
Average		22574	1772	4288	4860	5413	6114	6859	8074
Coef. of Var.		.01	.04	.06	.05	.05	.06	.07	.05

[a]Load ranges are as follows: low, 6,000 to 9,000 lbf; medium, 14,000 to 16,000 lbf; and high, 22,000 to 25,000 lbf.

ods. Therefore, only time and temperature differences are used in the comparisons. Seasonal variations in FWD measurements are also presumed to exist as a logical extension of daily variations, but this effect is most easily examined by using backcalculated moduli.

Load and deflection measurements were taken at four points on each slab, under several air temperature conditions but within the same 3-day period. Table 2 gives examples of the influence of air temperature fluctuations on FWD measurements made at center slab positions only (data are for Sheppard Feature T04A, Slab 1, at the center slab position). Joints and corners, as will be observed later, are significantly affected by air temperature changes, and therefore would not provide a meaningful comparison with the constant temperature case.

The trends displayed in this table closely parallel the findings for the constant temperature cases presented earlier. The coefficients of variation for load and particularly deflection measurements are noticeably better at the higher load levels. The modest 2 percent coefficient of variation in load/deflection ratios for high load levels over a 20-degree range in air temperature indicates that excellent consistency is available in FWD results at the center slab position. The 3 percent improvement in load/deflection ratio consistency over joint and corner positions that was measured under nearly constant temperature conditions demonstrates the strong dependency of joint and corner measurements on temperature.

The data in Table 3 present an interesting phenomenon that occurs as temperatures decrease. As air temperatures approach freezing, the FWD loads measured by the load cell increase significantly, but without a proportionate increase in the deflections. Loads that typically showed less than 2 percent variation in warm temperatures displayed 8 to 9 percent variation in cold temperatures, while deflections remained relatively unaffected.

It appears that for center slab conditions only, the moderate temperature fluctuations (15 to 20°F) experienced throughout the course of a normal test day do not add to the existing, constant temperature variation found in the equipment and pavement materials unless testing is done below 40 degrees. At these lower temperatures, the rubber buffers of the FWD apparently stiffen and impart a more sharply spiked impulse load to the pavement, creating higher load measurements. This same effect can also appear during early morning testing at air temperatures above 60 degrees. If the FWD has been stored overnight in cool conditions and the rubber buffers have not been allowed to warm up before testing, greater impulse loads will be imparted. The 8:00 a.m. reading on March 15 in Table 3 is a good example of this (data are for Sheppard Feature T04A, Slab 1, at the center slab position). However, these higher loads do not increase deflections appreciably. The results of this phenomenon on backcalculated moduli will be examined in more detail later in this paper.

JOINT LOAD TRANSFER

Joints have long been recognized as the major focal point for pavement distress in jointed concrete pavements, and yet are largely ignored in most of today's evaluation schemes. The load transfer efficiency of a joint, defined as the ratio of the deflection of the unloaded slab to the loaded slab, has a significant effect on the stresses that are developed at the bottom of the slab, and, therefore, on the performance of the slab under load. It quickly became evident during the field testing program that the high degree of repeatability of center slab load and deflection measurements did not exist at the joints as temperatures changed. Both the magnitude of the deflections and the load transfer efficiencies were affected.

TABLE 2 Repeatability of FWD Load/Deflection Ratio Under Varying Temperatures

Load Range	Temp. Cond No.	Load (lbf)	Sensor Load/Deflection Ratios (lbf/mil)						
			D0	D1	D2	D3	D4	D5	D6
Low	1	8395	7631	8395	8395	9327	10493	11992	13991
	2	8300	7545	8300	8300	9222	9222	10375	13833
	3	8125	7386	8125	9027	9027	10156	10156	11607
	4	7998	7998	7998	8886	8886	9997	11425	11425
Average		8205	7640	8204	8652	9115	9967	10987	12714
Coef. of Var.		.02	.03	.02	.04	.02	.05	.08	.11
Medium	1	15534	6472	7397	7767	8175	9137	9708	11095
	2	15582	6492	7082	7420	7791	8656	9165	10388
	3	15852	6892	7205	7926	8343	8806	9324	11322
	4	15964	6940	7601	7982	8402	8868	9977	11402
Average		15733	6699	7321	7773	8177	8866	9543	11051
Coef. of Var.		.01	.04	.03	.03	.03	.02	.04	.04
High	1	23389	6496	7796	8065	8353	9355	10631	11694
	2	23484	6907	7575	7828	8387	9393	9785	11742
	3	23357	7077	7785	7785	8650	9342	10616	11678
	4	23071	6991	7690	7955	8544	9228	10486	11535
Average		23325	6867	7711	7908	8483	9329	10379	11662
Coef. of Var.		.01	.04	.01	.02	.02	.01	.04	.01

Note: Temperature Condition No. 1 existed on July 10 at 1:55 p.m. at an air temperature of 101°F. Temperature Condition No. 2 existed on July 11 at 8:45 a.m. at an air temperature of 89°F. Temperature Condition No. 3 existed on July 11 at 9:20 a.m. at an air temperature of 91°F. Temperature Condition No. 4 existed on July 12 at 10:00 a.m. at an air temperature of 82°F.

TABLE 3 Repeatability of FWD Load and Deflection Measurements Under Varying Temperatures

Load Range	Temp. Cond. No.	Load (lbf)	Sensor Positions (mils)						
			D0	D1	D2	D3	D4	D5	D6
Low	1	7304	1.1	1.0	0.9	0.9	0.7	0.7	0.6
	2	8376	1.1	1.0	1.0	0.9	0.9	0.7	0.7
	3	8848	1.2	1.0	1.0	1.0	0.9	0.8	0.7
	4	9632	1.1	1.0	1.0	1.0	0.8	0.8	0.7
Average		8540	1.13	1.00	0.98	0.95	0.83	0.75	0.68
Coef. of Var.		.11	.04	<.005	.05	.06	.12	.08	.07
Medium	1	15432	2.4	2.1	2.0	1.8	1.7	1.5	1.4
	2	16504	2.4	2.1	2.1	1.9	1.8	1.6	1.5
	3	17720	2.5	2.3	2.1	2.0	1.9	1.7	1.5
	4	18824	2.5	2.2	2.2	2.0	1.8	1.7	1.4
Average		17120	2.45	2.18	2.10	1.93	1.75	1.63	1.45
Coef. of Var.		.09	.02	.04	.04	.05	.03	.06	.04
High	1	23532	3.6	3.2	3.0	2.8	2.5	2.3	2.0
	2	24295	3.6	3.2	3.1	2.8	2.6	2.4	2.1
	3	25965	3.8	3.2	3.1	2.9	2.7	2.4	2.2
	4	28318	3.7	3.3	3.2	2.9	2.7	2.4	2.0
Average		25527	3.68	3.23	3.10	2.85	2.63	2.38	2.08
Coef. of Var.		.08	.03	.02	.03	.02	.04	.02	.05

Note: Temperature Condition No. 1 existed on March 13 at 12:30 p.m. at an air temperature of 61°F. Temperature Condition No. 2 existed on March 15 at 8:00 a.m. at an air temperature of 65°F. Temperature Condition No. 3 existed on March 17 at 4:15 a.m. at an air temperature of 45°F. Temperature Condition No. 4 existed on March 19 at 8:20 a.m. at an air temperature of 36°F.

Load Transfer Efficiency

The importance of load transfer at joints on the overall performance of rigid airfield pavements is intuitively obvious but not well documented. A perfectly efficient system for transferring load from one side of the joint to the other can reduce the free edge stress by 50 percent (6,7). Many different systems have been developed and tested for establishing and maintaining high degrees of load transfer across joints during the life of the pavement. The objective of these systems is simple: to minimize the tensile stresses and deflections in the concrete that result when loads are applied at the edge of the slab. Keeping concrete edge stresses at a minimum dramatically reduces fatigue damage and greatly increases pavement life, while reducing deflections minimizes the potential for pumping.

In the evaluation of remaining pavement structural life, the level of stress developed under an aircraft gear at the slab joint must be determined. Unfortunately, it is impractical to quickly or economically measure actual stresses developed at joints. However, it is possible to determine how well the load transfer mechanism is performing by measuring the relative deflection on both sides of the joint. This relative deflection is a direct indication of the load transfer efficiency of the joint. Normally, a correction is applied to the deflection measured by the D1 sensor (see Figure 1) to account for slab curvature due to bending, but the finite element mesh has been designed to automatically make this adjustment. By coupling the load transfer efficiency with a good analytical model of joint behavior, such as ILLI-SLAB, the edge stresses under actual loads can be calculated.

Effect of Load Magnitude on Load Transfer Efficiency

To investigate the possibility that the load transfer efficiency at joints is dependent on the magnitude of the loads used to create the relative deflections, the data presented in Table 4 were extracted from the constant temperature repeatability study discussed earlier. These data represent three slab thicknesses, two joint types, loads from 6,500 to 24,000 lb, and load transfer efficiencies between 30 and 100 percent.

The results given in Table 4 support the conclusion that load transfer efficiency is independent of the load magnitude, at least within the load range of the FWD (this may not be true for light load devices that generate loads less than 5,000 lb). With the exception of Slab 1 in Feature T04A, load trans-

TABLE 4 Relationship Between Magnitude of Load and Load Transfer Efficiency as Measured at Undoweled Transverse Contraction Joints and Keyed Longitudinal Construction Joints

Feature	Slab No.	Undoweled Transverse Contraction				Keyed Longitudinal Construction			
		Load (lbf)	D0 (mils)	D1	LTE (%)	Load (lbf)	D0 (mils)	D1	LTE (%)
T04A	1	7456	1.6	1.2	75	6936	1.8	1.2	67
		15400	3.9	2.6	67	15032	4.3	2.4	56
		23055	6.1	3.7	61	23103	6.7	3.4	51
	2	6840	1.1	0.9	82	6968	1.3	1.2	92
		14648	2.6	2.2	85	14640	3.0	2.7	90
		22514	3.9	3.4	87	22673	4.4	4.1	93
	3	6752	1.2	1.2	100	6688	1.5	1.3	87
		14656	2.8	2.7	96	14808	3.4	3.1	91
		23150	4.2	4.1	98	22848	5.2	4.6	88
A03B	1	7496	1.8	1.7	94	7216	2.3	0.9	39
		16296	4.0	3.8	95	15496	4.9	2.2	45
		23914	6.0	5.7	95	23421	7.3	3.4	47
	2	7528	5.0	2.7	54	7400	4.5	4.0	89
		15368	11.4	5.2	46	15512	9.6	8.3	86
		23246	17.6	7.3	41	23373	14.4	12.2	85
	3	6872	3.1	1.0	32	6936	2.8	1.0	36
		14992	7.4	2.3	31	15064	6.4	1.9	30
		23071	11.3	3.6	32	23150	9.5	2.8	29
A05B	1	6888	1.6	1.5	94	6896	2.1	1.8	86
		14936	3.6	3.3	92	14944	4.8	4.3	90
		22801	5.4	5.0	93	22976	7.2	6.5	90
	2	6680	1.9	1.9	100	6792	2.2	1.9	86
		14840	4.5	4.3	96	14824	5.1	4.4	86
		22928	6.6	6.4	97	22769	7.6	6.6	87
	4	7696	2.1	2.0	95	7240	2.3	2.1	91
		15584	4.5	4.2	93	15280	4.8	4.4	92
		23532	6.6	6.2	94	23007	7.2	6.5	90

fer efficiencies are remarkably consistent, particularly in view of the inherent variation in the equipment and materials highlighted earlier. With this result, the extrapolation of load transfer efficiencies under actual aircraft loadings can be made confidently.

Variation of Load Transfer Efficiency Along the Joint

Two additional aspects of joint load transfer that the engineer must be concerned with during field testing are (a) the direction in which the relative deflections are measured, and (b) the location of the measurement along the joint. It has been demonstrated that, for example, on highway pavements load transfer efficiency measured with the loading plate on the approach slab is much different from when measured from the leave slab (8). In addition, the highly channelized nature of highway traffic causes variation in load transfer efficiency along the joint. To investigate these concerns for airfield pavements, 21 positions on 3 slabs for 3 separate features were tested at low and high temperatures. Typical results of this investigation are shown in Figure 2 (data are for Feature T04A, Slab 1). Two sets of measurements are included to dramatize the effect that temperature has on load transfer efficiency.

Several general trends can be observed from these results. First, there appears to be little difference in load transfer efficiency at transverse joints when measured from the approach or leave slabs. This conclusion is not surprising for the airfield situation in which traffic is usually bi-directional along taxilines and centerlines. However, for longitudinal joints this is not the case. Several slabs show marked increases in load transfer efficiency when measured from the leave slab, indicating that loading history can influence joint behavior. Again, this result is not surprising when it is considered that aircraft gears ride consistently along the same side of the longitudinal joint, regardless of the direction of travel. Therefore, the engineer must determine where the majority of the gears track and adjust his test pattern accordingly.

Load transfer efficiencies are consistent, for the most part, along the joint. This permits some latitude in trying to position the FWD somewhere near the aircraft gearpath on the slab. However, in several instances the efficiencies drop off as the corner of the slab is approached. This tendency could result from loss of subbase support at the corner, and thus the effect of shear in the base or subgrade, or it could be due to the absence of dowel bars near the corners in each of the adjacent slabs. In any event, the normal test pattern is intended to identify potential problem areas near corners. Finally, the effect of increased temperature on load transfer efficiency is unmistakable; significant increases in joint performance accompany higher temperatures. This effect will be examined in more detail.

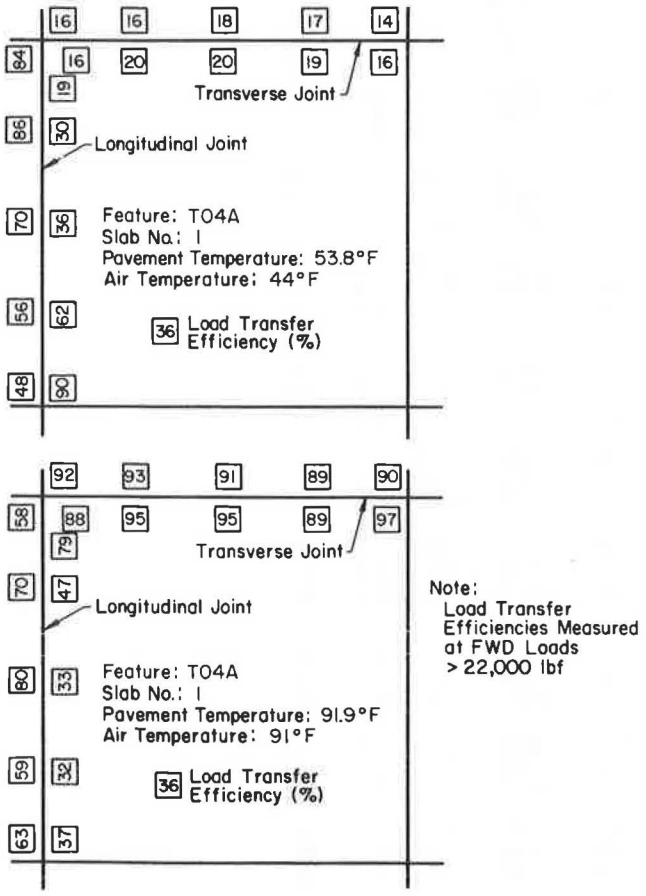

FIGURE 2 Joint load transfer efficiencies at various locations.

Effect of Temperature on Load Transfer Efficiency

One of the most disturbing aspects of NDT & E of any pavement system is the variability of results due to temperature. In flexible pavement systems, this effect is most pronounced on the stiffness of the asphaltic concrete materials. In rigid pavements, temperature changes influence load transfer efficiency more than any other characteristic of the system. Although temperature has been known to affect load transfer for some time, no attempts have been made to accurately quantify this phenomenon. One of the major objectives of this research effort was to describe the behavior of different joint types under changing temperature conditions. From this background, it was expected that a technique could be developed to account for the temperature effect in predicting the remaining life of rigid pavements. This temperature effect is undoubtedly composed of both curling effects and expansion and contraction effects, but only the combined effect is considered important in joint load transfer efficiency.

The repetitive nature of the FWD testing at Sheppard Air Force Base, coupled with the extremes in temperature that are routinely experienced in field testing, provided the basis on which to quantify load transfer changes with temperature. Load transfer efficiencies were measured at 20 dummy groove transverse joints and 20 keyed longitudinal joints, encompassing a range of pavement thicknesses from 10 to 20 in. Dowelled joints were not available for testing and, therefore, are not included in this study. Pavement surface temperatures were recorded for each test by inserting a digital thermometer probe into a predrilled, 1-in. deep, 1/8-in. diameter, oil-filled hole in each slab. Air temperatures were also obtained from the base weather station for each hour with the view that either could be used for analysis. A minimum of 5, and generally 12, temperature levels were obtained for each joint.

Figures 3 and 4 are graphic displays of the distinct relationship between joint load transfer efficiency and air temperature over a wide spectrum (for Feature T04A). The highly significant aspect of this behavior lies in the characteristic shape of this

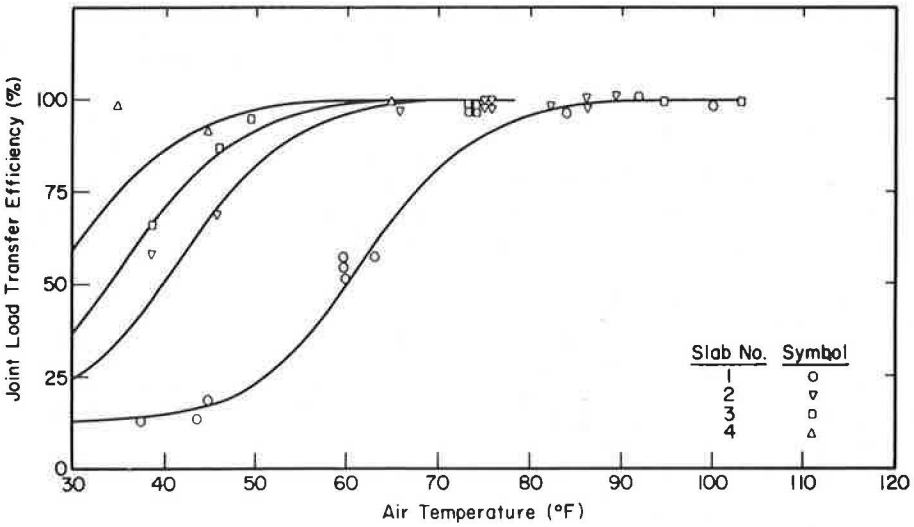

FIGURE 3 Relationship between air temperature and transverse joint load transfer efficiency.

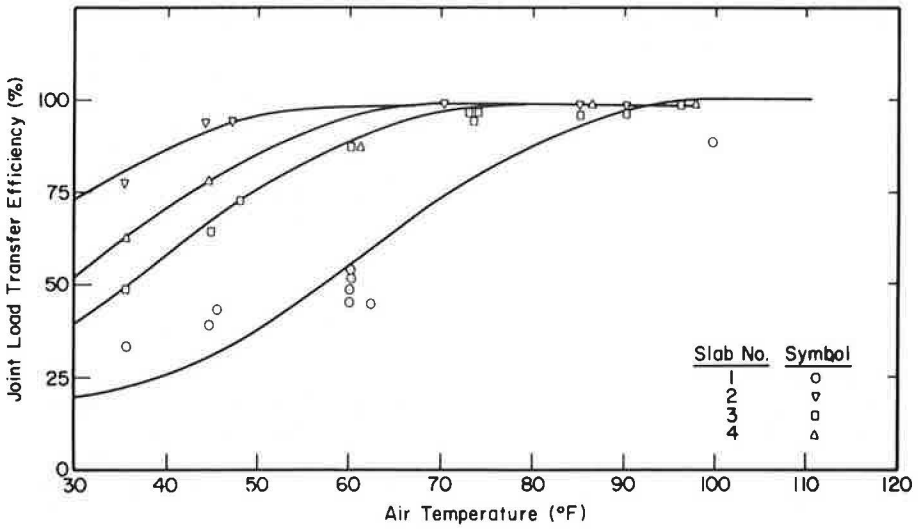

FIGURE 4 Relationship between air temperature and longitudinal joint load transfer efficiency.

relationship, an S-shaped curve. Each joint appears to take on the same shape and is nearly identical for both pavement temperature and air temperature. The variety of horizontally shifted positions for joints within the same feature is typical, and makes it difficult to select a joint that is representative of the entire feature.

Each joint tends toward a maximum load transfer efficiency of 100 percent as temperatures increase, and toward a minimum value of 20 to 25 percent as temperatures decrease. In many instances, the joint opening is so small that good load transfer exists throughout the temperature range, regardless of how much the slab contracts. In contrast, some joints have such poor load transfer at all temperatures in the normal range that they display a nearly flat response. However, this behavior does not mean that the characteristic shape of the load transfer efficiency-temperature curve cannot be described by an S-shaped curve. It merely means that the curve is shifted significantly, in either direction, from the norm.

The explanation for this consistent behavior is complex and involves the interaction of aggregate particles along the face of the transverse crack, or the contact between the male and female portions of the longitudinal keyed joint. Presumably, as the joint opens up under falling temperatures, less concrete surface area is available for contact and deflection resistance. When the joint opens completely, a certain minimum amount of load transfer is still available through the shear strength of the base course or subgrade material. Thus, the upper bound of 100 percent and a somewhat variable lower bound of 20 to 25 percent are reasonable. Additional research might correlate the lower bound with the material type used directly beneath the PCC surface.

With upper and lower bounds established, the only characteristic of the curve remaining to be identified is the slope, or rate at which the load transfer efficiency approaches the bounds. Inspection of Figures 3 and 4 reveals that each curve of similar joint type has approximately the same slope, and that a distinctly steeper slope exists for transverse dummy groove joints than for the longitudinal keyed joints. It appears that the type of joint construc-

tion affects the rate at which load transfer diminishes with temperature, which is not a surprising result.

Prediction of Load Transfer Efficiency

The discovery that the load transfer efficiency-temperature relationship of a given joint type closely follows an S-shape curve with certain upper and lower bounds and diminishing rate makes it possible to establish the horizontal location of this curve for any joint, if the load transfer efficiency at some temperature is known. However, this is precisely what is determined in the field with the FWD. Therefore, it becomes possible to rely on only one measurement of load transfer efficiency for a joint to predict the efficiency that will occur for any temperature that joint might experience. Only in those instances in which measured load transfer efficiency is near the upper or lower bound are additional measurements recommended. This can mean tremendous savings in personnel and equipment costs in field data collection; retesting of the same joint at several temperatures to determine its behavior pattern is eliminated. In addition, knowing the load transfer efficiency for the entire temperature range permits a much more accurate determination of cumulative fatigue damage from aircraft operations over an entire year.

An S-shaped curve with a positive slope has the following general form:

$$LTE = A_1 + (A_2 - A_1)e^{-(SF/AT)^{A_3}} \quad (1)$$

where

LTE = load transfer efficiency,
A_1 = lower bound,
A_2 = upper bound,
SF = shift factor in kelvin,
AT = air temperature in kelvin, and
A_3 = slope at inflection point.

Note that the air temperature and shift factor must be converted to the absolute scale to avoid the mathematical impossibilities that would occur when temperatures at or below zero on either the Fahrenheit or Centigrade scale are encountered. Figure 5 shows the generalized form of the S-shaped curve and its five fundamental parameters.

In Equation 1, the values of the constants A_1 and A_2 were determined by inspection of many data plots similar to those in Figures 3 and 4, whereas the value of A_3 must be determined for each type of joint construction. This was done using the Nonlinear Computer Analysis of the Statistical Package for the Social Sciences (SPSS) (9). The value of A_3 was calculated for each of the 20 transverse joints and 20 longitudinal joints and averaged to obtain a single curve that describes the load transfer efficiency versus temperature relationship for that joint type. The following equations were developed for each joint type:

For transverse dummy groove joints:

$$LTE = 0.25 + 0.75e^{-(SF/AT)^{40.0}} \quad (2)$$

For longitudinal keyed joints:

$$LTE = 0.25 + 0.75e^{-(SF/AT)^{25.0}} \quad (3)$$

These two equations can now be used to predict the load transfer efficiency that will exist at a given joint for any temperature if the load transfer efficiency is known for only one temperature. In making this calculation, it is assumed that the load transfer efficiency measured in the field lies somewhere between 25 and 100 percent, exclusive. Otherwise, the shift factor cannot be determined uniquely for that joint.

BACKCALCULATION OF CONCRETE ELASTIC MODULUS AND MODULUS OF SUBGRADE REACTION

When any type of load is placed on a rigid pavement slab, the slab will deflect nearly vertically to form a basin. The deflected shape of that basin is a function of several variables, including the thickness of the slab, the stiffness of the slab (characterized by E), the stiffness of the underlying

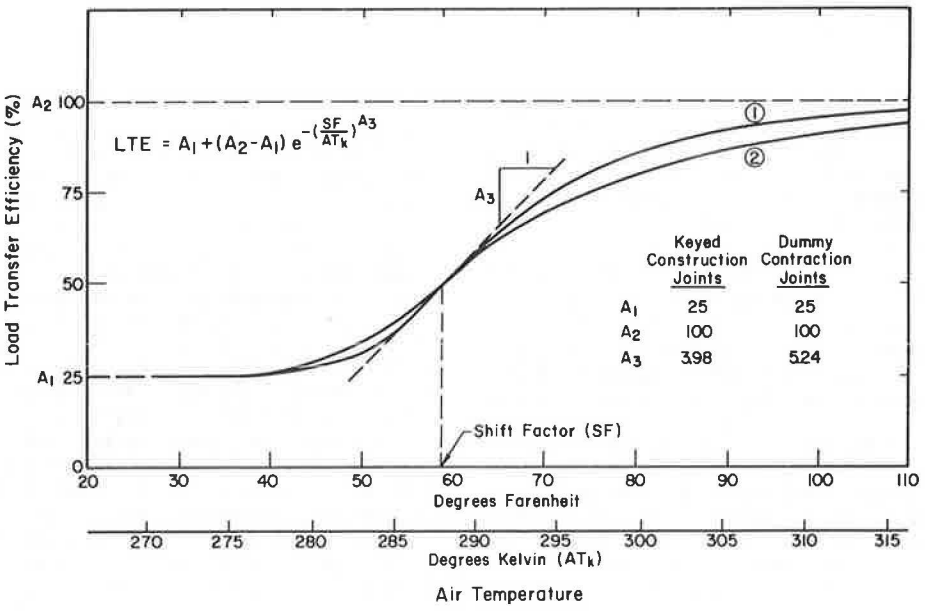

FIGURE 5 Generalized S-shaped curve and its fundamental parameters.

support systems (characterized by k), and the magnitude of the load. This interaction between E and k results in a characteristic deflection basin for a given magnitude and duration of load and thickness of concrete. If the approximate shape of the basin can be measured under loading conditions similar to an aircraft gear, and if two independent parameters describing the shape of the basin can be developed, then a unique value for both E and k can be backcalculated for a given load and slab configuration.

Hoffman and Thompson (10) found that it was possible to characterize a two-parameter model for flexible pavements by using the maximum deflection under the load (D0) and a parameter they called the basin area. This area concept, shown in Figure 6, combines all the measured deflections in the basin into a single number to minimize the effect of an erroneous geophone reading. The area being determined

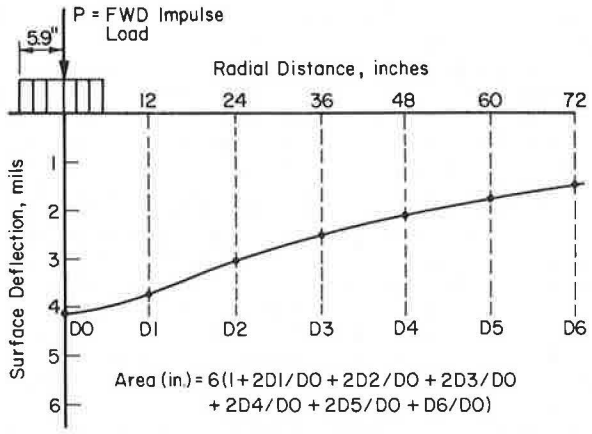

FIGURE 6 Deflection basin area concept.

is essentially one-half of the cross-sectional area of the deflection basin taken through the center of the load. To eliminate the effect of variable loads and to restrict the maximum and minimum values of the area, each deflection reading is normalized with respect to the maximum D0 deflection. Thus, the basin area has the units of length and is a function of the number and location of the sensors. Using the FWD with seven sensors spaced 12-in. apart and the trapezoidal rule, the following equation is employed to calculate area for rigid pavements:

$$\text{Area (in.)} = 6 \times (1 + 2 \times D1/D0 + 2 \times D2/D0 + 2 \times D3/D0 + 2 \times D4/D0 + 2 \times D5/D0 + D6/D0) \quad (4)$$

By visualizing a perfectly stiff slab, that is, all deflections equal, the maximum area possible from Equation 4 is 72 in. Conversely, a practical minimum area of about 11 is obtained if Boussinesq techniques are employed (the slab is as stiff as the foundation).

The independence of the D0 and area parameters is assured by the normalizing process. The same D0 could produce an area of 72 in. just as easily as one of 11 in. With the deflection basin area and the maximum deflection D0, it is possible to solve for that unique combination of dynamic E and k that produces the same characteristic basin as measured with the FWD.

The determination of dynamic E and k from deflection basin measurements can be accomplished graphically for any given slab configuration, Poisson's ratio of the concrete, and magnitude of load. This technique has proven successful in backcalculating dynamic E and k values that, when input back into the ILLI-SLAB model, very accurately reproduce FWD-measured deflections (7). However, its use has been limited primarily to thinner highway pavements on which only four sensors on the FWD are needed to describe the deflection basin accurately.

Several drawbacks to this graphic technique should be noted because they severely limit its application for large airfield evaluation programs. First, this technique requires hand plotting of the backcalculation grid, which can only be done after several ILLI-SLAB computer runs have been annually input. Second, a new grid must be developed for each pavement thickness and slab size encountered, which can mean up to 25 separate grid formulations for each airfield. Third, individual FWD deflections must be normalized to a standard load, usually 24,000 lb, to avoid a separate grid for each drop of the FWD. Finally, inaccuracies can easily be introduced through poor interpolation of dynamic E and k values within the grid. This source of error can be minimized somewhat, but only if more ILLI-SLAB runs are made to develop a finer grid.

Computer-Based Iterative Solution for Dynamic E and k

One of the major objectives of this research was to develop a complete, computer-based rigid pavement evaluation system that would relieve the engineer of hand manipulation of large amounts of data. Initially, efforts centered on the development of a large, computer-generated data base from which algorithms for estimating dynamic E and k, given the deflection basin characteristics and the geometry of the slab, could be formulated. Although showing some potential, these efforts failed to produce the accuracies that could be obtained from the graphic solutions.

Consequently, a simple iterative scheme was devised by using ILLI-SLAB as a computer subroutine that accurately backcalculates the unique dynamic E and k combination by matching measured and observed deflections. The program contains checks after each iteration and terminates when prescribed tolerances are satisfied. Up to five iterations may be required to close within these tolerances, but three or four iterations are typical. The greater sensitivity of both area and D0 in the higher ranges of E and k will dictate how many iterations are ultimately required. A complete description of the technique involved in this computer solution for E and k can be found in a paper by Foxworthy (2).

Comparison of Measured and Predicted Deflection Basins

The validity of any analytical model is truly tested when predicted response is compared with measured response. To verify the accuracy of ILLI-SLAB and the backcalculated dynamic E and k moduli, each individual slab at Sheppard Air Force Base was used to compare measured and predicted deflections for FWD loads of more than 22,000 lb. Figure 7 graphically shows the results for one feature (Feature A06B). This figure shows the outstanding precision with which ILLI-SLAB models a pavement's response to load.

An analysis of the deflection data reveals trends similar to those established during the FWD repeatability study. As deflections decrease away from the loaded area, the percent error between measured and predicted deflection at each sensor tends to increase. This is reasonable if each sensor carries about the same built-in error (the sensors are ac-

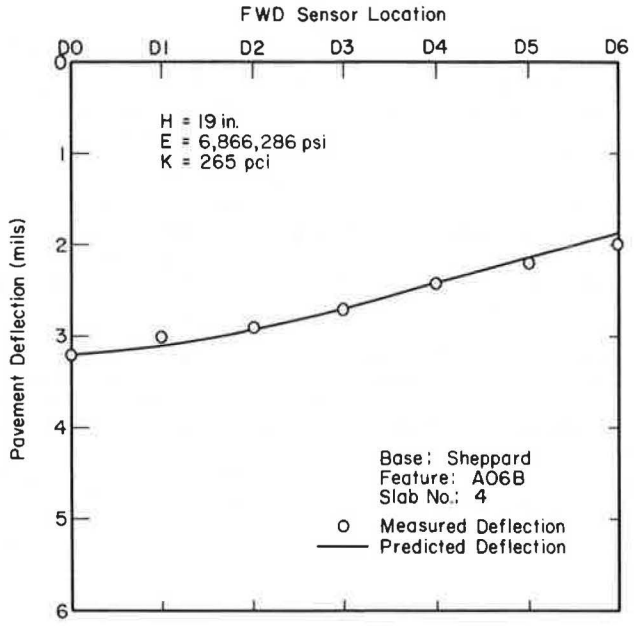

FIGURE 7 Comparison of measured and predicted FWD deflections.

curate to within 0.0005 in.). Typically, 1 to 2 percent error is observed for the D0 reading whereas 5 to 6 percent is common for the D6 value. However, in most cases this match between measured and predicted deflection basins is remarkable, particularly in light of the inherent variation in the sensors and paving materials, and the very small deflections involved.

Repeatability of Backcalculated Dynamic E and k Moduli

Table 5 gives the results of backcalculated dynamic moduli at constant temperature for two features at Sheppard Air Force Base. Each table entry for the given temperature (e.g., 78.6, 82.2, etc.) represents at least eight tests performed within 45 min of each other. Several important conclusions can be drawn from this table and the results of extensive analyses of variance.

First, at slab center, no apparent relationship exists between the magnitude of load and k, other than a decrease in the coefficient of variation of k as load increases for these features. This indicates that the dynamic k is not stress sensitive for the interior FWD loads used or the base and subgrade materials involved.

Second, although the coefficients of variation decrease with increased load, they remain somewhat higher for backcalculated k than those observed for FWD-measured loads and deflections.

Third, a pattern does exist with regard to dynamic E values and magnitude of load. Consistently higher, and often unrealistic, dynamic E values are backcalculated for low load levels, as evidence by Feature A05B in Table 5. The differences are much more pronounced between low and medium loads than between medium and high loads. The coefficients of variation for dynamic E values display much the same tendencies, with the higher loads showing significantly greater consistency. Again, higher load levels appear to give more realistic and reliable results, suggesting that the highest load levels attainable with the FWD should be used. Unrealistic values of E or k can be flagged by the computer for further study.

One of the most puzzling aspects of NDT & E is the effect of changing environmental conditions on

TABLE 5 Repeatability of Backcalculated Dynamic E and k Moduli at Constant Temperature at the Center Slab Position

				k		$E \times 10^6$		
Feature	Slab No.	Pvmt Temp. (°F)	Load[a] Range	Average (pci)	Coef. of Var.	Average (psi)	Coef. of Var.	No. of Tests
T04A	1	78.6	Low	294	.19	4.2	.33	8
			Medium	280	.15	3.8	.26	8
			High	286	.11	3.6	.18	8
	2	82.2	Low	434	.09	2.9	.13	8
			Medium	349	.07	3.3	.14	8
			High	358	.07	3.2	.12	8
	3	80.8	Low	206	.14	5.5	.15	8
			Medium	205	.17	4.7	.27	8
			High	215	.12	4.6	.22	8
A05B	1	68.4	Low	181	.11	6.6	.18	9
			Medium	178	.16	6.0	.11	9
			High	190	.05	5.8	.12	9
	2	74.5	Low	156	.12	7.9	.17	8
			Medium	158	.04	6.9	.04	8
			High	181	.06	6.2	.08	8
	4	89.1	Low	125	.18	7.9	.29	8
			Medium	141	.07	6.0	.13	8
			High	150	.05	5.7	.07	8

[a]Load ranges are as follows: low, 6,000 to 9,000 lbf; medium, 14,000 to 17,000 lbf; and high, 22,000 to 26,000 lbf.

the parameters that characterize the pavement system. Individual E- and k-value trends with pavement temperature indicate that all slabs within a feature display similar tendencies, but no overall predictable pattern is discernible. Dynamic k values tend to be slightly higher at colder temperatures, level off in mid-range, and then increase again slightly at higher temperatures. This kind of pattern would appear to be related more to moisture levels than temperature, but additional research into this aspect is needed to reach any meaningful conclusions. In any event, the fluctuation in k is not significant enough to affect the stresses generated to any great extent. Dynamic E values also exhibit a pattern similar to k values, tending to be moderately higher at colder temperatures and then leveling off. However, at higher temperatures the pattern is inconsistent.

Table 6 presents a summary of the results of backcalculated dynamic k and E values for eight slabs at pavement temperatures ranging from 36 to 101 °F. With at least five cases per slab, this table shows that the introduction of temperature as a variable has increased the coefficients of variation above the levels established by the constant temperature situation, particularly for dynamic E values at low load levels. At recommended high load levels, this increase in the coefficient of variation is modest, averaging about 4 percent. Dynamic k values remain relatively unaffected by temperature fluctuations, with coefficients of variation similar to the constant temperature case. Figure 8 shows how the normal variation in E and k at constant temperatures is great enough to encompass the variation in E and k at different temperatures.

In conclusion, it appears that only temperature extremes substantially influence backcalculated dynamic E and k values. Temperature fluctuations between 40 and 90°F are relatively insignificant, producing little variation in addition to that which is already inherent in the equipment and pavement materials. The overwhelming temperature effect occurs at the joints, where load transfer plays an important role in the pavement response to load.

SUMMARY

The foundation for a complete system that will nondestructively test and evaluate rigid airfield pavements has been developed. The FWD has been shown to give consistent load and deflection measurements under a variety of temperature and slab location conditions. The effects of changing temperatures on joint load transfer efficiency have been described, and mathematical models have been formulated to incorporate these relationships into actual stress analyses. Finally, an iterative solution for E and k, based on FWD measurements, permits their consis-

TABLE 6 Repeatability of Backcalculated Dynamic E and k Moduli at Various Temperatures at the Center Slab Position

				k		$E \times 10^6$		
Feature	Slab No.	Pvmt Temp. Range (°F)	Load[a] Range (lbf)	Average (pci)	Coef. of Var.	Average (psi)	Coef. of Var.	No. of Cases
T04A	1	33.1	Low	275	.19	5.9	.31	8
		to	Medium	276	.15	4.2	.16	8
		121.8	High	316	.13	3.6	.19	8
	2	33.1	Low	422	.13	4.7	.26	8
		to	Medium	348	.12	4.4	.27	8
		121.8	High	396	.10	3.8	.27	8
	3	33.1	Low	268	.29	5.8	.38	8
		to	Medium	243	.27	1.3	.27	8
		121.8	High	261	.25	4.6	.26	8
	4	33.1	Low	448	.24	2.9	.53	5
		to	Medium	370	.13	4.4	.08	5
		121.8	High	391	.12	4.2	.12	5
A05B	1	34.2	Low	209	.17	7.1	.13	6
		to	Medium	189	.16	7.2	.13	6
		119.3	High	208	.18	6.5	.09	6
	2	34.2	Low	194	.31	9.1	.33	7
		to	Medium	176	.16	7.7	.21	7
		119.3	High	188	.08	7.6	.14	7
	3	34.2	Low	327	.23	10.0	.19	6
		to	Medium	287	.12	9.3	.24	6
		119.3	High	310	.09	8.8	.09	6
	4	34.2	Low	189	.14	7.5	.27	7
		to	Medium	173	.10	6.8	.15	7
		119.3	High	182	.07	6.8	.11	7

[a]Load ranges are as follows: low, 6,000 to 9,000 lbf; medium, 14,000 to 16,000 lbf; and high, 22,000 to 25,000 lbf.

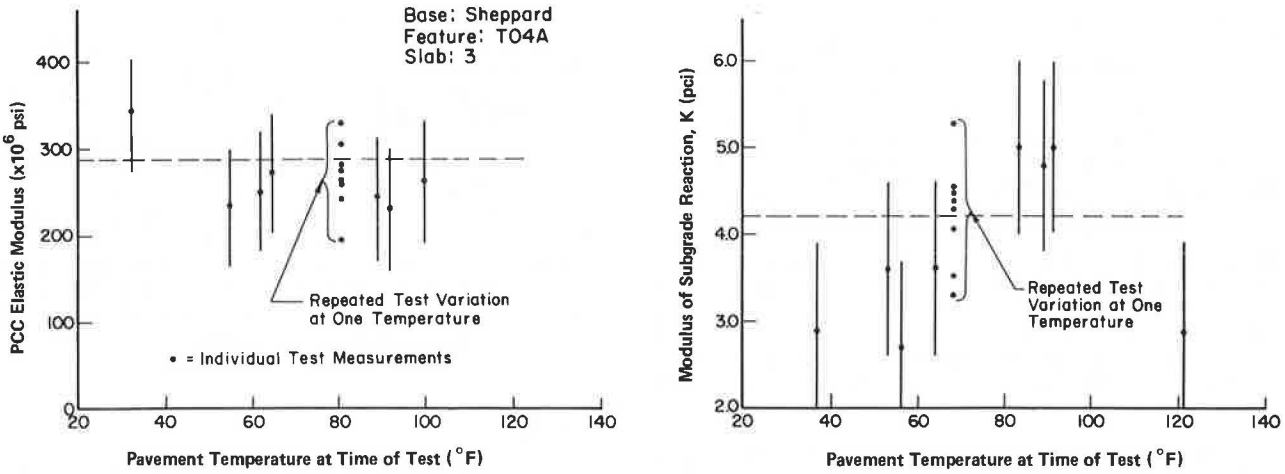

FIGURE 8 Typical variation in E and k at constant temperature applied to single observations of E and k at various temperatures.

tent determination under a wide range of temperatures.

ACKNOWLEDGMENTS

The authors wish to acknowledge the cooperation and financial support of the U.S. Air Force Engineering and Services Center and the University of Illinois, without which this research could not have been accomplished.

REFERENCES

1. R.E. Smith and R.L. Lytton. Synthesis Study of Nondestructive Testing Devices for Use in Overlay Thickness Design of Flexible Pavements. ERES Consultants, Champaign, Ill., Nov. 1983.
2. P.T. Foxworthy. Concepts for the Development of a Nondestructive Testing and Evaluation System for Rigid Airfield Pavements. Ph.D. dissertation. University of Illinois at Urbana-Champaign, Urbana, 1985.
3. A.M. Tabatabaie, E.J. Barenberg, and R.E. Smith. Longitudinal Joint Systems in Slip-Formed Rigid Pavements. Volume II--Analysis of Load Transfer Systems for Concrete Pavements. Report FAA-RD-79-4. Federal Aviation Administration, U.S. Department of Transportation, Nov. 1979.
4. A.M. Tabatabaie-Raissi. Structural Analysis of Concrete Pavement Joints. Ph.D. dissertation. University of Illinois, Urbana, 1977.
5. A.M. Ioannides, J. Donnelly, M.R. Thompson, and E.J. Barenberg. Analysis of Slabs-On-Grade for a Variety of Loading and Support Conditions. AFOSR-83-0143. U.S. Air Force Office of Scientific Research, Washington, D.C., Sept. 1984.
6. M.I. Darter. Concrete Pavement Evaluation. Proc., 7th Annual Airport Engineering and Safety Seminar, Federal Aviation Administration, Hershey, Penn., March 1983.
7. Nondestructive Structural Evaluation of Airfield Pavements. ERES Consultants, Champaign, Ill., Dec. 1982.
8. J.A. Crovetti and M.I. Darter. Joint Repair Methods for Portland Cement Concrete Pavements, Appendix C, Void Detection Procedures. University of Illinois, Urbana, March 1985.
9. N.H. Nie et al. Statistical Package for the Social Sciences. McGraw-Hill, New York, 1975 (2nd edition).
10. M.S. Hoffman and M.R. Thompson. Mechanistic Interpretation of Nondestructive Pavement Testing Deflections. Project IHR-508, University of Illinois, Urbana, June 1981.

Publication of this paper sponsored by Committee on Monitoring, Evaluation and Data Storage.

Mathematical Programming Models for the Development of a Unified Ranking System

HOSIN LEE, C. L. SARAF, and W. RONALD HUDSON

ABSTRACT

An important component of any rehabilitation and maintenance programming is an index or scale for selecting candidate projects for rehabilitation and establishing priority among the candidate projects. In the past two decades, tools and concepts of multiple attribute decision making (MADM) have been applied to developing an index for establishing priorities for pavement rehabilitation. However, virtually no effort has been made toward developing a unified ranking system for both rigid and flexible pavements. Presented is a univariate time series model dealing with a single common attribute existing in both rigid and flexible pavements, such as roughness. The single attribute method is extended by adding more attributes such as cracking, rutting, punchouts, and so forth is in order to form a MADM method. The goal programming model determines the relative weights for the multiple attributes. Several advantages of these models for practical application are discussed.

During the past 40 years, more than $1 trillion has been invested in the highway system of the United States. With much of the highway network system completed, national attention and interests have been directed toward the problems of maintaining highways. State and local governments spend $15 billion annually to maintain the nation's 4-million-mile network (1). Massive investments, which are estimated to be $400 billion by the year 2000, will be required for rehabilitating and maintaining pavement. Consequently, it has become necessary to develop a system for effectively programming the rehabilitation and maintenance of the pavement network.

Some agencies developed a combined index to express the overall condition of the pavement for rating purposes. This combined index is computed by adding up the deduct values for specific distress types and subtracting the sum from the perfect score, 100. The combined index method using deduct values is one of the so-called multiple attribute decision making (MADM) methods that have long traditions in many other disciplines (2).

In the past decade, the tools and concepts of MADM have been applied to the development of an index for establishing priorities for pavement rehabilitation. However, virtually no efforts have been made toward developing a unified ranking system for both rigid and flexible pavements based on the different sets of pavement attributes. Recently, the Texas State Department of Highways and Public Transportation (SDHPT) has indicated its interest in the development of a unified ranking system for selecting candidate projects in order to distribute rehabilitation funds to both types of pavement rehabilitation projects on an equitable basis.

The next section consists of a univariate time series model dealing with a single common attribute that exists in both rigid and flexible pavements, such as roughness. Then the problem with a single attribute is extended by adding more attributes such as cracking, rutting, punchouts, and so forth in order to form a multiple attribute decision making problem. Next, the goal programming model, which determines the relative weights for the attributes, is described. The paper concludes with a discussion of the practical applications of these models.

H. Lee and C.L. Saraf, Center for Transportation Research, The University of Texas at Austin, Austin, Tex. 78712. W.R. Hudson, The Dewitt C. Greer Centennial, University of Texas at Austin, Austin, Tex. 78712.

UNIVARIATE TIME SERIES OF SERVICEABILITY INDEX MODEL

The present serviceability index (PSI) represents a means for using objective data, such as roughness, to estimate present serviceability rating (PSR). Generally, a pavement section that is deteriorating, for example, losing serviceability index (SI) at a fast rate, should be ranked higher for rehabilitation than others because rapid loss of SI indicates probable rapid future deterioration of pavement. An increasing deterioration rate might be due to inadequate design, traffic heavier than was expected, more severe environmental conditions than expected, and so forth.

This concept can be demonstrated by comparing three pavement sections, as shown in Figure 1. The three pavement sections are currently at the 3.0 SI level and are 5, 8, and 10 years old, respectively. The question is, Which section should be ranked higher for rehabilitation? The time-dependent phenomenon of pavements includes many unknown factors and it is not possible to develop a deterministic model that allows exact calculation of the future pavement condition ranking. However, it can be observed that these pavements should be ranked in the order of A, B, and C, based on the different past performance histories of the pavements.

The model discussed here is based on a single time series that is a sequence of observed SI data at equally spaced time intervals, say X_t, $t = 1, 2, \ldots n$ (years). It is presumed that the observations in a time series are correlated. Therefore, the model relating X_t, X_{t-1}, and X_{t-2} can be developed as

$$X_t = b_1 X_{t-1} + b_2 X_{t-2} + a_t \quad (1)$$

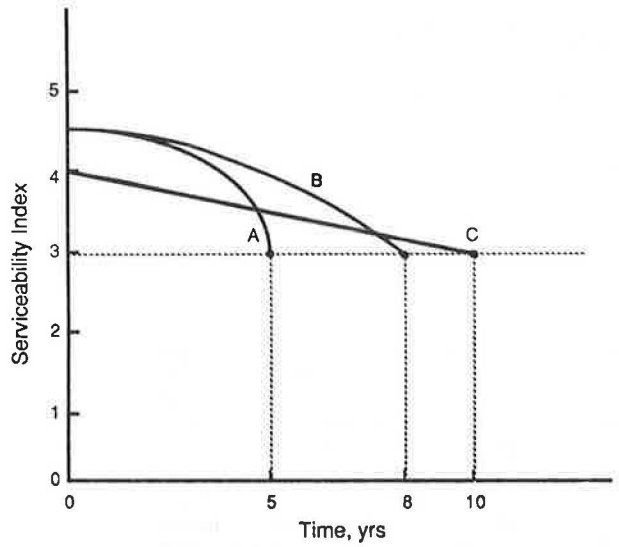

FIGURE 1 Three pavement sections with the same present SI but different rate of loss of SI.

where

X_t = SI at time t;
b_1, b_2 = parameters to be estimated; and
a_t = random error entering the the model at time t, which is assumed to be an independent, normally distributed random variable with mean zero and constant variance σ_a^2.

The model (Equation 1) expresses the dependence of the variable on itself at different points in time; in other words, the variable X_t is regressive. A set of data points is needed to estimate b_1 and b_2. To do this, data were obtained from the SI data base at the Center for Transportation Research (CTR), University of Texas at Austin, where historical SI data have been collected from the 22 test sections over 3 years beginning in 1982; these data are given in Table 1. By using an ordinary least-squares method, the cross-sectional data were fitted to the model as follows:

$$FSI = 0.98\ PSI - 0.55\ LSI \qquad R^2 = 0.96 \qquad (2)$$

where

FSI = future serviceability index (X_t),
PSI = present serviceability index (X_{t-1}), and
LSI = loss of serviceability index during the previous year ($X_{t-2} - X_{t-1}$).

This model can be used to predict SI in the future by using the current serviceability index and the LSI over recent time. This predicted SI can be used as a common index for rehabilitation. The model can be updated from time to time as more data become available. In those cases in which past history data for more than 3 years are available, the model can be expanded to consider the more distant past history of SIs.

VALIDATION OF THE MODEL

In this section, diagnostic checks are applied to the fitted model. To check the prediction capability of the model, the observed values were plotted against the predicted values, as shown in Figure 2.

TABLE 1 Annual SI Data for 22 Test Sections in Austin

Section No.	Year 1983	1984	1985
7	4.47	4.77	4.69
5	4.54	3.64	3.41
33	4.48	4.42	4.33
36	4.42	4.45	4.37
32	4.41	4.42	4.33
23	4.20	4.18	3.98
34	3.96	3.94	3.82
28	3.81	3.06	3.03
8	3.70	3.67	3.49
40	3.66	3.60	3.68
19	3.62	3.61	3.54
9	3.60	3.27	3.19
3	3.57	3.35	3.25
12	3.53	2.82	2.14
41	3.50	3.50	3.53
15	3.38	2.32	1.07
2	2.62	2.11	2.00
35	2.48	2.69	2.44
6	2.39	2.41	2.36
38	2.08	1.88	1.62
44	1.17	1.21	1.12
39	1.05	0.90	0.77

It can be observed that the model predicts the future serviceability reasonably well. High R^2 value supports this explanatory power of the model. The F-statistic value of the fitted regression falls in the critical region at a 1 percent level of significance. Therefore the null hypothesis (H: $b_1 = b_2 = 0$) is rejected, and thereby the notion that the regression slopes are different from zero purely by chance is also rejected (3). Parameters of independent variables were found to be significantly different from zero, by using a t-statistic at the level of significance $\alpha = 0.01$.

An error term exists in any model unless the model is a perfect representation of reality. In a good regression model, an error term is assumed to be normally distributed with a mean of zero and a constant standard deviation. Furthermore, the errors are assumed to be independent. The residual is an estimate of the error. The residuals can be used to test the original assumptions: normality, constant variance, and independence in the error term.

To check the normality assumption, a frequency histogram for the residuals was constructed. The bell-shaped distribution that was observed in the frequency histogram is supportive of the normal distribution. A normality of residuals was assured by the Shapiro-Wilk test (W = 0.937). A hypothesis of normality could not be rejected at $\alpha = 0.05$ (4).

To check common variance and independence assumptions, residuals were plotted against the PSIs. It is difficult to detect heteroscedasticity (the case in which the error term has no constant variance) because of the randomness of errors. A pattern in the residuals neither supports the heteroscedasticity nor shows any dependency of residuals. A hypothesis of autocorrelation (that successive residuals tend to be close together) was rejected by the Durbin-Watson test (D = 2.64) at $\alpha = 0.05$ (5).

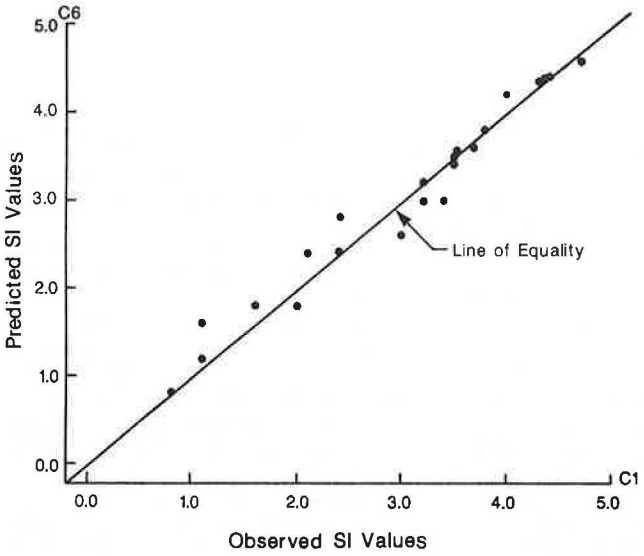

FIGURE 2 Plot of predicted SI values against observed SI values.

Multicollinearity is said to exist when any independent variable is correlated with another independent variable. It is one of the main causes of misinterpretation and misuse of regression. The correlation between variable PSI and LSI in Equation 2 is -0.219. This low value indicates that the correlation between these two independent variables is not significant. In other words, a hypothesis of no correlation could not be rejected at $\alpha = 0.05$ (6).

All of these test statistics and plots indicate that the regression equation satisfies all the assumptions and requirements. The negative parameter associated with the rate of loss of SI indicates that rapid loss of SI probably indicates rapid deterioration of a pavement in the future. The intercept was not significant enough to be included in the final equation. The model should be further verified as more data become available.

APPLICATION OF UNIVARIATE TIME SERIES MODEL

To show how the procedure is used for developing a common index, a number of hypothetical pavement sections were set up, as presented in Table 2. By using Equation 2, the predicted SI was calculated for each of the sections given in Table 2. The predicted SI can be used as a common index for assigning priority rankings to the given sections. These rankings are included in Table 2.

The results indicate that the pavement with the faster deterioration rate should be ranked higher for rehabilitation work. This equation may give some credit to rigid pavements, which generally deteriorate at a slower rate than do flexible pavements.

GOAL PROGRAMMING MODEL FOR MULTIPLE ATTRIBUTE DECISION MAKING

In the past two decades, a substantial advancement in MADM has been made. The results of a literature review of methods and applications using MADM have been classified systematically by Hwang and Yoon (2). In recent years, a great deal of research has been done on MADM; in particular, there has been rapid theoretical development in multiattribute utility theory, which is a solution approach to MADM uncertainty (7). However, the basic proposition that motivates pavement research is the idea that pavement selection for rehabilitation is influenced by perceptions of and values for specific attributes of the pavement sections.

This concept has been used in marketing research to predict consumer preferences for brands of a particular product class (8). The methods require that the decision maker be able to indicate his preference between two alternatives. LINMAP techniques (LINear programming techniques for Multidimensional Analysis of Preferences) were originally developed to explain, rationalize, lead to understanding of, and predict decision behavior, but they are well fitted for normative decision making (9-11). The original model

TABLE 2 Hypothetical Pavement Sections Ranked According to Future Serviceability Index

Section No.	Pavement Type	Present SI	Loss of SI	Future SI	Ranking for Rehabilitation
1	Flexible	3.40	0.80	2.89	18
2	Rigid	3.40	0.60	3.00	20
3	Flexible	3.20	0.50	2.86	17
4	Rigid	3.20	0.40	2.92	19
5	Flexible	3.00	0.30	2.78	16
6	Rigid	2.90	0.20	2.73	15
7	Flexible	2.80	0.10	2.69	14
8	Rigid	2.70	0	2.65	13
9	Flexible	2.60	0.80	2.11	10
10	Rigid	2.50	0.60	2.12	11
11	Flexible	2.40	0.50	2.08	9
12	Rigid	2.40	0.40	2.13	12
13	Flexible	2.20	0.30	1.99	7
14	Rigid	2.20	0.20	2.05	8
15	Flexible	2.00	0.10	1.91	6
16	Rigid	1.90	0	1.86	5
17	Flexible	1.80	0.80	1.32	1
18	Rigid	1.70	0.60	1.34	2
19	Flexible	1.60	0.20	1.46	3
20	Rigid	1.50	0	1.47	4

was modified to estimate weights for both flexible and rigid pavements simultaneously.

Consider a set of preference judgments (j,k) such that pavement section j is preferred to section k in a pairwise comparison. It is assumed that the judgments are implicitly made by a highway engineer or other professional on the basis of some global criteria, possibly with some error. A highway professional makes paired comparison judgments such as the following: pavement section k needs to be rehabilitated before section j. Overall, pavement performance is the global criterion; presumably a highway engineer makes his overall judgment considering some of the pavement attributes, such as cracking, punchouts, and so forth, but exactly which attributes are considered cannot be known.

Let d_{jq} denote the difference of the condition of pavement section j from the perfect condition in terms of pavement attribute q. Let W_q denote the weight or importance of the attribute q. Then the global criterion D_j for the pavement section j is given by

$$D_j = \sum_{q \epsilon Q} W_q \, d_{jq} \qquad (3)$$

The global criterion model states that given any pair (j,k), the condition of pavement section j is better than the section k only if $D_j < D_k$.

The global criterion is but a model of a highway engineer's decision-making process. It is not necessary that a highway engineer solve Equation 3 to arrive at his decision. The objective of this model is to develop a set of weights such that the global criterion D_j defined in Equation 3 is as consistent as possible with the given pairwise comparison judgments by a highway engineer. Inconsistencies of judgments will be minimized by assigning lower weight to the attributes that involve inconsistent decisions. This leads to the following formulation, which belongs to a particular class of linear programming problems known as goal programming (7,12,13).

$$\text{Minimize} \sum_{(j,k) \epsilon S} Y_{jk} \qquad (4)$$

Subject to the constraints

$$\sum_{p \epsilon P} W_p \, d_{kp} - \sum_{q \epsilon Q} W_q \, d_{jq} + Y_{jk} \geq 0 \text{ for } (j,k) \epsilon S$$

$$\sum_{p \epsilon P} A_p \, W_p - \sum_{q \epsilon Q} A_q \, W_q = 1$$

$$Y_{jk} \geq 0 \qquad \text{for } (j,k) \epsilon S$$

$$W_p, W_q \geq 0 \qquad \text{for } p \epsilon P, \; q \epsilon Q$$

where

- j = pavement section that decision maker prefers to section k;
- S = set of all ordered pairs (j,k) of the n pavement sections;
- Y_{jk} = amount of violations to be minimized by selecting optimum W_p, W_q;
- p = pavement attribute of nonpreferred section k;
- P,Q = {1, 2 . . . t}: t pavement attributes of either rigid or flexible pavement;
- W = $\{W_q\}$, $q \epsilon Q$: weights to be assigned to pavement attribute Q;
- d_{kp} = distance of pavement section k from ideal point of attribute p;
- q = pavement attribute of preferred section j;
- d_{jq} = distance of pavement section j from ideal point of attribute q;

$A_p = \sum_{k \epsilon S} d_{kp}$; and

$A_q = \sum_{j \epsilon S} d_{jq}$.

A goal programming model was developed to estimate the weights of multiple attributes in a global criterion measure. The inputs to this model consist of (a) a set of pavement sections, with each section defined by its pavement attribute values; and (b) a set of paired preference judgments that were made on the pavement sections by highway engineers in terms of the global criterion (Gestalt).

A survey was conducted using 27 highway engineers who were participating in the Pavement Management Training Program in Austin. A set of choices between two pavement sections in different types and conditions was obtained from highway engineers. A typical pairwise comparison set is shown in Figure 3 with four selected attributes for each pavement type. Eight pavement attributes were described briefly in the survey form. A total of 31 pairwise comparison sets were presented individually on a projection screen to prevent highway engineers from relating a current selection to the previous selections.

Flexible Pavement

Attribute \ Section	Section 1
Patching	0 %
Rutting (inches)	1.0 in
Alligator Cracking	20 %
Serviceability Index	2.5

Rigid Pavement

Attribute \ Section	Section 2
Patches (#/mile)	10
Spalled Cracks (#/mile)	5
Punchouts (#/mile)	0
Serviceability Index	2.0

FIGURE 3 Typical pairwise comparison set of flexible and rigid pavements.

The objective of this research is to estimate the average response of the group. A separate analysis of each highway engineer's judgments was also performed to ascertain whether his set of estimated weights differed significantly from others. An equation representing the group opinion of highway engineers has been developed by using a linear programming computer package as follows:

$$\text{Common Index} = 3.8 \cdot RD + 0.08\,AL + 2.86\,(5.0 - SI) + 0.38 \cdot PU \qquad (5)$$

where

- RD = average rut depth (in.),
- AL = alligator cracking (%), and
- PU = number of punchouts.

Patches in either flexible or rigid pavements and spalled cracks did not affect the group's decision-making process significantly. They were dropped out of the equation because too much inconsistency existed with these four attributes in the decision-making process. Weights can be compared between attributes considering their different measurement units. For example, three punchouts will have the

same effect on pavement performance as approximately 15 percent alligator cracking, according to Equation 5. The higher number in the common index means a higher priority for rehabilitation. Perfect pavement should have an index value of zero.

A second survey was conducted to verify the equation derived by using the data from the first survey. A highway engineer may perceive pavement attributes differently in different situations. He may make pairwise comparison judgments differently with different sets of comparison pairs. He may possibly commit some error because of fatigue, boredom, or other reasons. The main objective of the second survey was to find whether these errors significantly affect his decision-making process.

The same group of highway engineers was asked to evaluate another 31 comparison pairs under conditions different from those during the first survey. Another equation was derived in the same way as was the first equation, but by using data from the second survey, as follows:

$$\text{Common Index} = 0.03\,PA + 3.54\,RD + 0.06\,AL + 2.71\,(5.0 - SI_F) + 0.24\,PU + 3.43\,(5.0 - SI_R) \quad (6)$$

where

PA = percentage patching in flexible pavement,
RD = rut depth (in.),
SI_F = SI of flexible pavements, and
SI_R = SI of rigid pavements.

Patches or spalled cracks in rigid pavement still did not affect the group's decision-making process significantly in the second survey. The second equation is similar to Equation 5 except that patching was included in flexible pavements, and the weight for the SI of rigid pavement went up whereas the weight of punchouts went down. Equation 5 is proved to be stable over random errors discussed previously by Equation 6. Equation 5 will be further verified by Equation 6, using a Spearman rank correlation measure with a sample application of the model in the next section.

APPLICATION OF GOAL PROGRAMMING MODEL

In this section, an application of the goal programming model is briefly presented. To demonstrate how Equation 5 is used in establishing priorities for rehabilitation work, a set of hypothetical pavement sections was set up, as presented in Table 3. By using Equation 5, the common index was calculated for each of the sections listed in Table 3. The rankings based on this common index are included in Table 3. The results indicate how the procedure produces a common index using multiple pavement attributes. The ranking numbers appear to be realistic and applicable in practice.

VERIFYING CONSISTENCY OF GOAL PROGRAMMING MODEL

An application of the goal programming model was made by using the set of hypothetical pavement sections in Table 3. However, Equation 5 was developed by using only a subset of the entire highway network. Therefore, the consistency of Equation 5 needs to be verified with random errors associated with other pavement sections in different conditions. To do this, another equation, Equation 6, was developed with the results of the second survey, which was conducted by using another set of pavement sections under different conditions. Even though there is no direct statistical test of the hypothesis that the two equations are identical, correlation analysis can be applied if the equations are expressed as ranked data.

The rankings of 20 hypothetical pavement sections based on Equation 5 are given in Table 3. Another ranking of the same pavement sections, using Equation 6, is given in Table 4, together with the rankings obtained by using Equation 5. The consistency of the two rankings is of interest.

The measure of the degree of association between the two rankings can be obtained with a nonparametric method called rank correlation. A widely used measure of the correlation between ranked series is a coef-

TABLE 3 Hypothetical Pavement Sections Ranked According to Common Index by Using Condition Survey Data

Section No.	Pavement Type	Patching (Percent)	Rut Depth (Inches)	Alligator Crack (Percent)	Punchout (Percent)	SI	Common Index	Ranking for Rehabilitation
1	Flexible	0	0	25	---	4.0	4.86	19
2	Rigid	---	---	--	0	4.0	2.86	20
3	Flexible	25	0	25	---	3.5	6.29	16
4	Rigid	---	---	--	5	3.5	6.19	17
5	Flexible	0	0	50	---	3.0	9.72	13
6	Rigid	---	---	--	0	3.0	5.72	18
7	Flexible	0	1.0	25	---	3.0	11.52	9
8	Rigid	---	---	--	10	3.0	9.52	14
9	Flexible	25	0	50	---	2.5	11.15	10
10	Rigid	---	---	--	0	2.5	7.15	15
11	Flexible	25	1.0	25	---	2.5	12.95	7
12	Rigid	---	---	--	10	2.5	10.95	11
13	Flexible	0	0	75	---	2.0	14.58	3
14	Rigid	---	---	--	5	2.0	10.48	12
15	Flexible	50	0.5	25	---	2.0	14.48	4
16	Rigid	---	---	--	10	2.0	12.38	8
17	Flexible	0	1.0	50	---	2.0	16.38	1
18	Rigid	---	---	--	15	2.0	14.28	5
19	Flexible	25	1.0	0	---	1.5	13.81	6
20	Rigid	---	---	--	15	1.5	15.71	2

TABLE 4 Hypothetical Pavement Sections Ranked According to Equations Developed by Using First and Second Surveys and the Difference in Their Rankings

	First Survey		Second Survey		Difference in Ranking	
Section No.	Common Index	Ranking	Common Index	Ranking	d	d^2
1	4.86	19	4.21	19	0	0
2	2.86	20	3.43	20	0	0
3	6.29	16	6.32	18	-2	4
4	6.19	17	6.35	17	0	0
5	9.72	13	8.42	15	-2	4
6	5.72	18	6.86	16	2	4
7	11.52	9	10.46	12	-3	9
8	9.52	14	9.26	13	1	1
9	11.15	10	10.53	11	-1	1
10	7.15	15	8.58	14	1	1
11	12.95	7	12.57	8	-1	1
12	10.95	11	10.98	10	1	1
13	14.58	3	12.63	7	-4	16
14	10.48	12	11.49	9	3	9
15	14.48	4	12.90	5	-1	1
16	12.38	8	12.69	6	2	4
17	16.38	1	14.67	2	-1	1
18	14.28	5	13.89	3	2	4
19	13.81	6	13.78	4	2	4
20	15.71	2	15.61	1	-1	1
					$\Sigma d = 0$	$\Sigma d^2 = 66$

ficient of rank correlation developed by Spearman in 1984 (8). This measure is expressed by

$$r_s = 1 - \{(6 \Sigma d^2)/[n(n^2 - 1)]\} \quad (7)$$

where d is the difference in rank between paired items in a series and n is the number of pairs of ranked items in a series.

Using the value of d in Table 4,

$$r_s = 1 - \{(6 \times 66)/[20(400 - 1)]\} = 0.95 \quad (8)$$

Coefficient r_s computed from sample data should be tested for significance because it is subject to a sampling error. The value of $r_s = 0.95$ obtained from a sample of 20 paired pavement section rankings is significant at the 0.01 level of significance. This result confirms that the rankings obtained by using Equation 5 are highly correlated and, therefore, consistent with the rankings obtained by using Equation 6.

SUMMARY, CONCLUSIONS, AND RECOMMENDATIONS

Two methodologies are presented for the selection of pavement sections for rehabilitation. An application of the univariate time series of SI method is shown to be useful in establishing an objective way to assign priorities by taking the past history of the pavement into consideration. As expected, the deterioration rate is shown to be a significant factor in the model. However, this empirical result is by no means definitive. The equation was generated by using a rather small sample of data collected from flexible pavements in Austin, Texas. The model should be tested with a broad range of data in different situations, such as cold weather for rigid pavement.

The goal programming model using pairwise comparison data appears to be useful in explaining the process of how decisions are made. This method does not place significant judgmental demand on the decision maker as do other methods, such as utility function. The procedure is generalized so that a common set of weights can be estimated using the paired comparison judgments of a group of highway engineers, who use two different types of pavements with different pavement attributes. Only five of eight pavement attributes were found to be used by the raters for comparing rigid pavements with flexible pavements.

The goal programming formulation is extremely flexible; thus, many additional features can be built into the basic model, such as the following:

1. Additional constraints on weights can be readily imposed. For example, if it is known from a previous analysis that SI is more important than the number of spalled cracks, such a constraint can be added.
2. The quadratic utility concept can be used instead of the linear utility function used in the model procedure developed.
3. An individual highway engineer may state his confidence in comparing a pair of pavement sections.

The application of this method to developing a common index will be helpful in understanding the behavior of decision makers in aggregating information across the attributes, and improving the quality of their decision making.

In general, the analysis of setting priorities demonstrates the equivocal nature of the phenomenon. The different rankings resulting from different analyses of setting priorities could be considered

as a strength rather than a weakness because (a) each procedure for setting priorities is based on some rational strategy and (b) each different strategic approach affords a different view of the phenomenon.

The time-series model can be considered a quick-and-simple solution to comparing rigid and flexible pavements, but the model is a good start toward the development of a unified ranking system. The model produces a reasonable answer and it can be easily applied in practice.

Highway engineers can provide information with more confidence through the pairwise comparison approach that through other approaches, such as the utility theory and the scaled rating method. Therefore, the pairwise comparison approach is recommended for collecting subjective opinions about two different types of pavements with different pavement attributes. Moreover, pairwise comparison is simpler and easier than probabilistic assessment of values for utility function development or direct rankings of pavements in different types and conditions.

One major limitation of the method is that it is not guaranteed with only paired preference data that an internally scaled multiattribute function exists. Even if such a function exists, the actual decision-making process of highway engineers may not be a simple additive function, which was assumed in the model. Another limitation of this procedure is that appropriate statistical tests of significance for the parameter estimates are lacking.

Consequently, it is recommended that future research effort be directed towards verifying the models developed with different sets of SI data and other groups of highway engineers. The model should be tested with more data obtained under different conditions in terms of traffic volume, pavement type and structure, environment, and so forth. It is also recommended that historical serviceability data should be collected for a longer time period, which will allow testing of the model at different points in time.

It is recommended that the goal programming model that uses pairwise comparison data be tested and implemented by using a group of engineers from the state highway agency. The group of raters should include one engineer from each highway district or region. The equation developed could be considered a consensus of different engineers' views about pavement rehabilitation programming, which would also allow testing of the model with different groups of people. The involvement of users such as district engineers in the modeling process would facilitate implementation of the goal programming model.

Finally, it is recommended that these two methods for developing a unified ranking system be implemented by state highway agencies at an early date.

ACKNOWLEDGMENTS

The authors are pleased to acknowledge the combined efforts and support of the Center for Transportation Research at the University of Texas at Austin and the Texas State Department of Highways and Public Transportation, in cooperation with the FHWA, U.S. Department of Transportation.

REFERENCES

1. America's Highways: Accelerating the Search for Innovation. Special Report 202, TRB, National Research Council, Washington, D.C., 1984.
2. C.L. Hwang and K.S. Yoon. Multiple Attribute Decision Making. Springer-Verlag, New York, 1981.
3. A.H. Bowker and G.J. Lieberman. Engineering Statistics. Prentice-Hall, Englewood Cliffs, N.J., 1972, 2nd edition.
4. W.J. Conover. Practical Parametric Statistics. Wiley, New York, 1980, 2nd edition.
5. G.O. Wesolowsky. Multiple Regression and Analysis of Variance. Wiley, New York, 1976.
6. T.C. Clark and L.L. Schkade. Statistical Analysis for Administrative Decisions. Southwestern, Cincinnati, Ohio, 1979, 3rd edition.
7. R.L. Kenney and H. Faiffa. Decision with Multiple Objectives: Preferences and Value Tradeoffs. John Wiley & Sons, Inc., New York, 1976.
8. D. Pekelmen and S.K. Sen. Mathematical Programming Models for the Determination of Attribute Weights. Management Science, Vol. 20, No. 8, April 1974, pp. 1217-1229.
9. F.M. Bass, E.A. Pessemier, and D.R. Lehman. An Experimental Study of Relationships Between Attitudes, Brand Preference, and Choice. Behavioral Science, Vol. 17, No. 6, Nov. 1972, pp. 532-541.
10. V. Strinivasan and A.D. Shocker. Linear Programming Techniques for Multidimensional Analysis of Preferences. Psychometrika, Vol. 38, No. 3, Sept. 1973, pp. 337-369.
11. V. Strinivasan and A.D. Shocker. Estimating the Weights for Multiple Attributes in a Composite Criterion Using Pairwise Judgments. Psychometrika, Vol. 38, No. 4. Dec. 1973, pp. 473-493.
12. A. Charnes and W.W. Cooper. Management Models and Industrial Applications of Linear Programming. Vol. 1, John Wiley & Sons, New York, 1961.
13. F. Hillier and G. Lieberman. Introduction to Operations Research. Holden-Day, Inc., San Francisco, 1980, 3rd edition.

Publication of this paper sponsored by Committee on Strength and Deformation Characteristics of Pavement Sections.

Development of an Expert System for Pavement Rehabilitation Decision Making

STEPHEN G. RITCHIE, CHE-I YEH, JOE P. MAHONEY, and NEWTON C. JACKSON

ABSTRACT

In recent years, continued deterioration of the nation's highway infrastructure has led to increased emphasis on pavement rehabilitation, with national annual expenditures of billions of dollars. The nature of the analysis and design process suggests that a new technological approach, knowledge-based or expert system, could play an important role in addressing pavement rehabilitation problems and needs. An overview of expert system characteristics is provided; the pavement rehabilitation analysis and design process is discussed; and a prototype, microcomputer-based, surface condition expert system (SCEPTRE 1.1) for flexible pavement rehabilitation is described. Based on user inputs and a knowledge-base constructed from several human experts, the system can deduce a set of feasible project-level rehabilitation strategies for subsequent detailed analysis and design. The system can also readily explain its reasoning and conclusions, and is easily modified. It can therefore make its body of specialized knowledge accessible to a much broader range of potential engineering users.

In recent years, highway pavements in the United States have been wearing out faster than they can be repaired. This has led to increased emphasis on pavement resurfacing, restoration, and rehabilitation work, or simply pavement rehabilitation strategies, in order to restore highways to their original safe, usable condition without expansion of the original capacity. Large sums of money are currently invested in such programs, but in the future even greater emphasis is likely to be placed on maintaining and rehabilitating existing infrastructure (of which highway systems are a major part) rather than embarking on major capital investment in new facilities. In the state of Washington alone, about $100 million is spent annually on pavement resurfacing (seal coats, overlays, rehabilitation) for a state highway system approximately 7,000 miles long. In comparison, the combined length of the nation's 50-state highway systems is approximately 790,000 miles (1). Estimates of the national annual expenditures by similar state and federal agency programs run into billions of dollars.

Successful pavement rehabilitation strategies are developed by a relatively small number of pavement engineering specialists, using their knowledge, judgment, experience, and usually a limited amount of data--often uncertain in nature--from which inferences are derived and design and investment decisions made. Such experts are only to be found in some federal and state agencies, universities, and private firms. Because the analysis and design of project-specific rehabilitation strategies relies so heavily on expert pavement engineers, and the tasks involved are both complex and ill-defined, conventional computer tools are of limited use. Nevertheless, a pressing need exists to formalize this expertise and make it available to a larger number of engineers to ensure that the most cost-effective designs are constructed statewide. However, this situation is compounded by predictions that one-third of the most experienced engineers in state departments of transportation (DOTs) and county highway agencies will retire during the coming decade (2). It is a premise of the research described in this paper that expert systems can play a significant role in addressing these problems.

Expert systems are basically interactive, problem-solving computer programs that emulate the knowledge of a human expert in a specific professional domain. To date, no attempt has been made to systematically formalize the knowledge, experience, and thought process used by pavement engineering experts. Moreover, only recently has it become technically feasible to automate such a knowledge base in a computer program that could perform as an expert consultant and even as an instructor for other engineers. Such a program would be oriented particularly to engineers at the state DOT district level, but also to those at the county and local agency levels. In this paper, an overview of expert system characteristics is provided; the pavement rehabilitation analysis and design process is discussed, including the role of pavement management systems (PMSs); and a prototype, microcomputer-based surface condition expert system that has been developed for flexible pavements is described. This system represents the first phase of a much more extensive expert system under development for project-level analysis and design of pavement rehabilitation strategies for state-maintained highways. Ongoing research in these areas is also described.

RESEARCH OBJECTIVE

The quality of engineering analysis and design is a function of at least the following: quality of the

S.G. Ritchie, Department of Civil Engineering and Institute of Transportation Studies, University of California, Irvine, Calif. 92717. C-I. Yeh, Institute of Transportation Studies, University of California, Irvine, Calif. 92717. J.P. Mahoney, Department of Civil Engineering, University of Washington, Seattle, Wash. 98195. N.C. Jackson, Materials Laboratory, Washington State Department of Transportation, Olympia, Wash. 98504.

data; quality of the analysis tools; and judgment, experience, and training of the engineer. The ultimate objective of this research is to develop an easy-to-use, generalized microcomputer program that (a) embodies the knowledge, experience, and judgment of expert pavement engineers, and (b) provides the local engineering user with an interactive analysis and design tool (that is also an instructional aid) for development of pavement rehabilitation strategies. The program could also, perhaps with some modifications, be utilized as a more general educational tool for development of skills in the pavement rehabilitation area.

The research described in this paper is oriented toward developing a tool for state-maintained highway systems. A parallel effort is under way for rural counties and local agencies. The development of these programs represents an exploratory but high-potential basic research effort in the area of knowledge-based expert systems from the field of artificial intelligence. Such systems are discussed in the following section.

OVERVIEW OF EXPERT SYSTEMS

Description

In recent years, expert systems have emerged from decades of research into artificial intelligence, which addresses problems traditionally believed to require human intelligence (e.g., natural language processing, speech recognition, computer vision, and robotics) in order to find a solution. Expert systems are designed to emulate the performance of an expert, or group of experts, in a particular problem domain. Such systems are primarily applicable to situations requiring specialized knowledge, skill, experience, or judgment for determination of a solution or development of a solution strategy. In such cases, the problem is usually said to be ill-structured in the sense that a numerical algorithmic solution is not available or is impractical. Because so many of the problems that transportation professionals face are of this kind (e.g., designing an optimal transit route network or making decisions about how to rehabilitate a deteriorated section of highway), it can be said that, in general, the potential appears high for knowledge-based expert systems to become useful tools for the practicing transportation planner and engineer. Such systems can be envisaged as functioning as expert consultants, capable of explaining their reasoning and why they arrive at certain conclusions. Thus, one could eventually expect to learn from an expert system in the same way that one currently learns from an actual dialogue with an expert consultant.

In a number of disciplines, operational expert systems have already been developed. Examples include the following: MYCIN, for medical consultation and diagnosis (3); DIPMETER, for oil-well logging (4); PROSPECTOR, for mineral exploration (5); and R1, for computer system configuration (6). In civil engineering, systems developed to date include SACON, for structural analysis (7); SPERIL, for assessing earthquake damage to buildings (8); HYDRO, for watershed management (9); and HI-RISE, for preliminary design of high-rise buildings (10).

In the transportation field, little work on expert systems had been reported until recently. However, a number of systems are now in various stages of development. These include CHINA, for highway noise barrier design (11); DIRECTOR, for urban transportation education (12); TRALI, for traffic signal setting (13); and SCEPTRE, for pavement rehabilitation, which is discussed in more detail later in this paper. Further discussion of high-potential applications of expert systems in the transportation field can be found in Yeh et al. (12).

However, not all problems are suitable candidates for expert system formulation. Evaluation criteria include the following:

- Algorithmic solutions are impractical because of complex physical, social, political, or judgmental components, which generally resist precise description and deterministic analysis.
- Recognized experts exist in the field.
- An expert is often not physically available, or the knowledge transfer is too difficult or costly or may take too long.
- An expert's solution time is finite, typically taking a few minutes to a few hours.
- Tasks are largely cognitive.
- Faulty or incomplete data may be encountered during the problem-solving activity.
- Factual elements of the domain knowledge are routinely taught to beginners, who can eventually become experts.
- The potential pay-offs are high.

It is argued that the majority of these criteria indicate that pavement rehabilitation analysis and design has strong potential for expert system application.

Differences from Conventional Programs

Expert systems are fundamentally different from conventional computer programs. One principal difference is that an explicit problem-solving algorithm is not needed because a separate knowledge processor determines when, where, and how to apply every individual knowledge element. This is advantageous for many practical problems in which the knowledge is difficult to represent in a numerical form and a sequence of steps that will produce a solution is unknown. In addition, expert systems can readily accommodate nonnumeric, qualitative, or symbolic data; they provide an explanation capability for their conclusions, and utilize a reasonably natural dialogue user interface. Many expert systems can also handle incomplete or uncertain data by making inferences from their own knowledge base; this knowledge base can be updated more easily than the knowledge in a conventional program can because it is separated from the rest of the program.

Figure 1 shows the basic architecture of an expert system. The two main components are the knowledge base and the inference engine, or control process. The knowledge base is the power of an expert system in the sense that it contains all the empirical and factual information for the problem domain. The inference engine searches through the knowledge base or the context to find a conclusion for each subgoal and, thus, the entire problem. The result of the user interface can be that the user is queried for information needed to reach a conclusion. The context is the work space or short-term memory of the system. It stores currently relevant facts and knowledge, successively placed there by the inference engine. Finally, a user-friendly interface contains an explanation module to explain the system's problem-solving strategy to the user, and often contains a knowledge acquisition module to help experts articulate their knowledge in a form acceptable to the system's architecture.

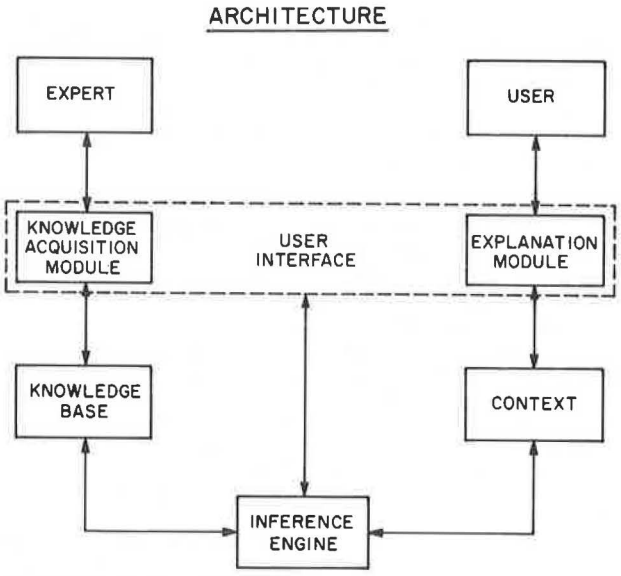

FIGURE 1 Basic architecture of an expert system.

PAVEMENT REHABILITATION

Role of Pavement Management Systems

For many years, state and federal highway agencies have collected pavement condition data with which to make maintenance and rehabilitation decisions. In the past, this was generally done on a project-by-project basis, and the data were used to determine which projects to maintain or rehabilitate and what action was required to correct observed pavement deficiencies. Decisions were made on a year-to-year basis in an environment in which resources (both manpower and money) were usually more plentiful than they are today (1).

More recently (in the past decade), many highway agencies have concluded that they can no longer manage their roadways on the basis of field observations alone. As a result, computerized PMSs have been developed for networks of highways. These systems establish priorities among projects currently in need of maintenance or rehabilitation and the general types of rehabilitation strategies required (often in the form of an annual rehabilitation action plan). The more sophisticated systems also project future pavement performance and the associated need for future rehabilitation strategies to minimize life-cycle costs or maximize net benefits.

An example of the type of pavement performance curve underlying these analyses, for the Washington State Department of Transportation (WSDOT), is shown in Figure 2. Such curves relate the pavement's performance rating to the age of the pavement. The performance rating is a function of a combined ride and surface condition rating. The ride rating is obtained with a Cox Ride Meter, and the surface condition rating reflects a weighted combination of the severity and extent of several types of distress. A pavement in perfect condition has a rating of 100 (15). As indicated in Figure 2, as a pavement ages, its condition gradually deteriorates. WSDOT defines two rehabilitation levels on each performance curve: one in which the pavement should be rehabilitated, and a later one in which the pavement must be rehabilitated. The must level corresponds to a rating of 40, and represents the minimum allowed pavement condition. Beyond this level, temporary fixes may retard the rate of deterioration. When a rehabilitation treatment is applied, the pavement rating increases abruptly and a new performance cycle begins.

A major function of PMSs is programming the rehabilitation process, which results in an objective, optimized mating of rehabilitation needs and available funding. Rehabilitation priority programming also serves as an effective management tool by identifying both those projects that could be implemented at varying funding levels and, conversely, the costs associated with varying levels of service. This flexibility is invaluable when dealing with a state legislature or the general public (16).

Currently only a handful of states actually have operational PMSs, although many are in the process of developing such systems. In addition, applications at the county level are being investigated and appear promising (17), particularly in Washington, which is acknowledged to have one of the most advanced programs in the country (16).

However, a PMS is not a project-specific design tool, and is not intended to be such. It can help identify the locations of pavement problems in a network and general types of solution strategies, but not at the level of detail necessary for design purposes. Most PMSs do not address a basic need of the district, county, or local agency engineer, who may already know where the problems are but is unable to determine (through lack of training, experience, or time) how those problems arose, how serious the situation is, what procedures to follow, what data to assemble, how to interpret those data, how to

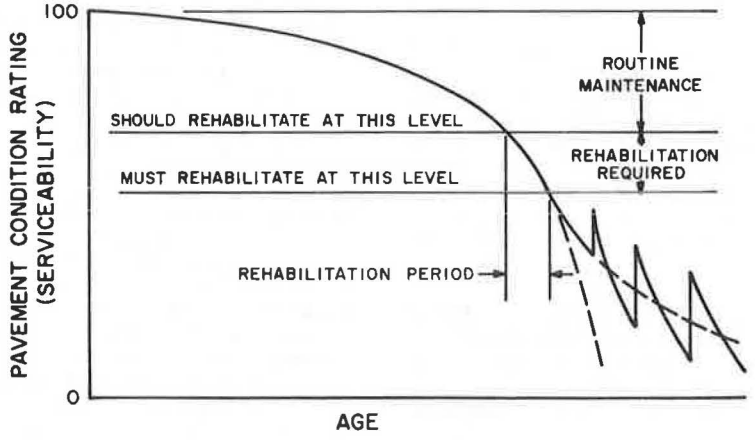

FIGURE 2 Example of WSDOT pavement performance curve.

develop feasible rehabilitation strategies, and how to select an optimal design. The expert system described in this paper represents the first phase (i.e., developing feasible rehabilitation strategies) of more extensive expert systems that will address exactly these analysis and design issues. The respective roles of these expert systems and those of a PMS are therefore different, but complementary.

Surface Condition Evaluation

In theory, the pavement rehabilitation process is composed of at least the following four tasks:

1. Evaluation of pavement surface condition,
2. Analysis and evaluation of structural adequacy,
3. Design of alternative strategies, and
4. Selection of an optimal strategy.

An overall objective of the research described in this paper is to systematically formalize the process by which human pavement experts interpret limited and uncertain data in a specific highway and project context, determine a range of feasible pavement rehabilitation strategies, and develop a recommendation and detailed design for an optimal strategy. After this process is formalized, it can be transformed into an expert system that comprises formal rules necessary for automating the process in a computer program. A first step is therefore to attempt to relate feasible pavement rehabilitation strategies to an evaluation of pavement surface condition. The expert system SCEPTRE 1.1, described in the next section, performs this task.

Although surface condition evaluations provide valuable and necessary information, it is recognized that they do not provide sufficient information for design; such information is obtained from structural adequacy evaluations. However, evaluation of a pavement's surface condition enables a judgment to be made of the adequacy of the existing pavement for current service. It is also used to determine the need for structural evaluation, establish the probable cause of surface distress, and determine the need and establish priorities for maintenance or more extensive rehabilitation. Surface condition evaluations can also indicate the rate of change in pavement conditions and acceptability so that the approximate time for scheduling future work can be predicted (14).

DEVELOPMENT OF SCEPTRE

Description

SCEPTRE 1.1 is the Surface Condition Expert for Pavement Rehabilitation. It evaluates pavement surface distress in order to recommend feasible rehabilitation strategies for detailed analysis and design. SCEPTRE 1.1 is applicable to state-maintained highways and flexible pavements. Rigid pavements will be included in the future. A major effort is also under way to address the needs of bituminous pavements in rural counties.

The major task in building an expert system is to acquire and encode the expertise and knowledge of one or more experts into the knowledge base. The mission of expert system developers (knowledge engineers) is to carry out such a transformation, ensuring that the performance of the resulting system reaches the desired level. The factual and empirical information in the knowledge base can be represented in various ways. The most common is by means of production rules, which take the following format: IF premise THEN action; for example, IF transverse cracking exists AND crack size is at least 1/8 in., THEN fill cracks.

General-purpose programming languages, such as LISP or PROLOG, can be used to build expert systems. However, a much faster route is to use one of several so-called knowledge engineering tool kits (or shells), which comprise an inference engine, empty knowledge base, and context structure. The system developer then simply has to enter the rules into the knowledge base. In the initial prototyping of SCEPTRE reported in this paper, such a shell was utilized, namely EXSYS (18). EXSYS is an expert system development package for IBM personal computers and compatible microcomputers. In the current case, EXSYS was used with a Compaq Portable microcomputer.

The knowledge base for SCEPTRE was derived from the combined expertise of two pavement specialists, with extensive experience of pavement rehabilitation in Washington and Texas.

The following types of surface distress and defects are considered by the system: longitudinal cracking in wheelpath(s), alligator cracking in wheelpath(s), block cracking, transverse cracking and/or longitudinal cracking outside wheelpath(s), and rutting. These are compatible with those used in developing the WSDOT pavement condition ratings discussed earlier. A copy of the actual pavement rating form is shown in Figure 3.

The following is a list of the rehabilitation and maintenance strategies (RAMs), from which a subset is drawn by SCEPTRE to form a feasible set for any particular combination of distress types.

- Do nothing,
- Fog seal,
- Chip seal,
- Double chip seal,
- Make thin asphalt concrete overlay ($\leq$0.10 ft),
- Make medium asphalt concrete overlay (0.10 < thickness < 0.25 ft),
- Make thick asphalt concrete overlay ($\geq$0.25 ft),
- Friction course,
- Fill cracks,
- Reconstruct,
- Hot recycle asphalt concrete,
- Level up, mill, and make medium asphalt concrete overlay (0.10 < thickness < 0.25 ft), and
- Level up, mill, and make thick asphalt overlay ($\geq$0.25 ft).

The knowledge base also contains multiple estimates, both subjective and data based, of the mean survival time (years) and standard deviation of survival time for each RAM in the list just given for various types of distress and other conditions. These estimates, provided by experts, relate to the service life of any rehabilitation strategy until the pavement rating score again reaches the must-rehabilitate level of 40. In the current version of SCEPTRE, this information on service life is used to calculate the probability that a given RAM, under given conditions, will provide acceptable performance for at least as long as a minimum desired service life input by the user. This is believed to be a useful, although approximate, measure of the comparative risk and performance associated with each RAM, and one that can be readily appreciated by potential users. In future versions of SCEPTRE, this information will be complemented by a life-cycle cost analysis for each RAM to provide an indication of the financial impacts of each strategy.

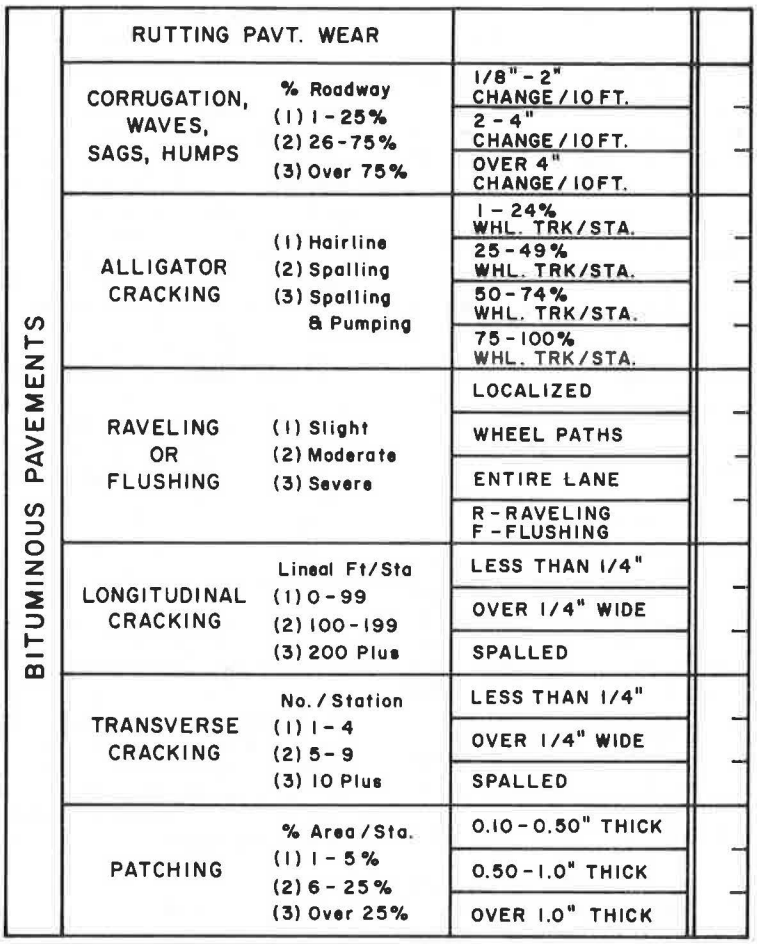

FIGURE 3 WSDOT pavement rating form.

Selection of Strategies

The selection of feasible RAMs in SCEPTRE is keyed to specific measures of pavement surface distress or defects. A structured approach to deriving project-specific RAMs for each defect type has been used, involving complex decision trees. A similar but much simpler (by comparison) set of procedures was incorporated in the California PMS (16). Such an approach lends itself readily to a rule-based representation of knowledge, as used in SCEPTRE. As an example, for alligator or fatigue cracking in the wheelpath(s), Table 1 gives a list of the levels of information that are utilized in determining RAMs feasible for this distress type; similar procedures are used for other distress types. The list of all feasible RAMs is then refined to include only those appropriate to the distress types for the particular pavement section.

Most of the information SCEPTRE seeks for each project, which is currently input by the user interactively, can be obtained from data files for the WSDOT PMS. A new version of this PMS is currently being developed for counties and local agencies. The authors believe that variations of the surface condition rating surveys used by this PMS, and SCEPTRE, will increasingly be adopted by other states and agencies. SCEPTRE could be modified to accommodate any regional or agency differences.

Figures 4-8 show selected examples of a sample session with SCEPTRE 1.1 (the output has been edited slightly for presentation). Figure 4 shows the log-on welcome-to-SCEPTRE message. Figure 5 shows the starting dialogue for flexible pavements. Figure 6 shows a sample interaction in the case of a segment with alligator cracking in the wheelpath(s). Figure 7 shows part of SCEPTRE's explanation capability. Figure 8 shows an example of the final set of feasible RAMs determined by SCEPTRE for the segment, together with the probability that each RAM will

TABLE 1 SCEPTRE Knowledge-Base Levels for Alligator Cracking in Wheelpath(s)

Level	Description
1. Climate	Region A: marine-dominated climate Region B: high solar radiation, temperature extremes
2. Amount of surface distress	Based on percent length of both wheelpaths distressed: 1. ≤10% 2. 10% < amount < 25% 3. ≥25%
3. Severity of surface distress	1. Hairline cracking 2. Spalling or spalling and pumping
4. Existing pavement performance	Based on predicted or actual life to a rating score of 40[a]: 1. ≤5 years 2. 5 < performance < 10 yr 3. ≥10 yr
5. Traffic levels	1. ADT < 800 veh/lane 2. 800 ≤ ADT ≤ 4,000 veh/lane 3. ADT > 4,000 veh/lane
6. RAMs	See list in text

[a] Pavement life is the time since original construction or the last resurfacing to a pavement condition rating of 40 (based on a scale of 0 to 100).

Welcome to

SCEPTRE 1.1

The Surface Condition Expert for PavemenT REhabilitation

SCEPTRE provides expert advice on feasible rehabilitation strategies for flexible state-maintained highways. You will now be asked to respond to a number of statements related to a pavement segment's surface condition.

Press any key to start __

FIGURE 4 Welcome-to-SCEPTRE message.

In this segment, alligator cracking in wheel path(s)

1 exists

2 does not exist

1__

Enter number(s) of value(s), WHY for information on the rule or <H> for help

FIGURE 5 Starting dialogue for flexible pavements.

The % length of both wheel paths alligator cracked is

1 10% or less

2 between 10% and 25%

3 25% or more

3__

Enter number(s) of value(s), WHY for information on the rule or <H> for help

FIGURE 6 Sample interaction in the case of segment with alligator cracking in the wheelpath(s).

```
The observed or predicted service life of the existing pavement (to a WSDOT
rating score of 40) is


1  5 years or less
2  between 5 and 10 years
3  10 years or more


WHY


RULE NUMBER:  51


IF:
     (1) In this segment, alligator cracking in wheel path(s) exists
and  (2) The regional climate has high solar radiation and temperature
         extremes
and  (3) The % length of both wheel paths alligator cracked is 25% or more
and  (4) The severity of alligator cracking involves spalling and/or pumping
         and rutting
and  (5) The observed or predicted service life of the existing pavement (to
         a WSDOT rating score of 40) is 5 years or less
and  (6) The AADT on this segment is between 800 veh/lane and 4000 veh/lane


THEN:
         Do-nothing
and      Fog seal
and      Thin asphalt concrete overlay
and      Medium asphalt concrete overlay
```

FIGURE 7 Sample of SCEPTRE'S explanation capability.

```
* * * * * * * * * * * * * * * * * * * * * * * * * * * * * * * * * * * * * *

YOUR MINIMUM DESIRED RAM SERVICE LIFE FOR THIS SECTION IS 5 YEARS.
IN THE OUTPUT BELOW, P IS THE PERCENT PROBABILITY THAT THE ACTUAL SERVICE
LIFE FOR EACH RAM WILL BE AT LEAST THIS LONG.

THE LIST OF FEASIBLE STRATEGIES FOR THIS PAVEMENT SECTION IS AS FOLLOWS:

DO-NOTHING                        P =  0% (EXPECTED LIFE = 2 YEARS)
FOG SEAL                          P = 25% (EXPECTED LIFE = 3 YEARS)
THIN ASPHALT CONCRETE OVERLAY     P = 37% (EXPECTED LIFE = 4 YEARS)
MEDIUM ASPHALT CONCRETE OVERLAY   P = 75% (EXPECTED LIFE = 7 YEARS)

* * * * * * * * * * * * * * * * * * * * * * * * * * * * * * * * * * * * * *
```

FIGURE 8 Feasible RAMs determined by SCEPTRE.

equal or exceed the minimum desired service life input by the user; the expected life for each RAM is also displayed.

ONGOING RESEARCH

Ongoing research with SCEPTRE is proceeding on several fronts. It is planned that the expert system be implemented by using an originally developed shell, which will allow greater flexibility in representing knowledge and controlling program operation. This would also facilitate distribution of the program to users. A prototype shell, written in LISP, has already been developed, although at this point only for a mainframe computer. A major effort will be devoted to interfacing SCEPTRE with a PMS data base to further automate the operation of the system and to incorporate pavement performance analysis over time and life-cycle costing for feasible RAMs. The knowledge base will also be expanded to include rigid pavements. To facilitate the system's use as an educational tool, the user interface will be improved significantly and the explanation capability enhanced. Because SCEPTRE is to become part of a larger detailed analysis and design expert system, it is planned to link SCEPTRE's output to design and analysis subroutines, particularly for pavement overlay design.

A significant knowledge engineering effort remains in tackling these issues. Consideration may also be given to linking SCEPTRE's output to a network optimization program to determine optimal project-level RAMs and budgets before performing the detailed analysis and design. The authors believe that the feasibility of the expert system approach to pavement rehabilitation has been proven with SCEPTRE 1.1, and that the research outlined in this paper will make the system a powerful and useful tool.

SUMMARY AND CONCLUSIONS

Rehabilitating the nation's highway infrastructure will continue to require both major effort and investment in years to come. However, the nature of the pavement rehabilitation analysis and design process suggests that a new technological approach, knowledge-based or expert system, could play an important role in addressing pavement rehabilitation problems and needs. Expert systems represent an emerging technology and may revolutionize professional activities in some areas. This paper has presented an overview of expert system characteristics, a discussion of the pavement rehabilitation analysis and design process, and a description of a prototype, microcomputer-based, surface condition expert system (SCEPTRE 1.1) for rehabilitation of flexible pavements. This system will become part of a much larger expert system to assist practicing engineers in analyzing and designing optimal and cost-effective rehabilitation strategies on a project-by-project basis. However, even in its current form SCEPTRE can make its body of specialized knowledge accessible to a broad range of potential engineering users.

ACKNOWLEDGMENT

This paper is based on research supported in part by the National Science Foundation.

REFERENCES

1. C.H. Oglesby and R.G. Hicks. Highway Engineering, John Wiley & Sons, New York, 1982, 4th ed.
2. D.J. Kulash and W.A. Hyman. Future Demand for Transportation Professionals: The Outlook for Engineers in State Departments of Transportation. In Special Report 210: Transportation Education and Training: Meeting the Challenge, TRB, National Research Council, Washington, D.C., 1985, pp. 18-36.
3. E.H. Shortliffe. Computer-Based Medical Consultation: MYCIN. American Elsevier, New York, 1976.
4. R. Davis, et al. The Dipmeter Advisor: Interpretation of Geologic Signals. Proc., Seventh International Joint Conference on Artificial Intelligence, University of British Columbia, Vancouver, 1981, pp. 846-849.
5. R.O. Duda et al. A Computer-Based Consultant for Mineral Exploration. SRI International, Menlo Park, Calif. 1979.
6. J. Bachant and J. McDermott. R1 Revisited: Four Years in the Trenches. AI Magazine, Fall, 1984.
7. J.S. Bennett and R.S. Elgelmore. SACON: A Knowledge-Based Consultant for Structural Analysis. Proc., Sixth International Joint Conference on Artificial Intelligence, 1979, pp. 47-49.
8. M. Ishizuka, K.S. Fu, and J.T.P. Yao. SPERIL I--Computer Based Structural Damage Assessment System. Technical Report CE-STR-81-36. Purdue University, Lafayette, Ind., Nov. 1981.
9. J. Gaschnig, R. Reboh, and J. Reiter. Development of a Knowledge-Based Expert System for Water Resource Problems. SRI Project Report 1619. SRI International, Menlo Park, Calif., Aug. 1981.
10. M.L. Maher. An Expert System for the Preliminary Structural Design of High Rise Buildings. Ph.D. dissertation. Department of Civil Engineering, Carnegie-Mellon University, Pittsburgh, Pa., 1984.
11. R.A. Harris, L.F. Cohn, and W. Bowlby. An Application of Artificial Intelligence in Highway Noise Analysis. In Transportation Research Record 1033, TRB, National Research Council, Washington, D.C., 1985.
12. C-I. Yeh, S.G. Ritchie, J.B. Schneider, and N.L. Nihan. Knowledge-Based Expert Systems in Transportation Planning and Engineering: An Initial Assessment. Department of Civil Engineering, University of California, Irvine, 1985.
13. C. Zozaya-Gorostiza and C. Hendrickson. An Expert System for Traffic Signal Setting Assistance. Department of Civil Engineering, Carnegie-Mellon University, Pittsburgh, Pa., 1985.
14. Asphalt Overlays and Pavement Rehabilitation. Manual Series No. 17 (MS-17). The Asphalt Institute, College Park, Md., Nov. 1977.
15. T.L. Nelson and R.V. LeClerc. Development and Implementation of Washington State's Pavement Management System. Report WA-RD50.1. Washington State Department of Transportation, Olympia, 1983.
16. Pavement Management Rehabilitation Programming: Eight States' Experiences. Federal Highway Administration, U.S. Department of Transportation, Aug. 1983, 109 pp.
17. R. Kulkarni, F. Finn, and A. Lamont. Feasibility Study of a Pavement Management System for Washington Counties. Final Report. Woodward-Clyde Consultants; Washington State Department of Transportation, Olympia, 1984.
18. EXSYS Expert System Development Package User's Manual. EXSYS, Inc., Albuquerque, N. Mex., 1985.

Publication of this paper sponsored by Committee on Monitoring, Evaluation and Data Storage.

Continuous Assessment of Performance History of Pavement Structures in France

ALAIN RASLE, JEAN-BAPTISTE BOUZIGUES, and MICHEL RAY

ABSTRACT

An overview is provided of observations made in connection with maintenance operations conducted on more than 11 000 km of French national roads as part of a preventive maintenance program, which also covered state-run (nonconcessionary) freeways. The primary purpose of making these observations was to evaluate the performance under traffic of various new or reconstructed (resurface, overlaid) pavement structures in order to assess the results of the design options made and to determine where changes were required. Making the observations also made it possible to reveal and analyze any abnormal conditions and to evaluate maintenance costs. The observations indicated the consistency of pavement design rules applied in France, and the validity of the decision to develop hydraulic-binder-treated granular materials. Road network managers now have a relatively wide range of pavement construction and reconstruction techniques, which are both operational and competitive not only with respect to initial capital cost but also to subsequent maintenance. A road data bank also enables comparisons between projects completed or those to be completed, and specific project data permit an assessment of service levels actually achieved. This provides a means of rectifying pavement designs and comparing the performance of different structures.

After the long, harsh winter of 1962-1963, which revealed the shortcomings of maintenance on France's road network at that time, the French highway department laid the groundwork for a comprehensive highway engineering program (design, maintenance), which it has implemented since 1969. There are three aspects to this program:

1. Design of new pavements capable of handling aggressive commercial traffic (13-ton legal axle weight). This design is based on a set of standards: a catalog of precalculated standard structures (1), and directives concerning the manufacture and placement of materials whose use is provided for in the catalog (2).
2. Rehabilitation of unsuitable old pavements (the coordinated overlays program initiated in 1969). This program has already enabled the resurfacing of some 20 000 km of France's 28 000-km road network. This reconstruction program is based on the directives mentioned previously and a design guide for flexible pavement overlays (3).
3. Scheduled preventive maintenance of new or reconstructed roads, a policy that was initiated in 1972, based on the application of a preventive maintenance guide (4).

At the same time, and as part of a more global policy of service to the user--covering in particular the geometrical, environmental, and road operation aspects--information handling facilities have been developed: the road data bank. These facilities are currently operational and provide considerable potential for the efficient use of the large amount of data collected. Much of these data are provided by surveys and through projects completed in accordance with the maintenance policy and specifications just described, providing an exceptional experimental field for the reliable evaluation of in situ pavement behavior.

In this paper, an assessment is provided of observations concerning maintenance tasks carried out in France on more than 11 000 km of national roads within the framework of a preventive maintenance program, as well as on nonconcessionary freeways. Most of the pavements (newly constructed or resurfaced) were opened to traffic between 1970 and 1983, the oldest being 25 years old.

The ultimate aim of such an assessment is first to determine the performance under traffic of various new or overlaid pavement structures in order to assess the technical options adopted and define changes, if needed. It is also designed to detect and analyze any abnormal conditions and, finally, to evaluate maintenance costs and provide (with certain reservations) for future needs, thereby contributing to the working out of corresponding budgets.

At this stage, two objections may occur to the reader:

1. First, the performance of various pavement designs is judged by maintenance work actually carried out. It would have to be verified that the service levels actually obtained are comparable with one another. At this stage, this can be reasonably assumed because of existing preventive maintenance guide specifications.
2. Finally, the perspective for making a sound judgment is limited with regard to most of the standard structures appearing in the basic documents currently governing the structural design of new pavements and flexible pavement overlays. This lack of perspective--which is due both to the average age of the structures and the pavement lengths involved (the population of certain structures is relatively small)--means that great care is required in interpretation, particularly because major technological developments may have taken place since the launching of the coordinated reconstruction program in 1969.

Pavements and Earthworks Division, SETRA, 46 avenue Aristide Briand, BP 100, 92223 Bagneux, France.

For the most common structures considered here, the trends observed nevertheless appear to be clear and provide solid grounds for assessing existing and foreseeable highway engineering technology.

On a more general level, these investigations indicated the following:

- Effectiveness of the pavement design specifications used, even though certain points require additional study;
- The value of an important decision of the seventies; namely, the development of hydraulic-binder-treated granular material (HBTGM); and
- The existence of a relatively broad range of application-ready competitive pavement construction and resurfacing methods currently available to highway engineers and authorities.

(Note that in France, the HBTGM technique is a standard technique for both the subbase and base layers. The technique involves, in particular, the use of cement, slag, fly ash or other hydraulic binders, high-quality granular materials, and treatment in plant and not in situ.)

France's road data bank makes it possible to compare work performed or to be performed, and the parameters will permit an evaluation of the effectiveness of highway service. A means of adjusting design parameters and evaluating the performance of structures will thus be provided.

It is with this in mind that the methods and computer programs developed can be made available to all agencies who so desire, with the common approach adopted making it possible to communicate in the same language and make valid comparisons.

The methodology is meant to be open ended and perfectible. The authors are interested in receiving suggestions concerning both the methods used and the results achieved, in particular from agencies, contractors, and materials and equipment suppliers.

OBJECTIVES

New or resurfaced pavement structures are monitored regularly for four purposes:

1. To assess the comparative behavior of various groups of pavement structures in situ, in both physical and financial terms;
2. To allow a judgment concerning decisions made about design specifications and the selection of road-building techniques and materials;
3. To provide data for technological forecasting; and
4. To contribute to the reliable estimation of future maintenance budgets.

METHODOLOGY

For the various groups of pavement structures used in statistically significant quantities, the distribution by age and traffic class was determined. For each category defined, successive maintenance operations were specified by date of implementation and type. All maintenance work performed, for both structural and surface aspects (permeability, stripping, peeling, etc.), was taken into account. Moreover, by an automatic statistical adjustment method, it was possible to calculate the probability of maintenance interventions at a given age of the pavement structure in question. The required data acquisition is carried out each year by a correspondent appointed in each of the seven Centres d'Etudes Techniques de l'Equipement (CETE) (Technical Study Centers for Equipement, which are regional agencies, backing the technical departments of the central government office) and the Regional Equipment Laboratories of the Paris region. The data are transmitted regularly to the Bordeaux CETE, which acts as a retrieval center for these studies and developed the data processing and operating systems.

CHARACTERISTICS OF THE POPULATION CONCERNED

The studies presented here cover a total of 11 210 km, or 2580 km of new pavement and 8630 km of resurfaced pavements. The initial works (construction or resurfacing) were carried out between January 1, 1960, and December 31, 1983, and all maintenance work carried out up to December 31, 1983, has been taken into account.

To avoid having an overly specific environment, which would induce nonrepresentative local patterns, the population (in the statistical sense) adopted for this study includes only sections of pavements on national roads or public freeways located outside of towns. Moreover, any sections likely to cause special problems of inputting or interpretation were removed from the sample (e.g., crossroads, road widening, sections of insufficient length).

Three groups of structures were considered for new pavements and four for resurfacing. Table 1 gives the length involved and the weighted mean age in 1983 for each group and Figure 1 shows the typical cross sections. For all the sections defined, the study consisted of indicating the age of the pavement structure at maintenance interventions and the nature of the tasks performed. Maintenance tasks were divided into five types:

- Type 1: Surface dressing or similar [slurry seal, surface regeneration with application of less than 2 cm of new material, bituminous concrete (BC) of thickness < 3 cm].
- Type 2: BC in a 3- or 4-cm layer (or surface regeneration with application of more than 2 cm of material).
- Type 3: BC in a layer of 5 to 8 cm.
- Type 4: BC in a layer of 9 to 14 cm.
- Type 5: Reconstruction (base layer and wearing course).

TABLE 1 Length and Weighted Mean Age of Pavement Structures

Structures Studied	Length (km)	Weighted Mean Age (yr)
Resurfacing with hydraulic-binder-treated granular material before 1975 (R/HBTGM < 75)	2 230	11.3
Resurfacing with hydraulic-binder-treated granular material in 1975 and after (R/HBTGM > 75)	2 560	5.9
Resurfacing with bituminous concrete (R/BC) strictly 10 cm thick	970	7.8
Resurfacing with bitumen-treated granular material (R/BTGM)	2 870	7.3
New pavements with HBTGM base and subbase (N HBTGM/HBTGM)	1 450	6.3
New pavements with BTGM base on HBTGM subbase (N BTGM/HBTGM)	530	6.4
New pavements with BTGM base on untreated granular material subbase (N/BTGM/UGM)	600	9.9
Total	11 210	
Average		7.8

Note: Pavements in cement concrete represent only 116 km on the network in question and were unable to be taken into account in the current study.

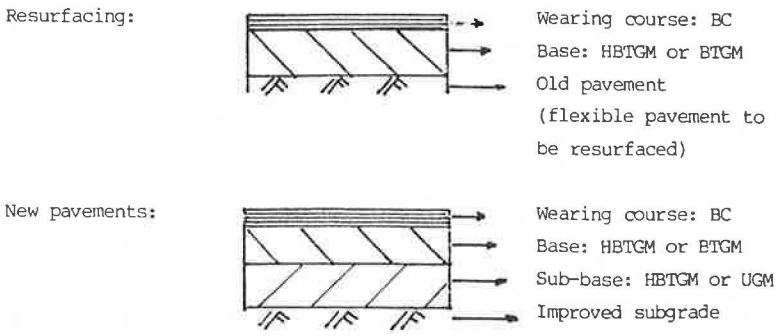

FIGURE 1 Typical cross sections.

Because of data acquisition difficulties, sealing of cracks was not taken into account.

SIGNIFICANCE AND LIMITS OF ANALYSIS

The analysis made endeavored to relate maintenance requirements to two explanatory variables: the construction (or resurfacing) technique and traffic. Other important parameters are also involved in such a correlation, including the environment, in particular, the climate; this was taken into account indirectly by an analysis of regional disparities (which are only partly explained by climatic differences). Other parameters could not be taken into account at the current stage of the study for want of reliable recording or interpretation facilities. In particular, such parameters are

- Subgrade bearing capacity class (which is taken into account in structured design),
- Structural design (considered to be in conformity with applicable documents and methods during the design phase),
- Material quality, manufacture, and placement conditions (assumed to be in conformity with current specifications), and
- Local climatic data (temperature, precipitation, and sunshine).

The method and practical conditions of the study, while they do not affect the validity of the conclusions given in the following list, nevertheless require certain reservations and great care regarding their interpretation, particularly if used for planning purposes.

- With experience, every technique is gradually improved, and only radical changes that can be easily located in time have been able to be taken into account. Accordingly, resurfacing with HBTGM applied before 1975 has been distinguished from HBTGM resurfacing done in 1975 and after because at that time the design rules were thoroughly modified.
- Numerous coordinated reconstruction projects employed HBTGM for special reasons, such as frost protection. The stresses on the various structures are therefore not always strictly comparable.
- The maintenance work performed does not always correspond to the work required, notably because when carried out suitable techniques were not available for all cases (thin-layer coated maintenance materials, surface dressings for heavy traffic, crack sealing, etc.).
- Finally, and above all, a causal analysis on the basis of maintenance work actually performed presupposes that budgetary constraints are not significant and do not introduce excessive trade-offs between what is needed and what is done, and also that decision-making rules are uniform for all the roads studied.

In other words, it has been assumed that the provisions of the Preventive Maintenance Guide Specifications are correctly applied by all agencies and that they actually make it possible, in conformity with the objective assigned to them, to constantly provide a comparable level of service on all pavements, irrespective of their initial structure. In practice, until 1983, budgetary constraints made it possible to a large extent to meet maintenance requirements, and accordingly have not introduced major bias into the results, whether in absolute value or in relative value.

MAIN RESULTS

Computerized data processing produces two types of printouts: (a) for each structure, maintenance performed year by year, through successive maintenance work and by type of task (Type 1, 2, 3, 4 or 5); and (b) cumulative maintenance frequencies, giving for each age the percentage of length maintained on sections having at least the age in question, both by type of structure and for successive maintenance operations. Each of these printings covers the sphere of action of each CETE. For all of France, it was possible to add a distinction by traffic class to these data.

These results are translated into more explicit curves, the chief of which are shown in the figures later in this paper. It should be noted that the traffic considered is that for 1980 expressed in numbers of vehicles exceeding 5 tons of payload, average annual daily traffic (AADT) on the busiest lane, and not the traffic of the first year of service. In the following table, TE is exceptional traffic.

Traffic Class	No. of Heavy Vehicles
T3	50-150
T2	150-300
T1	300-750
T0	750-2,000
TE	>2,000

ANALYSIS OF CUMULATIVE MAINTENANCE FREQUENCIES BY TECHNIQUE

National Results

Only the curves concerning structures having a sufficient population (cumulative length of sections) for their statistical interpretation to be reliable

have been selected. This criterion rules out most breakdowns according to the type of maintenance task performed. However, such information is provided in a later section entitled Analysis of Type and Cost of Maintenance Tasks.

Resurfacing with Bituminous Concrete (R/BC)

This resurfacing technique is special because it often represents a gradual-strengthening solution, used chiefly in regions with mild climates. Under such conditions (Figure 2), the need for rapid service is not surprising (50 percent of the length was resurfaced after 7 yr). The influence of traffic is small, which tends to indicate that this solution has been used discerningly.

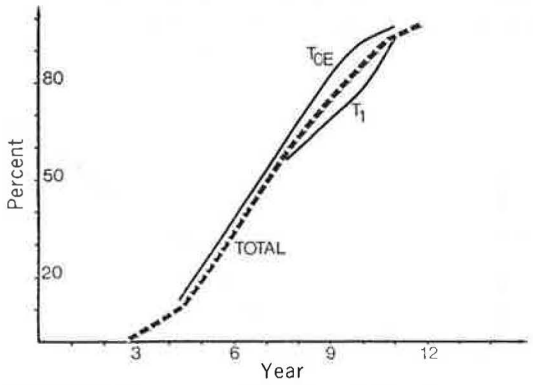

FIGURE 2 Percentage of length maintained as a function of age on pavements resurfaced with 10 cm of bituminous concrete.

Bases in Hydraulic-Binder-Treated Granular Materials

Figure 3 shows the radically different behavior of the resurfaced pavements in HBTGM applied before and after 1975, the year representing a turning point marking the almost systematic use of layers 25 cm thick and greater. This figure shows the importance of good structural design of semirigid pavements, which is also the subject of discussions at the international level.

Figure 4 shows that the maintenance performed on

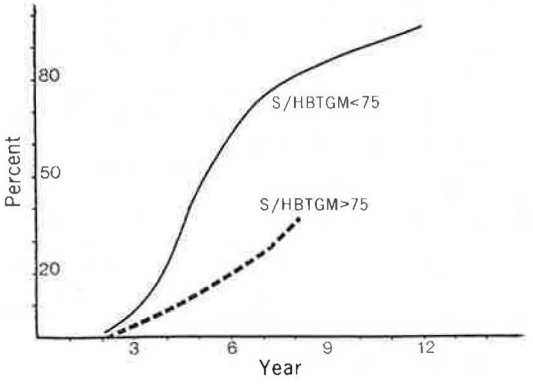

FIGURE 3 Percentage of length maintained as a function of age on pavements resurfaced with hydraulic-binder-treated granular material (all traffic).

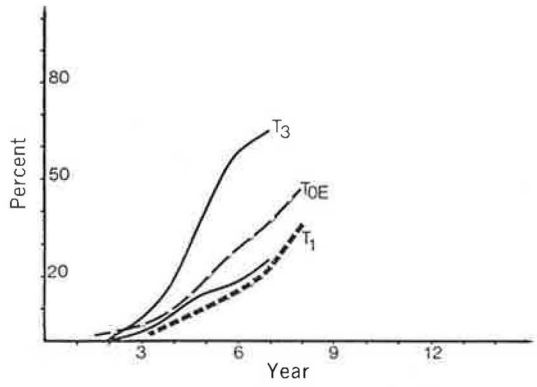

FIGURE 4 Percentage of length maintained as a function of age on pavements resurfaced with hydraulic-binder-treated granular material after 1975.

resurfacing with hydraulic-binder-treated granular material after 1975 (R/HBTGM > 75) differs according to the various traffic classes. For light traffic (T3), major maintenance requirements appear, but the population is too small to draw any definite conclusions. Very dense traffic (T0 and TE) requires far more maintenance than T1 and T2 levels of traffic. In these cases, the thicknesses of the wearing courses and the quality of the BC/HBTGM interfaces perhaps require more thorough study.

Figure 5, concerning new pavements, shows that the present all-HBTGM structures are subject to far earlier maintenance under dense traffic. It is possible that in practice the structures are sometimes undersized by comparison with the reference catalog and that problems remain concerning subbase-base bonding in certain cases.

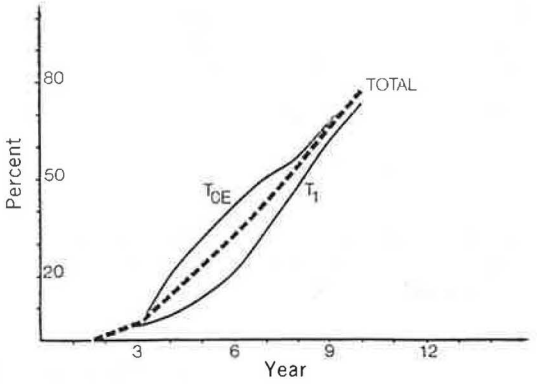

FIGURE 5 Percentage of length maintained as a function of age on new pavements with base and subbase layers in hydraulic-binder-treated granular material.

On the whole, it appears that, by comparison with Figure 6 [all structures taken together, except resurfacing with hydraulic-binder-treated granular material before 1975 (R/HBTGM < 75)], which will be used as a reference, the R/HBTGM > 75 structures are located exactly at the median point (50 percent will probably be resurfaced at 9 yr), whereas the new pavements with base and subbase layers in hydraulic-binder-treated granular material (N HBTGM/ HBTGM) show a less favorable result (median age of first maintenance is 7 3/4 yr), particularly under intense traffic (50 percent at 7 yr).

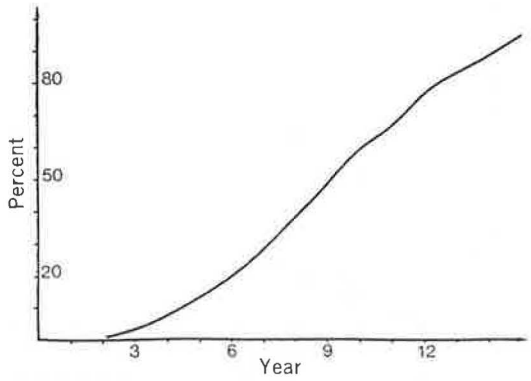

FIGURE 6 Percentage of length maintained as a function of age on all new and resurfaced pavements (excluding overlays with hydraulic-binder-treated granular material before 1975 and bituminous concrete overlays).

Bases in Bitumen-Treated Granular Material

Figure 7 shows the remarkable overall behavior of resurfacing with bitumen-treated granular material (R/BTGM) (50 percent maintained for more than 9 1/2 yr), irrespective of the level of traffic (which appears to confirm the validity and uniformity of their design).

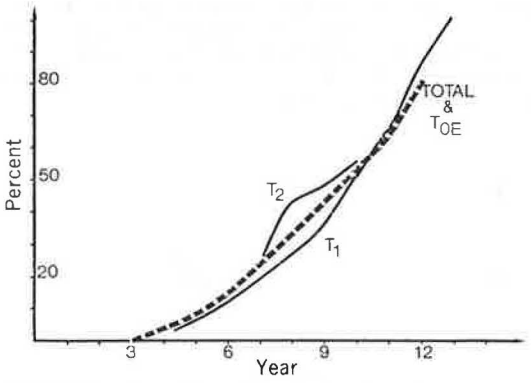

FIGURE 7 Percentage of length maintained as a function of age on pavements resurfaced with bitumen-treated granular material.

Figures 8 and 9, concerning new pavements with a BTGM base layer, show that the overall behavior of these pavements is satisfactory (50 percent maintained for approximately 9 yr). In this respect, two points should be noted. First, Figure 8 clearly shows (in spite of an inadequate population after Year 9) a peculiar feature of mixed pavements handling traffic at the level of T1. Such pavements appear to require maintenance relatively soon after their commissioning. No satisfactory explanation can at present be proposed for this, and a thorough study of the phenomenon should be made. At the same time, it should be noted that two differentiated subunits appear within this group of structures: pavements built in the sphere of action of the Western CETE (50 percent of the total length), behaving significantly better than others with respect to the date of execution of first maintenance. Second, the performance record of BTGM and subbase in untreated granular material (BTGM/UGM) is good, which should help to dispel concerns about this.

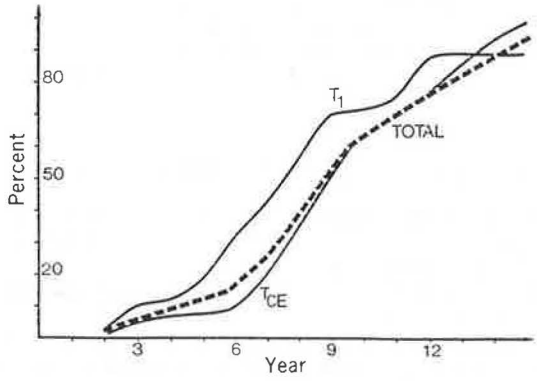

FIGURE 8 Percentage of length maintained as a function of age on new pavements with a base layer in bitumen-treated granular material and subbase in hydraulic-binder-treated granular material.

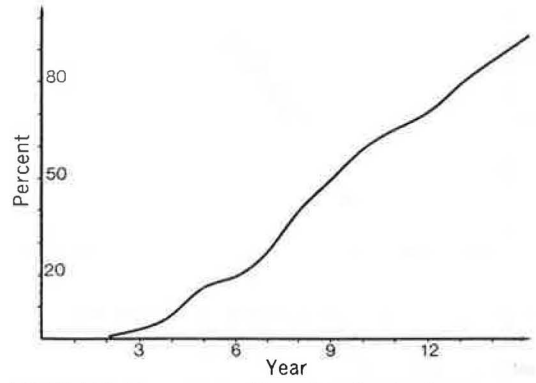

FIGURE 9 Percentage of length maintained as a function of age on new pavements with a base layer in bitumen-treated granular material and subbase in untreated granular material.

Synthesis

Table 2 provides a summary of the main information drawn from Figures 2-9.

If former deviations (R/HBTGM < 75) and the R/BC corresponding to a different strategy are excluded, it can be observed that (a) only the N HBTGM/HBTGM structure received maintenance significantly earlier than the other structures [chiefly in the case of very heavy traffic (T0 and TE levels)], and (b) the R/HBTGM > 75 and R/BTGM structures perform better than new pavements, which can be partly explained by better compliance with design rules and no doubt improved subbase uniformity.

Table 3 presents serious failures by type of structure, defined on the basis of two criteria: (a) the percentage of the length receiving maintenance during the first 3 yr; and (b) the percentage of the length maintained twice in 10 yr.

The data in Table 3 confirm that resurfaced pavements perform better than new pavements; and that the R/BC structures, although they experience few immediate failures, in many cases leave the pavement undersized and require relatively rapid subsequent compensation, which is normal within the framework of a progressive strategy.

The failure rate brought to light is on average relatively low. It does not call into question the design (although certain points remain to be examined) because this can be explained by hazards related to the materials and supports. On the whole,

TABLE 2 First Maintenance on Various Structures

Structure	Percentage Maintained at 5 yr	8 yr	10 yr	Median Age at First Maintenance (yr)
R/HBTGM < 75 (reminder)	45	81	90	5 1/4
R/BC	18	63	85	7
R/HBTGM > 75	14	36	–	9[a]
R/BTGM	7	33	54	9 3/4
N HBTGM/HBTGM	23	52	76	7 3/4
N BTGM/HBTGM	11	37	64	8 3/4
N BTGM/UGM	17	41	61	9
Total[b] HBTGM[c] + BTGM = Reference	12	38	61	9

Note: See Table 1 for definitions of structures.
[a]Estimate.
[b]Weighted average based on length (see Table 1 for lengths).
[c]R/HBTGM < 75 and R/BC excluded.

the results of the assessment can be regarded as satisfactory. In particular, the small spread observed around the mean date of occurrence of first maintenance indicates the effectiveness of design methods (catalogs) and the quality of the materials.

REGIONAL RESULTS

Regional analysis faces various uncertainties stemming notably from the often small size of the populations concerned. Moreover, it should be considered that local adaptations may be made to specifications established on the national level, which may result in different maintenance thresholds and consequently different service needs. In addition, reactions to certain problems (e.g., cracking) may be very different.

Without going into detail concerning the regional differences observed, it should be pointed out in particular that (a) new pavements have a wider spread of performance than resurfaced pavements, which can perhaps be explained by the greater preciseness and the centralization inherent in coordinated overlay projects; and (b) regions in northern and northeastern France require more maintenance on the average than do the other regions. Particularly affected are new pavements with base and subbase layers in HBTGM (N HBTGM/ HBTGM).

A research program will be worked out to allow a thorough study of the causes of the disparities observed. The authors are relying on this causal analysis to explain the good performance of regional projects as well as the shortcomings; important progress factors should be revealed in this way.

ANALYSIS OF TYPE AND COST OF MAINTENANCE TASKS

The considerations discussed in the preceding section refer only to the time at which first maintenance operations were performed on the various groups of structures. The conclusions drawn from this initial phase may undergo closer analysis taking into account the nature of the maintenance work performed.

To facilitate the making of summaries and comparisons, it was found helpful to define a global index of the cost of maintenance work. Adopting as reference (Index 1) the cost per square meter of Task No. 1 (surface dressing or similar) and considering the unit costs and average tonnages of the materials employed for Tasks 2 to 5, the following mean cost scale can be derived:

Type of Task	Cost Index
1	1
2	2.5
3	5
4	7
5	10

This procedure avoids any effects of price fluctuation. It should be noted that crack sealing has not been taken into account, which could affect slightly the results obtained for HBTGM, even though the financial cost is low (cost index is approximately 0.15).

By assigning these indices to the percentages of lengths on which the various types of tasks were performed, a weighted mean cost index (WMCI) can be obtained for each type of task. An analysis of this procedure is given in Table 4.

It should be pointed out that the development of maintenance techniques, particularly with the obligation to save bitumen, led to the development of surface dressings and thin-layer mix materials from 1981 onwards. This does not affect the comparisons made.

To obtain a higher level of aggregation, it is interesting to consider a global indicator incorporating both the date of first maintenance and the type of maintenance. The authors have adopted the ratio M/WMCI, where M is the median age at first maintenance (given in Table 2). It should be noted that this ratio can differ from those used in other countries, where reference is made to the service life or to the initial construction cost. In France, the latter comparison would be of no interest because the application of the catalog of structures (1) leads to the adoption of the same service life regardless of the type of structure considered. The choice is made after a call for bids, the most inexpensive structure then being selected. Comparing different structures of different cost and different service lives would thus be meaningless. The ratio adopted here, in contrast, reflects damage experienced by the structures and contributes to the verification of the initial assumptions.

It is thus possible to construct Table 5, which presents the short-term efficiency of the various structures (the ratio increases with the structure's performance).

TABLE 3 Assessment of Early Maintenance Operations

	Percentage of Length Maintained						
	R/BC	R/HBTGM > 75	R/BTGM	N HBTGM/HBTGM	N BTGM/HBTGM	N BTGM/UGM	Mean
During first 3 years	2	3	1	4	7[a]	3	2,5
Twice in 10 years	12	1.2[b]	2	6.5	3	2	3

Note: See Table 1 for definitions of structures.
[a]Note that smoothing of the curve would result in adoption of the value 5 percent. This value, which is relatively high, is chiefly due to failures observed on half of the population (pavements constructed outside Western CETE).
[b]8 years.

TABLE 4 Percentage of Length and Weighted Mean Cost Index During First Maintenance by Type of Task for Various Structures

Structure and Population (rounded)	Percentage of Length					Weighted Mean Cost Index
	Task 1[a]	Task 2[b]	Task 3[c]	Task 4[d]	Task 5[e]	
R/HBTGM < 75 (2230 km)	20	6.5	66.5	4	3	4.3
R/BC (970 km)	23	10.5	53	11	2.5	4.2
R/HBTGM > 75 (2560 km)	49	17	23	7	4	3
R/BTGM (2870 km)	29	17	43	8	3	3.7
Weighted average R (6400 km)	36	16	37	8	3	3.5
N HBTGM/HBTGM (1450 km)	13	11.5	53	14	8.5	4.9
N BTGM/HBTGM (530 km)	5	36.5	55.5	0	3	4
N BTGM/UGM (600 km)	18	6.5	57	13	5.5	4.7
Weighted average N (2580 km)	12.5	15.5	54.5	11	6.5	4.7
Weighted average (8980 km)[f]	29	16	42	9	4	3.8

Note: See Table 1 for definitions of structures. The percentages given are means calculated during the period 1974 to 1982.

[a]Cost index = 1.
[b]Cost index = 2.5.
[c]Cost index = 5.
[d]Cost index = 7.
[e]Cost index = 10.
[f]Not including the R/HBTGM < 75.

The tables confirm most of the trends previously noted, in particular: (a) the good performance of recent overlays, particularly those in HBTGM (Table 5); and (b) the relatively less favorable behavior of new pavements; when maintenance is required, it concerns a layer of 5 to 8 cm of BC in more than 50 percent of the cases (Table 4). The data in Table 4 also indicate that the breakdown of the various tasks is unequal. In particular, it is interesting to observe the high proportion of HBTGM overlays maintained by a surface dressing (in 49 percent of cases) during the first maintenance after commissioning.

Before proceeding with a more general analysis of the relation between traffic and maintenance performed, the influence of traffic on the type of task should be noted, even if the populations are sometimes too small for the analysis to be comprehensive. The data in Tables 6 and 7, concerning overlays and new pavements of significant length, indicate that the following logic is generally complied with: the higher the traffic density, the more costly the maintenance.

GLOBAL ANALYSIS OF TRAFFIC EFFECTS

The current study would not be complete without a comparison of stresses experienced by groups of structures studied in terms of loads borne. The data available are not detailed, but an order of magnitude is adequate to indicate the relevant trends in this respect.

By using a method similar to that used for maintenance task costs, an index of weighted mean traffic borne by each structure has been determined on the basis of the following scale (corresponding to the mean of each class, with Index 1 for the mean of class T3, or 100 commercial vehicles/day/direction).

Traffic Class	Traffic Index Adopted
T3	1
T2	2
T1	5
T0	13
TE	22

Table 8 gives the results of the detailed calculations.

It can thus be seen that

- Overlays are on average less traveled on than new pavements;
- The R/HBTGM > 75 structures bear lighter traffic than do the other overlays. Priority was given to the resurfacing of roads handling the heaviest traffic.
- The N BTGM/UGM structures are among the most traveled on, with a good part of them being for freeway pavements.

However, to put these considerations in perspective, it should be noted that the maintenance requirements of a structure (for equivalent design) do not vary in proportion to the level of traffic handled. Concerning this point, the authors note the theoretical maintenance scenarios evaluated for various structures and various traffic densities at the 1981 Road and Energy Symposium in Paris (5) (see Table 9).

If the calculation method described previously (Table 4) is applied to the data in Table 9, it can be observed that the WMCI ranges from 2.8 (between 8 and 10 years) for T3, to 4 (at 8 or 9 years) for T0. It is possible to determine an adjustment relating the WMCI to the traffic index (iT) between the two limits:

$$WMCI = 2.8 + 1.11 \log iT.$$

It should also be pointed out that the conclusions of the Organisation for Economic Cooperation and Development's report on the Impacts of Heavy Freight Vehicles indicate that the maintenance-versus-traffic-expense curve has an elasticity of 0.1 to 0.2 (6); that is, maintenance expenses increase 5 to 10 times less quickly than traffic (mean for several countries). The results obtained by these two approaches are in agreement and indicate the relatively small influence of traffic on maintenance expenditures.

Three conclusions may be made:

1. Differences in levels of traffic cannot justify the differences in behavior observed between one structure and another.
2. The BTGM/UGM structure appears to be valid for use under high traffic densities, which is not

TABLE 5 Short-Term Efficiency of Various Structures

Technique	Structure							
	R/HBTGM < 75	R/BC[a]	R/HBTGM > 75	R/BTGM	N HBTGM/HBTGM	N BTGM/HBTGM	N BTGM/UGM	Mean
M/WMCI	1.2	1.7	3	2.6	1.6	2.2	1.9	2.4

Note: See Table 1 for definitions of structures.

[a]The concept of efficiency is different for a progressive strategy; the value given here could not be compared directly with the other values.

TABLE 6 Percentage Maintained by Type of Task and Traffic Class for Various Overlay Structures

	R/BC		R/HBTGM			R/BTGM		
Task	T1	T0E	T2	T1	T0E	T2	T1	T0E
Type 1	33	16	61	46	51	57	32	14
Type 2	8	10	32	12	9	7	20	17
Types 3-5	59	74	7	42	40	36	48	69

Note: See Table 1 for definitions of structures. Traffic classes are defined in the section Main Results.

TABLE 7 Percentage Maintained by Type of Task and Traffic Class for Various New Pavement Structures

	N HBTGM/ HBTGM		N BTGM/ HBTGM		N BTGM/ UGM	
Task	T1	T0E	Total	T0E	Total	T0E
Type 1	34	4	5	5	18	4
Type 2	5	13	36	16	7	7
Types 3-5	61	83	59	79	75	89

Note: See Table 1 for definitions of structures. Traffic classes are defined in the section Main Results.

provided for in the current design catalog for new structures. This is why it would be interesting to know the subgrades on which structures of this type were built (because, even more than other structures, flexible structures adapt to a subgrade that cannot be deformed).

3. The requirements estimated at the Road and Energy Symposium are similar to what is actually observed in the current assessment. For the T1 level of traffic (500 commercial vehicle/day/direction on average), the predicted WMCI was 3.6 at 8 or 9 years, while the results of the current study indicate a mean WMCI of 3.8 at 9 years for 700 commercial vehicles/day/direction. However, the predicted theoretical breakdown of the various tasks is not obtained; current practice indicates much greater use of surface dressings, at the same time compensated for by more costly maintenance on other sections.

APPLICATIONS TO FORECASTING OF MAINTENANCE REQUIREMENTS

Apart from the evaluation that can be made of the performance of given structures and the questions thus raised, other applications have been considered for the assessment presented here. Such applications are (a) determination of the long-term discounted cost of construction and maintenance scenarios, and (b) forecasting of future maintenance budgets.

For both of these applications, the curves presented in the figures have been converted into maintenance probabilities at a given age by means of a computerized adjustment program. It turns out that Gauss's (normal) and Galton's (log-normal) laws are adjusted with satisfactory coefficients of correlations, Galton's law being slightly more suitable. This is in particular due to the curves' passing through the point of origin, which is not the case with Gauss's law. However, the computer costs involved make its use too costly compared with the advantage it affords.

The authors have not considered it worthwhile to present an evaluation of future maintenance budgets merely on the basis of the assessment of pavement structural behavior because various obstacles exist and a suitable methodology would first have to be worked out. The analysis made concerns the first maintenance work, and the population of subsequent maintenance operations recorded is too small to determine significant means and standard deviations, or to establish a reliable relationship between the nature of two consecutive maintenance operations. Additional analysis would be required, namely, a forecast of technical developments and their relative cost, the costs associated with maintenance, and in particular the nuisance caused to the users, which is particularly noticeable in the case of regular works (e.g., crack sealing). It should also be noted that the assessment worked out is largely a reflection of previous maintenance budgets and that no forecast of needs could be confined to a mere extrapolation from past trends.

Similarly, the authors have not considered it worthwhile to calculate the discounted cost of maintenance, or of long-term construction (or resurfacing) plus maintenance, for the various structures considered. In addition to the reasons already mentioned, the following should also be noted:

- To allow for a mean cost of construction or resurfacing by technique would falsify the analysis because there is reason to believe that, in each specific case, the structure with the lowest initial cost was used. The real question is determining the initial capital investment difference that can be

TABLE 8 Percentage of Length Bearing Given Traffic and Weighted Traffic Index by Traffic Class for Various Structures

	Length Bearing Given Traffic (%)					
Structure and Population (rounded)	Traffic Class T3[a]	Traffic Class T2[b]	Traffic Class T1[c]	Traffic Class T0[d]	Traffic Class TE[e]	Weighted Traffic Index[f]
R/HBTGM < 75 (2230 km)	1	10	49	39	1	795
R/BC (970 km)	3	14.5	53	29	0.5	685
R/HBTGM > 75 (2560 km)	8	26	56	10	0	470
R/BTGM (2870 km)	6	14.5	50	29	0.5	673
N HBTGM/HBTGM (1450 km)	2	9	48	38	3	820
N BTGM/HBTGM (530 km)	0	7	46	33	14	981
N BTGM/UGM (600 km)	4	17.5	32	26.5	20	983
Weighted Mean (rounded)	4.5	15	50	28	2.5	700 (T1 high level)

Note: See Table 1 for definitions of structures. Traffic classes are defined in the section Main Results.

[a]Index = 1.
[b]Index = 2.
[c]Index = 5.
[d]Index = 13.
[e]Index = 22.
[f]The result obtained was multiplied by 100, giving the order of magnitude of the mean traffic borne by the structure, expressed in heavy vehicles per direction (AADT).

TABLE 9 Theoretical Maintenance Scenarios Planned for Various Structures and Traffic Densities

Structure	Traffic Class T0		Traffic Class T1		Traffic Class T2		Traffic Class T3	
	Time (yr)	Maintenance	Time (yr)	Maintenance	Time (yr)	Maintenance	Time (yr)	Maintenance
Structures treated with hydraulic binders	4	33% CS	3	33% CS	4	30% CS	4	30% CS
	5	33% CS	4	33% CS	5	30% CS	5	30% CS
	6	33% CS	5	33% CS				
	8	60% 4-cm BC 40% 8-cm BC	8	20% SD 40% 4-cm BC 40% 8-cm BC	8	20% SD 40% 4-cm BC 40% 6-cm BC	8 10	40% SD 20% 4-cm BC 40% 6-cm BC
	12	50% CS	12	50% CS	12	60% CS	15	40% CS
	16	60% 4-cm BC 40% 8-cm BC	16	20% SD 40% 4-cm BC 40% 8-cm BC	16	20% SD 40% 4-cm BC 40% 6-cm BC	18	40% 6-cm BC
	24	60% 4-cm BC 40% 8-cm BC	24	20% SD 40% 4-cm BC 40% 8-cm BC	24	20% SD 40% 4-cm BC 60% 6-cm BC	20	20% 4-cm BC 40% SD
Composite structures with a hydrocarbon base	5	20% CS	5	20% CS				
	9	60% 4-cm BC 40% 8-cm BC	9	20% SD 40% 4-cm BC 40% 8-cm BC	9	20% SD 40% 4-cm BC 40% 6-cm BC	10 20	40% SD 20% 4-cm BC 40% 6-cm BC
	17	60% 4-cm BC 40% 8-cm BC	17	20% SD 40% 4-cm BC 40% 8-cm BC	17	20% SD 40% 4-cm BC 40% 6-cm BC	20	40% SD 20% 4-cm BC 40% 6-cm BC
	25	60% 4-cm BC 40% 8-cm BC	25	20% SD 40% 4-cm BC 40% 8-cm BC	25	20% SD 40% 4-cm BC 40% 6-cm BC		
WMCI (at 8–10 yr)[a]	4.0		3.6		3.2		2.8	

Note: The WMCI calculated in this way is the same for both groups of structures in question (at a given traffic density) when allowance is not made for crack sealing and the present cost account method is used.

[a]The WMCI was calculated using the following indices: SD (surface dressing): 1; CS (crack sealing): 0; and BC (bituminous concrete): 4 cm–3, 6 cm–4.5, and 8 cm–5.5.

offset by differences in maintenance costs, which implies a more global calculation, incorporating factors other than those provided by the current assessment. Moreover, this analysis remains to be made.

- It would be necessary to take into account not only the median date of maintenance but also the spread around this mean, which requires a more thorough study.

However, the assessment of structural performance summarized in this paper may provide a precious basis for estimating future maintenance needs, to the extent that it provides a distribution of pavements by age and clear information on the type and date of first maintenance. However, among other things, pavement mechanics should be applied to determine a relation between the various types of successive maintenance operations in order to comply with the objective assigned to the entire national network, namely, to constantly provide a high level of service and adapt the pavement structure to prevent foreseeable traffic growth.

GENERAL CONCLUSIONS

In addition to the specific conclusions and avenues of research outlined in this paper, it appears to be necessary to make four general conclusions, in spite of the reservations expressed throughout the study concerning the interpretation of results.

First, applicable design specifications in France for new pavements as well as for flexible pavement overlays are consistent and valid. However, certain specific problems deserve study, among which are the following:

- Research on the causes of the disparities observed with respect to maintenance of overlays in HBTGM as a function of traffic.
- For new pavements in HBTGM, verification of structural design, both theoretical and practical, and study of base-subbase bonding, which would enable closer analysis of immediate failures.
- Analysis of the causes of certain regional disparities.
- Study of the possibility of making more extensive use of BTGM/UGM under heavy traffic loads (after analysis of the subgrades).

Second, concerning the past, the major innovation of the seventies was the development of HBTGMs in pavement subbases, and the decisions made by the French highway authorities in this respect are now confirmed as being highly judicious, both technically and economically.

Third, concerning the present, a relatively wide range of operational pavement construction and reconstruction techniques is now available, competitive in all respects, none of which appears to involve additional initial cost because of the reduced subsequent maintenance requirements.

Fourth, concerning the future, the results achieved on R/BC apparently justify the belief that this progressive resurfacing strategy could be developed in temperate regions (e.g., seaboards).

It should be noted that the authors have not dealt with the case of cement concrete pavements, which are therefore not encompassed by the conclusions. Moreover, the results set out above should be extended by more general studies, in particular: (a) detailed theoretical study of the link between types of successive maintenance operations, and (b) more global and more precise updated long-term calculations for various structures and strategies.

The facilities set up for this assessment should be maintained. However, the basic data will be supplied by the road data bank, which is able to merge and sort the different files and permit rapid detailed statistical correlations (e.g., data on soil types). Some of the information expected from the pursual of this project includes (a) regular updating of the trends described here; (b) illustration of phenomena that do not appear at present for want of sufficient populations and perspective; and (c)

analysis of maintenance sequences beyond the first maintenance, and in particular the probability of occurrence of a maintenance operation of a given type according to the nature of tasks previously carried out.

Finally, it should be emphasized that the current assessment of the performance of pavement structures is simply a report on observed deviations from and approaches to problems in the form of explanatory hypotheses. However, it cannot as such explain the causes and the solutions to be found, which require additional studies and research. Therefore, it is essential to warn against the making of hasty conclusions concerning the choice of pavement structures and also against possible misinterpretations.

REFERENCES

1. 1977 Catalog of New Pavement Standard Structures. Laboratoire Central des Ponts et Chaussées (French Road Research Laboratory), Service d'Etudes Techniques des Routes et Autoroutes (Road and Freeway Technical Studies Department), Ministry of Transport, Paris, France, 1977.
2. Directives and Recommendations for the Construction of Pavement Subbases and Wearing Courses. Service d'Etudes Techniques des Routes et Autoroutes (LCPC-SETRA), Paris, France, 1969-1985 (updated regularly).
3. Guide to the Design of Flexible Pavement Overlays. Service d'Etudes Techniques des Routes et Autoroutes (LCPC-SETRA), Paris, France, 1976.
4. Technical Guide for Preventive Maintenance of the National Road Network. Service d'Etudes Techniques des Routes et Autoroutes (LCPC-SETRA), Paris, France, 1979 (plus list of deficiencies).
5. Revue Générale des Routes et Aérodromes. Special Issue. La Route et l'Energie (Roads and Energy), No. 577, July-August 1981.
6. Impacts of Heavy Freight Vehicles. Organisation for Economic Cooperation and Development, Paris, France, 1983.

Publication of this paper sponsored by Committee on Monitoring, Evaluation and Data Storage.

A Comprehensive System for Nondestructive Testing and Evaluation of Rigid Airfield Pavements

PAUL T. FOXWORTHY and MICHAEL I. DARTER

ABSTRACT

A complete system is presented for nondestructive testing and evaluation of rigid airfield pavements based on the falling weight deflectometer and the ILLI-SLAB finite element analysis model. This system was developed to provide the engineer with specific guidelines for planning and conducting extensive evaluations of major installations, calculating stresses generated by aircraft gear loads, and predicting the future performance of rigid pavement features under a variety of loading conditions. Techniques are presented for determining the location of maximum damage to rigid pavement slabs for one or any combination of aircraft, and the validity of the calculated stresses is established through comparisons of measured and predicted deflections at joints. These stresses are then related to actual field performance of rigid airfield pavements through a complete ILLI-SLAB reanalysis of accelerated traffic test data. A correlation between backcalculated concrete elastic modulus and flexural strength is reported, and the procedures to determine total accumulated Miner's damage at the critical stress location are explained. Realistic formats for reporting remaining pavement structural life to operations personnel are suggested. Major study findings include (a) new feature designations based on actual loading conditions, (b) a statistical sampling plan to reduce testing requirements, (c) techniques for determining the location of maximum accumulated damage for each feature, (d) a field performance curve to relate stress to available coverages, and (e) computer programs for predicting remaining structural life for one or any combination of aircraft.

This research effort was undertaken to develop the concepts necessary for a complete nondestructive testing and evaluation (NDT & E) system for rigid airfield pavements that was capable of field testing and analyzing the many distinct features that typically exist on modern commercial and military airfields. Past destructive methodologies and current elastic layered analysis procedures are not capable of assessing the true impact of aircraft operations at rigid pavement joints under a variety of temperature conditions. After an extensive review of currently available NDT equipment and mechanistic models, the falling weight deflectometer (FWD) and the ILLI-SLAB finite element program were chosen for their tremendous versatility.

In another paper in this Record, the authors establish the repeatability of FWD loads and deflections over a wide range of temperature, load, and thickness conditions; when coupled with an ILLI-SLAB-based iterative computer scheme to backcalculate dynamic elastic and subgrade moduli, accurate predictions of FWD-generated deflections were achieved. Therefore, after the pavement feature has been characterized by the NDT equipment and analytical model, confidence can be placed in the accuracy of the stress calculations that must be made at the joints for a variety of gear loads and configurations operating on major airfields.

In that same paper, in addition to validating measurement consistency and deflection predictions of the FWD/ILLI-SLAB system, techniques are presented to describe the temperature-dependent behavior of joint load transfer. Thus, accurate stress calculations can be made at the point of maximum accumulated damage (invariably at one of the joints) for each feature at any temperature. It now remains to formulate these components into a comprehensive methodology that will guide and direct the engineer toward realistic projections of remaining pavement life. This objective will be accomplished in this paper by (a) introducing several new concepts into the evaluation process that are intended to link the major components, and (b) providing specific examples from Seymour-Johnson Air Force Base (AFB) in North Carolina, Plattsburgh AFB in New York, and Sheppard AFB in Texas to demonstrated the NDT & E process. The result will be a complete system on which to expand and improve. Figure 1 shows a flow chart that can be used as ready reference for the entire NDT & E procedure; Foxworthy should be consulted for particular details on its development (1).

PLANNING AND CONDUCTING THE FIELD TESTING PROGRAM

The structural evaluation of any pavement network (such as all pavements at an airfield) is a twofold process: general network-level evaluation and specific project-level evaluation. The engineer must initially be concerned with the collection and analysis of information for all identifiable pavement features on the airfield network. By necessity, such a testing program must be broad enough in scope to permit the most efficient use of limited resources, yet detailed enough to identify potential problem areas. This general network evaluation program need not be overly concerned about the underlying causes

P.T. Foxworthy, Civil Engineering Research Division, U.S. Air Force Weapons Laboratory, Kirtland AFB, N.Mex. 87111. M.I. Darter, University of Illinois, Urbana, Ill. 61801.

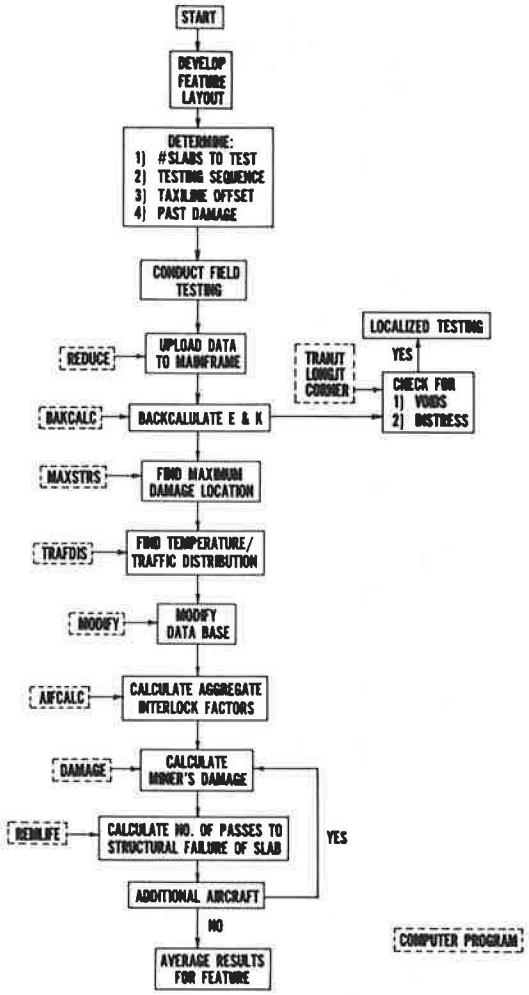

FIGURE 1 Flow chart of nondestructive testing and evaluation process.

of pavement distress, but rather should provide remaining structural life predictions for each feature and identify those features warranting additional investigation during the specific phase of the evaluation. The methodologies described here will address the first of these two phases, the general network-level evaluation.

Feature Identification

The tremendous challenge facing the engineer in planning and conducting an NDT & E program must begin in much the same way as conventional destructive evaluations. All available sources of information on the design, construction, maintenance, and repair of the airfield facilities must be reviewed, along with the results of any previous testing and condition surveys, to identify each distinct group of continuous pavement slabs that display nearly identical material properties, dimensions, construction histories, and maintenance practices. No limitations exist on the maximum or minimum feature size; however, the two primary purposes of feature designations are to (a) provide uniform pavement sections for ease of analysis, and (b) provide a convenient breakdown of the entire pavement system into smaller sections for maintenance and repair planning. This suggests that features smaller than about 10 slabs should be avoided to reduce testing and analysis requirements. Similarly, large parking aprons or entire runway widths seldom require maintenance or repair over the entire surface; generally keel sections and aircraft tie-down locations would receive priority for repair. Thus, the use of the pavement plays an important role in feature identification.

Historically, the concept of traffic area has been used in design to further subdivide pavement features into sections that not only have similar material properties, design, and geometrics, but also have consistent loading conditions. The designation of traffic areas has been based on the degree of channelization of the traffic and whether the airplanes are at full mission weight. These convenient designations have permitted reductions in the design of pavement thicknesses to take advantage of the lateral distribution of traffic along runway interiors and aprons, and lower fuel loads along ladder taxiways. In addition, construction difficulties are minimized by the designation of entire aprons and runway widths as single features.

However, for purposes of evaluation the use of current traffic area designations must be modified to more accurately reflect actual loading conditions. This will result in a substantial increase in the number of features for evaluation than were required for design, but the speed with which data can be collected and analyzed with this system justifies this recommendation. For parking aprons, this will mean further subdivisions for (a) the highly channelized taxilanes, (b) the statically loaded parking spots, and (c) the unloaded pavement areas between parking rows and taxilines. For runways, separate features must be established for the highly channelized areas surrounding the centerline. This centerline feature may only be two slabs wide for the first 1,000 ft, and then expand to a four-slab width for the remainder of the runway interior to account for increased wander. The exact location of this widening point will vary with the gross loads of the mission aircraft and, therefore, cannot be fixed a priori. Observation of surface distress will be the primary indicator of proper feature change points on runways as well as aprons.

Figures 2 and 3 show examples of proposed feature designations on the runway at Plattsburgh AFB and the operational apron at Seymour-Johnson AFB. The A, B, C, and D identifiers used for design have been replaced by S, T, and U designations representing static, transient, and unloaded conditions, respectively. These three categories encompass the entire spectrum of loading conditions that are encountered and readily describe the relative importance of the feature in putting maintenance and repair work in priority order. When used in conjunction with pavement thickness, construction history, and distress patterns, a realistic feature layout can be developed for NDT & E of an entire airfield.

The vast majority of features on an airfield will receive either T or U designations, with only those slabs actually supporting parked aircraft falling in the S category. Unloaded or U features can, in many instances, be omitted altogether from the NDT & E program if the potential for their use by aircraft, now or in the future, is low. Later in this paper, the proper use of pass-per-coverage ratios for each of these feature designations will be discussed.

Random Sampling Within Features

Even with the ability to collect and analyze vast amounts of data, it would be highly impractical in the general evaluation to test every slab in every feature. Therefore, a sampling program must be developed to systematically test each feature. This sampling program must specify, through the use of

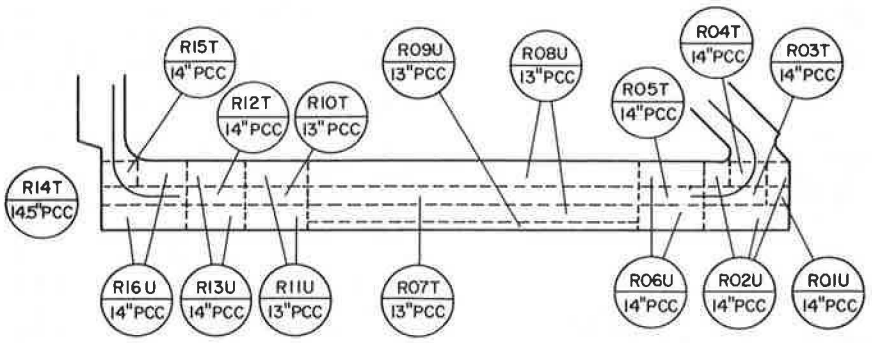

FIGURE 2 Proposed feature designations for Runway 17-35 at Plattsburgh Air Force Base.

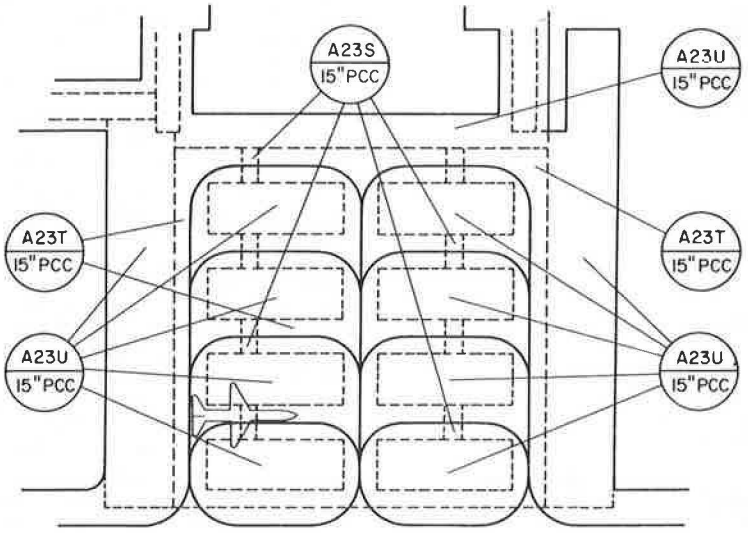

FIGURE 3 Proposed feature designations for the strategic air command apron at Seymour-Johnson Air Force Base.

statistical concepts, the number of slabs to be tested in a feature (or the number of replications) for a given level of desired precision. Because the engineer is unlikely to have the opportunity to return to the site for additional tests, the procedure must include a means by which to determine the number of tests required based on the previously established variability of the data being collected. The sampling program presented here is similar to the program developed for the pavement condition index (PCI) methodology described by Shahin et al. (2). Use of this statistical sampling plan will reduce testing requirements without significant loss of accuracy.

The number of slabs to be tested in a feature depends on the following:

- How large an error (e) can be tolerated in the estimate of the mean (X_E) of the feature elastic concrete modulus E (chosen over the subgrade reaction modulus K because of its greater variability; this is shown by the authors in another paper in this Record).
- The desired probability that the estimated mean of E (X_E) will be within this limit of error (e), usually set at 95 percent.
- An estimate of the variation of E from one slab to another within the feature, usually expressed as the variance (s^2) or the coefficient of variation (s/X_E).
- The total number of slabs (N) in the feature.

The allowable error (e) must first be expressed in terms of confidence limits. If e is the allowable error in estimating the mean elastic modulus (X_E) of the feature, and the desired probability that error will not exceed e is 95 percent, then the 95 percent confidence limits, computed from an approximately normally distributed sample mean, are

$$X_E \pm 2s/n^{0.5} \quad (1)$$

where n is the number of tested slabs. Therefore,

$$e = 2s/n^{0.5} \quad (2)$$

Solving for the required sample size n gives

$$n = 4s^2/e^2 \quad (3)$$

This expression can be used if the total number of slabs in the feature is large (more than 1,000). However, if the computed value of n is higher than 10 percent of the total number of slabs in the feature, a modified value n' should be used:

$$n' = Ns^2/[(e^2/4)\ (N-1) + s^2] \quad (4)$$

Before Equation 4 can be used to compute the required number of slabs to be tested, the total number of slabs in the feature must be estimated and the standard deviation and allowable error must be de-

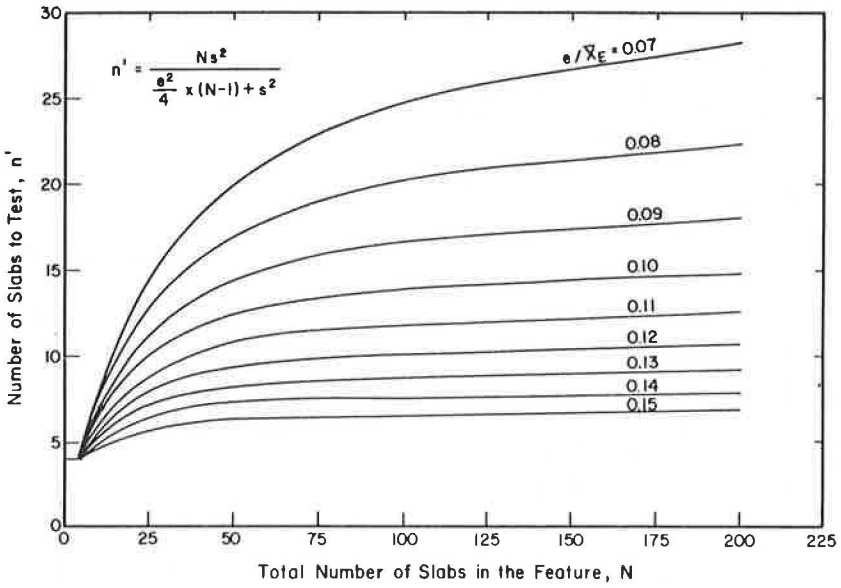

FIGURE 4 Determination of FWD testing requirements.

termined. From the repeatability studies on backcalculated FWD elastic modulus reported by the authors elsewhere in this Record, a coefficient of variation of about 20 percent was found for dynamic E. Because E values center around 5 x 10^6 psi, the standard deviation of E is approximately 1.0 x 10^6 psi. If an allowable error of 0.5 x 10^6 psi is permitted, the maximum number of slabs to be tested in a feature is

$$n = 4(1.0)^2/0.5^2 = 16 \text{ slabs.}$$

Figure 4 was developed from Equation 4 to permit a rapid determination of the number of slabs to be tested, if the total number of slabs in the feature has been estimated. Several alternatives for the allowable error, expressed as a percentage of the mean (e/X_E), are presented. A minimum of four slabs is required for every feature. As additional field verification of this procedure takes place, more accurate information on the true variance of the expected value of the mean of E will become available. This will probably result in a lower standard deviation and, therefore, a reduced testing requirement. Basing the determination of the number of slabs to be tested on the elastic modulus will ensure that modulus of subgrade reaction values, which display smaller variances, are determined with more than adequate precision.

The selection of which slabs to test is as important as the number to test. Not only is a random selection required to assure an unbiased estimate of the k and E parameters, but ideally they should be tested in a random order. However, such a procedure would be impractical because it would increase travel time between test locations dramatically. Therefore, it is recommended that the testing sequence shown in Figure 5 be used to systematically test the required number of slabs. A stratified random sampling procedure is recommended. The total number of slabs in the feature (N) is divided by the number to be tested (n) to establish the number of slabs skipped between tests. Testing should be accomplished in both directions along the feature unless only unidirectional movement of aircraft is allowed on the feature, in which case testing should proceed in that direction. Finally, only intact slabs should be tested because they are the only slabs that can be modeled relatively easily by the finite element program. Variation from the testing sequence of Figure 5 by one or two slabs to avoid broken slabs will not affect the random nature of the sequence.

The Nose Dock Apron at Seymour-Johnson AFB that was chosen as an example of the NDT & E process is

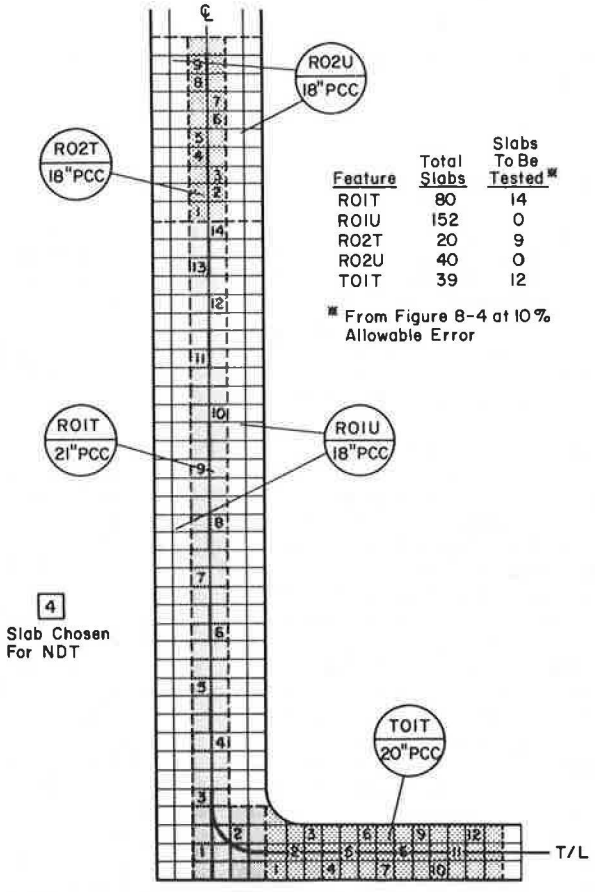

FIGURE 5 Recommended stratified testing sequence.

shown in Figure 6. Two features have been identified from the observed usage of the pavement: Feature A20T carries the aircraft loadings while Feature A20U remains unloaded. According to the information in Figure 4, 6 of the total of 24 slabs in Feature A20T are to be tested at an allowable error of 14 percent; Feature A20U does not require evaluation. Figure 6 shows which slabs were tested and the crack pattern development for the entire feature.

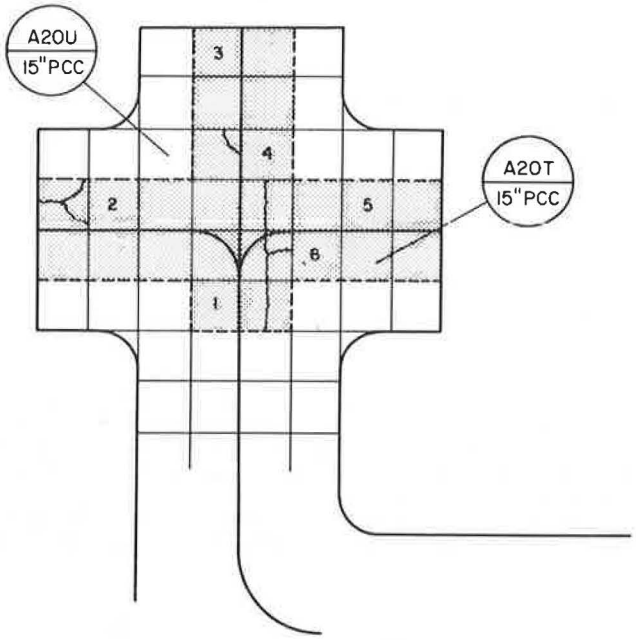

FIGURE 6 Crack development and testing sequence for Feature A20T.

Individual Slab Testing

During the field research, the testing pattern shown in Figure 7 was demonstrated to be an efficient method of testing the four key stations on each slab. This sequence is recommended for all general network-level evaluation testing. In addition, three drops of the FWD should be made at each station from a height that will produce loads in the 24,000-lb range. These three drops can then be averaged by the computer to improve deflection gauge sensitivity and reduce testing error for the backcalculation program.

The computer software supplied with the FWD can be programmed to create a data file for each feature on the airfield, with the total number of slabs to be tested input before beginning each feature. In addition, several other important pieces of information can be recorded on tape at this time for later use by the mainframe computer, including the installation name, the feature designation, transverse and longitudinal slab dimensions and joint types, pavement thickness, date and time of testing, and any remarks about the feature that may be pertinent. The air temperature will also be required, but is usually only available from the base weather station or the Federal Aviation Administration (FAA) Flight Service Station at the end of each day, and will have to be added separately to the mainframe's comprehensive data file. The taxiline offset distance, the transverse offset distance, and Miner's past damage, which will be discussed later, can be input to the FWD computer at the time of testing and will be retained throughout the evaluation sequence.

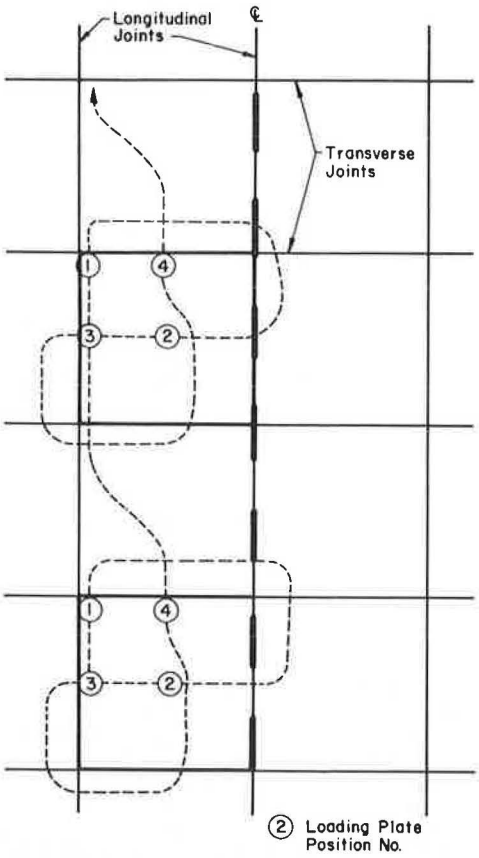

FIGURE 7 Recommended FWD testing pattern for network-level evaluations.

DATA PREPARATION

The field data collection program will typically result in the accumulation of more than 100 data files containing information on from 6 to 22 separate slabs and 12 drops per slab. These files must be transferred to a mainframe computer by using a terminal emulation program. In addition, the information stored on the cassette tapes is in metric units and unformatted, making it difficult to read the information directly from the file.

To solve this problem, a computer program REDUCE was written to create new individual files for each feature, with the information formatted for input into the backcalculation program. The metric units are converted to pounds force and mils of deflection, and the three FWD drops are averaged. The paper by Foxworthy should be consulted for specific examples of the computer inputs and products for REDUCE and the other programs described throughout the remainder of this paper (1).

BACKCALCULATION OF E, k, AND AGGREGATE INTERLOCK FACTORS

Backcalculation of the dynamic elastic modulus of the concrete and the dynamic modulus of subgrade reaction for each slab is performed by the computer program BAKCALC. This program is the first in a series of programs developed to analyze the response of the pavement slab to FWD loads at the key locations. The program uses an iterative scheme (1) and the ILLI-SLAB finite element program as a subroutine to determine these moduli values. These values are then reinput to compute the predicted deflections.

For the most part, measured and predicted deflections will be within about 2 percent of each other, particularly for the D0 reading. In the event that the two D0 deflections do not agree within this tolerance, an error in the estimation of the pavement thickness is probably to blame. A brief investigation into this phenomenon during analysis of the research data revealed that, when this occurs, a trial and error search for the thickness that will produce nearly identical values of measured and predicted D0s will provide the correct thickness. This technique has potential for the NDT & E of airfields for which pavement thickness information is unavailable.

Three other computer programs were developed as part of the rigid pavement evaluation process to compare predicted and measured deflections at the transverse joint (TRANJT), longitudinal joint (LONGJT), and corner (CORNER) of the slab. These programs utilize the backcalculated moduli from the center slab position, along with an iterative solution for the ILLI-SLAB aggregate interlock factor (AIF), discussed by Foxworthy (1), to provide the engineer with supplemental information about the performance of individual joints within a feature. Ideally it would be desirable to use actual joint measurements for the determination of E, k, and the AIFs, but the complexities surrounding support conditions at the joints makes such an undertaking impractical at this time. However, if the backcalculated values for the center slab could be assumed to exist at the joints as well, then selection of the proper aggregate interlock factor, based on a comparison of measured and predicted deflections at the joints, is reduced to an iterative computer solution.

The impact of making this assumption is much more significant for k than for E. Obviously, making this assumption for k ignores the potential loss of support that can occur at the joint from plastic deformation, pumping, and so forth. It also ignores the assumed nonexistence of shear across joints in the Winkler foundation. However, if this assumption will permit reasonably accurate ILLI-SLAB modeling of the joint's behavior under FWD loads, great confidence can then be placed in the calculated stresses under actual gear loads.

Table 1 presents the results of typical measured and predicted deflections across joints for a variety of pavement thicknesses and load transfer efficiencies. This remarkable agreement between measured and predicted deflections, across such a stark discontinuity as a keyed construction joint or dummy contraction joint, further reinforces the ability of ILLI-SLAB to accurately model behavior of joints. In the event predicted joint and corner deflections are well below measured deflections, subbase or subgrade support has probably been lost along that joint. If the opposite is true, that is, predicted values are much higher than measured, it is probably the result of a very low E modulus that was transferred from the center of the slab to the edges. Such an artificially low E value could arise from testing near a structural crack.

DETERMINATION OF CRITICAL STRESS LOCATION FOR EACH FEATURE

The next major task facing the engineer is the determination of that one key location on each feature where the critical stress is developed for each aircraft. At first glance, this might appear to be an extensive undertaking, but four simplifying assumptions ease this task considerably. First, aircraft do not generally operate randomly over the surface of a feature; they follow specific paths dictated by painted taxilines. Second, the location of this taxiline remains a constant distance from the slab's longitudinal joints throughout the feature. If not, a new feature should be designated where the taxiline shifts location. Third, the load transfer efficiency along transverse and longitudinal joints remains nearly constant, as shown by the authors in another paper in this Record. Finally, the critical tensile stress (and thus maximum damage) in a slab will occur at a transverse joint unless the gear travels within an average distance of about 12 in. from the longitudinal joint, in which case the critical stress is developed midway between transverse joints along the longitudinal joint.

Critical Gear Position

The four assumptions discussed in the preceding section permit the engineer to make a rapid assessment of the critical stress location of the aircraft gear to produce the maximum damage to the concrete slab. As shown in Figure 8, the combination of fixed taxiline to longitudinal joint distance and aircraft centerline to outside of the gear distance firmly establishes the position of the gear relative to the longitudinal joint. If the gear is not within about 12 in. of this joint, the point at which it crosses the transverse joint becomes the critical stress location.

Undoubtedly many occasions will occur on which a particular slab width, load transfer efficiency, taxiline location, and aircraft gear configuration combine to make the critical stress location uncertain. To assist the engineer in such an eventuality, a computer program called MAXSTRS was developed, based on the ILLI-SLAB finite element model, to calculate the maximum tensile stress at the bottom of the slab for any position of the gear. Inputs to the program include the aircraft type; slab dimensions; backcalculated k, E, and aggregate interlock factors; and distances from each joint to the nearest point on the gear. The type of aircraft specified automatically sets up the proper finite element mesh, and the offset distances from the joints specify the gear position. Each potential critical location for the gear can then be checked quickly, including the remote possibility that it could lie in the interior of the slab if load transfer at the joints is high enough (at least 95 percent).

Effects of Mixed Traffic

At this stage in the evaluation process, a few comments on the effects of mixed traffic will greatly reduce or even eliminate repeated stress calculations for other than the primary aircraft utilizing the pavement feature. First, the failure of a slab, defined as the appearance of the first load-associated crack throughout the evaluation procedure, begins at only one point on the bottom of the slab, the point of greatest repeated stress damage. Second, this point of greatest damage will usually occur under the mean wander point of the primary aircraft gear. Third, unless the wheelpaths of two or more aircraft overlap, resulting in additive stresses at the bottom of the slab, only the primary aircraft needs to be included in the evaluation of the feature.

In special instances, such as for thicker pavements and certain aircraft mixes, the actual point of maximum stress damage might not be located directly under a wheel of either aircraft. This situation can be accommodated by analyzing the stress distribution of each gear separately and then summing the stresses to find the point of maximum total stress. This point then becomes the location of maximum damage.

TABLE 1 Comparison of Measured and Predicted FWD Deflections Across Longitudinal and Transverse Joints

Feature	Slab No.	Load (lbf)	Measured (M) or Predicted (P)	Sensor Deflections (mils) D0	D1	D2	D3	D4	D5	D6	Load Transfer Efficiency (%)
Longitudinal Joints											
T04A	1	23182	M	5.3	4.1	3.6	3.2	2.8	2.4	2.0	77
			P	5.6	4.4	3.6	2.9	2.3	1.7	1.1	79
	2	23087	M	4.3	3.9	3.5	3.0	2.6	2.3	1.9	91
			P	4.3	3.9	3.3	2.6	2.1	1.6	1.1	92
	3	22626	M	5.0	4.5	4.1	3.6	3.1	2.8	2.3	90
			P	4.9	4.5	3.9	3.3	2.8	2.2	1.7	92
	4	23071	M	4.3	3.9	3.5	3.0	2.7	2.3	2.0	91
			P	4.2	3.9	3.3	2.7	2.2	1.7	1.2	92
A05B	1	25170	M	9.1	6.0	5.1	4.3	3.6	2.9	2.4	66
			P	8.5	5.7	4.8	4.0	3.2	2.5	1.8	67
	2	22896	M	7.6	7.2	6.3	5.4	4.6	3.9	3.3	95
			P	7.2	6.9	5.8	4.8	4.0	3.2	2.4	95
	3	26871	M	5.7	5.2	4.4	3.9	3.3	2.9	2.5	91
			P	5.5	5.1	4.2	3.4	2.8	2.1	1.5	93
	4	26505	M	8.6	6.9	5.9	5.0	4.3	3.7	3.1	80
			P	8.2	6.9	5.8	4.8	4.0	3.2	2.4	83
A08B	1	23055	M	17.2	10.4	8.5	6.7	5.2	4.1	3.1	60
			P	16.8	10.4	8.1	6.0	4.5	2.9	1.4	62
	2	24136	M	34.1	6.4	5.2	4.3	3.3	2.8	2.3	19
			P	28.1	4.1	3.1	2.3	1.7	1.0	0.4	15
	3	23898	M	22.9	6.7	5.7	4.7	3.9	3.2	2.7	29
			P	22.8	5.9	4.4	3.2	2.3	1.4	0.5	26
	4	22578	M	15.9	14.8	11.9	9.1	6.9	5.4	3.7	93
			P	15.5	14.5	11.1	8.2	6.1	3.9	1.8	94
Transverse Joints											
T04A	1	23914	M	6.2	4.0	3.5	3.2	2.8	2.5	2.1	65
			P	6.1	4.0	3.3	2.7	2.2	1.7	1.2	65
	2	26537	M	5.0	3.4	3.0	2.7	2.3	2.0	1.7	68
			P	5.0	3.5	2.9	2.4	2.0	1.5	1.1	69
	3	25520	M	4.5	4.1	3.8	3.5	3.1	2.8	2.6	91
			P	5.2	4.8	4.1	3.5	2.9	2.4	1.9	93
	4	25726	M	8.7	2.2	2.0	1.9	1.5	1.4	1.3	25
			P	8.6	2.2	1.8	1.4	1.1	0.9	0.6	25
A05B	1	25631	M	11.9	3.4	3.1	2.7	2.4	2.1	1.8	29
			P	11.7	3.0	2.5	2.1	1.7	1.3	0.9	26
	2	25138	M	7.7	7.0	6.0	5.2	4.5	3.8	3.3	91
			P	7.5	6.9	5.9	5.0	4.2	3.4	2.6	92
	3	25106	M	6.7	4.3	3.8	3.3	3.0	2.6	2.2	64
			P	6.8	4.4	3.6	3.0	2.4	1.8	1.2	64
	4	25822	M	8.1	7.3	6.3	5.4	4.5	3.9	3.3	90
			P	8.3	7.6	6.4	5.3	4.3	3.4	2.5	92
A08B	1	24359	M	11.6	11.4	9.3	7.5	6.3	4.8	3.8	98
			P	12.2	11.6	8.9	6.7	5.0	3.3	1.6	95
	2	23580	M	13.8	13.4	11.2	9.2	7.1	5.9	4.6	97
			P	14.1	13.5	10.4	7.7	5.8	3.8	1.9	95
	3	25615	M	12.5	11.8	9.7	7.6	5.9	5.0	4.2	94
			P	13.0	12.3	9.4	6.9	5.1	3.3	1.5	95
	4	23739	M	25.7	8.6	7.3	6.2	5.1	4.4	3.6	33
			P	23.1	7.0	5.4	4.0	2.9	1.9	0.8	30

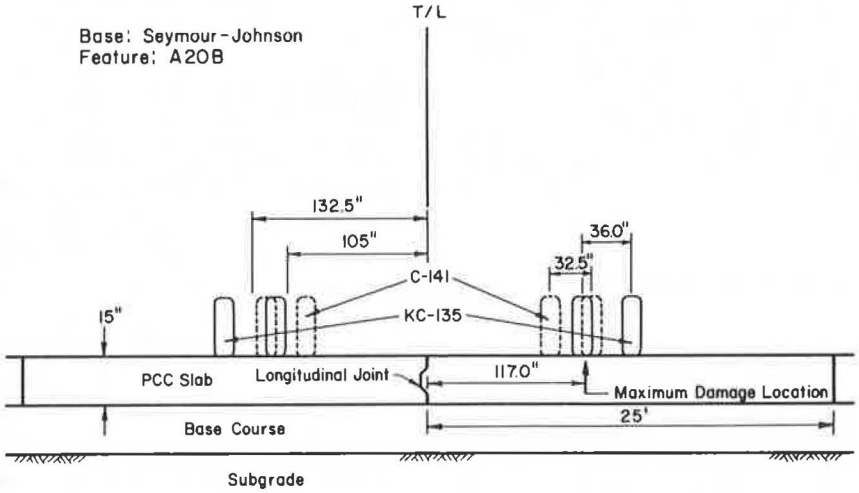

FIGURE 8 Determining the location of maximum accumulated damage for two or more aircraft.

The final determination of the critical aircraft gear may or may not coincide with the primary mission aircraft for the feature. It is entirely possible, for instance, that an aircraft producing high stress levels for 10 operations per day may cause more accumulated damage at its gear mean wander point than a lower stress-producing aircraft operating at 100 passes per day would cause at some other point on the slab. Generally, the critical aircraft for a feature will be apparent from the comparison of wheelpaths of all aircraft using the feature, particularly if an analysis of the critical stress has been performed on other similar features. In the event two or more wheelpath mean wander points do coincide, Miner's Damage Law must be used to account for the cumulative effects (3). This procedure will be discussed in detail later in this paper.

ACCOUNTING FOR TEMPERATURE AND PAST TRAFFIC EFFECTS

The tremendous variation of load transfer efficiencies experienced by any joint over the range of temperatures that joint is subjected to annually must be accounted for in the cumulative damage effects of the critical aircraft gear load. It is not sufficient to simply use an average annual load transfer efficiency exhibited by the joint when calculating the maximum stress because that stress is not linear with temperature or load transfer efficiency. It is possible, however, to distribute the total annual traffic at an installation into several temperature zones, calculate the maximum stress that would be generated by the critical gear at the average temperature of each zone, determine Miner's damage for that stress in each zone, and then sum the damage for each temperature zone to obtain the overall damage to the pavement in a year. This approach is recommended in this evaluation procedure.

A typical daily temperature cycle can be described approximately by the trigonometric relationship

$$T_H = [(T_{max} - T_{min})/2] \times \sin[15 \times (H - s)] = T_{avg} \quad (5)$$

where

T_H = temperature at any hour of the day;
T_{max} = maximum daily temperature (°F);
T_{min} = minimum daily temperature (°F);
H = hour of the day, from 1 to 24;
s = number of hours, from 1 to 24, between midnight and the occurrence of T_{avg}; and
$T_{avg} = (T_{max} + T_{min})/2$.

From this relationship, the temperature at any hour of the day can be approximated. If it is assumed that the variable s remains constant throughout the year, and that T_{max} and T_{min} are relatively stable over an entire month, then the average temperature of each hour of the year could be used to place that hour into 1 of 12 temperature zones. These zones were established in increments of 10°F from 0 to 100, as a compromise between the accuracy of smaller intervals and the increased analysis effort; temperatures below 0°F and above 100°F each comprise a zone. From the total number of hours in each zone, the percentage of the total hours in a year falling within each zone can easily be calculated.

If aircraft operations are assumed to be distributed evenly throughout the day, week, and year, the percentages just given become the percentages of aircraft operations on any feature within each temperature zone. Because the load transfer efficiency at any joint can be calculated for each temperature zone, the critical stress generated by the primary aircraft can be calculated for each of the 12 temperature zones in which it might operate. A computer program called TRAFDIS was written to perform these calculations.

The three assumptions made to complete this analysis do not appear to compromise the accuracy of this approach. The time of the day at which maximum and minimum temperatures occur remains fairly constant from month to month. The use of readily available monthly maximum and minimum mean daily temperatures will obviously not include those few hours of each year when temperature extremes exist, but the effect of these few hours on the total percentage is small. The greatest criticism could be levied at the assumption of evenly distributed traffic over time, particularly for commercial airport operations. However, for military airfields this assumption is not unreasonable because of their commitment to 24-hr readiness. The results of an analysis based on even distribution of traffic would probably lead to somewhat conservative estimates of remaining life because greater damage would be accumulated for night operations at colder temperatures. If an accurate traffic distribution pattern could be determined for a particular installation, it could be incorporated into the computer scheme to provide a more realistic analysis.

Estimating Past Traffic Damage

The prediction of remaining structural life in any pavement system must begin with an estimate of the past accumulated load damage based on Miner's Damage Law, which states that

Total Damage = Past Damage + Future Damage

Past damage can be estimated in two different ways, depending on the availability of past traffic loading data. If adequate data are available, a stress analysis can be conducted for each aircraft that has used the pavement, taking into account all of the factors that influence stress levels. From this extensive analysis, a summation of load damage can be made by using Miner's Damage Law. Usually, however, records on the movement of aircraft are inadequate, particularly for taxiways and aprons. Therefore, it is recommended that the estimate of past damage be obtained by using existing load-associated slab cracking information from the current PCI survey. If only load-associated damage is used, this technique will provide a quick, reasonable assessment of the accumulated damage, regardless of the type and mix of aircraft that produced it. The importance of an accurate distress survey thus becomes obvious.

The estimate of past damage is made by counting the number of slabs in the feature that contain any of the following distress types: corner breaks, longitudinal and transverse cracking, diagonal cracking, and shattered slabs. This number of distressed slabs is divided by the total number of slabs in the feature to arrive at the percentage of cracked slabs for the feature. Because the failure criteria have been established at 50 percent of all slabs with at least one load-associated crack dividing the slab into two pieces, a percentage of cracked slabs equaling 50 constitutes a Miner's damage of 1.00. It then becomes simply a linear transformation between the percent cracked slabs (%CS) and Miner's damage number (MDN). Expressed mathematically,

$$MDN = \%CS \times 0.02 \quad (6)$$

Only in those rare instances in which no load-associated cracking can be detected within the feature

will an analysis of past traffic damage be necessary. In these cases, the feature would probably have been recently constructed, and such an analysis would be feasible.

Two points must be emphasized in making this estimate of the past damage. First, care must be taken during the initial counting of the distressed slabs to avoid including slabs that have cracked from other than load-associated causes. It is often difficult, for instance, to distinguish between a longitudinal crack caused primarily from load damage and a crack caused primarily from environmental or construction factors. Many cracks are caused by a combination of load and curling, warping, and shrinkage stresses. Cracking due to construction deficiencies, such as poor joint alignment or late sawing of contraction joints, must not be counted. Conversely, slabs that have been replaced must be counted as cracked slabs to avoid biasing the damage estimate for the other slabs (unless more than one-half of the slabs have been replaced, in which case it becomes a new feature). Good engineering judgment must be used to make this estimate because it has such a tremendous impact on the projection of remaining life.

The second point of interest is the potentially unconservative nature of the final damage estimate from distress survey results. It is entirely possible that, because of the mechanics of crack propagation, load-associated cracking may not have quite reached the surface of several slabs, where it could be counted. Thus, a feature could possibly exhibit no load-associated distress during the survey, and two weeks later 5 to 10 percent of the slabs display their initial crack. Only through the long-term monitoring programs currently under way will trends of this type be discovered. In the interim, this procedure provides the most reasonable approach to estimating past damage, certainly far better than the only other alternative.

Figure 6 shows the required crack development pattern to make this estimate of the total accumulated past damage. Of the 24 slabs in the feature, 5 contain a load-associated crack. From Equation 6, Miner's damage number for Feature A20T becomes 0.42.

DEVELOPMENT OF FINAL EVALUATION DATA BASE

The analyses conducted in the last sections have resulted in the establishment of three additional pieces of information, critical to the evaluation of each feature, which must be added to the data base. The taxiline offset distance is the distance from the taxiline of the feature, either painted or projected, to the closest longitudinal joint. This distance is used in conjunction with the airplane's configuration to position the gear on the slab for stress calculations. The transverse joint offset distance allows the positioning of the gear at some point other than the transverse joint, if the critical stress analysis revealed, for instance, that the maximum stresses were developed along the longitudinal joint. Finally, the past, accumulated, load-associated damage, expressed as a Miner's damage number, must be added to the data base. A simple computer program MODIFY has been written to generate this file.

Aggregate Interlock Factors for Each Temperature Zone

The dependence of the critical stress on air temperature, and hence load transfer efficiency, requires that the maximum tensile stress at the bottom of the slab be calculated for each of the 12 temperature zones. To accomplish this, aggregate interlock factors must be determined for each zone at both longitudinal and transverse joints for inclusion into the ILLI-SLAB program. Thus 24 aggregate interlock factors must be iterated for each slab tested. Fortunately, the computer program AIFCALC performs these calculations quickly and efficiently.

AIFCALC makes two assumptions in determining these aggregate interlock factors. First, load transfer efficiencies below 25 percent are elevated to 25 percent to avoid precision errors when slopes of lines near zero are encountered. Similarly, load transfer efficiencies above 95 percent are automatically assigned an aggregate interlock value of 30 x 10^8 psi to avoid a problem much the same as that which exists at the lower values. Second, the program assumes that load transfer efficiencies below 25 percent and above 95 percent, as measured in the field, have just reached these values at the time of measurement. Otherwise, no prediction of their behavior with temperature could be made (see paper by the authors elsewhere in this Record). The only alternative to this assumption would be a retesting of the slab joint at another time to obtain a load transfer efficiency between 25 and 95 percent. Fortunately, this situation does not occur often if testing is accomplished between 40 and 90°F.

PREDICTING THE REMAINING LIFE

The DAMAGE program reads the slab dimensions, backcalculated moduli, and aggregate interlock factors for the first temperature zone to calculate the maximum stress generated by the specified aircraft, with adjustments to the dynamic k moduli for static loading conditions, if necessary. This stress is used as the basis for determining the stress in each of six gross weight categories. For example, an aircraft loaded at 80 percent of its gross weight will produce a stress at the bottom of the slab equal to 80 percent of the stress produced at its maximum gross weight.

The flexural strength of the concrete is then determined through a correlation developed during this research with backcalculated concrete elastic moduli, adjusted for traffic area. When divided by the calculated stress for each gross weight category, the evaluation factor for each category is established. Equation 7, developed from an ILLI-SLAB reanalysis of accelerated traffic test data and shown graphically in Figure 9 is as follows:

$$\text{Log}_{10}\ \text{COV} = 1.323 \times (\text{FS}/\text{CS}) + 0.588 \quad (7)$$

where

COV = coverages to initial crack failure,
FS = flexural strength,
CS = critical stress,
R^2 = 0.64, and
SEE = 0.52.

Equation 7 then relates the evaluation factor to the number of coverages that can be expected for each gross weight category in the first temperature zone. Next, the damage caused by one coverage of the aircraft is distributed among the temperature zones according to the percentage of total aircraft operations occurring in each zone. Finally, this entire process is repeated for each of the 12 temperature zones, and the damage from each zone is summed to provide the total damage resulting from one coverage of the aircraft in each gross weight category.

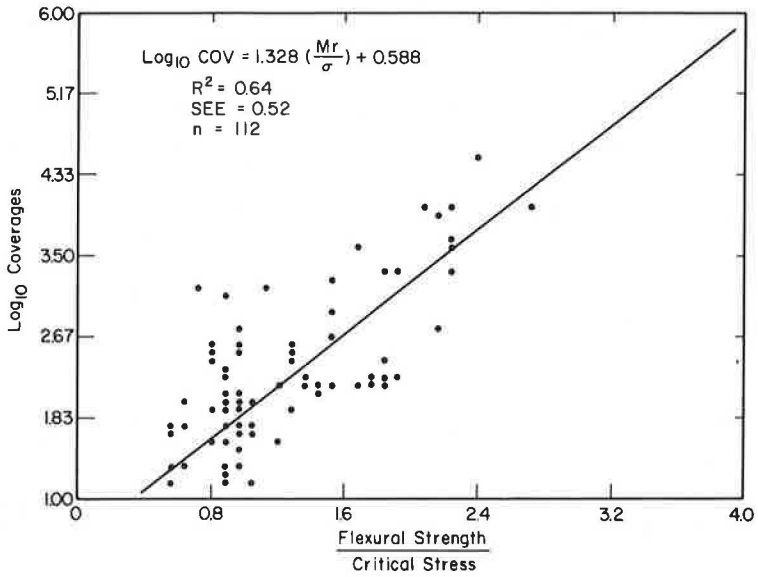

FIGURE 9 Relationship between strength and stress of concrete slabs and their field performance—the transfer function.

Relating Future Damage to Remaining Coverages

From the calculation of the damage caused by one coverage of the specified aircraft, it is a simple procedure to calculate the remaining coverages to initial crack failure. REMLIFE calculates the future damage allowed for one coverage of the aircraft by subtracting the past damage from a total permitted Miner's damage of 1.0. The remaining coverage level for each gross weight category is simply the total future damage divided by the total damage for one coverage of the aircraft. This entire process is then repeated for every slab tested.

Pass-per-Coverage Ratios

Brown and Thompson documented the background, development, and application of the current procedure for converting coverages to passes, and provided a limited amount of data on which the current pass-per-coverage (P-C) ratios, still in use by many agencies, are based (4). These data were collected at several Air Force bases in 1956 and 1960, using B-47, KC-97, B-52, and KC-135 aircraft. Approximately 1,176 observations of aircraft taxi, takeoff, and landing operations were made at 1,000-, 2,000-, and 5,000-ft points on runways, and along curved portions of taxiways.

The primary result of the study was a method for calculating P-C ratios based on a channelized traffic wander width of 70 in. and a nonchannelized wander width of 140 in. Recognizing that the lateral distribution was continuously changing along the runway for each aircraft, these wander widths were arbitrarily established for design purposes.

In 1975, the Federal Aviation Administration sponsored an extensive research effort by HoSang to determine realistic lateral distribution patterns for commercial aircraft traffic at civil airports (5). Data were collected at nine airports representing a wide range of operating and environmental conditions. More than 10,000 observations of lateral distribution were made at three runway locations and on parallel and high-speed taxiways.

The results of this study verified the P-C ratio calculation procedures developed by Brown and Thompson, and also provided lateral distribution characteristics more representative of today's aircraft operations. Particularly noteworthy is that, for all practical purposes, the standard deviations along the entire length of runways and taxiways can be assumed constant. On runways, some additional wander was evident at the point of rotation, but in general, a standard deviation of 6.5 ft is representative of the entire length. On taxiways and apron taxilanes, a standard deviation of 3.0 ft is typical. The vast amount of data collected and the instrumentation utilized make this report extremely valuable in the pavement evaluation process. The P-C ratios presented in Table 2 were developed from HoSang's recommendations and allow the user to select values that are appropriate for a given situation (5). The average P-C ratios stated here are used in the REMLIFE computer program.

Final Evaluation

The last step performed by REMLIFE in the evaluation for a single aircraft is the application of the aircraft's P-C ratios to the calculated coverage level for each gross weight category. This produces the predicted number of aircraft passes remaining in each slab until initial crack failure occurs. However, it remains for the engineer to condense these individual slab predictions into a single prediction for the entire feature.

Ideally, a representative slab could have been developed for the evaluation of each feature by averaging FWD deflections and backcalculating an overall E and k for the feature. This technique was shown as a part of this research to produce results that agree precisely with backcalculated E and k values obtained for each slab and then averaged for the entire feature. The savings in computer processing time is substantial, and such a procedure is recommended if only E and k values are desired from FWD deflections.

However, when the evaluation process is extended to remaining life projections, the representative slab concept will not work. The required average load traffic efficiency for each joint in such a representative slab would not accurately reflect the

TABLE 2 Pass-per-Coverage Ratios for Selected Aircraft at Various Standard Deviations of Wander Width for Rigid Pavements

	Standard Deviations of Wander Width (ft)								
Aircraft	1	2	3	4	5	6	7	8	9
F-4	3.42	6.84	10.26	13.67	17.06	20.26	22.92	24.67	25.24
A-10	4.78	9.55	14.32	19.10	23.81	28.15	31.58	33.54	33.95
F-15	3.54	7.08	10.62	14.15	17.55	20.43	22.26	22.75	23.16
F-16	4.56	9.11	13.13	14.57	15.38	16.84	18.59	20.50	22.50
T-38	7.72	15.43	23.10	29.95	33.84	34.56	36.25	38.66	41.48
F-111	1.99	3.98	5.95	7.57	8.21	8.46	9.69	10.46	11.29
C-130	0.85	1.71	2.56	3.41	4.20	4.79	5.04	5.11	5.28
DC-9	2.24	3.00	4.17	5.41	6.65	7.75	8.54	8.89	8.97
B737	2.45	3.14	4.20	5.37	6.56	7.66	8.50	8.94	9.03
B727	2.17	2.99	3.76	4.72	5.72	6.70	7.54	8.14	8.41
C-141	1.16	1.50	1.98	2.53	3.09	3.61	4.02	4.26	4.31
KC135	1.10	1.48	1.89	2.39	2.91	3.44	3.95	4.41	4.77
C5	0.83	1.31	1.39	1.52	1.72	1.94	2.17	2.40	2.61
DC10	1.00	1.80	1.98	2.33	2.76	3.21	3.67	4.14	4.62
L1011	1.01	1.78	1.97	2.34	2.77	3.23	3.71	4.19	4.67
E4	1.00	1.53	1.81	2.14	2.33	2.40	2.43	2.45	2.46
B52[a]	0.55	0.75	0.95	1.16	1.29	1.31	1.37	1.45	1.54

[a] These pass-coverage ratios are one-half of the values calculated by the program to account for the large distance between the bicycle gears.

increased stresses that develop as joints open in colder temperatures. Therefore, each slab must be evaluated separately for remaining passes to failure, and then an average remaining pass level for the feature can be determined easily.

The evaluation of the feature for a mix of aircraft requires an additional step in the REMLIFE program. The DAMAGE outputs for each aircraft must be combined in a specific manner for each gross weight category and slab to determine the total damage from the assumed traffic. The P-C ratio for each aircraft and the proportion of each aircraft in the total are utilized to arrive at the final remaining life predictions. The current capabilities of the REMLIFE program will permit any mix of aircraft.

SUMMARY

A complete system for NDT & E of rigid airfield pavements has been presented. Techniques for identifying and statistically sampling individual features will reduce testing and analysis costs while ensuring accurate results. Computer programs have been developed to calculate stresses at joints for any gear configuration and for any temperature profile. These stresses are related to field performance by a transfer function derived from accelerated traffic test data. Finally, the structural life of the feature can be predicted for any mix of aircraft.

ACKNOWLEDGMENTS

The authors wish to acknowledge the cooperation and financial support of the U.S. Air Force Engineering and Services Center and the University of Illinois, without which this research could not have been accomplished.

REFERENCES

1. P.T. Foxworthy. Concepts for the Development of a Nondestructive Testing and Evaluation System for Rigid Airfield Pavements. Ph.D. thesis. University of Illinois at Urbana-Champaign, Urbana, 1985.
2. M.Y. Shahin, M.I. Darter, and S.D. Kohn. Condition Evaluation of Jointed Concrete Airfield Pavement. ASCE Transportation Engineering Journal, Vol. 106, No. TE4, July 1980, pp. 381-399.
3. M.A. Miner. Cumulative Damage in Fatigue. Journal of Applied Mechanics, Sept. 1945.
4. D.N. Brown and O.O. Thompson. Lateral Distribution of Aircraft Traffic. Miscellaneous Paper S-73-56. U.S. Army Engineer Waterways Experiment Station, Vicksburg, Miss., July 1973.
5. V.A. HoSang. Field Survey and Analysis of Aircraft Distribution on Airport Pavements. FAA-RD-74-36. Federal Aviation Administration, U.S. Department of Transportation, Feb. 1975.

Publication of this paper sponsored by Committee on Monitoring, Evaluation and Data Storage.

Pavement Condition Data Analysis and Modeling

MARIA MARGARITA NUNEZ and MOHAMED Y. SHAHIN

ABSTRACT

To maximize the benefits of pavement management, a reliable method of pavement condition forecasting is extremely important. Described is a methodology for pavement condition data analysis and a modeling technique for use in the PAVER pavement management system. The latest PAVER data bases from 18 civilian agencies and 2 military installations were used to verify this methodology. Several models were developed for each location to account for the wide variety of factors affecting pavement performance. Relevant information of the pavement sections was organized into pavement families; a family is defined by the pavement type, pavement rank, and pavement functional classification. A screening procedure was designed to examine the data retrieved for obvious errors. A statistical outliers analysis was implemented to detect any unusual observations. The family model accepted for pavement condition index prediction was developed from the pavement AGE variable averaged every 3 years to obtain a representative point for each 3-year period. This point was then used in the final polynomial regression analysis. Pavement condition forecasting for each section was accomplished by customizing the prediction depending on the present condition in relation to the family curve. The family models were designed for continuous update as more data are gathered for a given location and entered in the PAVER data base.

Prediction of pavement performance using nondestructive testing (NDT) results has been studied by O'Brien, Kohn, and Shahin (1). For model development, O'Brien et al. included several variables: pavement type, condition rating, NDT information, pavement construction, traffic information, and pavement layer thicknesses. The independent variables included in the final model for pavement condition prediction were pavement construction history, a weighted traffic variable, and NDT deflection parameters. The pavement construction history was reflected in three pavement layer age variables: time since last overlay, time from construction to first overlay, and total pavement age. The NDT parameters were a normalized deflection factor given by the slope of the deflection basin, and a measure of the deflection basin area. The traffic variable included in the prediction model is the natural logarithm of current traffic count weighted by traffic type (passenger vehicles, two-axle trucks, three or more axle trucks). The relative significance of each variable group was 60 percent for the age variables, 30 percent for the NDT variables, and 10 percent for the traffic variable.

The prediction model presented by O'Brien et al. was considered adequate for network condition projection but not for the project-level condition prediction. An overall regression model based on all the variables originally included was not considered satisfactory particularly for project-level analysis. This was attributed to the complexity of accurately accounting for all variables in one model. The model was developed from data for one location; therefore climatic effects were not included. Also, the model is static in that it would be difficult for the average pavement manager user to update the model when additional pavement condition data become available.

To maximize management benefits, a reliable method of pavement condition forecasting is extremely important. Proper selection of an optimum maintenance strategy at the network and project levels depends on the availability of an accurate prediction model that reflects local conditions. In this paper, a methodology for pavement condition data analysis and the development of a prediction model for use in the PAVER pavement management system are described (2). In this methodology, models are developed for each specific location and models are continuously updated as more data are gathered and entered in the PAVER data base.

U.S. Army Construction Engineering Laboratory, P.O. Box 4005, Champaign, Ill. 61820-1305.

PAVER DATA BASES

The condition rating procedure used in this study is the pavement condition index (PCI) of the PAVER pavement management system developed by the U.S. Army Construction Engineering Research Laboratory (USA-CERL) (1,2). The PAVER system provides the user with data storage and retrieval, pavement network definition, establishment of project priorities, inspection scheduling, determination of current and future network condition, maintenance and repair needs, economic analysis, and budget planning. PCI is a composite index of the pavement's structural integrity and operating condition. PCI of a pavement section is determined based on distress type, quantity, and severity. It is a numerical index from 0 to 100 that has been divided into seven categories that range from failed to excellent, as shown in Figure 1.

PAVER is a pavement management system that improves the maintenance decision-making process at the network and project levels. The prediction methodology presented here and developed as part of the PAVER program can be effectively utilized by other management systems. The PAVER system has been widely implemented by many military installations and has been adopted by the American Public works Association for use by cities and counties. The latest PAVER

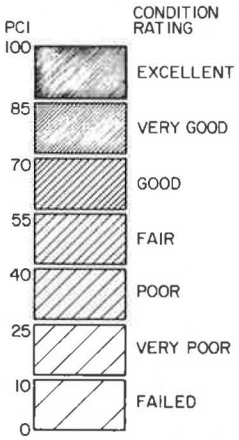

FIGURE 1 Pavement condition index and condition rating scale.

data bases from 18 civilian agencies (cities and counties) and military installations were used to verify the methodology presented in this paper.

Data available in PAVER for each of these agencies include pavement identification, pavement rank or functional classification (primary, secondary, etc.), condition history, layer material properties, and traffic records.

MODELING PROCEDURE

The overall procedure for model development is shown in Figure 2. By using a program developed to access the PAVER data base and retrieve information for each pavement section, it was possible to obtain data for more than 6,300 cases. This program takes the users' request for family definition based on the uniform conditions of the pavement sections and prints information pertinent to pavement identification, pavement condition, time since the pavement was built or last reconstructed, pavement structure, layer material properties, and traffic. Although the data retrieved are sufficient for family definition, most of the information currently stored in the PAVER

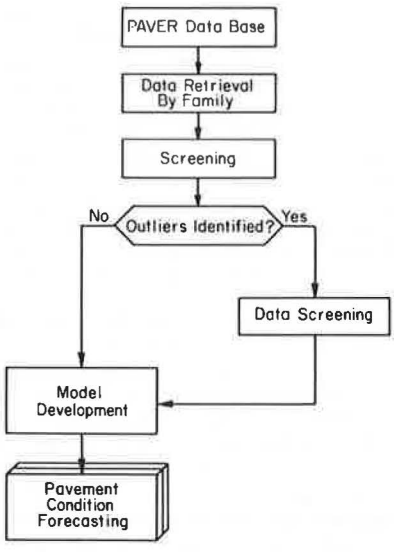

FIGURE 2 Flow diagram of modeling procedure.

data bases pertains to a one-time survey for each section during the lifetime of the pavement. To ensure adequate model development, it would have been desirable to have replicate measurements of pavement field condition and also information for different time periods.

Information on several pavement sections was found to be in error; these errors originated during data collection, coding, or entering in the data base. A screening program that examines the data retrieved for obvious errors was also developed, as explained in a subsequent section of this paper. As shown in the flow diagram in Figure 2, screened data are also examined for outliers that may have a great influence in the model selection phase. A model for pavement condition prediction is developed for each family of pavements, in which the data are averaged every 3 years to obtain a representative point for each 3-year period. The selection of the best prediction model for mathematical condition is based on minimizing prediction errors, as explained later. Finally, PCI prediction of a given section is determined by modifying the prediction curve, depending on the section's present condition relative to the prediction model curve for the pavement family.

CONCEPT OF PAVEMENT FAMILIES

More than one model should exist for a given location to account for the wide variety of factors affecting pavement performance. Therefore, a model should be developed for each family of pavements at each pavement location. Relevant information elements of the pavement sections in the PAVER data bases have been reorganized into pavement family files in which every family is defined by the pavement type, pavement use, and the pavement rank or functional classification. Grouping pavement sections with similar characteristics makes it possible to develop relationships for prediction at an acceptable level of confidence.

The several choices for the selection of a pavement family are as follows:

- Pavement type: asphalt concrete (AC), portland cement concrete, (PCC), asphalt concrete overlay on portland cement concrete (APC), and asphalt concrete overlay on asphalt concrete (AAC);
- Pavement use, which is identified by the service rendered, such as roadways, streets, parking lots, runways, taxiways, or aprons; and
- Pavement rank or functional classification, such as arterials (primary), collectors (secondary), and local roads and streets (tertiary).

The data collection summary for roadways (by pavement family) is given in Table 1 for original pavements (without overlay) and in Table 2 for overlaid pavements. The tables include data from 15 data banks and 94 families for a total of more than 6,300 cases.

DATA SCREENING PROCEDURE

Errors have been identified as those pieces of data in which a mistake was committed when gathering, coding, or entering the data. Pieces of inaccurate data can be found because they break basic system rules; examples are PCI values greater than 100 when the PCI scale is from 0 to 100, or two identical AGE records that show different PCIs. One of the assumptions of this modeling technique is that a section of pavement deteriorates with time at different rates during the life of the pavement; therefore, to eliminate obvious errors but not questionable data the methodology allows the user to define data

TABLE 1 Data Collection Summary for Original Pavements by Pavement Rank for Two Surface Types

	AC					PCC				
Base	Principal	Arterial	Collector	Industrial	Residential	Principal	Arterial	Collector	Industrial	Residential
Ada Co., Idaho	100	110	140	148	188					
Abilene, Texas	159	53				2				
Bellingham, Washington										
Billings, Montana			2	16	75					
Bloomingdale, Illinois	7	12	119	25						
Bryan, Texas		9	17	128	131		4	2	26	19
Calgary, Canada	693					4				
Glenn Ellyn, Illinois		15	25		120					3
Hayward, California	50	22	565							
Niagara, Canada					614					3
Overland Park, Kansas	111	194								
Tacoma, Washington	66	50	55	3	2	9	7	16		
Winnipeg, Canada	4									
Fort Eustis, Virginia	2	4	13			3	4	18		
Great Lakes, Illinois	21	109	72			2	4	12		

Note: AC is asphalt concrete and PCC is portland cement concrete. The numbers in each cell indicate the number of cases in that family.

TABLE 2 Data Collection Summary for Overlaid Pavements by Pavement Rank for Two Surface Types

	AC/AC					AC/PCC				
Base	Principal	Arterial	Collector	Industrial	Residential	Principal	Arterial	Collector	Industrial	Residential
Ada Co., Idaho	17	5	10	12	3	5	2		2	
Abilene, Texas										
Bellingham, Washington	31	22	25	183					2	
Billings, Montana										
Bloomingdale, Illnois										
Bryan, Texas										
Calgary, Canada	194									
Glenn Ellyn, Illinois							8	22		78
Hayward, California	82	42	475							
Niagara, Canada										
Overland Park, Kansas										
Tacoma, Washington	30	35	30	9			2			
Winnipeg, Canada						109				
Fort Eustis, Virginia	44	36	93			2		2		
Great Lakes, Illinois	36	104	95			37	50	17		

Note: AC is asphalt concrete and PCC is portland cement concrete. The numbers in each cell indicate the number of cases in that family.

boundaries. The questionable data are analyzed in a separate part of this methodology under outliers identification.

A flow diagram of the screening procedure is shown in Figure 3. The data are first sorted by pavement section number, time since pavement was built or last reconstructed (AGE), and PCI. Cases of the same section are listed and two rules are applied. First, sequential cases of the same section are compared; if the increase in PCI is greater than 20 points, the case with the high PCI is listed in the Errors file. This indicates either that there is an error in one of the records, or that major rehabilitation has been performed between condition surveys, thus constituting a different family of pavements. Second, for a pavement section with more than one case of the same AGE, if the PCIs are the same, only one case is retained, and if the PCIs are different, all cases are removed and listed in the Errors file.

The following general tests are also applied to every case. Is AGE greater than 30? Is PCI greater that 100? Is the PCI-AGE point outside the boundary? Given that the answer to any of these questions is yes, the case is listed in the Errors file. This mechanistic procedure eliminates obvious problems; however, to ensure appropriate model building, further examination of the data for any unusual observations was performed in the outliers analysis.

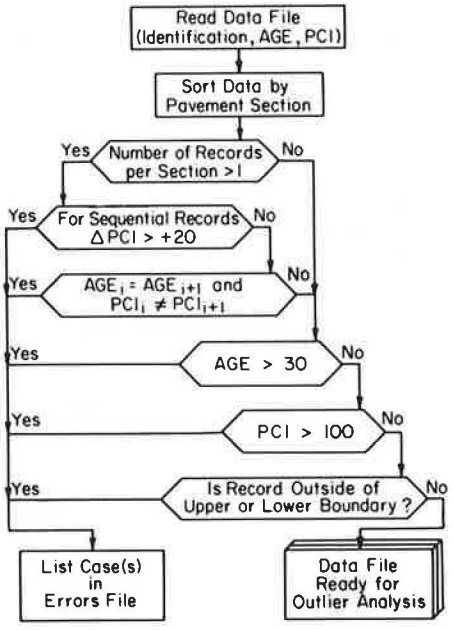

FIGURE 3 Flow diagram of the screening procedure.

OUTLIERS ANALYSIS

Cases with unusual values can have substantial impact in the statistical analysis of pavement condition modeling of a family. Therefore, to identify data with very large or very small values, every family file was subjected to an analysis of residuals based on linear regression analysis. The rate of deterioration, which represents the reduction in PCI over a given time period, was initially included for outliers identification. The frequency distribution of the rate of deterioration was plotted and found to be skewed to the left, that is, the concentration of the rate of deterioration values was greatest around the lower rate of deterioration. Therefore, setting a confidence interval for data screening based on the rate of deterioration was not possible because data points with very low rates of deterioration could not be observed.

A technique for outliers identification based on residuals analysis was then applied to the data. Residuals are calculated as the difference between the observed value and the value predicted by a linear regression model of PCI against AGE. The frequency distribution of residuals was found to be normal, thus lending itself to setting confidence intervals. This is always the case with the residuals frequency plot even if the distribution of the components is markedly nonnormal (3). The standard deviation of the residuals was used as a measure of spread to observe the relative magnitude of any particular residual.

The regression subprogram of the Statistical Package for the Social Sciences (SPSS) software for personal computers was used to find the best-fit mathematical function between PCI as the dependent variable and AGE as the independent variable (4). A sample output of the regression analysis using SPSS is shown in Figure 4. A straight-line function obtained by the least-squares analysis was used to predict PCI values. After building an equation, several types of residuals and related statistics were requested from the analysis of residuals feature of SPSS. These residuals were used to locate outliers and examine basic regression assumptions. A list of the 10 most extreme normalized residuals was generated along with a histogram of normalized residuals. The normal probability of the residuals and cases

```
SHOW.
INCLUDE 'C:\SPSS\DATA\2ADACA.FIL'.
DATA LIST FILE = '\SPSS\DATA\2ADACA.PRN'/
                 AGE 1-6 (3) PCI 7-10.
VARIABLE LABELS  AGE   'TIME SINCE LAST DAY OF CONSTRUCTION'
                 PCI   'PAVEMENT CONDITION INDEX'.
REGRESSION VARIABLES = AGE PCI /
The raw data or transformation pass is proceeding
SPSS/PC has written      99 cases to the active file
STATISTICS = SES DEFAULTS/
DEPENDENT = PCI/
METHOD = ENTER AGE/
RESIDUALS = ID (AGE) DEFAULTS.

Page   2                    SPSS/PC  Release 1.10                    2/11/86

        * * * *   M U L T I P L E   R E G R E S S I O N   * * * *

Listwise Deletion of Missing Data

Equation Number 1    Dependent Variable..   PCI   PAVEMENT CONDITION INDEX

Beginning Block Number  1.  Method:  Enter       AGE


Variable(s) Entered on Step Number
   1..     AGE        TIME SINCE LAST DAY OF CONSTRUCTION


Multiple R            .43175
R Square              .18641
Adjusted R Square     .17802
Standard Error      13.91469

Analysis of Variance
                    DF        Sum of Squares       Mean Square
Regression           1           4303.08850        4303.08850
Residual            97          18780.99231         193.61848

F =      22.22458        Signif F =  .0000

---------------------- Variables in the Equation -------------------------

Variable                B         SE B        Beta     SE Beta          T  Sig T

AGE             -1.05768       .22436     -.43175      .09158     -4.714  .0000
(Constant)      73.75811      3.07865                              23.958  .0000


End Block Number   1   All requested variables entered.
```

FIGURE 4 Sample output of the regression analysis using SPSS.

**** MULTIPLE REGRESSION ****

Equation Number 1 Dependent Variable.. PCI PAVEMENT CONDITION INDEX

Residuals Statistics:

	MIN	MAX	MEAN	STD DEV	N
*PRED	44.0552	72.6126	60.8283	6.6264	99
*RESID	-30.2089	28.7069	-.0000	13.8435	99
*ZPRED	-2.5313	1.7784	.0000	1.0000	99
*ZRESID	-2.1710	2.0631	-.0000	.9949	99

Total Cases = 99

Durbin-Watson Test = 1.56509

* *

Outliers - Standardized Residual

Case #	AGE	*ZRESID
23	8.083	-2.17101
40	5.167	2.06307
78	2.083	1.90051
29	6.917	-1.90030
56	2.000	1.89420
57	17.000	-1.85254
39	5.167	1.84747
15	14.000	-1.79311
7	24.083	1.77612
47	21.167	1.77006

Histogram - Standardized Residual

```
NExp N      (* = 1 Cases,    . : = Normal Curve)
0  .08   Out
0  .15  3.00
0  .39  2.67
0  .88  2.33 .
4 1.81  2.00 *:**
6 3.31  1.67 **:***
4 5.43  1.33 ****.
7 7.98  1.00 *******.
9 10.5   .67 ********* .
* 12.4   .33 ********** .
* 13.1  0.0  ************:**
* 12.4  -.33 ***********.
* 10.5  -.67 **********:*
8 7.98 -1.00 *******:
8 5.43 -1.33 ****:***
2 3.31 -1.67 **.
2 1.81 -2.00 *:
1  .88 -2.33 :
0  .39 -2.67
0  .15 -3.00
0  .08   Out
```

* *

Normal Probability (P-P) Plot
Standardized Residual

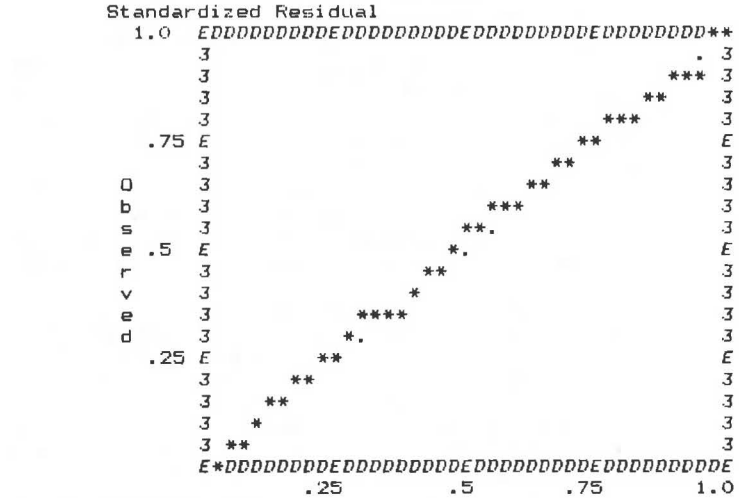

FIGURE 4 (continued)

that fall outside the normal curve were identified. The probability that a deviation in either direction will exceed three standard deviations is close to zero. Therefore, any deviation larger than three standard deviations was assumed to be out of the expected values and the case was listed as an outlier. The selection of three standard deviations for outliers may be ultraconservative and thus a normal probability value of 2.5 may be used for outlier analysis.

MODEL DEVELOPMENT

Preliminary analysis and results from previous studies (1) have shown that PCI is strongly related to AGE for a given pavement family and that no significant correlation can be found with the other data base variables, given that families of pavements were correctly defined. For example, runways and aprons were not combined in one family. Therefore, linear regression models and hi-order polynomial regression equations for PCI prediction as a function of AGE were investigated for their use in this research project.

After errors and outliers were eliminated from the data files, model development for each family followed. The first approach attempted for PCI forecasting was stepwise regression using the SPSS (4). A scattergram of the PCI and AGE variables was examined. The plot revealed a curvilinear relationship between the variables. This can be observed in Figures 5-7, in which PCI is plotted as a function of AGE for three different families. Although it was clear that the relationship between AGE and PCI follows a curve of second or third order, the least-squares stepwise regression method was always selecting a straight-line regression equation as the best fitting model. This was attributed to the imbalance of the number of cases in each pavement category and the inability of regression models to explain inflection points, as demonstrated by the figures.

The stepwise regression method is the best variable selection procedure: it is fast and works with one independent variable at a time while improving the equation at every step. However, stepwise regression makes an automatic insertion of a variable determined by a test of significance, and judgment is still required in the examination of the final model (5).

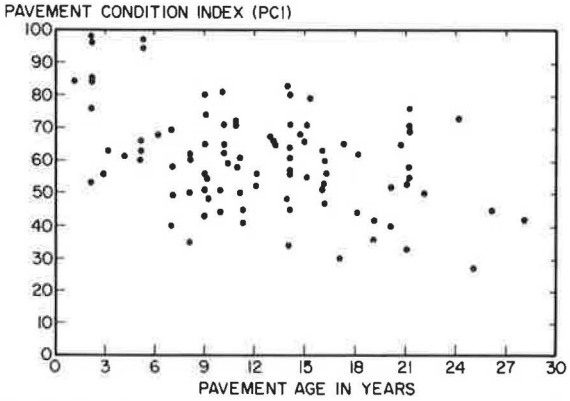

FIGURE 5 Scatterplot of PCI versus AGE for an AC surface pavement—primary road family.

Because a polynomial function based on stepwise regression could not be obtained for any family, the data were divided in two groups, one for pavement sections with a PCI of from 0 to 60 and the other for sections with a PCI of from 61 to 100. A PCI of 60 was assumed to represent the main inflection point in a PCI versus AGE curve. Multiple regression analysis was then performed for both groups and a curve of the desirable shape was found for each group of data. However, this procedure could not be used as an overall prediction model because the curves did not converge at the PCI point of 60, preventing the creation of a continuous curve for PCI prediction that would describe the total range of AGE.

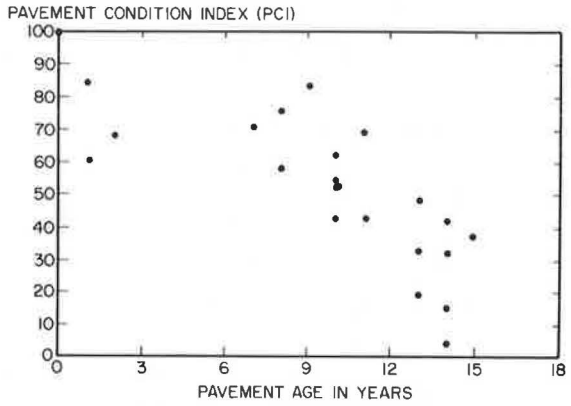

FIGURE 6 Scatterplot of PCI versus AGE for an AC surface pavement—tertiary road family.

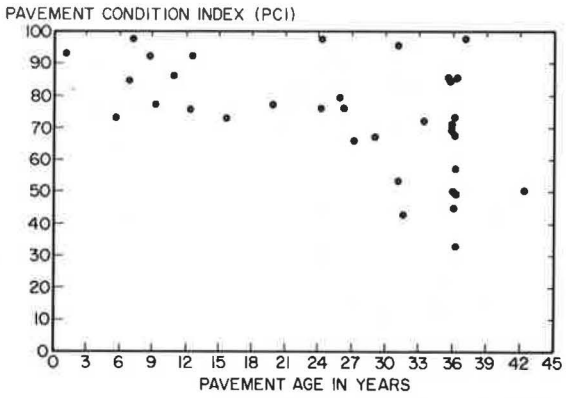

FIGURE 7 Scatterplot of PCI versus AGE for an AC/AC surface pavement—secondary road family.

The data were then grouped for different AGE ranges and the best regression line was fitted through points that represented the average of each group. This was done under the assumption that the average pavement condition in a given AGE range weighs equally regardless of the number of points existing in a given range. By grouping the data for AGE ranges of 3 years, a third-order polynomial could easily be fitted. This is shown in Figures 8, 9, and 10, in which third-degree polynomials were fitted for the data shown in Figures 5, 6, and 7, respectively.

To obtain a measure of the acceptability of this relationship, the mean squares (MS) of the deviations of the observed Yi from the predicted Yi by models representing first-, second-, and third-order polynomials were compared, as shown in Table 3. The root mean squares (RMSs) calculated as the square root of MS divided by the sample size is always lower for the third-order polynomial, thus showing the advantage of choosing a third-degree polynomial for modeling PCI-AGE of a given pavement family.

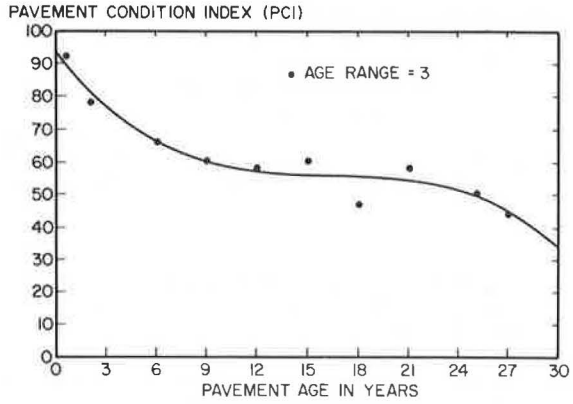

FIGURE 8 Third-order polynomial regression for an AC surface pavement—primary road family.

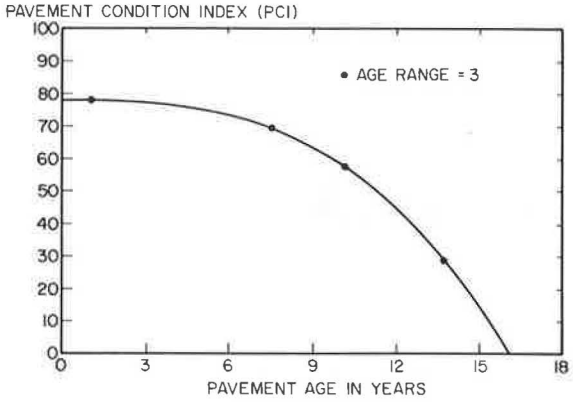

FIGURE 9 Third-order polynomial regression for an AC surface pavement—tertiary road family.

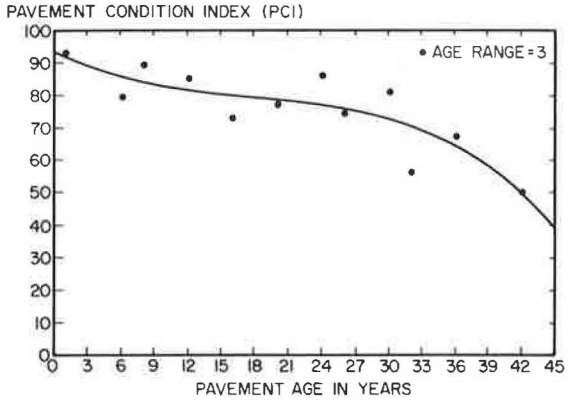

FIGURE 10 Third-order polynomial regression for an AC/AC surface pavement—secondary road family.

PAVEMENT CONDITION FORECASTING

The prediction models were developed to represent the average behavior of an entire pavement family. Therefore, PCI prediction for each section should be modified depending on its relative position to the curve. To predict the future PCI of a section, a curve is drawn through the present PCI-AGE point, which is parallel to the prediction model curve for the pavement family at equal condition. The PCI can then be determined at the desired future AGE by reading from the later curve. This is shown in Figure 11, in which a given section of the road presented by the dot is 10 years old with a PCI of 70. By drawing curve parallel to the family curve through the point and looking for the pavement condition at year 20, PCI is predicted to be 56 within 10 years.

In this technique, it is assumed that the deterioration of pavements is a function of their present condition regardless of AGE. Therefore, the technique is likely to produce more accurate results for short-term prediction than for long range (i.e., 20 years). Because budget planning for maintenance and repair is usually prepared for a 5-year period, and because the models are continuously updated when new condition data are made available, this technique is expected to yield acceptable results at the network and project levels. Other techniques are also currently being investigated by USA-CERL and will be reported on in the future.

TABLE 3 Comparison of Root Mean Squares

Family	Order of Polynomial Line		
	First	Second	Third
AC pavement, primary road	14.11	13.75	13.11
AC pavement, tertiary road	14.37	12.94	12.88
AC/AC pavement, secondary road	14.47	14.48	14.37

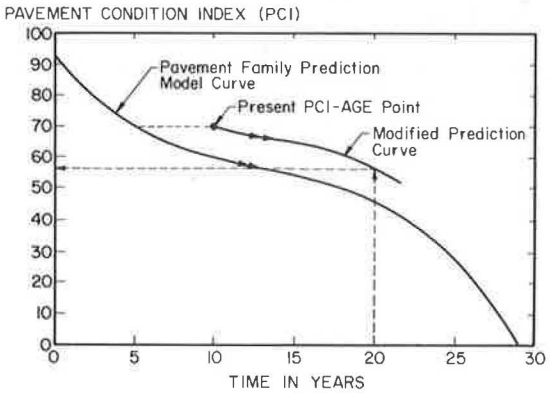

FIGURE 11 Example of pavement condition forecasting.

SUMMARY

Data available in the PAVER pavement management system were used in the form of pavement families for outlier analysis and modeling of pavement condition. A pavement family is defined by pavement type, pavement use, and pavement rank or functional classification. Grouping of pavement sections by their similar conditions made it possible to develop relationships for prediction at an acceptable level.

A screening procedure was designed to clean the data of each family from obvious errors. To ensure appropriate model building, a statistical outliers analysis was also developed. The outliers procedure is based on an examination of the residuals of a straight-line regression model. For pavement condition model development, the AGE data were averaged every 3 years to obtain a representative point for each 3-year period. This point was then used in the final polynomial regression analysis. Pavement condition forecasting was accomplished by customizing the prediction for each individual section depending on its condition in relation to the prediction model curve for the pavement family. The family models were designed to be easily updated by PAVER

users when new pavement condition data are entered to their PAVER data bases.

REFERENCES

1. D.E. O'Brien, S.D. Kohn, and M.Y. Shahin. Prediction of Pavement Performance by Using Nondestructive Test Results. In Transportation Research Record 943, TRB, National Research Council, Washington, D.C., 1983, pp. 13-17.
2. M.Y. Shahin and S.D. Kohn. Pavement Maintenance Management for Roads and Parking Lots. Technical Report M-294. Construction Engineering Research Laboratory, U.S. Army Corps of Engineers, Champaign, Ill., Oct. 1981.
3. D.V. Huntsberger and P. Billingsley. Elements of Statistical Inference. Allyn and Bacon, Inc., March 1979, 4th ed.
4. M.J. Norusis. Statistical Package for the Social Sciences (SPSS/PC for the IBM/XT). SPSS Inc., Chicago, Ill., 1984, 624 pp.
5. N.R. Draper and H. Smith. Applied Regression Analysis. Wiley Series in Probability and Mathematical Statistics, New York, Jan. 1981, 2nd ed.

The views of the authors do not purport to reflect the position of the Department of the Army or the Department of Defense.

Publication of this paper sponsored by Committee on Monitoring, Evaluation and Data Storage.

Use of Surface Waves in Pavement Evaluation

SOHEIL NAZARIAN and KENNETH H. STOKOE II

ABSTRACT

Material characterization of pavement systems in situ is required for determining load capacity and assessing the performance and possible need for rehabilitation or replacement of the system. Nondestructive tests are usually carried out for this purpose. Desirable features of nondestructive tests are speed of operation, economy, and a sound theoretical basis compatible with the in situ data collection procedure. The most popular methods in this category are the falling weight deflectometer (FWD) and the Dynaflect. These methods are fast for in situ data collection; however, a rigorous data-reduction algorithm that can result in a unique solution and take into account the effect of the dynamic nature of the load has only begun to be developed. An alternative method of nondestructive testing has been under continuous development at the University of Texas. This method is called the spectral-analysis-of-surface-waves (SASW) method and is based on the theory of stress waves propagating in elastic media. The SASW method can be utilized to determine Young's modulus profiles of the pavement structure and underlying soil as well as the thickness of each layer. In this paper the theoretical aspects of the SASW method are discussed in detail. The experimental procedure is included only briefly because it has been presented comprehensively in earlier papers. Several case studies on different types of pavements with various thicknesses are presented to demonstrate the utility and versatility of the SASW method. In each case, the results are compared with those of the well-established crosshole seismic test that was performed at the same locations. The Young's modulus profiles from these two independent methods compare closely.

The spectral-analysis-of-surface-waves (SASW) method of testing pavements in situ has been under development at the University of Texas since 1980. The objectives of performing SASW tests are to determine elastic moduli and thicknesses of the different layers nondestructively and rapidly. The method is based on generation and detection of stress waves, specifically surface waves. The theory of elastic waves in layered media is utilized to reduce and analyze data collected in the field.

The practical aspects of the SASW method have been presented by Heisey et al. (1), Nazarian et al. (2), and Nazarian and Stokoe (3). This paper concentrates on the theoretical aspects of the method. First, a brief background of the theory of wave propagation in an elastic, solid medium is discussed. The dispersion characteristics of surface waves, the basis for the SASW method, are presented. Data collection and reduction are then discussed. Finally, two case

University of Texas at Austin, Austin, Tex. 78712.

studies are presented that demonstrate the key theoretical aspects of the SASW method.

THEORETICAL BACKGROUND

Elastic Waves in a Layered Half-Space

If an elastic half-space is disturbed by a vertical impact on the surface, two types of waves will propagate in the medium: body and surface waves.

The first type, body waves, propagate radially outward in the medium. Body waves are composed of two different types: compression and shear waves. These waves are differentiated by the direction of particle motion relative to the direction of wave propagation. Particle motions associated with shear waves are perpendicular to the direction of wave propagation whereas particle motions associated with compression waves are parallel to the direction of wave propagation.

The second type of wave is the surface wave. Surface waves resulting from a vertical impact are primarily Rayleigh waves. Rayleigh waves propagate away from the impact along a cylindrical wavefront near the surface of the medium, and particle motion near the surface forms a retrograde ellipse. Miller and Pursey have shown that for a vertical impact more than 67 percent of the energy propagates as Rayleigh waves (4).

The velocity of propagation of the different waves are related by Poisson's ratio. Compression waves (P-waves) propagate faster than shear waves (S-waves). As Poisson's ratio (ν) increases from zero to 0.5, the ratio of P-wave to S-wave velocities increases from 1.4 to infinity. (A value of ν equal to 0.5 represents an incompressible material that theoretically has an infinite P-wave velocity.) This matter is also true for the ratio of Rayleigh wave (R-wave) to shear wave velocity. However, the variation of this ratio is small and varies from 0.86 to 0.95 for Poisson's ratios of zero and 0.5, respectively.

Velocity of propagation is a direct indicator of the stiffness of the material. In other words, Young's modulus and shear modulus of a layer can be easily determined if the shear wave velocity, compression wave velocity, or both are unknown. The relationships between velocities and moduli are as follows:

$$G = \rho (V_s)^2 \tag{1}$$

$$E = 2G(1 + \nu) = 2\rho\ (V_s)^2\ (1 + \nu) \tag{2}$$

or

$$E = \rho\ (V_p)^2\ [(1 + \nu)(1 - 2\nu)/(1 - \nu)] \tag{3}$$

where

G = shear modulus,
E = Young's modulus,
ρ = mass density,
V_s = shear wave velocity,
ν = Poisson's ratio, and
V_p = compression wave velocity.

As such, if the propagation velocities of body waves can be measured, the elastic moduli can readily be calculated by Equations 1-3.

Dispersive Characteristic of Surface Waves

In a homogeneous, isotropic, elastic half-space, R-wave velocity does not vary with frequency. However, R-wave velocity varies with frequency in a pavement system because of the layering (variation of stiffness with depth). This frequency dependency of surface wave velocity in a layered system is termed dispersion, and a plot of velocity versus frequency (or wavelengths) is called a dispersion curve.

The dispersive characteristic of surface waves can be demonstrated by examining the phase velocity. Phase velocity is defined as the velocity with which a seismic disturbance of a given frequency propagates in a medium. To investigate this matter, an idealized layered half-space is shown in Figure 1. Each layer of the half-space has a known shear wave velocity,

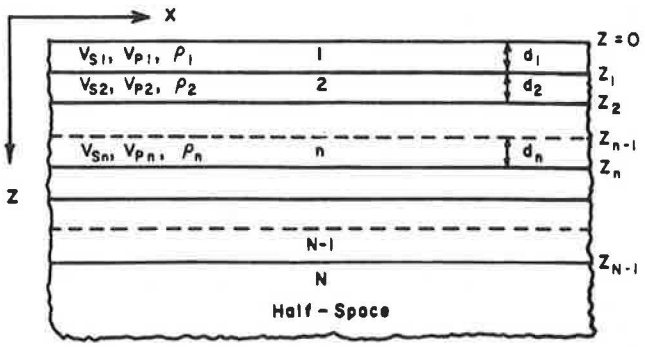

FIGURE 1 Idealized layered half-space.

compression velocity, Poisson's ratio, and mass density. For simplicity, assume that a harmonic disturbance with a known frequency (f) is applied to the surface of the medium and this disturbance propagates with a phase velocity (V_{ph}) in the horizontal direction. The objective is to find a relationship between frequency and phase velocity, that is, an equation with the form of

$$g\ (f,\ V_{ph}) = 0 \tag{4}$$

If the disturbance is not harmonic, it can be decomposed into a number of harmonic waves utilizing Fourier transform principles. Thomson introduced the first matrix solution to this problem in an elastic layered medium (5). However, this work contained a small error in assuming boundary conditions, which was later corrected and reworked by Haskell (6). In this approach, the relationship between phase velocity and frequency is obtained by setting a determinant equal to zero. The elements of the determinant are functions of propagation velocities and densities of the various layers as well as phase velocity and frequency. If there are N layers in the medium, 4N - 2 equations of motions will be obtained.

However, there will be 4N - 2 boundary conditions as well. These boundary conditions consist of compatibility of stresses and continuity of displacements at each boundary. In other words, at the interface of adjoining layers, normal and shear stresses at the bottom of the upper layer should be equal to those at the top of the lower layer. In the same manner, the horizontal and vertical displacements of each layer should be equal at the interface. The other boundary conditions consist of shear and normal stresses at the free surface, which are set equal to zero. The simultaneous solutions of these equations will result in a relationship in the form of Equation 4. The Haskell-Thomson solution forms the basis for a systematic computational procedure that can be easily programmed.

To elaborate on this matter, the equations of motion in the nth layer can be written as follows:

$$\nabla^2\phi_n = 1/(V_{pn})^2 \cdot \partial^2\phi_n/\delta t^2 \quad (5)$$

$$\nabla^2\psi_n = 1/(V_{sn})^2 \cdot \partial^2\psi_n/\delta t^2 \quad (6)$$

where

$$\nabla^2 = (\partial^2/\partial x^2) + (\partial^2/\partial z^2) \quad (7)$$

and where t = time, x = horizontal direction, z = vertical direction, and ϕ_n and ψ_n are two potentials corresponding to compression and shear wave velocities of the nth layer, respectively.

It can be shown that, by using the Fourier transform, Equations 5 and 6 can be written as

$$d^2\phi_n/dz^2 = r_n^2\phi_n \quad (8)$$

$$d^2\psi_n/dz^2 = s_n^2\psi_n \quad (9)$$

where

$$r_n^2 = k^2 - k_{pn}^2 = (\omega^2/V_{ph}^2) - (\omega^2/V_{pn}^2) \quad (10)$$

$$s_n^2 = k^2 - k_{sn}^2 = (\omega^2/V_{ph}^2) - (\omega^2/V_{sn}^2) \quad (11)$$

and k, k_{pn}, and k_{sn} are termed the wave numbers for V_{ph}, V_p, and V_s, respectively; Φ and Ψ are two potentials corresponding to compression and shear wave velocities of the nth layer, respectively (displacement potential in frequency domain). (Wave number is defined as the ratio of rotational frequency, ω ($\omega = 2\pi f$), to propagation velocity.) The solutions to Equations 8 and 9 are

$$\Phi_n = U_{pn}\exp(ir_nz) + D_{pn}\exp(-ir_nz) \quad (12)$$

$$\Psi_n = U_{sn}\exp(is_nz) + D_{sn}\exp(-is_nz) \quad (13)$$

where U_{pn} and U_{sn} are coefficients of terms corresponding to upgoing P-waves and S-waves, respectively; and $I = -1^{1/2}$. Similarly, D_{pn} and D_{sn} correspond to coefficients of terms associated with P-waves and S-waves propagating downward in the layer. To calculate these four factors for each layer, the boundary conditions discussed earlier must be applied. In other words, displacements and stresses should be continuous at each interface of two adjacent layers. Displacements and stresses are related to potentials Φ_n and Ψ_n as follows:

$$u_n = (\partial\Phi_n/\partial z) + (\partial\Psi_n/\partial x) \quad (14)$$

$$w_n = (\partial\Phi_n/\partial z) - (\partial\Psi_n/\partial x) \quad (15)$$

$$\sigma_n = \lambda_n\nabla^2\Phi_n + 2G_n[(\partial^2\Phi_n/\partial z^2) - (\partial^2\Psi_n/\partial z\partial x)] \quad (16)$$

$$\tau_n = G_n[(2\partial^2\Phi_n/\partial x\partial z) - (\partial^2\Psi_n/\partial x^2) + (\partial^2\Psi_n/\partial z^2)] \quad (17)$$

where

u_n and w_n = horizontal and vertical displacements in the nth layer,
σ_n and τ_n = normal and shear stresses in the nth layer, and
λ_n and G_n = Lame's constant and shear modulus of the nth layer.

U_{pN} and U_{sN} are equal to zero as no wave propagates upward from the last layer, which is considered to be a half-space. Also, it should be noted that σ_1 and τ_1 at the surface (i.e., top of Layer 1) should be equal to zero. By imposing these boundary conditions, the displacements at the surface can be related to the potentials of the bottom layer in matrix form as

$$\{P\} = [R]\{S\} \quad (18)$$

where

$$\{P\} = [U_{pN} = 0 \; U_{sN} = 0 \; D_{pN} \; D_{sN}]^T \quad (19)$$

$$\{S\} = [u_1 \; w_1 \; \sigma_1 = 0 \; \tau_1 = 0]^T \quad (20)$$

R is a 4 x 4 matrix that related potentials to displacements and has a twofold purpose: to propagate waves in each layer and to maintain continuity of stresses and displacements at each boundary.

In expanded form Equation 18 can be written as:

$$\begin{Bmatrix} 0 \\ 0 \\ D_{pN} \\ D_{sN} \end{Bmatrix} = \left[\begin{array}{cc:cc} r_{11} & r_{12} & r_{13} & r_{14} \\ r_{21} & r_{22} & r_{23} & r_{24} \\ \hdashline r_{31} & r_{32} & r_{33} & r_{34} \\ r_{41} & r_{42} & r_{43} & r_{44} \end{array}\right] \times \begin{Bmatrix} u_1 \\ w_1 \\ 0 \\ 0 \end{Bmatrix} \quad (21)$$

The matrices are subdivided as shown by dotted lines such that:

$$\begin{Bmatrix} 0 \\ A \end{Bmatrix} = \begin{bmatrix} R_{11} & R_{12} \\ R_{21} & R_{22} \end{bmatrix} \times \begin{Bmatrix} B \\ 0 \end{Bmatrix} \quad (22)$$

which leads to two equations. The equation of interest for this study for ease of mathematical operations is

$$R_{11} \cdot B + R_{12} \cdot 0 = 0 \quad (23)$$

or

$$R_{11} \cdot B = 0 \quad (24)$$

For a nontrivial solution, one must have

$$\det(R_{11}) = 0 \quad (25)$$

The only unknowns in this equation are frequency and phase velocity, so that by assuming a frequency, a corresponding phase velocity can be calculated; this function is called the dispersion function. To solve this problem for a certain frequency numerically, $\det(R_{11})$ is calculated for increments of phase velocity and the root is found when the value of the determinant changes sign.

In evaluating $\det(R_{11})$, the Haskell-Thomson solution encounters numerical instability at high frequencies that are necessary in pavement testing. This instability arises from the generation of large numbers at high frequencies in some intermediate steps. Dunkin proposed an approach to eliminate this instability (7); in his approach, the determinant is calculated directly, thus bypassing the generation of large numbers. [For more details, the reader is referred to Nazarian (8).]

Different characteristics of motion can be expected depending on the values of r and s defined by Equations 10 and 11, respectively. If r^2 and s^2 are both positive (i.e., phase velocity is less than P-wave and S-wave velocities) the roots of the dispersion equation are real and correspond to normal propagation modes of surface waves. However, if r^2 and/or s^2 becomes negative, r and/or s will become

imaginary, which results in modes of propagation analogous to so-called leaky modes. In this condition, the solutions are associated with the modes that give rise to complex phase velocities, which are attenuated with distance. The imaginary part of the complex velocity corresponds to viscous-type damping in the system (no geometrical damping is assumed in the solution). Therefore, the wave will attenuate with distance. In these cases, the solution is sought by assuming a multilayered plate resting on a layered half-space representing the pavement. The solution to this problem is similar to the normal mode solution presented and, to avoid redundancy, is not presented here; however, it can be found in Ewing et al. (9).

Parametric Study of Dispersive Characteristics of Surface Values

In the last section, the dispersion function was calculated, which is a relationship between frequency and phase velocity. If different frequencies are assumed and the phase velocity associated with each frequency is calculated and plotted, the outcome will be a curve called a dispersion curve. The shape of the dispersion curve is affected by three independent properties of each layer in a given profile. The factors being considered as independent are (a) shear wave velocity, (b) Poisson's ratio, and (c) mass density. Other combinations of parameters can be assumed, such as shear modulus instead of shear wave velocity, or compression wave velocity instead of Poisson's ratio. However, shear wave velocity is the major factor in determining a dispersion curve.

As mentioned earlier, surface waves are dispersive in a continuous elastic medium only if there are velocity contrasts in the layering. For instance, the dispersion curve of a stiff layer, say concrete, underlain by a softer half-space with a shear wave velocity equal to 1/7 of that of the thin layer, is shown in Figure 2. This velocity contrast corresponds to a ratio of elastic moduli of approximately 1:50 for values of Poisson's ratios and mass densities that are equal for the two materials. In the figure, the wavelengths are normalized relative to the height of the stiff layer, and the phase velocities are normalized relative to the shear wave velocity of the half-space. Theoretically, many different modes of vibration exist; however, in this discussion only the fundamental modes of vibration are considered.

The dispersion curve consists of two branches. The first branch, marked I, corresponds to the flexural mode of vibration of a plate (pavement) modified because of the existence of the underlying half-space (subgrade). The second branch, marked II, corresponds to the interfacial mode of propagation [Ewing et al. (9)], which at high frequencies becomes asymptotic to the P-wave velocity of the half-space (shown as II*).

It is also interesting to note in Figure 2 that for a normalized wavelength of 10 the ratio of phase velocity to S-wave velocity of the half-space is approximately 1.5. This clearly indicates that if inversion was not performed, the modulus determined for the half-space would be more than 2.2 times greater than actual modulus.

Also shown in Figure 2 is a dispersion curve corresponding to the same layering as the example just cited, except that the ratio of shear wave velocities of the thin layer relative to the half-space is equal to 3. In this case, the phase velocity reduces to the S-wave velocity of the half-space at a normalized wavelength of approximately 5.

A comparison of the dispersion curve of a two-layered system with that of a three-layered system consisting of a layer of stiff material, say concrete, over an intermediate layer, say base, over soil is shown in Figure 3. It can be observed that the addition of the extra layer has further shifted the dispersion curve toward higher velocities.

The effects of Poisson's ratio and density on the dispersion curves have been investigated and are found to be small [Nazarian (8), Ewing et al. (9)]. For instance, if Poisson's ratio varies from 0.15 to 0.49, the range of normalized velocity varies only

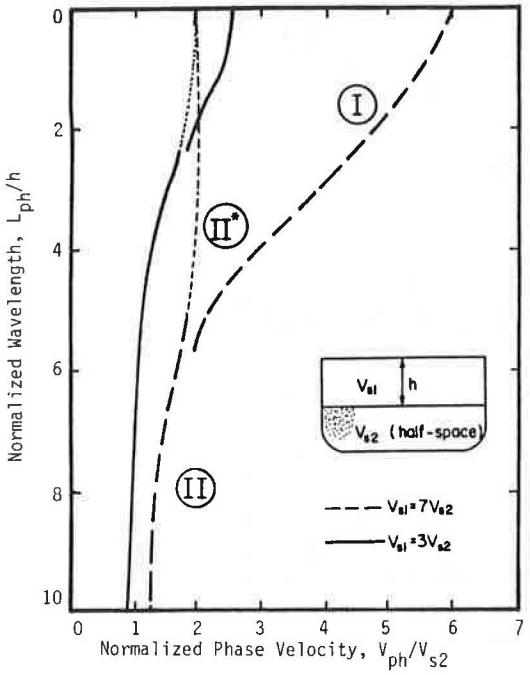

FIGURE 2 Theoretical dispersion curves for stiff layer underlain by elastic half-space.

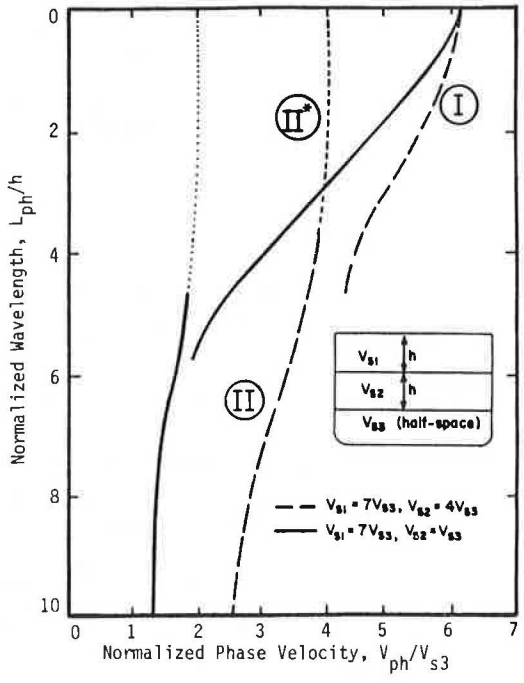

FIGURE 3 Comparison of theoretical dispersion curves for two-layered and three-layered media.

by about 10 percent in most profiles. The effect of density is even less than Poisson's ratio in the range of interest in most engineering problems.

TESTING PROCEDURE

Application of the SASW method to field testing has been discussed in detail by Nazarian et al. (2) and Nazarian and Stokoe (3). However, for completeness a brief overview of the method is presented here.

Field Procedure

Two receivers are attached to the surface of the pavement, as shown in Figure 4a. By means of a hammer blow, a transient impact is delivered to the pavement surface. Such an impact generates energy over a wide range of frequencies. Each frequency has an associated wave that propagates outward from the source along a cylindrical wavefront. Each wave has a wavelength that depends on the stiffness of the material and frequency of the wave. One important characteristic of the Rayleigh wave is that wave energy decays rapidly with depth such that at a depth equal to 1.5 times the wavelength the amplitude of the motion is only 1/10 that at the surface. As a result, different frequencies sample different amounts of material (different depths).

The signal generated by the impact is monitored by a recording device for further analysis. The recording device used is a waveform analyzer. The time-domain record from each receiver is transformed into the frequency domain. This process is repeated several times, and the records are averaged. Averaging is used as a tool to enhance and improve the quality of the signals. Spectral analyses are then performed on the enhanced records. The aspects of spectral analyses of interest in this method are the coherence function and the phase information of the cross power spectrum.

The coherence function is used to visually inspect the quality of signals being recorded in the field. On averaging the signals, the coherence function will have a real value between zero and one in the range of frequencies being measured. A value of one indicates perfect correlation between the signals being picked up by the receivers (which is equivalent to a signal-to-noise ratio of infinity). Similarly, a value of zero for the coherence function at a frequency represents no relation between the signals being detected. With this approach, data collected in the field can be conveniently checked in the field, and the test can be modified and repeated if necessary. In addition, the range of frequencies that is contaminated can be identified and omitted during in-house reduction.

The phase information of the cross power spectrum is used to obtain the relative phase shift at each frequency. This phase shift results from the waves sensed at the near receiver having to travel an additional distance X to be sensed at the far receiver. This phase shift can be translated into travel time, as discussed later (Equation 26).

To eliminate the effect of any internal phase shift associated with the receivers and recording device, the test is repeated from the reverse direction; that is, without removing the receivers the impact is applied to the other side of the receiver

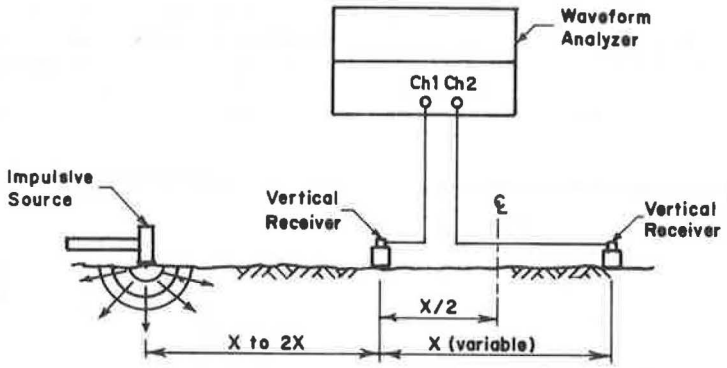

(a) General Configuration of SASW Testing

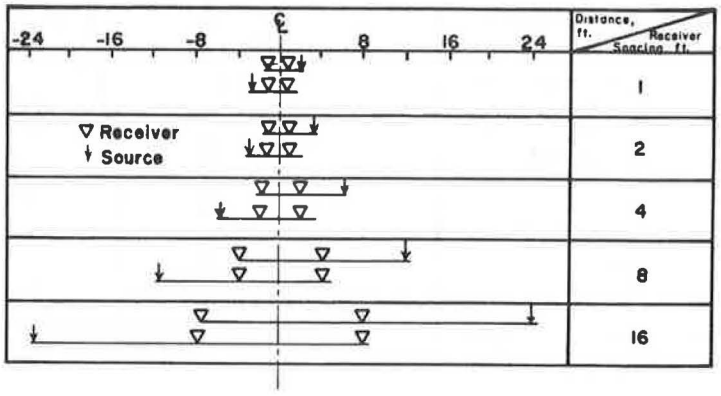

(b) Common Receivers Midpoint Geometry

FIGURE 4 Schematic of experimental arrangement for SASW testing *(3)*.

array. In this case the far receiver of the previous tests is the near receiver of the current test, as shown in Figure 4b.

Because of limitations of the recording device and range of frequencies that can be generated with a single source, testing is performed at several receiver spacings. A pattern for performing the test has been developed, which is called a common-receiver-midpoint array (shown in Figure 4b). In this pattern the receivers are spread equidistantly about an imaginary centerline. Close spacings are used to sample near-surface materials; hence, the source should be able to generate higher frequencies at these spacings. As the spacing is increased, deeper materials are sampled, and lower frequency ranges with more energy should be generated.

Data Reduction

Data reduction consists of two phases. First, data collected in the field have to be converted to a dispersion curve, which is considered the raw data. Second, the shear wave velocity profile is obtained by inverting the dispersion curve. By knowing the shear wave velocity profile and by estimating or knowing mass densities and Poisson's ratios, the Young's modulus profile can be obtained. Construction of dispersion curves has been discussed in detail in Nazarian and Stokoe (3). In summary, the range of frequencies with a coherence value of more than 0.90 is selected from the record. For each frequency (f) in this range, the phase shift is picked from the phase information of the cross power spectrum. Knowing the phase (ϕ), the travel time (t) can be calculated by

$$t = \phi/360f \quad (26)$$

and the phase velocity (V_{ph}) can be obtained by

$$V_{ph} = X/t \quad (27)$$

where X is the distance between the receivers. The wavelength L_{ph} is related to velocity and frequency by

$$L_{ph} = V_{ph}/f \quad (28)$$

The procedure can be demonstrated as follows. Typical records from spectral analyses performed on signals measured on an asphaltic-concrete pavement are shown in Figure 5. The upper record (Figure 5a) is the coherence function and the lower record (Figure 5b) is the phase information from the cross power spectrum. The dispersion curve constructed from this record is shown in Figure 6a in the range of wavelengths of 0.5 to 2 ft. The same curve is shown in Figure 6b except that only every sixth data point is plotted. The solid circles numbered 1 to 5 in Figure 6b correspond to the points marked as 1 to 5 on the phase information of cross power spectrum in Figure 5b. These points are positioned every 1,000 Hz at frequencies from 1,000 to 5,000 Hz. The process of calculation of phase velocity and wavelength from the phase and frequency data for Point 3 is as follows.

Given

Frequency = f = 3,000 Hz.
Raw phase = ϕ' = -32.50°, and
Receiver spacing = x = 1 ft.

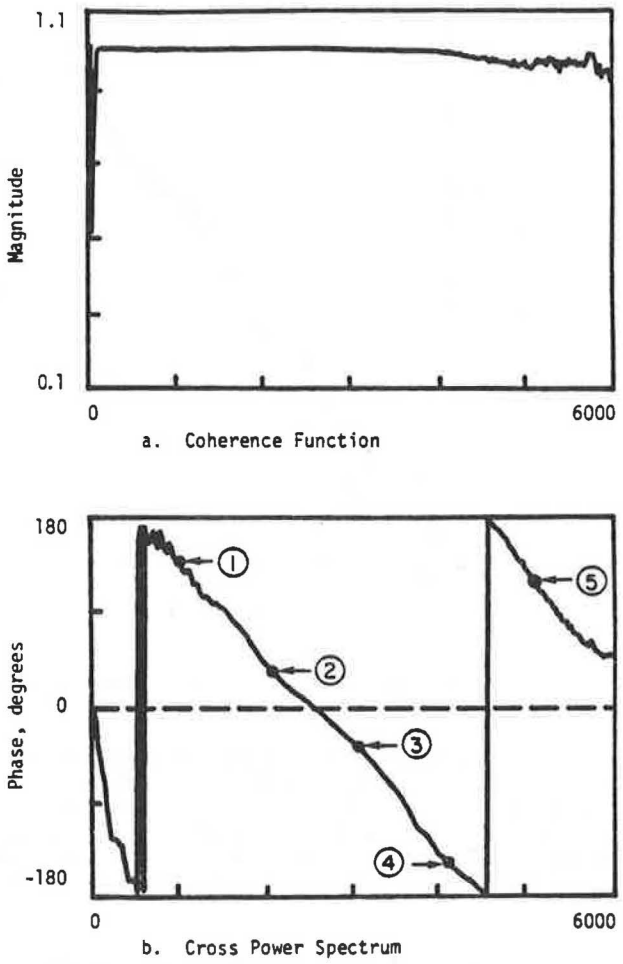

FIGURE 5 Typical spectral analysis measurements on a pavement.

Then

1. Actual phase (ϕ):

ϕ = 360 - (-32.50) = 392.50°

2. Travel time (t), using Equation 26:

t = 392.50/(360 x 3,000) = 0.36 x 10^{-3} sec

3. Phase velocity (V_{ph}), using Equation 27:

V_{ph} = 1/(0.36 x 10^{-3}) = 2,778 ft/sec

4. Wavelength (L_R), using Equation 28:

L_R = 2,778/3,000 = 0.92 ft

The dispersion curve between Points 1 and 2 (frequencies from 1,000 to 2,000 Hz) covers a range of wavelengths from 1.13 to 1.65 ft. However, for a similar increment in frequency range between Points 4 and 5 (frequencies from 4,000 to 5,000 Hz), a smaller portion of the dispersion curve corresponding to a range of wavelengths of 0.61 to 0.72 is obtained. As such, for a given record, the dispersion curve is better defined at the higher frequencies in the record, and for that reason the range of frequencies at different receiver spacings should be reduced to gain better resolution at lower frequencies.

The dispersion curve presented in Figure 6a is shown in Figure 7 along with a dispersion curve ob-

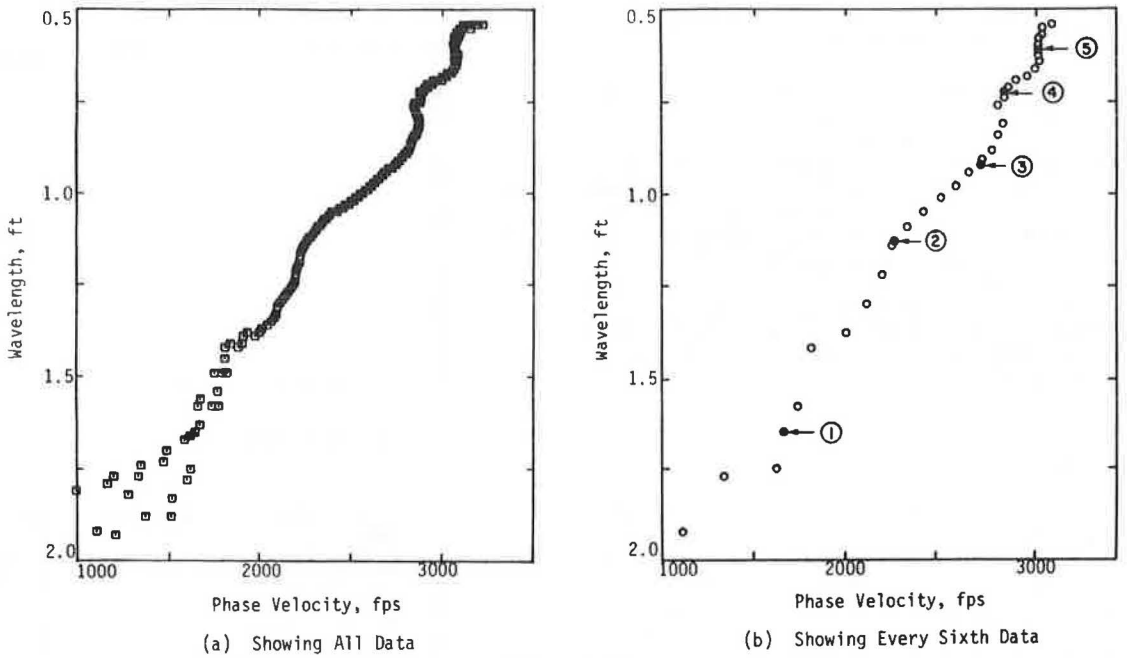

FIGURE 6 Dispersion curve constructed from record shown in Figure 5.

tained by repeating the experiment from the reversed direction (i.e., causing an impact from the opposite side of the receivers). In addition, the average curve actually used in the inversion process is included in Figure 7. The criterion being used for averaging data obtained at different spacings is as follows. At each frequency, the mean, standard deviation, and coefficient of variation of velocities are calculated. If the coefficient of variation is less than 7.5 percent, the mean is accepted as the average. However, if the coefficient of variation does not satisfy this criterion, points that are

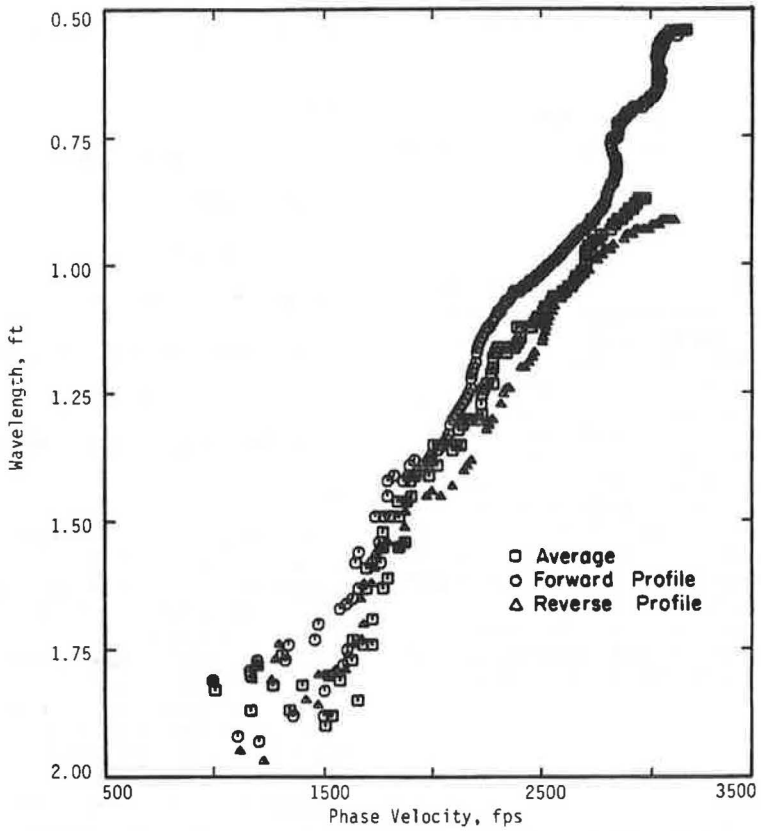

FIGURE 7 Dispersion curve constructed from record shown in Figure 5 and associated reverse profile record.

outside 0.67 times 1 standard deviation (outliers) are omitted, and the process is repeated.

Inversion Process

Inversion is the process of obtaining the true shear wave velocity profile from the dispersion curve. In other words, inversion is the process of determining the thickness and stiffness of different layers given the phase velocity-wavelength relationship. The inversion process is an iterative process in which a shear wave velocity profile is assumed and a theoretical dispersion curve is constructed. The experimental and theoretical curves are compared, and necessary changes are made in the assumed shear wave velocity profile until the two curves (experimental and theoretical dispersion curves) match within a reasonable tolerance.

The dispersive characteristic of surface waves was discussed earlier. Based on the theory discussed, a computer algorithm INVERT was developed to compute a theoretical dispersion curve from an assumed shear wave velocity profile. The program is interactive for ease of use. A range of frequencies and velocities is chosen for each search, along with the number of increments that should be used in each range. The higher the number of increments, the more accurately the dispersion curve is defined. However, computational time increases significantly as the number of increments increases. As such, instead of choosing a wide range of frequencies and velocities with a large number of increments, it is more economical to limit the ranges and number of increments and perform several runs. At each increment of frequency, the program computes the determinant presented in Equation 25. The phase velocity associated with each frequency is determined when there is a change of sign in the value of the determinant. An example output is shown in Figure 8, with the location of the roots marked by the dashed horizontal lines.

The value of the phase velocity is found by linear interpolation between the two velocities where the values of the determinant change sign. Because the dispersion equation is not linear, this interpolation introduces a small error. However, the velocity increments are kept small (usually approximately 5 percent of the expected velocity), and this error can be ignored. The results can be inspected and compared with the experimental data on the computer terminal screen or a hard copy can be produced.

The first step in the inversion process is assessment of a shear wave velocity profile from the dispersion curve. To avoid confusion, the dispersion curve should be divided into small sections and plotted with an expanded scale. Several layers (approximately 2 to 5) are selected, and a shear wave velocity is assigned to each layer. As a first approximation, it is useful to assume that the shear wave velocity is equal to 1.10 times the phase velocity and the depth of sampling is equal to 1/3 of the wavelength. These criteria are suggested as a simplified inversion process; however, the results from this process are not acceptable and will be significantly modified. With more experience, more realistic assumptions can be made. In addition, any

***** LAYER PROPERTIES *****

LAYER	THICKNESS (ft)	SHEAR WAVE VELOCITY (fps)	COMP. WAVE VELOCITY (fps)	DENSITY (slug)
1	1.0	1000.	2000.	3.4
2	1.0	1500.	3000.	3.4
3	1.0	1500.	3000.	3.4

(a) Layer Properties

***** DISPERSION CURVE DATA *****

NUMBER OF POINTS= 14

VELOCITY	WAVELENGTH
1342.	13.42
1298.	6.49
1228.	4.09
1120.	2.80
1028.	2.06
980.	1.63
957.	1.37
948.	1.18
1373.	1.53
938.	1.04
1340.	1.34
933.	.93
1298.	1.18
930.	.85

(c) Dispersion Curve Data

V_{ph} \ f*	100.00	200.00	300.00	400.00	800.00	900.00	1000.00	1100.00
1400	.12E+01	.72E+00	.11E+01	.88E+00	.33E-02	-.16E-01	-.59E-01	-.16E+00
1350	.11E+00	.25E+00	.53E+00	.11E+01	.30E-01	.14E-01	-.51E-02	-.16E+00
1300	-.55E+00	.84E-02	.24E+00	.30E+01	.50E-01	.33E-01	.20E-01	-.94E-03
1250	-.10E+01	-.18E+00	.55E-01	.13E+01	.67E-01	.49E-01	.36E-01	.24E-01
1200	-.14E+01	-.34E+00	-.73E-01	.29E+00	.86E-01	.64E-01	.49E-01	.37E-01
1150	-.17E+01	-.47E+00	-.10E+00	.62E-01	.12E+00	.84E-01	.64E-01	.49E-01
1100	-.19E+01	-.57E+00	-.23E+00	-.39E-01	.19E+00	.13E+00	.92E-01	.69E-01
1050	-.22E+01	-.66E+00	-.28E+00	-.96E-01	.24E+01	.60E+00	.26E+00	.16E+00
1000	-.24E+01	-.74E+00	-.32E+00	-.13E+00	.65E-01	.74E-01	.79E-01	.82E-01
950	-.26E+01	-.81E+00	-.35E+00	-.16E+00	.11E-02	.49E-02	.63E-02	.65E-02
900	-.28E+01	-.87E+00	-.37E+00	-.18E+00	-.22E-01	-.16E-01	-.13E-01	-.10E-01

number in each box represents value of det (R_{11})

dashed line represents one solution to Eq. 25

*f = frequency in Hz
+V_{ph} = phase velocity in fps
--- = location of fundamental root
=== = location of higher-mode root

(b) Values of Determinant R_{11} Presented in Equation 25

FIGURE 8 Representation of output from computer program INVERT.

additional information available about the site can be used to accelerate significantly the inversion process. It should be mentioned that this is mainly a preliminary trial only to obtain a reasonable starting point for the second stage of the matching process.

In the second stage, each layer in the shear wave velocity profile obtained in the first stage is divided into sublayers, and a more refined matching process is employed. When the theoretical and experimental curves match over the range of wavelengths available, the final shear wave velocity profile is obtained.

In the first stage, the dispersion curves can only be roughly matched because the resolution is not adequate for closer matching. However, in the second stage the resolution is much greater, and the theoretical and experimental curves can be compared and matched in a more refined manner simply by changing the velocities of the sublayers. As the number of sublayers increases, the accuracy with which the boundary between the actual layers can be defined also increases.

The reason for this two-stage process is to avoid large variations of shear wave velocities after the initial stage, which results in easier data analysis. It should be mentioned that small changes in a sublayer will have only local effects and will not cause significant variations in the theoretical dispersion curve.

A dispersion curve of a flexible pavement is shown in Figure 9. A portion of this curve over the range in wavelengths of 0.5 to 2 ft is shown in Figure 7. The profile at this site is approximately 5 in. of asphaltic concrete underlain by approximately 8 in. of lime-rock base and then subgrade. The outcome of the matching process during inversion is shown in Figures 10 and 11. The matching results have been expanded greatly to demonstrate the accuracy of the match. It can be observed that experimental and theoretical curves follow one another closely and at no point do the two curves disagree by more than about 5 percent. However, around wavelengths of 1.8 to 2.0 ft where the transition between the upper pavement system and subgrade is expected to occur, a portion of the curves cannot be matched because of a sharp change in velocity. This is a typical characteristic of transitional zones and almost occurs universally in all dispersion curves for pavements. Practically speaking, this transition zone appears as a step in the dispersion curve, and the data are so erratic that during construction of the dispersive waves the data points in this range will not fulfill the statistical criteria described previously. Another point of interest is a jump in the theoretical curve such as the one shown in Figure 10a in the range of wavelengths of 0.95 to 1.10 ft. These jumps occur in the vicinity of shear wave velocities of layers when a large contrast in velocities is present. This is due to a weakness in the program and at these boundaries the phase velocities are somewhat inaccurate.

CASE STUDIES

The SASW method has been utilized on many flexible and rigid pavements, both at airports and highways. Two cases are presented here to demonstrate the versatility of this method. In all cases, the results have been compared with crosshole seismic tests, a well-established in situ seismic test. The procedure of performing crosshole tests is discussed in detail by Stokoe and Hoar (10) and is not repeated here.

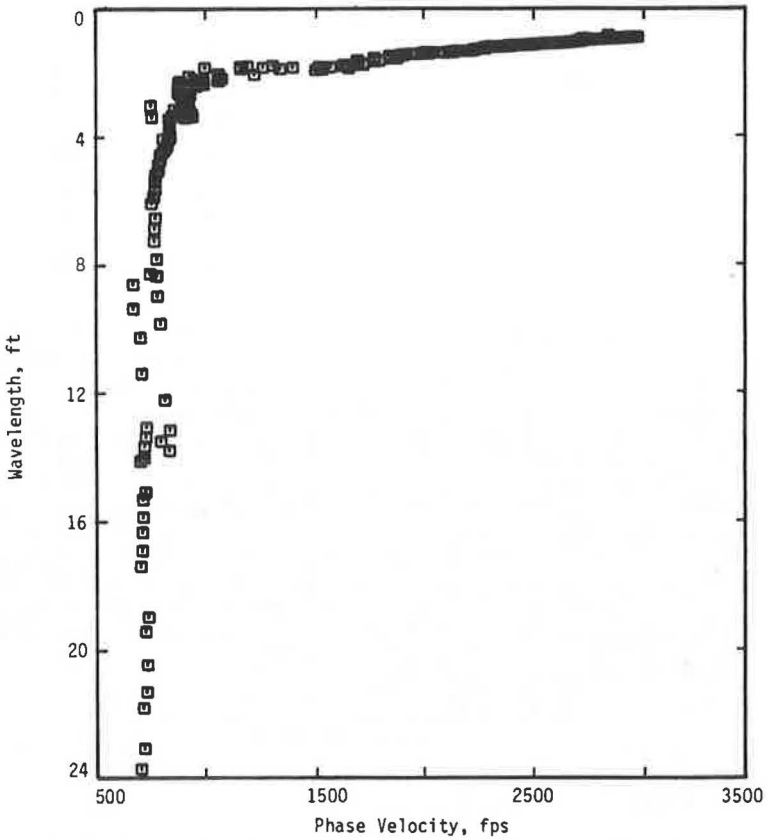

FIGURE 9 Dispersion curve constructed from SASW tests on a flexible pavement site.

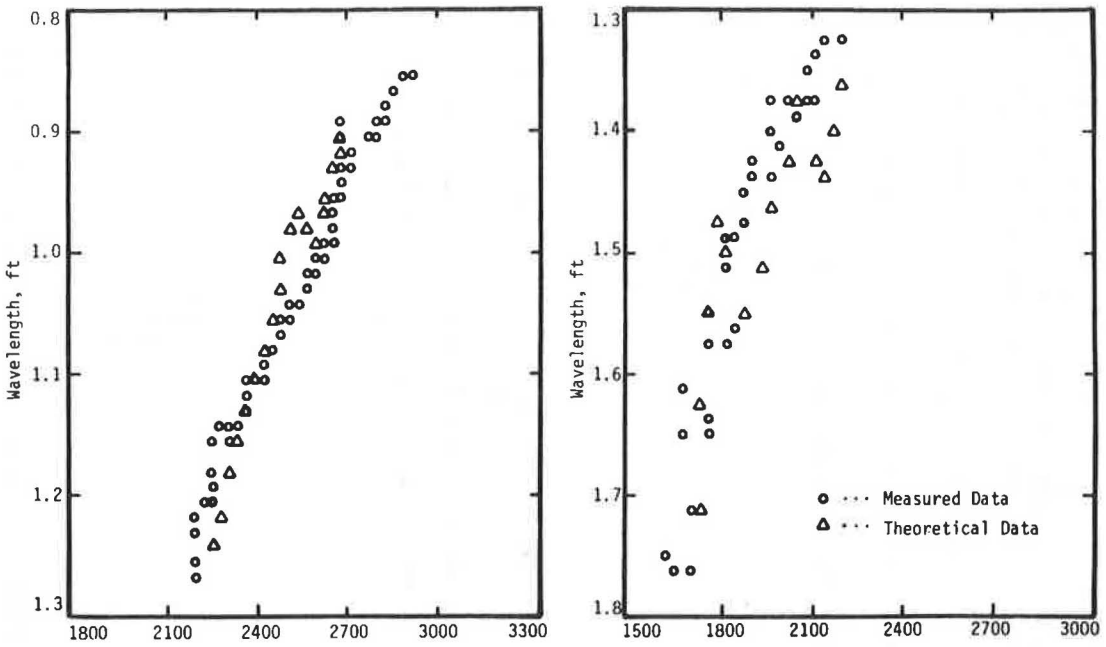

(a) Range of Wavelengths of 0.8 to 1.3 ft (b) Range of Wavelengths of 1.3 to 1.8 ft

FIGURE 10 Comparison of theoretical and experimental dispersion curves for short wavelengths for the flexible pavement site.

Case Study 1

The first case pertains to a flexible pavement site that was used as an example in the previous section. The profile consists of 5 in. of asphaltic concrete, 8 in. of lime-rock base, and subgrade (Figure 12b). The shear wave velocity profile determined at this site is shown in Figure 12c. The results from cross-hole tests are also shown in the figure, and the two compare well. Young's modulus profiles calculated from the shear wave velocity profiles, employing Equations 1-3, are shown in Figure 12d. Naturally, these curves agree well (because the velocities agreed), with a maximum and average differences of approximately 22 and 10 percent, respectively.

In Figure 11b, in the range of wavelengths of 4.5 to 5 ft, some theoretical data exist with no experimental data to be matched. At this point the transition between the upper and lower branches of the dispersion curve (such as the one shown in Figure 2)

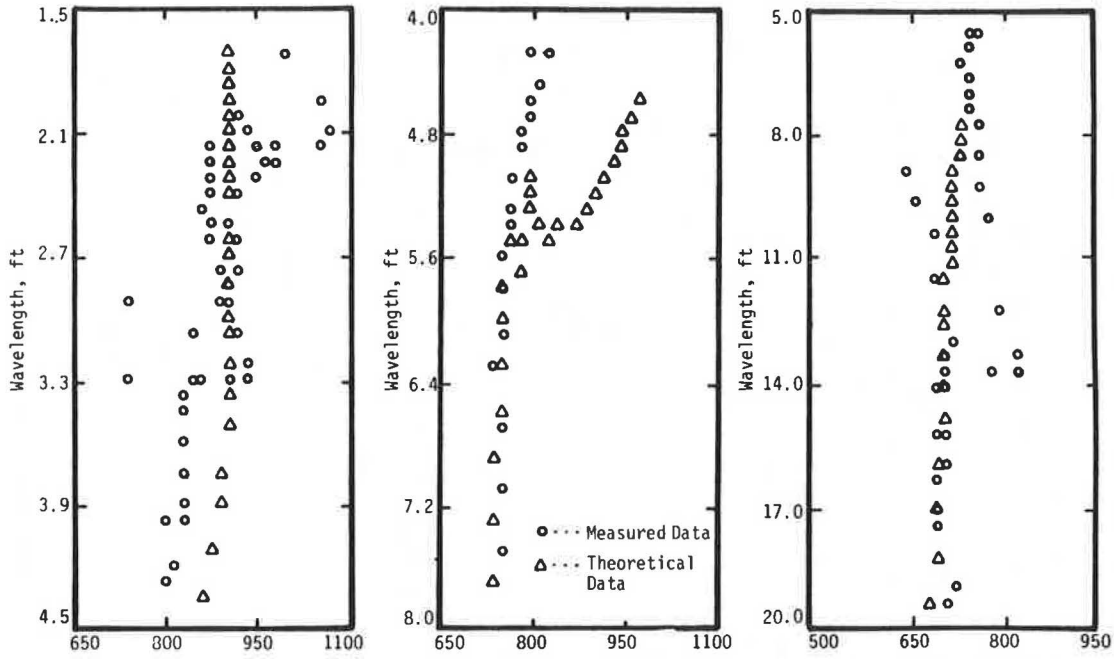

(a) Range of Wavelengths of 1.50 to 4.50 ft (b) Range of Wavelengths of 4.00 to 8.00 ft (c) Range of Wavelengths of 5.00 to 20.00 ft

FIGURE 11 Comparison of theoretical and experimental dispersion curves for longer wavelengths for a flexible pavement site.

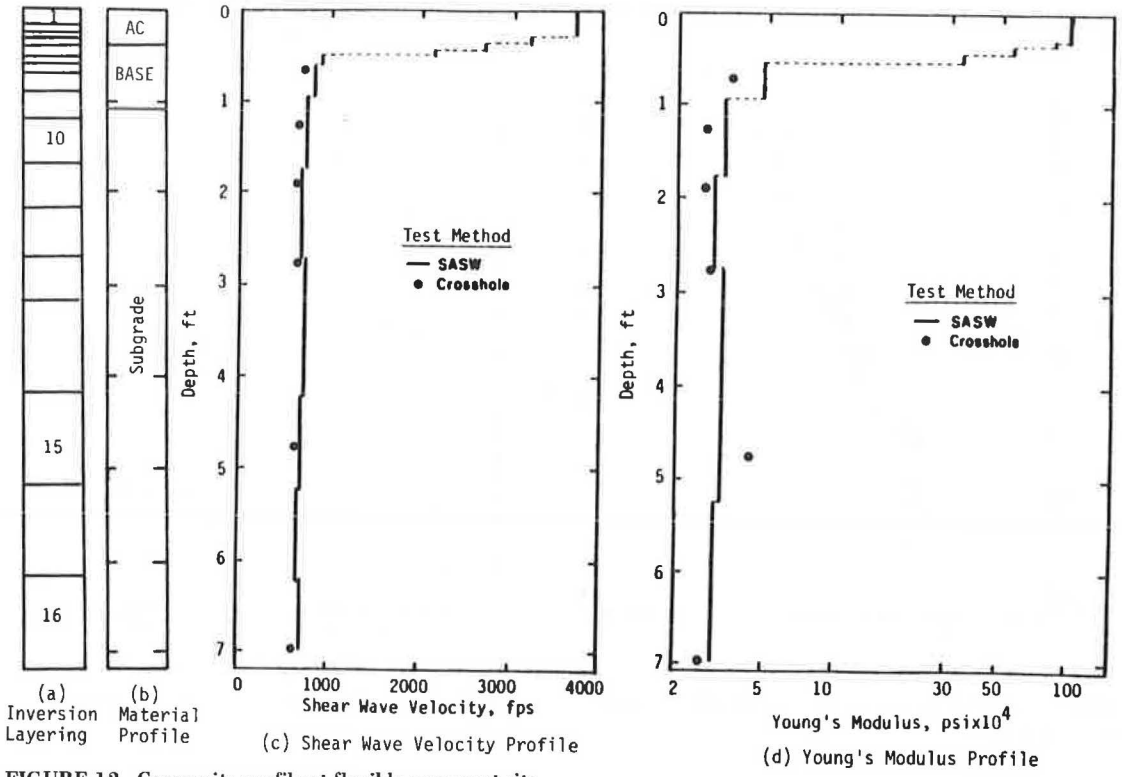

FIGURE 12 Composite profile at flexible pavement site.

is present. The reason for the lack of experimental data in this region is unknown but has little effect on the outcome.

Case Study 2

To test the utility of the inversion process, two series of tests for various profiles at the same site were performed on the embankment of an overpass. The first series of tests was performed after the embankment was raised to its final elevation but before placement of the pavement. The second series was performed after the granular base and pavement were placed. Nominal thicknesses of the asphalt and base layers are 2.5 and 15 in., respectively.

Shear wave velocity profiles from the two series of tests are presented in Figure 13d and their tabu-

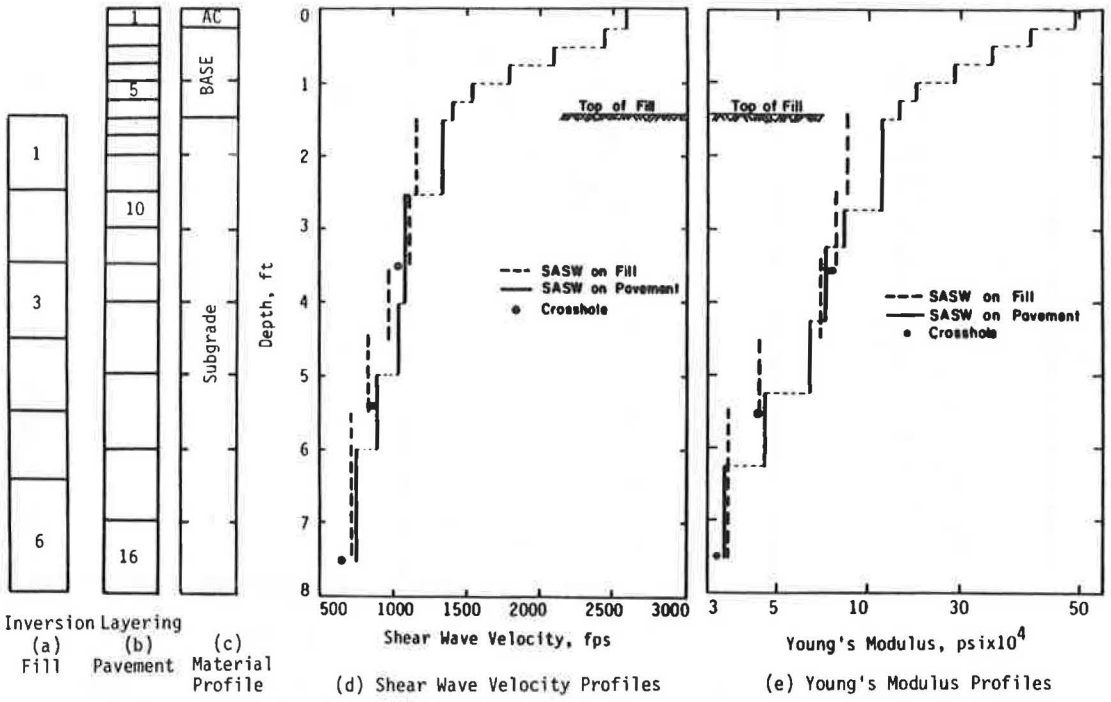

FIGURE 13 Composite profile at embankment site.

TABLE 1 Comparison of Young's Moduli and Shear Wave Velocities from SASW and Crosshole Tests at Embankment Site

Depth[a] (ft) (1)	Shear Wave Velocity (ft/sec) SASW First[b] (2)	SASW Second[c] (3)	Crosshole (4)	Young's Modulus (psi x 10^4) SASW First[b] (5)	SASW Second[c] (6)	Crosshole (7)	Difference (%) (5-6)/5 (8)	(7-6)/7 (9)
0.13	–	2,600	–	–	49	–	–	–
0.38	–	2,420	–	–	35	–	–	–
0.63	–	2,080	–	–	26	–	–	–
0.88	–	1,810	–	–	19	–	–	–
1.13	–	1,560	–	–	14	–	–	–
1.38	–	1,440	–	–	13	–	–	–
1.75	1,170	1,360	–	8.6	11.5	–	-33.7	–
3.50	1,120	1,100	1,010	7.9	7.5	6.5	5.1	-15.4
4.50	980	1,030	–	6.1	6.5	–	-6.6	–
5.00	840	1,030	–	4.4	6.50	–	-47.7	–
5.50	840	860	870	4.4	4.6	4.8	-4.5	+4.2
6.00	730	860	–	3.2	4.6	–	-43.7	–
7.50	730	740	720	3.2	3.4	3.3	-6.2	3.0

[a]Depths from ACP surface to middle of the layer.
[b]First series of SASW tests after placement of fill.
[c]Second series of SASW tests after placement of asphaltic-concrete pavement and base over fill.

lation is presented in Table 1. A total of 6 and 16 layers were used in the inversion of the dispersion curves for the before-and-after placement of the pavement layers, as shown in Figure 13.

Figure 13e shows the Young's modulus profiles from this site. The values of Poisson's ratio of 0.25, 0.25, and 0.33 were assumed for the pavement, base, and subgrade, respectively, and the assumed total unit weights were 135, 115, and 115 lb/ft^3 for pavement, base, and subgrade, respectively. Generally, the two curves match well. In the range of depths of 1.5 to 2.5 ft, the difference in Young's moduli is about 34 percent. Although the first few feet of the ground might have been compacted further because of placement of the base layer and pavement, it is believed that part of the difference is due to the weakness of the algorithm being used for data reduction at about the interface of subgrade and base material. At depths below 4.5 ft, the percentage deviation between moduli oscillate between high (48 percent) and low (4 percent) values. This occurs because of coarse layering being used to reduce the first SASW test series. It is believed that assumption of layers less than 1 ft in a soil site do not have any practical value and is a waste of computational time. Had finer layering been chosen, the result would have been in better agreement at depths of 5 and 6 ft.

SUMMARY

The main purpose of this paper is to present the theoretical aspects of the spectral-analysis-of-surface-waves (SASW) method because the experimental aspects have been presented by Nazarian et al. (2) and Nazarian and Stokoe (3). The SASW method is based on surface waves propagating in an elastic layered medium. The matrix solution for phase velocities of surface waves in this system has been developed by Thomson (5) and Haskell (6). To apply this solution to pavements, improvements in the numerical procedure made by Dunkin (7) have been adapted. All of this work has been combined, and an interactive computer program, INVERT, has been developed with which phase velocities can be determined. Phase velocities determined in this manner constitute the theoretical dispersion curve.

In the field, phase information of the cross power spectra as well as coherence functions is collected and used to construct an experimental dispersion curve. Factors that affect the shape of a dispersion curve are shear wave velocity, Poisson's ratio, and mass density of the different layers in a given profile. It is shown that the effects of the last two factors on the analytical results are not significant, hence, greatly simplifying data analysis. After experimental dispersion curves have been determined, the stiffness (Young's modulus) and thickness of each layer in the pavement system are evaluated by matching the theoretical dispersion curves to them. This step is called inversion.

Two case studies are included to demonstrate the actual performance of this method. The results from the method are compared with other independent tests. Young's moduli from these tests agree well with those obtained by the SASW method.

ACKNOWLEDGMENTS

This work was supported by the Texas State Department of Highways and Public Transportation; this support is greatly appreciated. Richard B. Rogers and Jerry F. Daleiden acted as technical monitors, and their comments and guidance are appreciated.

REFERENCES

1. J.S. Heisey, K.H. Stokoe II, and A.H. Meyer. Moduli of Pavement Systems from Spectral Analysis of Surface Waves. In Transportation Research Record 852, TRB, National Research Council, Washington, D.C., 1982, pp. 22-31.
2. S. Nazarian, K.H. Stokoe II and W.R. Hudson. Use of Spectral Analysis of Surface Waves for Determination of Moduli and Thicknesses of Pavement Systems. In Transportation Research Record 930, TRB, National Research Council, Washington, D.C., 1983, pp. 38-45.
3. S. Nazarian and K.H. Stokoe II. Nondestructive Testing of Pavements Using Surface Waves. In Transportation Research Record 993, TRB, National Research Council, Washington, D.C., 1984, pp. 67-79.
4. G.G. Miller and H. Pursey. On the Partition of Energy Between Elastic Waves in a Semi-Infinite

Solid. Proc., Royal Society, Vol. 223, London, England, 1955, pp. 251-541.
5. W.T. Thomson. Transmission of Elastic Waves Through a Stratified Solid Medium. Journal of Applied Physics, Vol. 21, Feb. 1950, pp. 89-93.
6. N.A. Haskell. The Dispersion of Surface Waves in Multilayered Media. Bull. Seismological Society of America, Vol. 43, No. 1, 1953, pp. 17-34.
7. J.W. Dunkin. Computation of Modal Solutions in Layered, Elastic Media at High Frequencies. Bull. Seismological Society of America, Vol. 55, 1965, pp. 335-358.
8. S. Nazarian. In Situ Determination of Elastic Moduli of Soil Deposits and Pavement Systems by Spectral-Analysis-of-Surface-Waves Method. Ph.D. dissertation. University of Texas, Austin, 1984, 452 pp.
9. W.M. Ewing, W.S. Jordetsky, and F. Press. Elastic Waves in Layered Media. McGraw-Hill Book Co., Inc., New York, 1957, 380 pp.
10. K.H. Stokoe II and R.J. Hoar. Variables Affecting In Situ Seismic Measurements. Proc., Conference on Earthquake Engineering and Soil Dynamics, ASCE, Pasadena, Calif., 1978, pp. 919-939, Vol. II.

Publication of this paper sponsored by Committee on Subsurface Drainage.